SAINT PETERSBURG STATE UNIVERSITY
Department of Nuclear Physics Research Methods

14th International Youth School-Conference

MAGNETIC RESONANCE AND ITS APPLICATIONS

Abstracts

an AMPERE event

April 23-29, 2017
Saint Petersburg, Russia

Schola **Spinus**

14th International Youth School-Conference

MAGNETIC RESONANCE AND ITS APPLICATIONS

SPINUS-2017

ORGANIZING COMMITTEE

Chairman	Denis Markelov, associate professor, SPSU
Vice-chairman	Alexander Ievlev, researcher, SPSU
Committee members	Andrey Egorov, associate professor, SPSU Andrey Komolkin, associate professor, SPSU Andrei Chudin, assistant researcher, SPSU Pavel Kupriyanov, engineer, SPSU Sergey Bystrov, graduate student, SPSU Sevastyan Rabdano, trainee researcher, SPSU Konstantine Tutukin, senior researcher, SPSU Timofey Popov, SPSU
Layout of Abstracts Book	Aleksandr Levantovskii

CONTACTS

1, Ulyanovskay st., Peterhof, 198504, St. Petersburg, Russia
Department of Nuclear Physics Research Methods
St. Petersburg State University

Tel.	(812) 428-99-48
Fax	(812) 428-72-40
E-mail	spinus@nmr.phys.spbu.ru
Website	http://nmr.phys.spbu.ru/spinus

PROGRAM COMMEETEE

SCIENTIFIC ADVISER OF THE SCHOOL-CONFERENCE

Vladimir Chizhik	Honored scientist of Russia, Professor, SPSU

ADVISORY BOARD

E. B. Aleksandrov	Acad., Prof., St. Petersburg, Russia
V. Balevicius	Prof., Vilnius, Lithuania
Yu. M. Bunkov	Prof., Grenoble, France
V. I. Chizhik	Prof., St. Petersburg, Russia
D. Fruchart	Prof., Grenoble, France
L. Yu. Grunin	Associate. prof., Yoshkar-Ola, Russia
E. Lähderanta	Prof., Lappeentanta, Finland
D. Michel	Prof., Leipzig, Germany
V. I. Minkin	Acad., Prof., Rostov-on-Don, Russia
B. Rameev	Prof., Gebze, Turkey
N. R. Skrynnikov	Prof., St. Petersburg, Russia, Purdue, USA
M. S. Tagirov	Prof., Kazan, Russia
S. Vasiliev	Prof., Turku, Finland

Spinus

SPONSORS

Alkor Technologies
alkor.net

Bruker Corporation
bruker.com

Russian Foundation for
Basic Research
rfbr.ru

SciJob.ru
Карьера для исследователей
и инженеров

scijob.ru

APG Eastern Europe
preforma.ru

Magicplot Systems, LLC
magicplot.com

Archaeophysics
nearsurface geophisics

archaeophys.com

P&L
Scientific

plscientific.se

Contents

Schedule of Spinus-2017

	23.04.17 Sunday	24.04.17 Monday	25.04.17 Tuesday	26.04.17 Wednesday	27.04.17 Thursday	28.04.17 Friday	29.04.17 Saturday
08:45 – 09:45		BREAKFAST				9:30-10:30 BREAKFAST	BREAKFAST
10:00 – 11:30		**Registration 30** **Chizhik 40** **GROUP PHOTO 20**	Koplak 30 **Volkov 60**	**Excursion day**	**Zubkov 60** **Eichhof 30**	**Grunin 40** Ievlev 20	**Departure**
11:30 – 12:00		COFFEE BREAK			COFFEE BREAK		
12:00 – 14:00		**Skrynnikov 60** Rabdano 20 Babicheva 20 Baranauskaite 20	**Bunkov 60** Slesarenko 30 Melnikova 30		**Cabal 60** Colet 30 Dvinskikh 30	**Vasil'ev 40** Salikov 20 **Matveev 60**	
14:00 – 15:30		LUNCH			LUNCH		
15:30 – 17:00	**Registration of participants**	**Michel 50** Denisov 20 Shubina 20	Soloninin 20 Shavykin 20 Markelov 20 **POSTER SESSION 16:30**		**Mozzhukhin 60** Kachala 30	Andronenko 30 Kosenkov, Neronov 30 **Awarding Closing**	
17:00 – 17:30		COFFEE BREAK			COFFEE BREAK		
17:30 – 19:00		**Fraissard 50** Chudin 20 Krylova 20	**POSTER SESSION**		**Sergeyev 30** Komolkin 20 Lähderanta 20		
19:00 – 20:00	**Welcome**	DINNER				DINNER	
20.00		Cultural and sporting activities			CONFERENCE DINNER		

Schedule

14-th International Youth School-Conference

«Magnetic Resonance and its Applications. Spinus-2017»

23 - 29 April, 2017

St. Petersburg

SUNDAY – 23 April 2017	
14:00 – 15:30	**LUNCH**
15:30 – 19:00	**REGISTRATION OF PARTICIPANTS**
19:00 –	**WELCOME PARTY «*EVENING IN KARELIA*»**

	MONDAY – 24 April 2017
08:45 – 09:45	**BREAKFAST**
10:00 – 10:30	**Registration**
10:30 – 11:10	**Vladimir I. Chizhik** A few details about Magnetic Resonance in Russia
11:10 – 11:30	***GROUP PHOTO***
11:30 – 12:00	**COFFEE BREAK**
12:00 – 13:00	**Nikolai R. Skrynnikov** Recent results from the Laboratory of biomolecular NMR @ SPbGU: from mechanism of anti-cancer peptides to characterization of flexible tails in amyloid fibrils
13:00 – 13:20	**Sevastyan O. Rabdano** Reconstruction of particle size-distribution from conjunction of NMR and DLS diffusion data
13:20 – 13:40	**Ekaterina S. Babicheva** Study of nanoemulsions of the hydrophobic phthalocyanine in pluronic aqueous solutions
13:40 – 14:00	**Valeriia E. Baranauskaite** Study of the structural-dynamic characteristics of the ternary system CsCl-LiCl-D_2O with NMR spectroscopy in the interval from 25 to the freezing temperature.
14:00 – 15:30	**LUNCH**
15:30 – 16:20	**Dieter Michel** Nuclear Spin Relaxation Studies of Mobility of Molecules Adsorbed in Porous Media: Small Molecules embedded in Zeolites and related materials
16:20– 16:40	**Gleb L. Denisov** Paramagnetic terpyridine complexes of d-metals by methods of the magnetic resonance spectroscopy
16:40– 17:00	**Natalia S. Shubina** NMR study of photoisomerization of AzoTAB and CTAB when interacting with cardiomyocytes
17:00 – 17:30	**COFFEE BREAK**
17:30 – 18:20	**Jacques Fraissard** NMR in Archaeology: Egyptian Pyramids and Blue Maya
18:20 – 19:40	**Andrei V. Chudin** Application of NMR for studies of archaeological pottery. Preliminary results

18:40 – 19:00	**Ekaterina A. Krylova** NMR study of water dynamics in copper-exchanged mordenites
19:00 – 20:00	**DINNER**
20:00 –	**CULTURAL AND SPORTING ACTIVITIES**
	TUESDAY – 25 April 2017
08:45 – 09:45	**BREAKFAST**
10:00 – 10:30	**Oksana V. Koplak** Spin dynamics studied by solid-state nuclear magnetic resonance and electron paramagnetic resonance in 29S:B crystals
10:30 – 11:30	**Vitaly I. Volkov** NMR investigation of ionic and molecular transport mechanism in ion-exchanger nanochannels
11:30 – 12:00	**COFFEE BREAK**
12:00 – 13:00	***Yuriy M. Bunkov*** Supermagnonics
13:00 – 13:30	**Nikita A. Slesarenko** NMR analysis of calixarenes-sulfonic acids
13:30 – 14:00	**Daria L. Melnikova** Investigation of α–casein translational mobility by NMR methods
14:00 – 15:30	**LUNCH**
15:30 – 15:50	**Alexey V. Soloninin** NMR study of $LiBH_4$ and solid solutions $LiBH_4$-LiI
15:50– 16:10	**Oleg V. Shavykin** The sensitivity of local dynamics and its manifestation in NMR to excluded volume in dendrimers
16:10 – 16:30	**Denis A. Markelov** The “Hollow Core” Structure of Copolymeric Dendrimers
16:30 – 17:00	**POSTER SESSION**
17:00 – 17:30	**COFFEE BREAK**
17:30 – 19:00	**POSTER SESSION**
19:00 – 20:00	**DINNER**
20:00 –	**CULTURAL AND SPORTING ACTIVITIES**

	WEDNESDAY – 26 April 2017
08:45 – 09:45	**BREAKFAST**
	EXCURSION DAY
19:00 – 20:00	**DINNER**
20:00 –	**CULTURAL AND SPORTING ACTIVITIES**
	THURSDAY – 27 April 2017
08:45 – 09:45	**BREAKFAST**
10:00 – 11:00	**Mikhail A. Zubkov** Basic MRI physics, methods and applications
11:00 – 11:30	**Uwe Eichhoff** Can MRI contribute to the understanding of mental diseases?
11:30 – 12:00	**COFFEE BREAK**
12:00 – 13:00	**C. Cabal Mirabal** Kinetics studies of complex biomedical process by Magnetic Resonance. Cuban experiences
13:00 – 13:30	**Jean-Marie Colet** A ^{1}H-NMR-based Metabonomic Study of the Nephroprotective Role of Taurine against Gentamycin Poisoning in Rats
13:30 – 14:00	**Sergey V. Dvinskikh** Solid-State NMR Study of Surfactant Mesophases at Solid Interfaces
14:00 – 15:30	**LUNCH**
15:30 – 16:30	**Georgy V. Mozzhukhin** TD NMR detection of energetic and illicit materials
16:30 – 17:00	**Vadim V. Kachala** Avance Neo NMR spectrometer
17:00 – 17:30	**COFFEE BREAK**
17:30 – 18:00	**Nikolay M. Sergeyev** «ISTINA» is Not TRUE at all
18:00 – 18:20	**Andrei V. Komolkin** Master programs in Physics at Saint Petersburg State University

18:20 – 18:40	**Erkki Lähderanta** Double Master Program of St. Petersburg State University and the Lappeenranta University of Technology
20:00 –	**CONFERENCE DINNER**
	FRIDAY – 28 April 2017
09:10 – 10:30	**BREAKFAST**
10:30 – 11:10	**Leonid Y. Grunin** Spin-Lattice NMR Relaxation in Polycrystalline Solids
11:10 – 11:30	**Alexandr V. Ievlev** ^{1}H NMR relaxation in emimAc-glycerol mixture.
11:30 – 12:00	**COFFEE BREAK**
12:00 – 12:40	**Sergey G. Vasil'ev** Magnetic Resonance Study of Atomic Hydrogen Isotopes Stabilized in Solid Hydrogen Matrices below 1K
12:40 – 13:00	**Vladislav A. Salikov** Analysis of NMR spectra of alizarin and alizarin red S
13:00 – 14:00	**Vladimir V. Matveev** NMR in Magnetic Materials: Current status
14:00 – 15:30	**LUNCH**
15:30 – 16:00	**Sergey. I. Andronenko** A Variable temperature X- and W-band EPR study of SiCN/Fe ceramics
16:00 – 16:30	**Denis D. Kosenkov, Yuriy I. Neronov** Experimental determination of magnetic resonance ratio of magnitometers based on Cesium-133 atoms and water protons in fields 10 .. 25 mTl
16:30 – 17:00	**AWARDING AND CLOSING**
17:00 – 17:30	**COFFEE BREAK**
17:30 – 19:00	**FREE TIME**
19:00 – 20:00	**DINNER**
	SATURDAY – 29 April 2017
08:45 – 09:45	**BREAKFAST**
11:00 –	**DEPARTURE**

Spinus

Welcome to the School-Conference "Spinus" of Saint Petersburg State University

Already not quite the 'Winter' International Youth School-Conference "Magnetic resonance and its application" SPINUS-2017 will be held at the St. Petersburg State University in the 14th time. It is organized in according to the subjects of researches and master's degree programs, which are developed and implemented in the educational process. In modern physics, the term "magnetic resonance" refers to a set of phenomena accompanied with the emission or absorption of electromagnetic waves of the radiofrequency diapason by quantum systems (nuclei, electrons, atoms, molecules, etc.). These phenomena, the physical nature of which is of independent interest, provided the basis of radiospectroscopic methods for studying the structure of matter and physico-chemical processes in it. They are also used for the creation of quantum generators, amplifiers, and magnetometers. For the development of ideas and applications of magnetic resonance six Nobel Prizes were awarded in the areas of physics, chemistry, biology, physiology and medicine (the latter was in 2003).

Primarily, magnetic resonance methods are:

- Nuclear Magnetic Resonance (NMR)
- Electron Paramagnetic Resonance (EPR)
- Nuclear Quadrupole Resonance (NQR)

These methods, being contactless, do not destroy an object under a study, that makes them unique and in demand not only in physics and chemistry, but also in medicine, geology, biology, archeology. Now, any medical center with high reputation has a magnetic resonance imaging (MRI). In Russia, NMR is used in oil well logging, laboratory analysis of the productivity of oil-bearing reservoirs, analysis of oil content and moisture of seeds; EPR technique is used for geological research, non-destructive control of precious stones; there are NQR applications for remote detection of solid explosives and narcotics. Magnetometry methods based on magnetic resonance are indispensable for carrying out archaeological researches.

The designation "school-conference" means that, on the one hand, the organizers will include in the program the lectures, which reflect the basics of magnetic resonance and current state of knowledge and experience in this field, and, on the other hand, as well as at any conference it is expected to discuss new results, obtained by young scientists, using magnetic resonance techniques. It should be emphasized that our school-conference aims not only to researchers specializing in the field of magnetic resonance, but also to representatives of other sciences, where these methods can be successfully applied.

Earlier the school organizers worked at the Department of quantum magnetic phenomena (QMPh) of the St. Petersburg State University, which was founded in 1993 on the initiative of Professor V.I. Chizhik on the basis of the laboratory, created in the 50s of the last century by F.I. Skripov at the Department of Radio Physics (the branch "Quantum Radiophysics"). On January 1, 2014, the Department of QMPh joined the united Department of nuclear-physics research methods (Head of the Department is Corresponding Member of the Russian Academy of Sciences, Professor Mikhail Kovalchuk). The QMPh collective has a number of priority works in the field of nuclear magnetic resonance. One of the most significant achievements is the first in the world implementation (in 1958) of the Fourier transform of a free induction signal in order to obtain a NMR spectrum. Concurrently with the research activity, the staff of the department are actively involved in the development of practical applications of magnetic resonance. The department graduates work not only in Russia and the CIS, but also in Sweden, USA, New Zealand, England, Germany, France,

Italy, occupying positions from a highly advanced operator of radiospectrometers to a professor.

The main research areas developing in the group of quantum magnetic phenomena:

- Nuclear magnetic relaxation in liquids;
- Nuclear magnetic resonance in solids, including magnetically ordered materials;
- NMR in liquid crystals;
- NMR in heterogeneous systems;
- MRI in weak magnetic fields;
- Electron paramagnetic resonance;
- Nuclear magnetic resonance in the magnetic field of the Earth;
- The quantum magnetometry in archeology.

It is evident from the above that the scope of our research interests is quite wide. We always open for the collaboration with researchers from various science fields.

Our team has published a series of monographs, textbooks and training manuals on Magnetic Resonance. For example:

1. Vladimir I. Chizhik, Yuri S. Chernyshev, Alexey V. Donets, Viatcheslav Frolov, Andrei Komolkin, Marina G. Shelyapina. Magnetic Resonance and Its Applications. 2014, Springer-Verlag. 782 pp. (Now more than 20700 downloads)
2. Квантовая радиофизика: магнитный резонанс и его приложения. Учеб. пособие. 2-е изд., перераб. Под ред. В. И. Чижика. – СПб.: Изд-во С.-Петерб. ун-та, 2009. 700 с.
3. В. И. Чижик. Ядерная магнитная релаксация. Учеб. пособие. 3-е изд. – СПб.: Изд-во С.-Петерб. ун-та, 2004. 388 с.
4. Практикум по магнитному резонансу. Учебное пособие. Под ред. В. И. Чижика. – СПб.: Изд-во С.-Петерб. ун-та, 2003. 184 с.

The Organizing committee
of the 14th International Youth School-Conference
"Magnetic resonance and its applications" Spinus-2017

Lectures

Supermagnonics

Yury Bunkov

Kazan Federal University, Kazan, Russia
MIPT, Dolgoprudnyy, Russia
E-mail: yuriy.bunkov@neel.cnrs.fr

Introduction

We consider the Bose-Einstein condensation (BEC) of quasi-equilibrium magnons which leads to a spin superuidity, the coherent quantum transfer of magnetization in magnetic materials. This phenomenon is beyond the classical Landau-Lifshitz-Gilbert paradigm. The critical conditions for excited magnon density in ferro- and antiferromagnets, bulk and thin films, are estimated and discussed.

Magnon BEC and Spin Supercurrent

At certain conditions the RF pumping of excited magnons may leads to a new state, so-called, magnon condensate, in which a macroscopic number of magnons forms a coherent quantum state. This state can significantly change the magnon gas properties, its dynamics and transport. Particularly, the magnetization precession may live in orders of magnitude longer than the T_2^* time of usual precession, so name long-lived induction decay signal. The spatial gradients of this state exhibit spin superfluidity, the coherent transport of deflected magnetization. The spin superuidity is an extremely interesting phenomenon both for fundamental and applied studies.

For the first time the existence of quasi-equilibrium Bose condensate was demonstrated in the experiment with nuclear magnons in the superfluid antiferromagnetic liquid crystal ^{3}He-B in 1984 [1]**.** The following phenomena were observed later: a) transport of magnetization by spin supercurrent between two cells with magnon BEC; b) phase-slip processes at the critical current; c) spin current Josephson ffect; d) spin current vortex formation; d) Goldstone modes of magnon BEC oscillations. The comprehensive reviews of these studies can be found in Ref. [2]. Currently magnon BEC found in different magnetic systems: i) in antiferromagnetic superfluid ^{3}He-A; ii) in in-plane magnetized yttrium iron garnet $Y_3Fe_5O_{12}$ (YIG) film with k about 10^{-5} 1/cm; iii) in antiferromagnetic $MnCO_3$ and $CsMnF_3$ with Suhl-Nakamura indirect nuclear spin-spin interaction.

Recently we have found the magnon BEC state and spin supercurrent in YIG film magnetized perpendicularly to the plain. We have observed the BEC state at k=0 with the properties very similar to one in ^{3}He-B. This discovery can be applied for number of applications. The results of our current investigations are the main topic of presentation. Particularly we have succeeded to observe the magnetization transport between two BEC states by a thin bridge between them. The stability of this spin supercurrent is protected by energetic gap, similar to one in usual supercurrent. This is why we are able to name this phenomenon “Supermagnonics”.

Acknowledgements

This work is supported by Russian Science Foundation (grant RSF 16-12-10359).

References

1. A. S. Borovik-Romanov, Yu. M. Bunkov, V. V. Dmitriev, Yu. M. Mukharskiy, JETP Lett. 40, 1033 (1984).
2. Yu. M. Bunkov, G. E. Volovik, Spin superfluidity and magnon BEC, Chapter IV of the book “Novel Superuids”, eds. K.H. Bennemann and J.B. Ketterson (Oxford, University press, 2013)

Kinetics studies of complex biomedical process by Magnetic Resonance. Cuban experiences

C. Cabal Mirabal[1,2], A. Fernandez Garcia[1], M. Lores Guevara[1], E. Gonzalez[2], L. Oramas Diaz[2]

[1]Medical Biophysics Center, University of Oriente, Cuba.
[2]Center for Genetic Engineering and Biotechnology, Cuba.
E-mail: carlos.cabal@cigb.edu.cu

Introduction

The potentials of the Magnetic Resonance (MR) methods in the research of biomedical system have been demonstrated during the 70 years of it existence, which we are celebrating this year. Cuban´s experiences concerning to quantitative MR associated with molecular, preclinical and clinical studies of significant diseases and the drug development are presented.

MR "in vitro" and "in vivo" studies of Sickle Cell disease (SCD) [1-4], the Diabetic Foot Ulcer (DFU) [5], the Brain Tumor Response (BTR) [6] and the Pharmacokinetics of Magnetic Nano Particles (MNP) [7], as example are presented. Furthermore, MR contributions to diagnostic and selection of therapeutic pathways are discuses.

MR Relaxation and Electron Spin Resonances studies of SCD

SCD is the first molecular disease described. Due to the polymerization of hemoglobin S (HbS), the erythrocyte is deformed, the permeability and elasticity of the membrane change, hemolysis is caused and rheology is modified, leading to painful vaso-occlusive crises [1, 4].

^{1}H T1 and T2 were determinate with the Cuban relaxometer at 4MHz using IR, Hahn and CPMG pulse sequences at 36 ^{o}C and with an error <5%. The measurements were performer during 8 h of the spontaneous deoxygenation of blood sample of more than 80 patients [2, 3].

Typical T1 and T2 temporal behaviors in HbA and HbS samples are shown in fig 1A [2, 3]. The kinetic of deoxyHbS polymerization are characterized by 3 stages: initial (I), nucleation (II) and termination (III) (1-4). The initial phase is delimited by the Delay time (tD) (9). After the tD, an autocatalytic formation of polymers takes place (II). Once nucleation concludes, ^{1}H relaxation tend to stabilize (III). The different MR behavior in HbA and HbS solutions could be associated with the molecular mobility or the Hb magnetism variations (oxyHb: diamagnetic and deoxyHbS: paramagnetic) and the appearance of micro in homogeneities at the end of the polymerization process [2, 3].

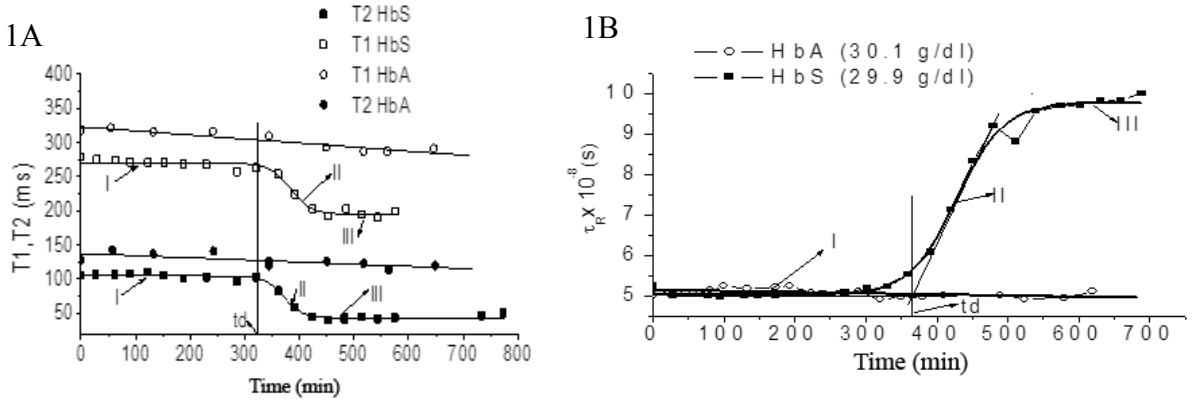

Figure 1. Temporal behavior of ^{1}H T1, T2 in 1A and τ_R, η_μ by ESR in 1B during the polymerization [2, 3]

From the T1, T2 and T1/T2 ratio values, in the regions I-III, can be concluded that $\tau_C \approx 4x10^{-8}$ s. A more precise quantitative evaluation of τ_C variation was done by ESR. Table 1 and figure 1B reports the values of typical temporal behavior of τ_R and the microviscosity η_μ determinate y ESR [3]. It's a good agreements between the 1H MR relaxation and ESR by the spin labeling method data.

Table 1. Rotation Correlation time and micro viscosity determinated by ESR [3]

Parameter	Region I (HbS)	Region II (HbS)	Region III (HbS)	HBA
τ_R ($x10^{-8}$ s)	5 ± 0.11	$5 \pm 0.11 \leq \tau_R \leq 9.8 \pm 0.22$	9.8 ± 0.22	5.8 ± 0.13
η_μ (mPas)	2.06 ± 0.1	$2.06 \pm 0.1 \leq \eta_\mu \leq 3.79 \pm 0.19$	3.79 ± 0.19	2.06 ± 0.1

The existing strong correlation between the MR parameters (T1, T2,τ_R, η_μ) with the t_D has been allowed to stablish a new diagnostic method for the differentiation between the Crises and Steady stages of the patients. Furthermore, this MR procedure made possible the discovery of the anti-sickling action of the Vanillin as a therapeutic drug [1-4].

MRI/MRS Quantitative Evaluation of Brain Tumor Response (BTR) and DFU response under treatment in Clinical trials

MR quantitative information for the evaluation of the BTR and DFU during treatment has been firstly reported [5, 6]. The purpose of this investigation was to set up the methodologies necessary for the study of two complexes pathological scenario. All MRI and MRS were performed with a 1.5 T Symphony Master Class system (Siemens).

Specifics MRI pulse sequences (FSE, IR, STIR, FLAIR, DWI), with and without Contrast agents (CA), was optimized in order to obtain reproducible quantitative data, reducing the Images Time and enhancing the contrast during the healing process [5, 6].

DFU response

A special device was created to be placed in the head RF coil in order to guarantee the reproducibility of the feet positioning. It was demonstrated that the RF coil parameters (Q and B1 homogeneity) don't change. The device provides two affixed sets of external markers connected with internal anatomic markers as a foot position reference [5].

MR studies of 10 DFU patients and were done previously and during treatment. DFU lesion sizes (Area and volume), Edema volume, as well as Apparent Diffusion Coefficient (ADC), and metabolites changes, were determined by MRI/MRS during a clinical trial phase IV.

Regardless of ADC complex dependence on tissue characteristics, if the measurements are performed under identical conditions (foot position, pulse sequence, slice orientation, etc.) we could hypothesize that ADC relative values changes, are connected to the tissue texture differences in the lesion. This was the first report of ADC and edema evolution of the DFU under treatment. This procedure is useful for evolution studies of other pedal disorders [5].

BTR

Fourteen pediatric patients treated with Monoclonal Antibody Nimotuzumab were evaluated on MRI/MRS for >2 years [6]. "In vivo" T1, T2 , and ADC maps, in the lesion and its surrounding was determinate in order to have a assessment of the relative changes of the Spectral Density function of MR relaxation process as consequences of the molecular mobility's changes in the tumor region. This evaluation was done with and without the standard CA [6]. It was possible to define three different tumor volume related to different molecular mobilities and activities. Furthermore, spectral amplitude ratios of NAA, Cho and Cr metabolites peaks has been determinates in the lesion and healthy areas located in the contra-lateral hemisphere.

The present MRI/MRS results are in perfect agreement with the clinical evaluation and confirm once again the MR possibilities when a standardized robust protocol is used [6].

MNP. Pharmacokinetics (PK) by MR relaxation and MRI

MNP are nowadays applied for diagnosis, drug delivery and thermotherapy agents amongst others [7]. MRI is a complementary technique to follow PK of MNP. By successive MRI we studied the evolution of contrast in the liver and measured the absorption, residence time and excretion of MNP-PEG-(NH2)2 during a one month in Winstar rats model by. A new metabolic routes is propose that determine the fate of MNP. MNP solutions Relaxivities was determinate "in vitro" and "in vivo" by MR relaxation and MRI [7].

The best RF coils for the study of rats in 1,5T MRI clinical machine was selected calculating the SNR, CNR and NUI of phantom of two different RF coils: the Head and Flexible coil; being the flexible one better in in more than 25 %.

The measured intensities Ii were normalized to the background I0 and the ratio (Ii-I0)/I0 was calculated as a time function after MNP injection. In Fig. 2 is represented the dependence of the ratio (Ii-I0)/I0, proportional to MNP concentration. Two different areas of the liver was evaluated (red and blue lines) and one muscle area (pink line), taken as a control. The graphics have three regions with different slopes. The first one with is associated with the entrance of the MNP in the liver: absorption period. The second can be attributed to the liver stationary state: residence. Finally the last region is connected to the excretion. From these measurements was possible to determine the principal MNP PK parameters is reported [7].

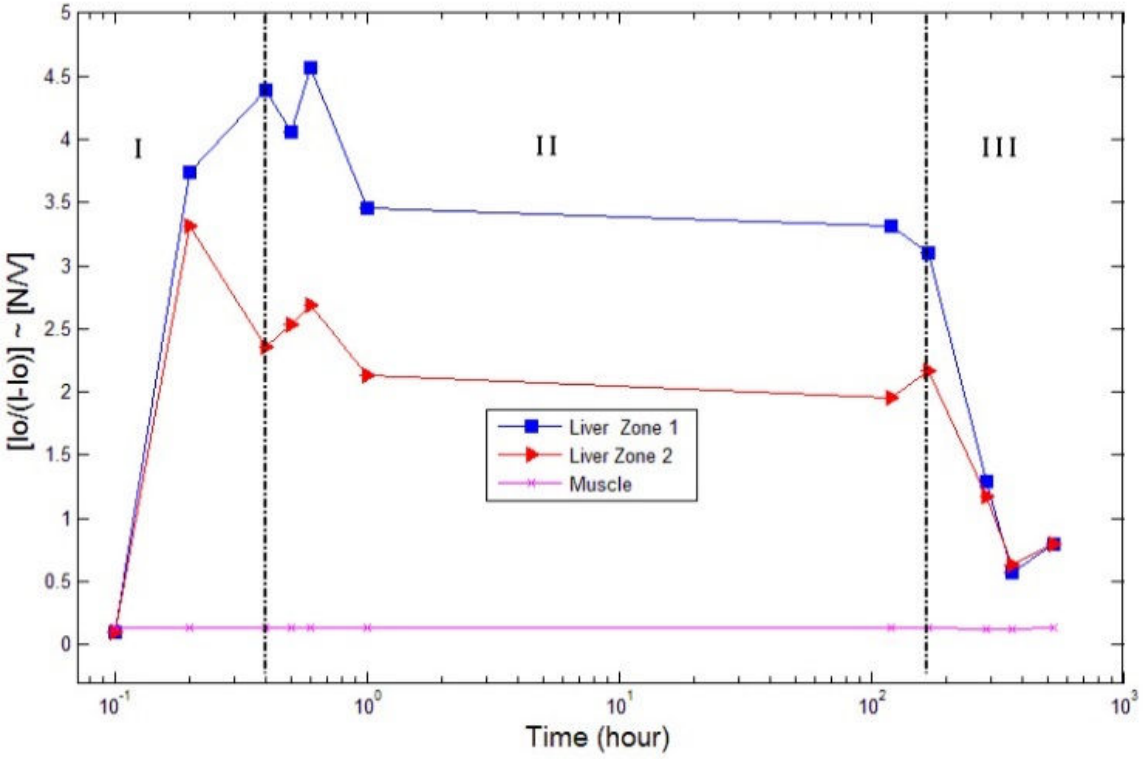

Figure 2. "In vivo" Temporal behavior of the normalize intensity T2 images after MNP injection [7]

Acknowledgements

Authors express gratitude to Lora Hospital, Santiago de Cuba and to the Medical-Surgical-Research Center, Havana. Likewise thanks patients and coworkers related to these studies.

References

1. A. Fernández, C. Cabal, J. Losada, E. Alvarez, et al, *Hemoglobin*, **29**, pp.181-187 (2005).
2. M. Lores, C. Cabal. *Appl Magn Resonan.*; **28**, 1, pp. 1 – 6 (2005).
3. M. Lores, C. Cabal, O.R Nascimento, A.M Gennaro. *Appl Magn Resonan*, **30**, pp. 121- 128. (2006).
4. A. Fernandez; C. Cabal; M. Lores; J. Losada; et al, *Hemoglobin*, **33**, pp. 206 – 213 (2009).
5. C. Cabal, E. González, J. Berlanga, D. Darias, et al, *J. of Radiology Research and Practice*, Article ID 783980, DOI: 10.5171/2014.783980 (2014).
6. E. González; C. Cabal; G. Sáurez; A. Lage; et al, *Pediatrics International*, **56**, pp. 43-46, doi: 10.1111/ped.12212 (2014).
7. A. Ruiz, Y. Hernández, C. Cabal, E. González, et al, *Nanoscale*; 5(23):11400-8. doi: 10.1039/c3nr01412f. Epub 2013 Jul 5. (2013).

Can MRI contribute to the understanding and therapy of mental diseases?

Uwe Eichoff

Bruker BioSpin GmbH (retired);
D 76287 Rheinstetten Silberstreifen Germany
E-mail: barbara.uwe@t-online.de

MRI is the most universal imaging modality and applied in clinical practice in almost any atomical locations. Furthermore in vivo spectroscopy allows the investigation of metabolic defects and molecular and cellular MRI, especially in transgenic animals contribute to the uderstanding of diseases on the molecular and cellular level.

But there are still diseases, where all imaging methods fail to deliver reproducible meaning full information, These are the mental diseases. I will try to give an overview of the possibilities of MRI in this field.

The nowadays most accepted hypothesis of the origin of such diseases is an impaired connectivity between various brain areas. Modern MRI methods allow the investigation of these connectvities. Diffusion Tensor Imaging (DTI) and MR-tractography reveals structural connectivities through neoronal fibers between brain areas. Functional Imaging in the Resting State (rs-fMRI) allows to vizualize functional connectivities. In this method the time course of rapidly repeated MRI scans is evaluated through the Blood Oxygen Level Dependent (BOLD) contrast. Even in complete rest the brain is active and oxygen is extracted from blood and fresh blood is supplied. The detection of the small signal changes needs highest sensitivity and the MRI scans must be repeated as fast as possible. Statistical evaluation and cross-correlation of the signals in all voxels show synchrony of signal level fluctuations even in remote brain areas. This allows to establish networks in the brain. The most important are the Default Mode Network (DMN), the Salience Network (SN) and the Centre Executive Network (CEN). Applications to Schizophrenia and Depression will be discussed. In Deep Brain Stimulation (DBS) the excitation, currently used for therapy of Parkinsons disease, is now introduced for therapy of Major Depressive Disorder (MDD) and can be taylored to the necessary brain location.

NMR in Archaeology: The Egyptian pyramids and the Maya Blue

Jacques Fraissard

University Pierre and Marie Curie, ESPCI-LPEM, Paris, France
E-mail: jacques.fraissard@upmc.fr

The Egyptian pyramids

The first pyramid in history was built at Saqqarah (City of Memphis) in about 2630-2605 bc. under the reign of the Pharaoh Djoser by his architect IMHOTEP. Two other important pyramids are the rhomboidal and the red from Sneferu, around 2600 b.c.. Naturally, when one thinks about Egyptian pyramids one thinks above all about those of Gizeh and specially about the pyramid of Kheops or the great pyramid (230 m ±10 cm square base and is 137 m high (initially 146 m) built more than 4500 years ago.. The time it took to build it is estimated to be 20-25 years. It contains some 2.3 millions blocks weighing on average 2.5 tons and with an average size of 1.3 m by 1.3 m by 0.7 m. But some other are much bigger (several tons).

I am not going to list in detail all that has been said or imagined in the attempt to explain how such an edifice could be constructed, assuming that it is made up of blocks cut out from nearby quarries.

Why am I speaking about these pyramids in a school devoted to NMR?

Professor Joseph Davidovits (France, USA) is an expert on cements and concretes, but also an experienced Egyptologist. This French scientist is the inventor of the geopolymerisation (1976). Geopolymers are the reciprocal of organic polymers. Instead of petrol derivatives and the carbon chain, one almost always uses a mineral matter consisting of silica and alumina; for example, silica (-Si-O-Si-O-), silico-aluminate (-Si-O-Al-O-), ferro-silico-aluminate (-Fe-O-Si-O-Al-O-) or alumino-phosphate (-Al-O-P-O-), created by a process of geopolymerisation

Davidovits proposed the idea that the blocks of the pyramids were cast in situ with a wet mix of limestone particles and an alumino-silicate-based alkali binder, which of course contradicts all the theories about quarrying.

A comparison was made of the solid-state ^{29}Si, ^{27}Al and ^{43}Ca MAS NMR spectra of the outer casing stone from Snefru's Bent Pyramid in Dahshour with two quarry limestones from the area. The NMR results suggest that the casing stones consist of limestone grains from the Tura quarry, cemented with an amorphous calcium-silicate gel formed by human intervention, by the addition of extra silica, possibly diatomaceous earth, from the Fayium area [1].

After these first NMR results many studies have been made using several modern techniques, such as elemental analysis, scanning and transmission electron microscopy, etc. All the conclusions are the same: the crucial parts of the pyramids are made of reconstituted limestone. This does not mean that all blocks were cast. Certain, probably at the lowest level, were doubtless carved.

These conclusions have been confirmed on the stele of the famine, the autobiographical funeral stele of Irtysen, the bas-relief of Rekhmire's tomb illustrating the procedure for moulding large blocks and the famous statue of the pharaoh Khafra.

The Secret of the Maya Blue

The adsorbed ^{129}Xenon detected by NMR is an excellent probe to determine microporous solid properties difficult to detect by classical physico-chemical techniques [2,3]. Indeed the very large and extremely polarisable electron cloud of xenon makes this atom particularly sensitive to its immediate environment. Small variations in the physical

interactions with the latter cause marked perturbations of the electron cloud which are transmitted directly to the xenon nucleus and greatly affect the NMR spectrum. The corresponding chemical shift depends on the dimensions and structure of the free space, on the chemical composition of the pore walls and on the ease of diffusion of the atoms in the crystallites. This technique has been mainly used to solve the secret of the Maya Blue (MB) synthesis [4].

The famous pre-Columbian Maya Blue pigment (2600 years b.c.) has been the subject of much research aimed at explaining the extreme stability of this hybrid organic/inorganic pigment present in mural paintings in Mayan Temples in the Yucatan, in many ceramic objects, in the large monolith, *Tlaltecuhtli,* representing the Aztec Earth god, etc.

In the MB pigment, the host is palygorskite clay (with tunnels having a 3.7 x 6.4 Å cross-section for the hydrated form), and the guest is the indigo molecule ($C_6H_{10}N_2O_2$). Depending on the various authors, the indigo lies in grooves at the surface of the clay fibers, inside the tunnels where it replaces the zeolitic water, or stays at the tunnel entrances. For this reason this research was focused on the mechanism of MB preparation and the final location of the indigo.

The dye was added to clay in three ways: i) the traditional Mayan technique, where palygorskite is mixed with an aqueous extract of leaves of the añil plant; ii) the synthetic method where the clay is mixed with synthetic indigo, either finely ground and heated to 180 °C or dissolved in DMSO, since it is not soluble in water. The treatment in an Accelerated Weathering Tester to simulate ageing corresponds to 10 years in real time.

NMR spectra of ^{29}Si, ^{27}Al, ^{13}C and adsorbed xenon ^{129}Xe show that, after ageing, only the sample prepared by the traditional technique contains indigo inside the palygorskite tunnels. With samples prepared from synthetic indigo, an interaction between indigo and the external surface of the clay is favoured.

Acid treatment of samples after ageing provides evidence for the chemical resistance of pigments prepared by the traditional technique as compared to the synthetic samples. This result agrees with the distribution of dye in the samples, as elucidated by NMR.

The indigo dye from añil leaves is water-insoluble; therefore, it must be deposited on the wall of the vessel and on the external surface of the clay without diffusion into the pores, according to the results on the synthetic samples. NMR spectra prove that indoxyl, a smaller precursor of indigo from añil leaves, is adsorbed on the clay surface and diffuse more easily into the pores, where it is ultimately oxidized by atmospheric oxygen, UV and hot climate, to provide indigo.

These NMR results have resolved the mystery regarding the preparation of MB and its final state.

References

1. Kenneth J.D. MacKenzie, Mark E. Smith, Alan Wong, John V. Hanna, Bernard Barry, Michel W. Barsoum. Were the casing stones of Senefru's Bent Pyramid in Dahshour cast or carved? Multinuclear NMR evidence. *Materials Letters* 65 (2011) 350–352 (and references therein)
2. J. Fraissard and T. Ito, *Zeolites*, **8**, 350-361 (1988**)** (and references therein)
3. J.Fraissard, Hyperpolarized Xenon-129 Magnetic Resonance, Royal Society of Chemistry,2015, Ed: Thomas Meersman and Eike Brunner.
4. Enrique Lima, Arial Guzmán, Marco Vera, Jose Luis Rivera, Jacques Fraissard, *J. Phys. Chem,* **116**, 4556-4563 (2013).

Spin-Lattice NMR Relaxation in Polycrystalline Solids

Leonid Grunin[1,2]

[1]*Resonance Systems GmbH, Seestrasse 28, D-73230, Kirchheim/Teck, Germany*
[2]*Volga State University of Technology, Lenin sq. 3, Yoshkar-Ola, 424000, Russia*
E-mail: mobilenmr@hotmail.com
http://www.nmr-design.com

Introduction

As far as Time-Domain NMR (TD-NMR) in recent years becomes really popular both for industrial Process Quality Control and for applied and fundamental material analysis, a particular attention is supposed to be paid to nano-scale quantum NMR effects as well as to experimental setups and processing software of proton magnetic relaxation measurements data. In previous lectures we have been discussing transverse NMR relaxation signals, their spectral editing and multiple-quantum transitions.

The presented talk is aimed to uncovering of longitudinal T_1 relaxation and spin diffusion phenomena, the influence of different material structure levels and molecular dynamics on the dissipation of the spin reservoir energy. The detailed description of pulse sequences is supposed as well.

Structure of the lecture

The lecture is organized as follows:

- Various structural organization of solid-state materials from small molecules crystals to polymers;
- Molecular and supermolecular dynamics and its description by the Correlation Function;
- Quantum Physics of modern TD-NMR: Spin Hamiltonian and Density operator;
- Semiclassical NMR Relaxation approach;
- Spin Diffusion as phenomenon and analytical tool;
- Different ways to simulation of the longitude magnetization build up
- Multi exponential T_1 NMR relaxation;
- Experimental setups and data processing;
- Conclusions: how to create a TD-NMR experiment for a particular task.

Additionally several examples of T_1 measurements, simulations and interpreting will show results for low and high molecular saccharides, polyethylene plastics and rubbery materials.

NMR in Magnetic Materials: Current Status

Vladimir. V. Matveev

Physical Faculty, Saint-Petersburg State University,
Ulianovskaya 1, Petrodvorets, Saint Petersburg, Ru-198504, Russia.

The lecture is devoted to nuclear magnetic resonance (NMR) in the magnetically ordered state also known as "NMR-in-magnetics" or "spin echo", or FNR *etc*. The technique, on one hand, is rather poorly known in comparison with the conventional NMR. On the other hand, this technique possesses a potential for very effective investigation and testing of various magnetic materials, especially in the nanocrystalline state.

In the first part of the lecture an introduction is done to basic physics of pulse NMR in magnetics together with a brief description of the method development since its appearance, more than 60 years ago. A lot of works during all these years are demonstrating that this technique is the useful addition to well known diagnostic methods and allow one to obtain unique information which cannot be reached by other methods. The technique was successfully applied to a lot of systems such as metallic cobalt and cobalt-containing materials, including films, multilayers and nanoparticles; various ferro- and ferrimagnetic compounds, Heusler alloys, intrinsically inhomogeneous perovskite-like CMR manganites *etc*.

In the second part of the lecture we review applications of the technique to some novel magnetic structures/materials during the last decade. As two examples are described a determination of the core-shell structure of bimetallic FeCo nanoparticles and an observation of ferromagnetic clusters far above Curie temperature in spin-glass manganites. We also discuss the most resent publications on assemblies of nanoparticles of different kinds, such as "molecular magnets" i.e., arrays of molecular complexes with several 3d-metal ions, Mn-doped magnetic semiconductors *etc*. As a separate item we analyze a detection of zero-field ^{13}C NMR signal in so-called "magnetic carbon" i.e., in carbon-based magnetic materials free from metallic elements.

It is interesting to note that the "NMR-in-magnetics" equipment is suitable also for investigation of acoustical absorption in superconductors. Namely, an observation of so-called "phonon echo" in superconductors was demonstrated for MgB_2 powder.

Nuclear Spin Relaxation Studies of Mobility of Molecules Adsorbed in Porous Media: Small Molecules embedded in Zeolites and related materials

Dieter Michel

Leipzig University, Faculty of Physics and Earth Sciences, Institute for Experimental Physics II, Linné-Strasse 5, 04103 Leipzig, Germany
E-mail: michel@physik.uni-leipzig.de; Phone: +49 341 97 32683

In extension to a lecture which I have presented on the St. Petersburg Winter conference in 2015, the aim of this contribution is to report about ^{1}H and ^{13}C spin-lattice relaxation studies to investigate the behavior of small molecules in zeolites and related materials with well-defined internal structure. The studies include traditional nuclear spin relaxation studies as well as more dimensional studies NOESY.

After a brief introduction into basic principles will be given and respective proton spin and carbon-13 relaxation measurements for molecules adsorbed in zeolites and related materials are treated. In the lecture we will show that the molecular mobility is both influenced by the size and shape of the internal voids and the interactions between the sorbed molecules. As a typical example for this combined action we will treat the changes in the conformation of adsorbed hydrocarbons the time of which is directly accessible in case of adsorbed simple olefins adsorbed in Y type zeolites. Furthermore changes in the chemical and physical properties of ethylene glycol (EG) adsorbed in zeolites are discussed. A clear differentiation between molecules within the zeolite cages and those ones at the outer surface is possible by means of NMR chemical shifts. Proton and deuteron relaxation studies will allow a selective study of the dynamics of different species and, in particular, to elucidate if the well-known glass-forming properties due to the molecule- molecule interactions in the pure liquid state of EG are also detectable in case of adsorbed species.

In a second part results for NMR measurements the interaction of small molecules (CO and CO_2) as well as water molecules with the host structure of various metal organic frameworks (MOF). This part refers also to a former presentation during the St. Petersburg conferences, and we will show that ^{13}C chemical shift anisotropy and isotropic chemical shift studies over a wide temperature range from 10 K to 353 K enable to derive a more detailed picture about solid and mobile fraction of mobile of the small molecules and in particular on the influence of the size of the internal voids of MOFs on the thermal mobility [1]. In this context it is very useful to investigate the local motion of the adsorbed molecules in more detail by means of ^{13}C nuclear spin-lattice relaxation for ^{13}CO and $^{13}CO_2$ molecules adsorbed in the MOFs over a wide range of temperature and at different resonance frequencies. It will be shown that the ^{13}C spin-lattice relaxation times are suitable for a more detailed analysis of local motion and the exchange dynamics. The results will also be discussed in relation to the structure of the MOFs [2]. ^{1}H MAS NMR measurements allow us to derive subtle information about the specific interaction of water molecules with the Cu metal sites in the MOFs and the intracrystalline and intercrystalline exchange dynamics [3].

The cooperation with Dr. M. Bertmer and Prof. J. Haase is greatly acknowledged.

References

1. F. Gul-E-Noor, M. Mendt, D. Michel, A. Pöppl, H. Krautscheid, J. Haase, M. Bertmer, Adsorption of Small Molecules on $Cu_3(btc)_2$ and $Cu_{3-x}Zn_x(btc)_2$ MOF as Studied by Solid-State NMR, J. Phys. Chem. C 2013, 117, 7703-7712

2. F. Gul-E-Noor, D. Michel, H. Kautscheid, J. Haase, M. Bertmer, Investigation of the Spin-Lattice Relaxation of ^{13}CO and $^{13}CO_2$ Adsorbed in the MOFs $Cu_3(btc)_2$ and $Cu_{3-x}Zn_x(btc)_2$, s. J. Phys. Chem. C 2013
3. F. Gul-E-Noor, D. Michel, H. Krautscheid, J. Haase, M. Bertmer. Time Dependent Water Uptake in $Cu_3(btc)_2$ MOF, Microporous and Mesoporous Materials 180 (2013) 8-13

«ISTINA» is Not TRUE at all

Nikolay. M. Sergeyev

Department of Chemistry Moscow State University
E-mail: sergeyev2010@yandex.ru

In the Moscow Lomonosov State University (MSU) the program ISTINA has been developed. As indicated in the preamble this program is designed to take into account and analyze the scientific activities of employees of organizations. ISTINA (using several letters from Russian writing of the name of the program *I*ntellectual *S*ystem of the *T*hematic *I*nvestigation of *NA*uchnoi information) is an information system that provides collection, systematization, storage in a bibliographic (reference) database, analysis and delivery of information characterizing the results of the activities of scientific and educational organization. The main language for the information in the database of the system is Russian. The program was developed by the Research Institute of Mechanics of MSU and put into operation in May 2012. In recent years, the ISTINA has become the main way to evaluate the work of researchers and teachers at MSU. And of course the program as any mechanical device is a purely formal procedure that hardly has anything to do with the essence of discoveries.

I was faced with the problem of evaluating of scientific staff at my re-attestation. I found two channels for the evaluation. The problem was that in English there are two types of writing my name as Sergeyev and Sergeev. Since all my articles published in foreign journals have my name as Sergeyev, but all the papers in Russian are available in English translations with my name as Sergeev. I even tried to protest, declaring in Russian editions that when preparing the translation of my papers they should write my name as Sergeyev. However, these requests were usually not taken into account. And as a whole, about 2/3 of my citation was accounted for Sergeyev and 1/3 for Sergeev.

All this is a reflection of the fact, established almost half a century ago, by one Russian remarkable scientist Vasily Vasilievich Nalimov, a mathematician, scientometrist, the author of many interesting books. He was also an employee of the Moscow State University. Back in the 60s of the last century he (see [1]) spoke about two information flows - in English and Russian languages. And these two flows do not agree. They exist independently. It must be admitted that, of course, the information flow in Russian is weaker.

There are of course the complexities associated with the low availability of journals in Russian for the world scientific community. We should admit that English has become the main language of science. And if you want your work to be read by others you need to publish in English. Many of our scientific journals are translated into English. But our journals have a rather long time between sending of the article to editor and publishing the paper. This is usually a year or more. And the English translation is published in general with a total delay of two or more years. The only reasonable way out of this situation is completely use English for publications in Russian scientific journals. There is nothing surprising or challenging in this approach. In medicine, in pharmacology, everybody till now uses Latin language. As you know, many outstanding Russian scientists (Pirogov, Lomonosov) wrote their works in Latin.

The priority of English is gradually recognized in other countries. For example the European Union created a number of new European journals (for example, the journal PCCP - Physical Chemistry Chemical Physics). Some countries (Italy, Sweden, and others) almost completely switched to scientific literature in English. Very important for understanding the current situation, a country such as China also gradually recognizes the priority of the English language. Almost half of the scientific journals in China are published in English.

But in general one must seriously fear another danger. This is bureaucratization and formalism. The scientific leader who seriously does not know his employees, who can not evaluate them without any ISTINA is not the leader at all [2].

About fifty years ago the founder of the sciencemetrics V.V. Nalimov warned [1]. He stated "In the literature, warnings against the vulgar use of the citation index for assessing the effectiveness of individual scientists have been repeatedly voiced. Here again we want to emphasize that quantitative assessments should always be subjected to additional semantic analysis".

Eugene Garfield [3] also writes that it would be completely ridiculous to believe that the most frequently cited scientists are worthy of the Nobel Prize. He stated "It will be catastrophically bad if planning departments or human resources departmnts of our universities will begin to make vulgar assessments on the level of citation".

References

1. V. V. Nalimov and Z. M. Mulchenko, Naukometria (in Russian), Nauka, 1969.
2. N.M. Sergeyev in Russ, Chem. Journ., 1999, N6 pp. 34-40
3. E. Garfield, The ethics of Scientific Publication, Current Contents, 1978, N 40

Recent results from the Laboratory of biomolecular NMR @ SPbGU: from mechanism of anti-cancer peptides to characterization of flexible tails in amyloid fibrils

Ivan S. Podkorytov[1], Irina I. Tyuryaeva[1,2*], Olga G. Lyublinskaya[2], Mikhail V. Belousov[3], Stanislav A. Bondarev[3], Kerstin Kämpf[4], Galina A. Zhouravleva[3], Sergei V. Dvinskikh[4], Nikolai R. Skrynnikov[1,5]*

[1]Laboratory of Biomolecular NMR, St. Petersburg State University, St. Petersburg 199034, Russia.
[2]Institute of Cytology, Russian Academy of Sciences, St. Petersburg 194064, Russia.
[3]Department of Genetics & Biotechnology, St. Petersburg State University, St. Petersburg 199034, Russia.
[4]Department of Chemistry, Royal Institute of Technology KTH, Stockholm SE 10044, Sweden.
[5]Department of Chemistry, Purdue University, West Lafayette, Indiana 47907, USA.
[*]These authors contributed equally to the presented work
E-mail: nikolai@purdue.edu

Antitumor GO peptides have been designed as dimerization inhibitors of prominent oncoprotein mucin 1. Here we demonstrate that activity of GO peptides is independent of the level of cellular expression of mucin 1. Furthermore, these peptides prove to be broadly cytotoxic. To explore molecular mechanism of their cytotoxicity, we have designed and tested a number of new peptide sequences containing the key CxC or CxxC motifs. Of note, these sequences bear no similarity to mucin 1 except that they also contain a pair of proximal cysteines. Several of the new peptides turned out to be significantly more potent than their GO prototypes. The results suggest that cytotoxicity of these peptides stems from their (moderate) activity as disulfide oxidoreductases. It is expected that such peptides, which we have termed DO peptides, are involved in disulfide-dithiol exchange reaction, resulting in formation of adventitious disulfide bridges in cell proteins. In turn, this leads to a partial loss of protein function and onset of apoptosis. At the same time, when applied at low doses, GO / DO peptides can apparently stimulate growth receptors and facilitate cell proliferation.

In the second part of my talk, I will speak about solution- and solid-state NMR investigation of translation termination factor Sup35p from *Saccharomyces cerevisiae*. In particular, the amyloidogenic portion of this protein, Sup35NM, has been a focus of our interest. One of the questions that remain unresolved is the status of M domain within Sup35NM: is it an integral part of the fairly rigid fibril architecture, or does it remain partially disordered? Historically, two types of experiments have been used to target flexible elements of protein fibrils: (*i*) solid-state HSQC experiments under MAS conditions and (*ii*) solution-state HSQC experiments on static samples. In both cases the underlying assumption has been that all protein material in the sample is sequestered in the fibrils. This assumption is, generally speaking, incorrect. Protein fibrils always exist in a state of dynamic equilibrium with monomeric (oligomeric) species. Our diffusion experiments on a solid-state sample of Sup35NM demonstrated that ca. 20% of the signal originates from monomers, characterized by high translational mobility, whereas the remaining 80% belongs to the flexible fibril tails. Furthermore, we have prepared a dilute solution sample of Sup35NM, where ca. 85% of the signal was associated with monomers and the remaining 15% represented the flexible fibril tails. A comprehensive series of diffusion and relaxation measurements produced a self-consistent picture of dynamic equilibrium involving monomers and fibrils. The addition of the diffusion filter to the standard HSQC sequence has allowed us to isolate the signals from the flexible parts of the fibril. Finally, the use of Sup35NM sample selectively labeled with ^{15}N in

valine positions made it possible to delineate the boundary between the flexible and the rigid portions of the polypeptide chain comprising the fibrils

Acknowledgments

This work was supported by the RSF grant 15-14-20038.

TD NMR detection of energetic and illicit materials

Bulat Rameev[1,2], Ayşe Maraşlı[1], Galina Kupriyanova[1,3], Georgy Mozzhukhin[1,3]

[1]Physics Department, Gebze Technical University, 41400 Gebze/Kocaeli, Turkey
[2]Laboratory of Radiation Physics, Kazan Physical-Technical Institute, 420029 Kazan, Russian Federation
[3]Instutute of Physics-Mathematical Sciences, Immanuel Kant Baltic Federal University, Kaliningrad, 236041 Russian Federation
E-mail:rameev@gyte.edu.tr
http://www.gtu.edu.tr

Introduction

One of the important problem of public security is the detection of explosive and illicit substances [1-4]. Recently, so-called improvised explosive devices (IEDs), made from commercially available chemical materials, became an issue of a growing importance. In the aviation and public transportation, a problem of non-invasive detection of the explosives in the baggage, suits, cars, and other containers has a profound significance to make the modern world more secure.

Minimum false alarm rate is provided by the techniques, which are directed to detect not the metal, or plastic enclose or fuses but the explosive itself. In other words, they should provide a possibility of the chemical-specific identification of explosive. Among such techniques, low-field nuclear magnetic resonance (NMR) is considered as very promising bulk (liquids) explosive detection method, based on the chemical identification of content. First successful applications of NMR method for detection of liquid explosives was demonstrated as early as in 90th years of XX century [5-7]. Most of researchers consider so-called time-domain NMR (TD-NMR) as a prospective technique for such applications. In the TD-NMR, the spectroscopic information (i.e. resonance frequencies) of the scanned material is neglected. It is NMR in moderate or low magnetic field ($\leq$1T) which is based on measurements of spin-lattice and spin-spin relaxation parameters (T_1 and T_2) of the proton nuclei. Specialized NMR analyzers of the liquid content of bottles have been demonstrated by Quantum Magnetics [5-7], *Bruker Inc.* [8] and *T_2 Biosystems* [9, 10]. It should be noted that in principle the time-domain NMR can be done in as low magnetic field as Earth's field (see, e.g. [11]). In very recent works, an application of this technique for the liquid identification in plastic bottles and metal cans have been demonstrated (see, [12] and [13], respectively).

In the TD NMR (or NMR relaxometry) measurements are usually made with use of low magnetic fields (and, correspondingly, low frequencies in the range of 1-60 MHz) with a magnetic field system based on the permanent magnet technology. Despite of low homogeneity of the DC magnetic field system of TD NMR devices, there are a few important advantages of this technique with respect its possible applications. The most important one is its relatively low price and maintenance expenses. However, as was already established in previous works [9, 15], the NMR measurements that provide only the relaxation parameters cannot make reliable discrimination between a ***large number*** of various substances, as well as in the case of multi-component liquid mixtures. It has been shown previously that the TD NMR measurements of diffusion (D) parameter in addition to the usually measured relaxation times (T_1, T_2) is a good method to improve discrimination between hydrogen-containing explosive/illicit materials and benign liquids [14]. In this work, another approach, based on the detection of ^{14}N NMR signal as an additional parameter to discriminate between various liquids, is studied. The feasibility of ^{14}N NMR detection has been checked. ^{14}N NMR signal of various nitrogen-based substances have been successfully detected and the relaxation parameters of the ^{14}N signal have been obtained.

Low field TD NMR of ^{14}N nuclear in illicit liquids.

It is well known that most of ***solid*** energetic and explosives materials includes the nitrogen nuclei of ^{14}N. However, the situation is similar in the case of ***liquids***: a number of energetic and explosive liquid substances contain nitrogen in their structure. For that reason, the detection of ^{14}N NMR signal as secondary parameter for more reliable detection of dangerous substances have been proposed by P. Prado et al [10]. There is, however, an issue in the detection of ^{14}N NMR, because the gyromagnetic ratio of ^{14}N nuclei is rather small in comparison to ^{1}H signal. Therefore, nitrogen NMR signal has a very small Signal to Noise Ratio (SNR). A special setup to check feasibility of ^{14}N NMR detection has been assembled. In the setup, a homemade permanent magnet system with the magnetic field of 0.475 T and a homemade RF probe with resonance frequency of 1.775 MHz have been used. Tecmag Apollo NMR console and 500 W Tomco power amplifier have been used in the NMR experiments.

Time domain ^{14}N NMR signal has been successfully detected in all nitrogen liquids, included in the test set. The results of ^{14}N NMR relaxation measurements of the nitrogen-containing liquids are summarized in Table 1, given below.

Table1. The results of the measurements of NMR N-14 (1 ml, room temperature, 1.777 MHz)

Name		T_2, ms	T_1, ms
Nitromethan		9.308±0.218	11.17±1.7
Nitroethan		5.271±0.114	5.87±0.39
Nitrobenzene		0.750±0.117	0.750±0.117
Nitric Acid (HNO_3)		10.06±0.48	11.12±0.7
Ammonium nitrate	1	29.442±1.21	44.36±3.42
	2	78.62±16.51	1325±220

Very interesting result (Fig.1) has been received in the NMR measurements of water solution of ammonium nitrate (AN). The NMR of AN is characterized by rather narrow ^{14}N lines due to small quadrupolar splitting of nitrogen in both coordinations (nitrate anion and ammonium cation), which is motionally averaged in liquid solutions. We have observed that frequency (Fourier transform) spectrum of this compound contain two lines in accordance with typical chemical shift values of nitrogen in above-mentioned coordinations.

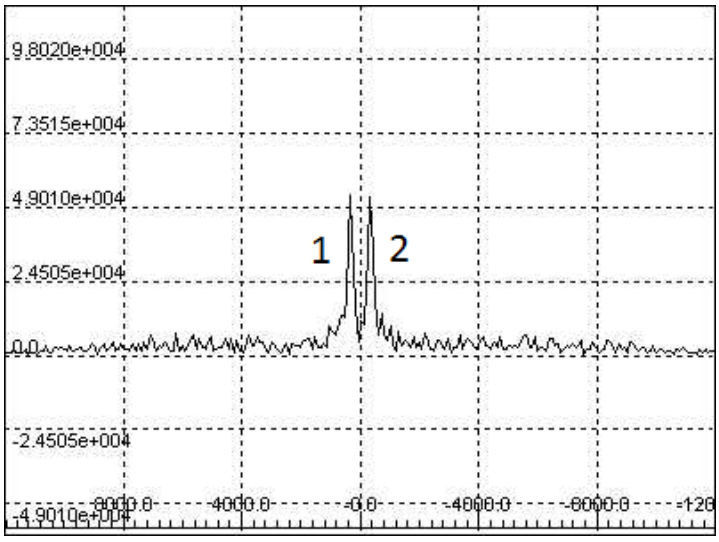

Figure 1. ^{14}N NMR spectrum of the ammonium nitrate solution.
The frequency shift between line 1 and line 2 is 683±97 Hz (385 ppm)

The relaxation parameters (excepting line No.2 of AN) have been calculated using *Tools capture* of *NTNMR* software. The parameters for the line 2 of AN have been calculated using *Origin* programme to exclude an influence of the magnet temperature shift during a long experiment time.

Conclusion

A novel approach, based on the detection of ^{14}N NMR signal as an additional parameter to discriminate between various liquids, has been studied. The feasibility of ^{14}N NMR detection of various energetic and illicit liquids has been demonstrated. ^{14}N NMR signals of various nitrogen-based substances have been successfully detected and the relaxation parameters of the ^{14}N signals have been obtained. It has been also shown that due to large chemical shift values of ^{14}N NMR signal, it is possible to observe splitting of FT NMR spectra of nitrogen-based compounds even by low field NMR device (in our case, at 0.475 T that corresponds to 1.775 MHz frequency of ^{14}N NMR).

Acknowledgements

G.K. and B.R. acknowledge support of TÜBİTAK for G.K.'s visit under 2221-Fellowship Programme for Visiting Scientists and Scientists on Sabbatical Leave. The work was supported by NATO Science for Peace and Security Programme, NATO SPS project No. 985005 (G5005). Authors also acknowledge a partial support by East Marmara Development Agency (MARKA, project No. TR42/16/ÜRETİM/0013) and by Research Fund of Gebze Technical University (grants Nos. BAP 2015-A-19 and BAP 2014-A-13). A. Maraşlı also acknowledge the support of Ministry of Science, Industry and Technology under Teknogirişim Program for Ideamag R&D Ltd. Co.

References

1. J.B. Miller, G.A. Barrall, “Explosives Detection with Nuclear Quadrupole Resonance”, American scientist, vol. 93, no. 1, 50, Jan.-Feb. 2005. DOI: 10.1511/2005.1.50
2. J.Fraissard and O. Lapina, Eds., Explosives Detection using Magnetic and Nuclear Resonance Techniques, NATO Science for Peace and Security Series B: Physics and Biophysics. Dordrecht, The Netherlands: Springer, 2009.
3. B.Z.Rameev, G.V.Mozzhukhin, and B. Aktas, Magnetic Resonance Detection of Explosives and Illicit Materials, Appl. Magn. Reson., vol. 43, no. 4, pp. 463-467, Dec. 2012. DOI: 10.1007/s00723-012-0423-9
4. T. Apih, B. Rameev, G. Mozzhukhin, and J. Barras, Eds., Explosives Detection using Magnetic and Nuclear Resonance Techniques, NATO Science for Peace and Security Series B: Physics and Biophysics, Dordrecht, The Netherlands: Springer, 2014.
5. L.J. Burnett, "Liquid Explosives Detection", Proceedings of the SPIE, vol. 2092, pp.208-217, Mar. 1994. DOI:10.1117/12.171241
6. S. Kumar, W.C. McMichael, Y.-W. Kim, A.G. Sheldon, E.E. Magnuson, L. Ficke, T.K.-L. Chhoa, C.R. Moeller, G.A. Barrall, L.J. Burnett, P.V. Czipott, J.S. Pence, D.C. Skvoretz, “Screening sealed bottles for liquid explosives”, Proceedings of the SPIE, vol. 2934, pp. 126-137, Jan.1997. DOI: 10.1117/12.265406
7. S. Kumar, “Liquid-content verification for explosives, other hazards, and contrabands by magnetic resonance”, Appl. Magn. Reson., vol. 25, 585-597, Sep. 2004. DOI: 10.1007/BF03166550.
8. J. Mauler, E. Danieli, F. Casanova, and B. Blumich, “Identification of liquids encountered in carr-on-luggage by mobile NMR”, in Explosives Detection using Magnetic and Nuclear Resonance Techniques, NATO Science for Peace and Security

Series B: Physics and Biophysics, J.Fraissard, O. Lapina, Eds., Dordrecht, The Netherlands: Springer, 2009, pp. 193-203.

9. S. Kumar, P.J. Prado, "Detection of concealed liquid explosives and illicit drugs in unopened bottles", in Explosives Detection using Magnetic and Nuclear Resonance Techniques, NATO Science for Peace and Security Series B: Physics and Biophysics, J.Fraissard, O. Lapina, Eds., Springer, Eds., Dordrecht, The Netherlands: Springer, 2009, pp.73-79.
10. P.J. Prado, I. Mastikhin, and M.T. Karlsson, Rapid Method to Screen Unopened Bottles to Detect Concealed Drugs , Appl. Magn. Reson., vol. 43, pp.531-540, Dec.2012, DOI: 10.1007/s00723-012-0325-x
11. Mohoric A., Stepišnik J., Progress in Nuclear Magnetic Resonance Spectroscopy, vol. 54, no. 3-4, pp. 166-182, Apr. 2009. DOI: 10.1016/j.pnmrs.2008.07.002
12. H. Sato-Akaba, H. Itozaki, Development of the Earth's Field NMR Spectrometer for Liquid Screening, Appl. Magn. Reson., vol. 43, no.4, pp.579-589, Dec. 2012, DOI: 10.1007/s00723-012-0346-5
13. E. Balcı, B. Rameev , H Acar, G.V. Mozzhukhin, B. Aktaş, B. Çolak, P.A. Kupriyanov, A.V. Ievlev, Y.S. Chernyshev, V.I. Chizhik. Development of Earth's Field Nuclear Magnetic Resonance (EFNMR) Technique for Applications in Security Scanning Devices. Appl. Magn. Reson., vol. 47, no. 1, pp. 87-99, Jan.2016. DOI: 10.1007/s00723-015-0730-z
14. B. Rameev, G.V. Mozzhukhin, R.Khusnutdinov, B.Aktas, A. Konov, N.A. Krylatyh, Ya.V. Fattakhov, D.D. Gabidullin, K.M. Salikhov, SPIE Proceeding. DSS12 - SPIE Defense, Security, and Sensing, 8357 - 33 V. 1, 83570Z(2012).

Magnetic Resonance Study of Atomic Hydrogen Isotopes Stabilized in Solid Hydrogen Matrices below 1K

S. Vasiliev[1], J. Ahokas[1], S. Sheludiakov[1], J. Järvinen[1], O. Vainio[1], L. Lehtonen[1], D. Zvezdov[1,2], D. M. Lee[3] and V. V. Khmelenko[3]

[1]Department of Physics and Astronomy University of Turku, 20500 Turku, Finland,
[2]Institute of Physics, Kazan Federal University, 18 Kremlyovskaya St., Kazan 42008, Russia,
[3]Department of Physics and Astronomy, Texas A&M University,
College Station, TX, 77843, USA
E-mail: servas@utu.fi
http://hturku.utu.fi

Solid hydrogen isotopes represent a special class of so-called quantum crystals, which are characterized by weak intermolecular interactions and large, zero-point energy. Hydrogen and **deuterium** atoms stabilized in such solid matrices become delocalized in the lattice sites and diffuse in a series of exchange tunneling reactions: $H+H_2=H_2+H$ and $D+D_2=D_2+D$. Similar exchange reactions $D+H_2=HD+H$ and $D+HD=D_2+H$, involving both hydrogen isotopes may take place in D_2:H_2 (HD) mixtures and result in a spectacular conversion of atomic deuterium into hydrogen atoms, while T-to-H conversion can be expected in T_2-H_2 mixtures. Impurity atoms are not stable and recombine into molecules if encounter each other in neighboring lattice sites.

In our experiments thin films of molecular hydrogen (50-500 nm) were deposited on a quartz crystal microbalance (QM) below 1K. The QM electrode works also as a flat mirror of 130 GHz ESR spectrometer enabling direct studies of the samples. High concentrations of atomic impurities in the range 10^{19} -10^{20} cm-3 were created by electron impact dissociation of the molecules. The electrons resulted from an rf discharge running close to the sample [1] or from the β-decay of tritium which was mixed to the sample gas before deposition. In this work we report the highest densities reached in the T_2 samples, approaching $2*10^{20}$ cm^{-3} for T in T_2 and $1*10^{20}$ cm^{-3} for H in T_2:H_2 mixture [2].

For the first time we studied the isotopic exchange reactions in a temperature range 0.1-1.5K which appear to be the lowest temperature where chemical reactions have been observed in a solid phase so far. We measured the reaction rate of $D+HD=D_2+H$ in HD and D_2:0.23% HD matrices and found, that the rate of the reaction is nearly independent of temperature within this range. Our results suggest that atoms remain mobile in the temperature range, even though both H and D recombination is strongly inhibited at temperatures below 1K.

We observed that Dynamic Nuclear Polarization (DNP) of H atoms in D_2:H_2 (HD) mixtures can be created by both the Overhauser and Solid effects efficiently. In addition to that, nuclear spins of hydrogen atoms can be polarized by saturating the center of the ESR spectrum resembling Overhauser effect in metals, the effect which is absent for H atoms in pure H_2 samples [3]. We suggested that a large number of H radical pairs formed during the course of the isotopic exchange reactions, coupled by strong exchange interaction. The radical pairs may possess an allowed transition at the center of the ESR spectrum while D atoms help to create a strong enough oscillating field at the position of ESR pumping.

References

1. S. Sheludiakov et al., Rev. Sci. Instrum, **85**, 053902 (2014).
2. S. Sheludiakov et al., Phys.Chem.Chem.Phys **19**, 2384 (2017).
3. S. Sheludiakov et al., Phys.Rev.Lett.,**113**, 265303 (2014).

NMR investigation of ionic and molecular transport mechanism in ion-exchange nanochannels

Vitaly I. Volkov[1,2]

[1]*Institute of Problems of Chemical Physics RAS,*
142432, Chernogolovka, Acad. N.N.Semenov av., 1, Russia
[2]*Science Center in Chernogolovka RAS,*
142432, Chernogolovka, Lesnaya str., Russia 9
E-mail: vitwolf@mail.ru

Introduction

Electrochemical energy sources like cation exchange membrane fuel cells are widely applied. The most important part of these systems is the high conductivity ion exchange membrane. The cation conductivity is controlled by ionic channel nanostructure, cation hydration processes and hydrated cation mobilities. The ionic transport nature revelation in polymeric ion exchanger is very important. Heteronuclear NMR spectroscopy and, especially, pulsed field gradient NMR technique, are successfully used for ionic mobility and solvatation investigations in ion-exchange membranes during last ten years. But, in spite of it, the above mentioned items are not completely understood.

The transport channels forming, ion-polymeric matrix interaction mechanism, ionic and molecular self-diffusion NMR investigations are summarized. The results were obtained by the Karpov Institute of Physical Chemistry, Institute of Problems of Chemical Physics RAS, Institute of General and Inorganic Chemistry RAS and USA, Japan and Europe scientific teams.

The next polyelectrolytes are discussed: Ion exchange membranes with differ polymeric matrix structures (perfluorinated membranes, styrene divinyl benzene, aromatic sulfocontaining polyamide and composite membranes).

The translational mobilities measured by pulsed field gradient NMR are compared with the ion conductivity impedance spectroscopy data. On the basis of polymer structure, hydration particularities and ionic and molecular mobility interconnections the ionic transport percolation mechanisms are proposed [1].

Ionic Channel Nanostructure

The Nafion perfluorinated sulfocation exchange membrane structure is shown in Fig. 1. Sulfonic acid groups counter ions and water molecules form nanochannels for ionic transport.

Cation Hydration

The hydration numbers of monovalent and bivalent cations were measured on the basis of ^1H chemical shift dependences on water content (see, for example, Fig. 2) [1].

The calculated hydration numbers h_0 (the average number of water molecules in the hydration shell of an cation) are as follows: for H^+, Li^+, Na^+, Cs^+ ionic forms of perfluorinated sulfonated MF-4SC and carboxylic F-4CF membranes are 2.3±0.3, 3.8±0.3, 3.5±0.3, 1.7±0.3 and 1.3±0.3, 2.8±0.3, 2±0.3, 1±0.3, correspondingly [1, 2]. It was mentioned that at low water content the hydration water are high mobile at temperature below 0^oC. This phenomenon is discussed in detail in paper [3].

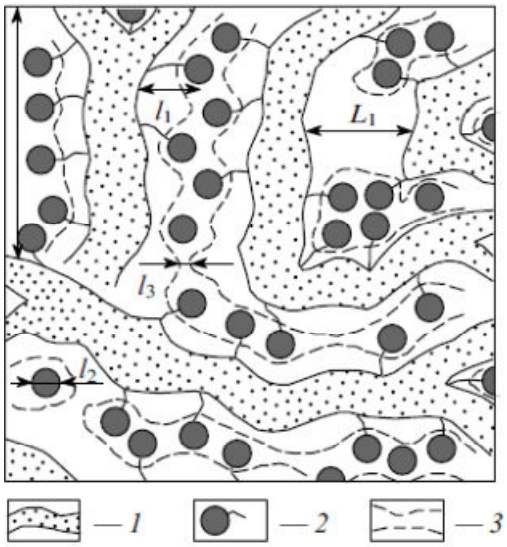

Figure 1. Structure of the amorphous part of a perfluorated sulfonate cation-exchange membrane [1]. (1) Polymer backbone; (2) hydrated counter-ions and functional groups at a low moisture content; (3) transport channels for ions and water molecules at a high moisture content; L_1=4 nm according to low-angle X-ray scattering data; L_2=10 nm according to Mössbauer spectroscopy; l_1=l_2=1 nm according to ENDOR and relaxation NMR data; l_3=1.5 nm according to standard porosimetry and ENDOR methods

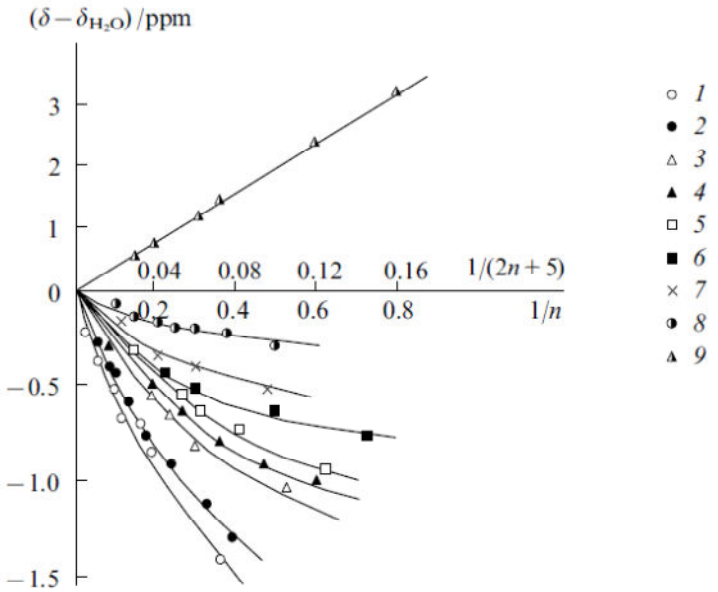

Figure 2. Dependences of ^1H chemical shifts of water on the water content in perfluornated sulfocation exchange MF-4SC membrane (n is the amount of water molecules per cation). Ionic forms are:
(1) Li+, (2) Na+, (3) K+, (4) Rb+, (5) Cs+, (6) Ba2+, (7) Ca2+, (8) Mg2+, (9) H+

Self-diffusion and Ionic Conductivity

Self diffusion coefficients of water molecules and LI^+ cations D_s were measured by pulsed field gradient technique. The ionic conductivities σ_{calc} were calculated on the basis of Nernst-Einstein equation. As it is shown in Fig.3, the dependencies D_s (n) and σ_{calc} (n) on water content are similar. It means that charge transfer is controlled by ionic and water self

diffusion. The σ_{calc} values calculated from water self diffusion data are more compare with experimental conductivity values σ_{exp}. For Li^+ cation σ_{calc} ($6{,}5\cdot10^{-3}$ S/cm) and σ_{exp}, ($6{,}2\cdot10^{-3}$ S/cm) are in an excellent agreement (Table 1). Self diffusion, by-turn, is determined by local motions, which parameters have been calculated from NMR relaxation data (Table 2).

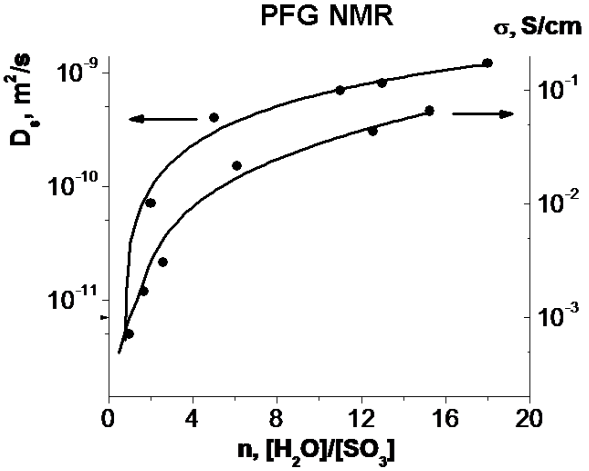

$$\sigma = n(ez)^2 \frac{D}{k_B T}$$

Figure 3

Table 1

Ionic form	MF-4SC			F-4CF	
	$\sigma_{exp.}$, S/cm	$\sigma_{calc.}$, S/cm		$\sigma_{exp.}$, S/cm	σ_{calc}, S/cm
H^+	$2{,}8\cdot10^{-2}$	$4.3\cdot10^{-2}$		$1{,}5\cdot10^{-7}$	$1.5\cdot10^{-6}$
Li^+	$6{,}2\cdot10^{-3}$	$1.1\cdot10^{-2}$	*$6{,}5\cdot10^{-3}$*	$1{,}01\cdot10^{-3}$	$4.3\cdot10^{-3}$
Na^+	$6{,}1\cdot10^{-3}$	$1.2\cdot10^{-2}$		$1{,}2\cdot10^{-3}$	$4.6\cdot10^{-3}$
Cs^+	$3{,}4\cdot10^{-4}$	$8.3\cdot10^{-4}$		$3{,}7\cdot10^{-4}$	$7.2\cdot10^{-4}$

Table 2

n	D^{calc}_{H2O}, m^2/s	D^{exp}_{H2O}, m^2/s	D^{calc}_{Li+}, m^2/s	D^{exp}_{Li+}, m^2/s
4	$5\cdot10^{-12}$	$4\cdot10^{-12}$	$2\cdot10^{-12}$	10^{-12}
20	$3\cdot10^{-10}$	$2\cdot10^{-10}$	$4\cdot10^{-11}$	$3\cdot10^{-11}$

Where D^{calc} is the self diffusion coefficient, calculated from Einstein equation $D^{calc} = r^2/ 6\tau_d$, τ_d is residence time of ions on the sulfonate group, obtained from ^1H and ^7Li NMR relaxation data, r is the particle jump distance. D^{exp} – self diffusion coefficient measured by Pulse Field Gradient ^1H and ^7Li NMR technique.

The mechanism of ionic and water transfer in membrane nanochannels was quantitatively explained on the basis of percolation theory [4].

References

1. V. I. Volkov, A. A. Marinin - Russian Chemical Reviews 82 (3) 248 - 272 (2013)
2. V. I. Volkov, A. A. Pavlov, E. A. Sanginov - Solid State Ionics 188, 124 (2010)
3. V. I. Volkov, S. L. Vasilyak, I-W Park, H J Kim, H Ju, E. V. Volkov, S H Choh - Appl. Magn. Res. 25, 43 (2003)
4. S. F. Timashev Fizikokhimiya Membrannykh Protsessov (Physical Chemistry of Membrane Processes) (Moscow: Khimiya, 1988)

Basic MRI physics, methods and applications

Mikhail Zubkov

International Research Centre for Nanophotonics and Metamaterials, Metamaterials laboratory, ITMO University, Saint-Petersburg, Russia
E-mail: m.zubkov@metalab.ifmo.ru
http://metalab.ifmo.ru

Introduction

Magnetic resonance imaging (MRI) is an essential application of the nuclear magnetic resonance (NMR) methodology, which has established its own set of nomenclature, its own scope of applications and its own diversity in aims, goals and methods. The underlying principles of MRI are nevertheless NMR-based and all the spectroscopy concepts still apply when the outcome of an experiment is an image rather than a spectrum. Here the basic methodology, including the principles of MRI, the ideas behind and the implementation of the basic MRI techniques and methods and their corresponding applications will be covered, while trying to establish a connection between the spectroscopic and imaging nomenclature.

Basics of MRI

The foundations of MRI are deeply rooted in NMR spectroscopy, thus it is only natural to start with something they are to have in common (assuming the basic description of a pulsed NMR experiment is well-known) – the equations describing the behavior of the bulk nuclear magnetization, i.e., the Bloch equations for free transverse and longitudinal magnetization in a rotating reference frame:

$$\frac{\partial M_z}{\partial t} = 0$$

$$\frac{\partial M_T}{\partial t} = 0$$

Here M_z is the magnitude of the longitudinal magnetization and M_T is the magnitude of the transverse magnetization. A critical point in the transition from the NMR spectroscopy to MR imaging experiment is the introduction of a temporary linear spatial magnetic field variation (i.e., the magnetic field gradient pulse, often referred to simply as gradient) and consequently the addition of a gradient term to the Bloch equations [1]. The behavior of magnetization during in presence of the field gradient can be described as

$$\frac{\partial M_z}{\partial t} = 0$$

$$\frac{\partial M_T}{\partial t} = -i\gamma(\boldsymbol{G}\cdot\boldsymbol{r})M_T$$

where γ is the gyromagnetic ratio of the observed nuclei, $\boldsymbol{r}$ is the spatial position and $\mathbf{G}$ is the magnetic field gradient magnitude. The solution of this equation can be shown to provide a means to obtain a spatial distribution of the NMR signal by two crucial MRI techniques, namely phase and frequency encoding. Additionally a technique called slice selection is often used for further localization of the spatial position NMR signal is acquired from.

Pulse sequences in MRI

While according to Bloch equations acquisition of an image requires only the application of a gradient pulse, in practice such application can be performed in a variety of ways depending on the desired outcome [2]. Commonly used spin-echo (SE), gradient echo (GRE), echo-planar (EPI), fast spin echo (FSE, TSE or RARE) and other sequences use

different strategies of excitation, refocusing, encoding and acquisition, making any categorization of the sequences problematic.

Here a notion of *k*-space [3] becomes useful as a tool to separate image acquisition from further processing and analysis. After *k*-space is introduced the aim of a pulse sequence is to provide correct magnetization handling and detection in order to obtain sufficient data for image formation (i.e., fill the *k*-space). After the acquisition of *k*-space is complete, a 2D Fourier transform is applied to the *k*-space data and an image is formed.

Contrast in MRI

It is not only the gradient interaction terms that can be added to Bloch equations. Relaxation and motion also add corresponding terms to Bloch equations, thus weighting the expression for the spatial distribution of the NMR signal.

Relaxation contrast

Incorporating the relaxation effects in the Bloch equations provides [4]

$$\frac{\partial M_z}{\partial t} = \frac{M_0 - M_z}{T_1}$$

$$\frac{\partial M_T}{\partial t} = -\frac{M_T}{T_2} - i\gamma(\boldsymbol{G}\cdot\boldsymbol{r})M_T$$

where T_1 and T_2 are the longitudinal and transverse relaxation times respectively, and M_0 is the equilibrium bulk magnetization. Note, that here M_T, M_z, T_1, T_2 and M_0 are usually considered to be spatial functions rather than constants. The solution for of the Bloch equations with relaxation terms for two spatial locations (or two pixels in an image as long as the acquired data is always digitized) can be differently weighted by corresponding contributions of the relaxation terms depending on the local value of T_1 and T_2. Contrast in an image is then defined by the difference of the NMR signal magnitudes in the two pixels [5].

The amount of weighting provided by the relaxation terms is determined by the pulse sequence timing and is usually the same for the whole image. A contribution of the relaxation terms can then be either minimized or maximized, leading to either longitudinal, transverse relaxation or none of the two providing most of the weighting. Weighting is then attributed to the whole image (and logically, to the pulse sequence timing) and depending on the prevalent factor can be T_1, T_2 or proton density weighting respectively (Fig. 1).

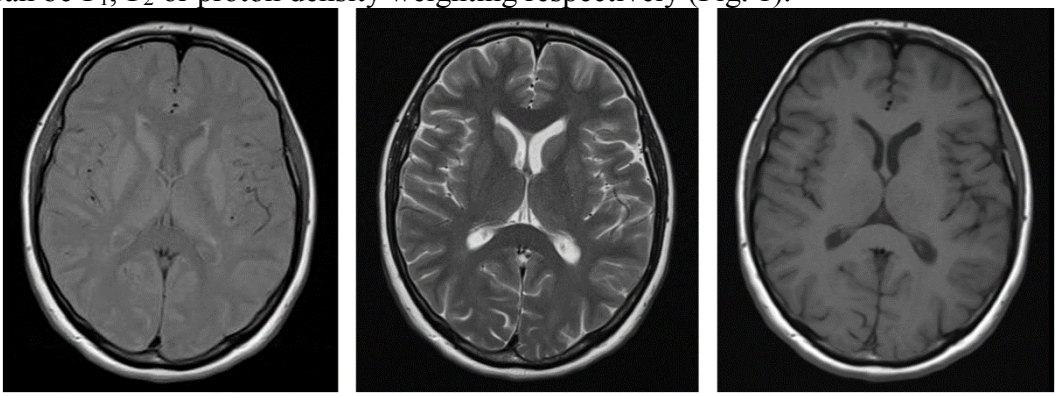

Figure 1. Images of one slice of a human brain obtained in a magnetic field of 1.5T (63 MHz ^{1}H resonance frequency) with SE pulse sequence. From left to right: proton density weighted image, T_2 weighted image and T_1 weighted image

Other types of contrast

Relaxation terms are not the only ones that can be included into Bloch equations. Macroscopic and microscopic motion can be incorporated into the magnetization behavior description as well. Microscopic motion can be accounted for with self-diffusion term [6]

$$\frac{\partial M_z}{\partial t} = \nabla \mathbf{D} \nabla M_z$$

$$\frac{\partial M_T}{\partial t} = -i\gamma(\boldsymbol{G} \cdot \boldsymbol{r}) M_T + \nabla \mathbf{D} \nabla M_T$$

where **D** is the self-diffusion tensor and ∇ is the gradient operator. Macroscopic motion on the other hand can be incorporated into Bloch equations by performing Taylor expansion of $\boldsymbol{r}(t)$ function (previously, **r** was considered constant) and truncating the series at first order terms

$$\frac{\partial M_z}{\partial t} = 0$$

$$\frac{\partial M_T}{\partial t} = -i\gamma(\boldsymbol{G} \cdot \boldsymbol{r_0}) M_T - i\gamma t \left(\boldsymbol{G} \cdot \frac{\boldsymbol{\partial r}}{\boldsymbol{\partial t}} \right) M_T$$

where $\boldsymbol{r_0}$ is the initial position of the unit magnetization. These two systems of equations, when solved, provide means to obtain either images where signal amplitude depends on the sample self-diffusion coefficient (diffusion-weighted images) or where signal phase of the signal depends on the substance velocity in a chosen volume.

Summary

The described MRI methods and concepts provide a variety of options to acquire an MR image. The resulting image can represent different parameters of the sample and thus provide different information to the user. This leads to an MRI experiment or examination usually being a combination of various acquisition strategies, allowing for complex analysis of a sample, tissue or organism.

References

1. P. C. Lauterbur, Nature 242, 190 (1973).
2. M. A. Bernstein, K. F. King, and Z. J. Zhou, *Handbook of MRI Pulse Sequences* (Academic Press, Amsterdam, 2004).
3. S. Ljunggren, J. Magn. Reson. 1969 54, 338 (1983).
4. A. D. Bain, in *eMagRes* (Wiley, DOI: 10.1002/9780470034590.emrstm0443.pub2, 2011).
5. C. Westbrook, *Handbook of MRI Technique*, 3rd ed. (Wiley-Blackwell, Chichester, West Sussex; Malden, MA, 2008).
6. W. S. Price, NMR *Studies of Translational Motion: Principles and Applications* (Cambridge University Press, Cambridge, 2009).

Oral Reports

A Variable temperature X- and W-band EPR study of SiCN/Fe ceramics

Sergey. I. Andronenko[1], A. Rodionov[1], Sushil K. Misra[2]

[1]Institute of Physics, Kazan Federal University, Kazan, Russian Federation, 420008
[2]Department of Physics, Concordia University, Montreal, Qc, H3G 1M8, Canada
E-mail: sergey.andronenko@gmail.com

Introduction

SiCN is a new class of materials for high-temperature electronics. Magnetic properties of SiCN materials doped with different transition metal ions can vary from paramagnetic to superparamagnetic and to ferromagnetic. Superparamagnetic materials are potentially useful in developing high-temperature magnetic-sensor devices. Magnetic composites, as well as electrically conductive ceramics, with properties varying from dielectric to semiconductor, can be easily produced using liquid silazane polymer as a base, and exploited to fabricate complex isolator-conductive-material structures in order to develop new MEMS-SiCN techniques [1]. Consequently, investigation of SiCN ceramics and its conductive and magnetic derivatives is currently of great interest. Further, sp^2 and sp^3-carbon related dangling bonds, which are usually formed in free carbon phase of SiCN [2] can be investigated by EPR, a powerful technique to detect various types of magnetic properties. It has turned out to be very effective in the study of such materials [3].

EPR study of SiCN/Fe ceramics

Polymer-derived SiCN ceramics, annealed at 1000º C, 1100º C, 1285º C, and doped with iron (III) acetylacetonate, were investigated at liquid-helium temperatures from 4 to 120 K. The X-band (9.425 GHz) EPR spectra are shown in Fig. 1. The broad EPR lines A and B belong to different Fe-containing crystalline phase with different temperature behaviour.

EPR study of dangling bonds

The narrow EPR line near g = 2.00 is due to two carbon related dangling bonds. It is without structure at X-band, but at W-band this structure becomes resolved. These two types of carbon-related dangling bonds are present (i) on the surface of the free-carbon phase (sp^2-carbon related dangling bonds) as defects, and (ii) within the bulk carbon phase (as sp^3-carbon related dangling bonds).

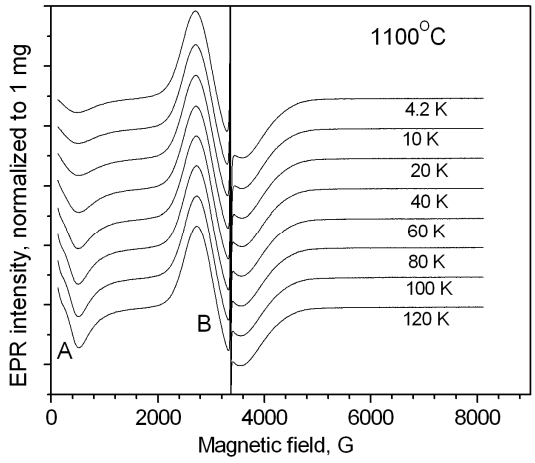

Figure 1. Temperature variation of EPR spectra of SiCN ceramic annealed at 1100° C at X-band

Temperature dependence of EPR linewidth of dangling bonds

The EPR linewidth of dangling bonds is strongly temperature dependent as shown in Fig. 2. The temperature dependence of EPR linewidth in the liquid-helium temperature range was found to be well described by the exchange interaction (J) in amorphous materials between carbon dangling bonds as deduced by Misra [4]. Accordingly, $\Delta B = A' + B' * T + C' / \left(1 + \exp\left(\frac{J}{T}\right)\right)$. In this expression, A′, B′, C′ are constants and T is the temperature. The second and third terms represent the relaxation of an exchange-coupled pair of spins in an amorphous solid. It was found by fitting the data that the value of the antiferromagnetic interaction was rather high (~ –80 K) in the various SiCN ceramic samples investigated here.

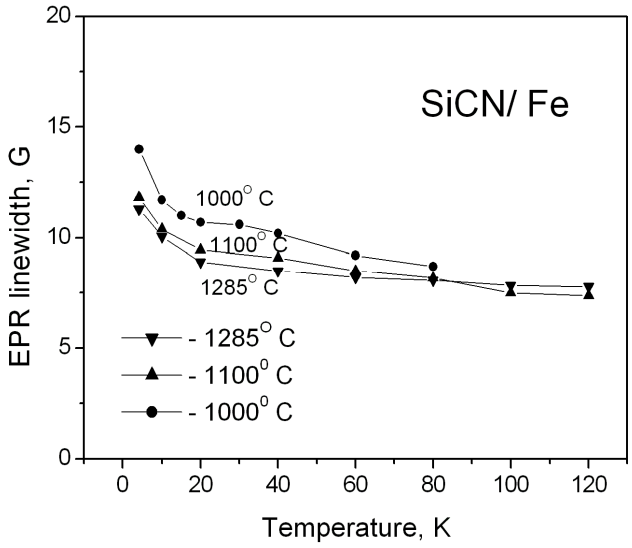

Figure 2. Temperature dependence of X-band EPR linewidth of dangling bonds for three samples annealed at 1285°, 1100°, and 1000°C

EPR/FMR study of SiCN/Fe ceramics: Fe-containing crystalline phase

The two FMR lines A and B in Fig. 1 are due to Fe ions, with different magnetic characteristics. They exhibit different temperature behavior. It is possible to use the temperature dependence of integrated FMR absorption linewidth to determine the Curie temperatures. This, in turn, can be used to determine the chemical composition of Fe-containing crystalline phase.

Critical temperature as determined from the FMR line A

As the temperature was increased from 290 K, the area under this absorption line, as obtained by double-integration of the first-derivative absorption curve, decreased and approached zero at 400 K. This integrated intensity is proportional to the magnetization of the ferromagnetic particles of Fe_5Si_3 in the sample.

The FMR linewidth of line A was fitted to the following expression [5] exhibiting the temperature (T) dependence:

$$\Delta B = \Delta B_0 + A|T_c - T|^{-0.7} \qquad (2)$$

The best fit yields the values: $\Delta B_0 = (220 \pm 10)$ G, $A = (5.2 \pm 0.5) \times 10^3$ G $\cdot K^{0.7}$, and $T_C = (393 \pm 5)$ K. This Curie temperature is very close to that for Fe_5Si_3 ($T_C = 393$ K).

W-band EPR study

The EPR study of SiCN ceramics, annealed at 1100° C was carried out at 300 K at W-band (93.96 GHz). EPR signals due to Fe ions were observed. The two well resolved sharp EPR lines at ~33,000 G are due to sp^2- and sp^3 – carbon-related dangling bonds.

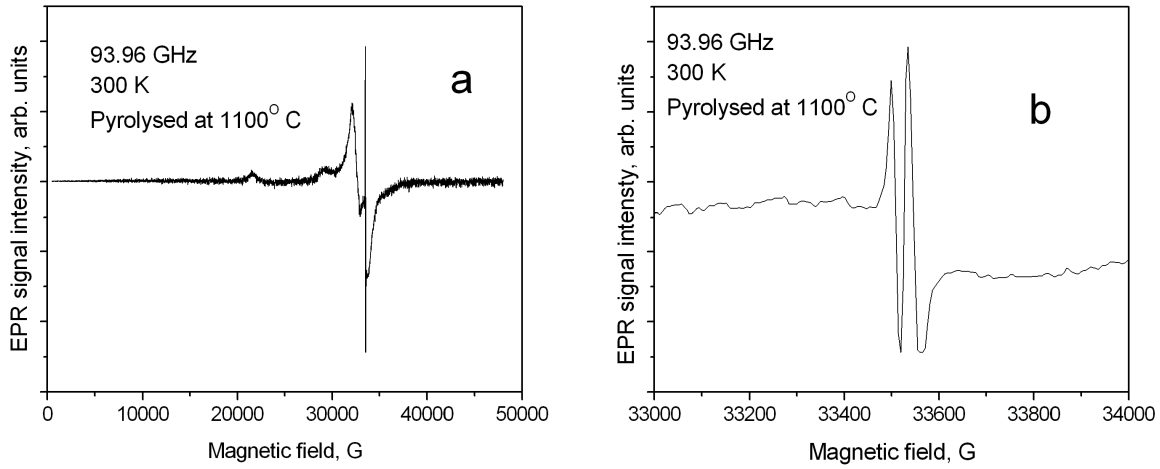

Figure 3. W-band EPR spectrum of SiCN/Fe ceramics (a) in the range 0-48,000 G and (b) in the range 33,000 – 34,000 G exhibiting EPR lines due to carbon-related dangling bonds

Conclusions

The low-temperature behavior of FMR and EPR signals in SiCN nanoparticles, activated with Fe ions is mainly due to the superparamagnetic nature of nanograins of Fe-containing compounds, mainly Fe_5Si_3. The low-field FMR signal, observed in SiCN/Fe near g = 10.0 at X-band, is not observed at W-band. It means, that this signal is not related to localized magnetic moments and, related to internal magnetic fields, determined by collective magnetic moments. High-frequency W-band EPR study of SiCN/Fe samples clearly shows, that central broad EMR lines observed at X-band are split into two different lines at W-band.

The two observed W-band EPR lines are due to carbon-related sp^2 and sp^3-dangling bonds. They are: (a) those associated with the aromatic rings of graphene layers with the g-value 2.0011 and (b) those existing in the bulk of "free" carbon phase with g = 2.0033 The EPR line with g = 2. 0033 is associated with sp^3-carbon related dangling bonds in amorphous carbon and the EPR line with g = 2.0011 is associated with sp^2-carbon related dangling bonds, which are located in broken aromatic rings of graphene layers.

Acknowledgements

This research was supported by the Natural Sciences and Engineering Research Council of Canada (NSERC) (SKM); SIA is grateful to Ministry of Education of Russian Federation, for partial support in the frame of research project, allocated to Kazan Federal University. SIA is grateful to Dr. S.B. Orlinskii for high-frequency measurements.

References

1. A. Leo, S. Andronenko, I. Stiharu, R. B. Bhat. – *Sensors*, **10**, 1338-1354 (2010).
2. S.I. Andronenko, I. Stiharu, S.K Misra. – *J. Appl. Phys.*, **99**, 113907 (2006).
3. S.I. Andronenko, I. Stiharu, S.K. Misra, C. Lacroix, D. Menard. – *Appl. Magn. Res.*, **38**, 385-402 (2010).
4. S.K. Misra. –*Phys. Rev.B.*, **58**, 14971-14977 (1998).
5. L.D. Landay, E. M. Lifshitz. Course of Theoretical Physics, v.5.: Statistical Physics. 4th ed. –"Nauka", Moscow, 1995; "Butterworth", London, 1999.

Study of nanoemulsions of the hydrophobic phthalocyanine in pluronic aqueous solutions

Ekaterina S. Babicheva[1], *Nataliia S. Shubina*[1], *Alexander M. Perepukhov*[1], *Alexander V. Maximychev*[1], *Vladimir M. Negrimovsky*[2]

[1]*Moscow Institute of Physics and Technology (State University)*
[2]*P. Hertsen Moscow Oncology Research Institute*
E-mail: esbabicheva@gmail.com

The solubilization of hydrophobic compounds is up to date in different spheres of human activities. This problem becomes particularly important in pharmaceutical applications where the most effective and save perspective compound could be inapplicable only due to its hydrophobicity. Solubilization of hydrophobic compound in surfactants aqueous solutions is one of the tools to resolve the problem, and understanding of solubilization mechanisms is rather actual. NMR spectroscopy is powerful technique for this purpose. It has been successfully applied on the intra- and intermolecular interactions in pluronic systems [1].

Phthalocyanines are a class of organic compounds widely used in different branches of science and technology, particularly as photosensitizers for photodynamic therapy of oncological diseases [2]. At the present work, we studied the solubilization of model phthalocyanine 1 in aqueous solution of polymeric non-ionic surfactant Pluronic F68 (fig.1).

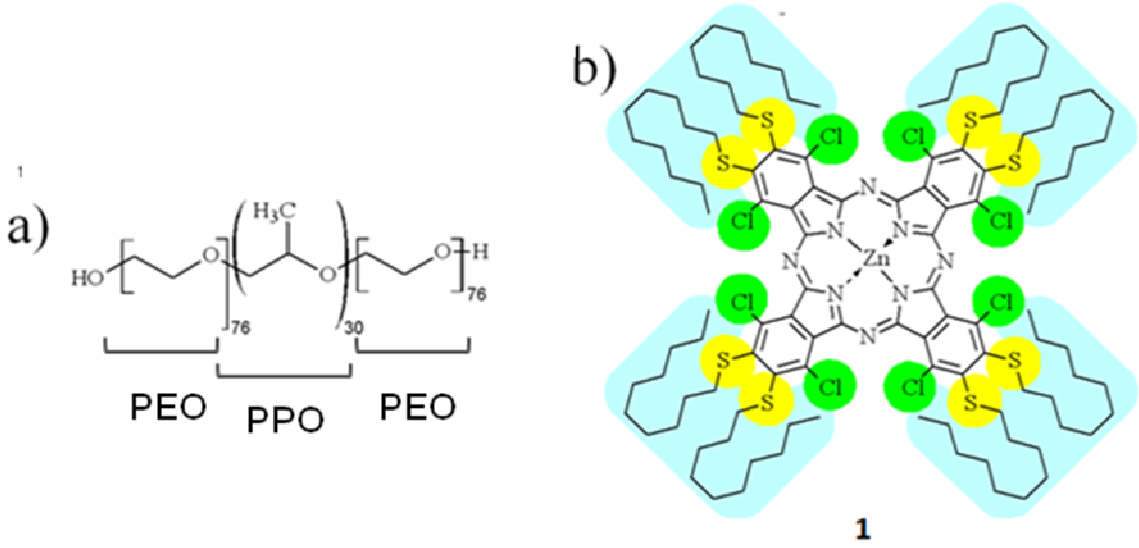

*Figure 1. Structures of pluronic F68 (a) and model phthalocyanine **1** (b)*

It is known that pluronics tend to aggregate with increasing of concentration and/or temperature. For pluronic F68 it was found, that its temperature-induced aggregation is accompanied by pronounced changes in its ^{1}H-NMR spectra: the appearance of a new resonance signal of propylene oxide CH_2-protons is observed. This phenomenon could be explained by conformational changing of propylene oxide fragments of the chain from *gauche* to his *anti* in course of micelle formation [2], which was also confirmed by FT-Raman and FT-IR studies [3, 4]. Increasing of the pluronic concentration results in the same effect. We found that at 25°C the micelle formation of pluronic F68 (new signal appearing) begins at ~ 20% (fig. 2) and solubilization of phthalocyanine **1** does not affect the conformational changes of pluronic at high concentrations as detected by ^{1}H-NMR spectra [5].

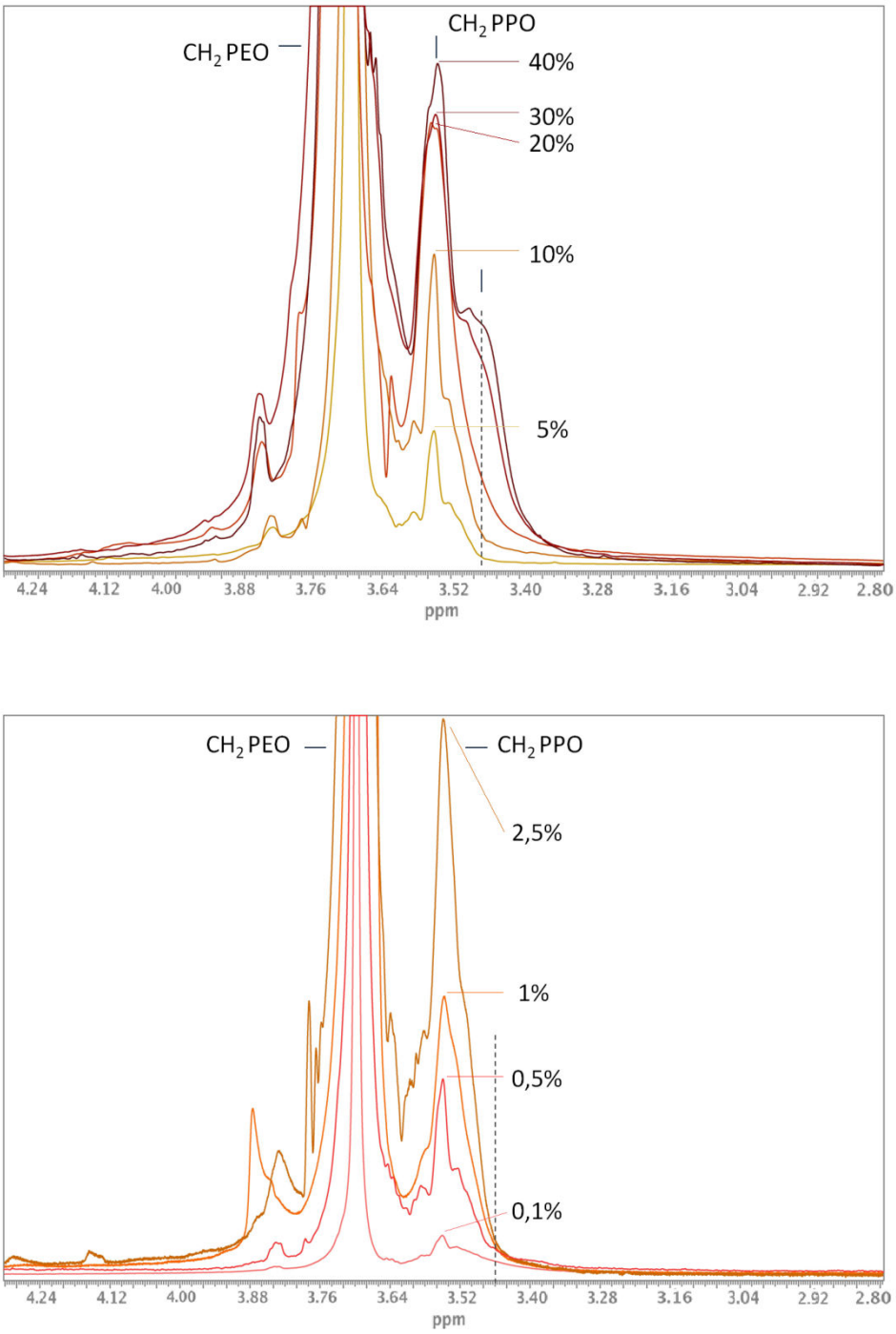

Figure 2. ^{1}H NMR spectra of F68 at various concentrations

Using UV-Vis spectroscopy we found, that dye **1** was solubilized in aqueous solution starting from concentration of the surfactant lower than 0,01%, and its concentration sharply increase at concentration of pluronic 1,0-2,5%. The order of this value corresponds with critical micelle concentration, determined for the same surfactant by pyrene solubilization - 0,4-0,8% [6].

As a result, two different methods allow observing changes in two different intervals of nanoemulsion concentration, and it could correspond to two different changes in nanoemulsion structure. The nature of these changes is currently being investigated.

References

1. Patent RF № 2164136. *Lukyanets E.A.* et al. Photosensibilizer for photodynamic therapy.
2. J. Ma et al. – *Langmuir*, **23**, 9596-9605 (2007)
3. Guo, C. et al. – *Langmuir*, **15**, 2703-2708 (1999)
4. Guo, C. et al. – *Colloid Polym. Sci.*, **277**, 376-381 (1999)
5. E. S. Babicheva et al. – *Materials of 13 International Youth School-Conference Spinus 2016*, 20-26 Nov. 2016, St. Petersburg, 72-74.
6. M. Yu. Kozlov. et al. – *Macromolecules*, ***33,*** 3305-3313 (2000).

Study of the structural-dynamic characteristics of the ternary system CsCl-LiCl-D2O with NMR spectroscopy in the interval from 25 to the freezing temperature

Valeria Baranauskaite, Olga Pestova, Andrey Efimov, Vasilyi Khripun

Instutite of Chemistry, Saint Petersburg State University

Introduction

Studies of the multicomponent water-salt systems' structures is an urgent task because peculiarity of the structure reflects in the variety of its properties including hygroscopicity, high solubility and heat capacity, low freezing temperatures, diversity of crystalline hydrates and of the double salts. Thus and so the study of formation mechanisms and conditions of joint compounds in these systems is a crucial task. The system under study is a model system for natural brines and is interesting, due to the different nature of the salts included: chaotropic CsCl and kosmostropic LiCl. The formation of the double salt goes by the structurally forced embedding mechanism [1].

The results of investigation of suchlike systems with NMR spectroscopy method allow one to receive a notion of the nearest surrounding of the ions and of the system structure on the whole, since the NMR method is sensitive to the appearance of microheterogenity in the solution. Discrepancy between natures of the salts reflects in their different influence on the water molecules mobility. Temperature studies NMR are suitable for the determination of a structural-dynamic characteristics. By applying of NMR method we received ^{2}D, ^{7}Li, ^{133}Cs spin-lattice (T1) and spin-spin (T2) relaxation times (sec), shifts (ppm) for the samples with constant ratio CsCl:LiCl = 1:2, at different concentrations, and for the different concentrations of CsCl, but constant LiCl concentration. We refined freezing points of these solutions, and deduced dependency of the velocity of the magnetic relaxation from the temperature at various concentrations as it can be seen at Fig. 1.

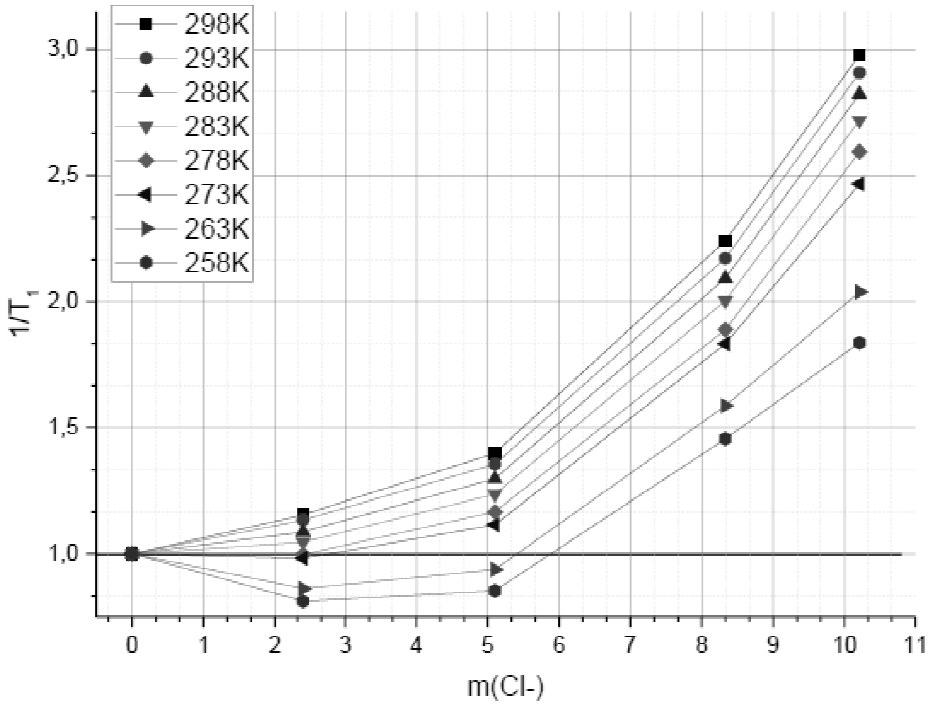

Figure 1. Relaxation velocity dependence from chlorine ion concentration (mol/l)

The temperature boundaries of microheterogenity appearance – formation of CG (cybotactic groups - precursors of solid phase) are detected. Acquired structural-dynamic parameters for the title system are compared with the ones for the binary systems. The activation energies are calculated as well as correlation times, what is shown at the Fig. 2. We state that for the positive temperatures (>273 K) activation energies are close to the ones of the pure heavy water D2O, 4 ccal/mol. This means that the relaxation mechanism of lithium and deuterium nuclei is alike. For the negative temperatures with the growths of salt concentration (Cl^-), the activation energies tend to the lower values. This is a result of the structure-breaking influence of ions on the water structure. Values of the activation energies for pure D_2O at positive and negative temperatures are taken from [2] and [3] respectively.

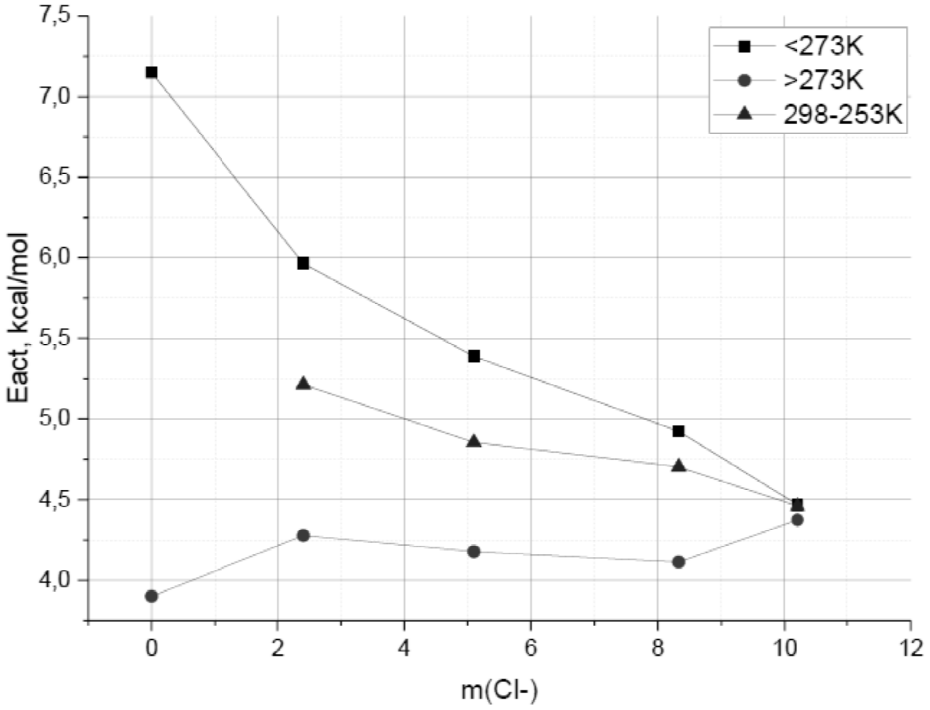

Firgure 2. Activation Energy dependence from chlorine ion concentration (mol/l)

References

1. Pestova Olga.N., Baranauskaite Valeria E., Khripun Maria K. - *J. of Gen. Chem.* V.86, 4, 577-581 (2016).
2. D. E. Woessner. - *The Journal of Chemical Physics* 39, 2783 (1963)
3. E. Lang, H. D. Lüdemann. - *Berichte der Bunsengesellschaft für physikalische Chemie* 84, 5, 462-470 (1980)

Application of NMR for studies of archaeological pottery. Preliminary results

Andrei Chudin

Saint-Petersburg State University, Lappeenranta University of Technology
E-mail: andrei.chudin@gmail.com

Introduction

Archaeological sites usually contain large amount of pottery, which is usually used for the archaeological attribution of the site. Investigations on pottery are of great interest, in particular when no historical witness is available. Therefore scientific effort is devoted to characterizing ancient ceramic artifacts and to investigating the possible sources of prime matter and the technology of production.

The «pottery» for physics means burned clay based material.

Clay minerals are:

- hydrous aluminium phyllosilicates, sometimes with variable amounts of iron, magnesium, alkali metals, alkaline earths, and other cations found on or near some planetary surfaces;
- weathering products;
- form flat hexagonal sheets;
- usually (but not necessarily) ultrafine-grained, normally considered to be less than 2 micrometers in size on standard particle size classifications.

Some time ago Chersonesos museum archaeologists asked us for few pottery samples investigation. There were 6 fragments from different amforas. Also we got a special fragment experimentally made by museum staff few years ago. The clay was taken from one of the 3 Chersonesos clay deposits. The same raw material base was used ancient masters also. The question was: can we combine or compare it by any physical settings?

For the first step we decided do use a couple of methods containing: lab. magnetometry, XRF and NMR. This set was chosen by the speed of results taking and probe safety (for next steps and other methods application).

Some words about NMR application for archaeological pottery artifacts investigation. For example, we know interesting results NMR application: successful trying to know the clay deposit origin and the temperature of burning. A multi-technique study of the firing process of an illite-rich clay in Italy was performed to study the modification induced by firing as a preliminary step to obtain information about ancient ceramic technology in this area [1].

The water absorption process in fired clay bricks was investigated by Pel et al. [2]. In these materials, a serious complication arises because of the presence of considerable amounts of paramagnetic ions which impair the use of the standard NMR imaging technique. The study was carried out with a home-built NMR imaging! The instrument allowed quantitative one dimensional moisture concentration profiles in the brick to be obtained [3]. The article by Ganna Zaytseva et al. [4] focuses on determining the chemical composition of the organic fractions in the pottery and the origin of the carbon. For this aim authors used the NMR method to identify the chemical compounds in the food residue and in the pottery matrix. Results obtained demonstrate that the food residue and the pottery matrix contain the same organic compounds, even if the relative abundances of various compounds are different in these materials.

The combination of NMR and isotopic ratio analyses of residues from prehistoric pots can give direct evidence of the use of the vessels and information about the diet of prehistoric

people. The cooking experiments show that there is very little change in the isotopic ratios by burning the foods to produce the residue. However, there is a change in the NMR spectra with the formation of a graphite-type material. The results of the residue analyses on vessels from complex, show two distinct uses: one were used for cooking fish stew, whereas another could have been used either as frying pans or fat-burning lamps [6].

Even LowField NMR is using in this specific area. Trudisca et. al. investigates individual characteristics related to the pottery firing technique through the low field single-sided NMR relaxometry. The approach is based on a recent method of analysis, the correlation of the longitudinal and transverse NMR relaxation times of a liquid probe (in this case distilled water) filling the porous system of ceramics [5].

Some preliminary results

Sample photo (Fig. 1) and magnified 500x photo (Fig. 2) of one of the sample (№10) are shown below.

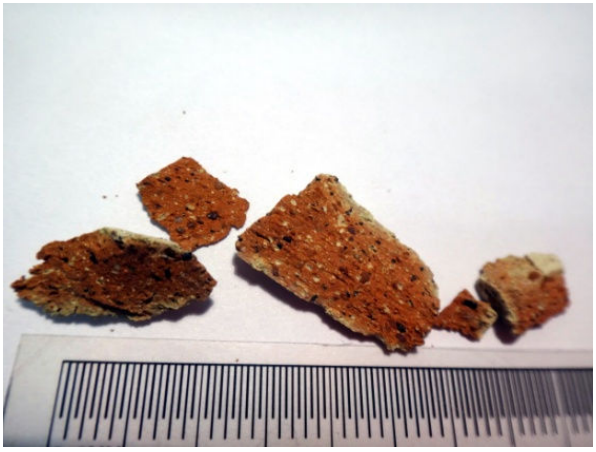

Figure 1. Sample 10 photo

Figure 2. Sample 10, magnified 500x photo

All the samples were handy milled down to 1 mm fraction. All the data during the 1st step was get with gross sample volume. Mass magnetic susceptibility of this sample has been measured as $1{,}4 \times 10^{-6}$ Si. Chemical element composition has been investigated with XRF spectrometer SHIMADZU EDX-800HS2. Results in relative values for Sample10 is shown in table below. Shown trusted data only (without the recalculation up to 100%).

Table1. XRF data for sample 10

Si	Al	Ca	Fe	K	Ti	Mn
40,7	21,3	19,3	12,8	3,7	0,9	0,2

MAS-NMR spectras were get on Bruker Avance 400. On the Fig. 3 shows the hysteresis loop for sample 10. Fig. 4 shows MAS-NMR ^{1}H spectra of the sample 10.

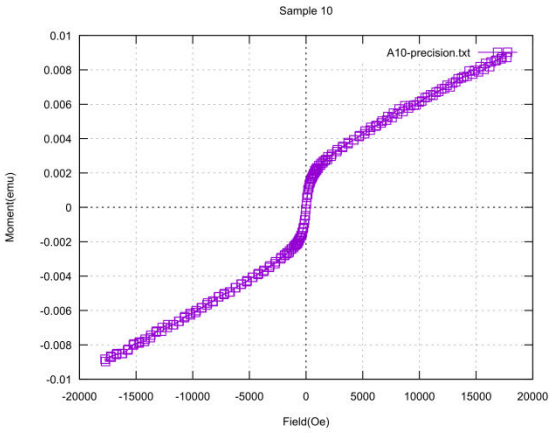

Figure 3. Sample 10 hysteresis

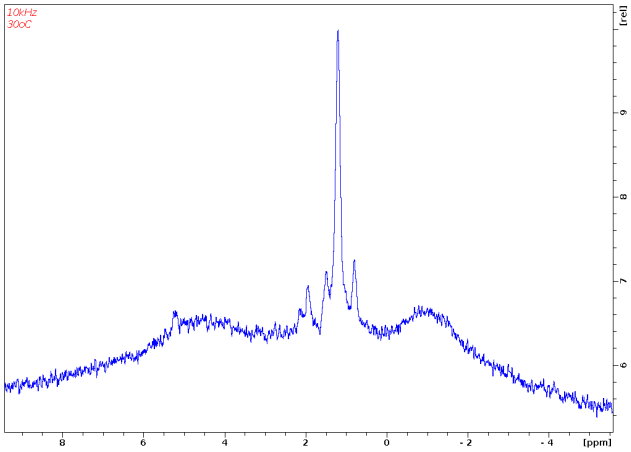

Figure 4. MAS-NMR ^{1}H spectra

Conclusions

The data get from all applied methods shows differences between samples good enough for grouping and differences. It gives us a possibility to answer to not only the given question, but also to know more about the technology and origin of pottery paste additions.

We have shown here the utility of using solid-state NMR spectroscopy in combination with lab. magnetometry and XRF to understand a complex archaeological material. There is about 10% of result showed only. The report is about very preliminary results and shows perspective direction of investigation.

References

1. Electron paramagnetic resonance, scanning electron microscopy with energy dispersion X-ray spectrometry, X-ray powder diffraction, and NMR characterization of iron-rich fired clays. F. Presciutti, D. Capitani, A. Sgamellotti, B.G. Brunetti, F. Costantino, S. Viel, A. Segre. J. Phys. Chem. B 109 (2005) 22147– 22158.
2. Water absorption in a fired-clay brick observed by NMR scanning. L. Pel, K. Kopinga, G. Bertram, G. Lang. J. Phys. D: Appl. Phys. 28, 1995.
3. One-dimensional scanning of moisture in porous materials with NMR. K. Kopinga, L. Pel. Rev. Sci. Instrum. 65,1994.
4. Radiocarbon pottery dating: The chemical compounds of organic fractions, the reliability of 14C dates (preliminary results) G. Zaytseva, E. Skakovsky, G. Possnert. Geochronometria, 2012.
5. Firing technique characterization of black-slipped pottery in Praeneste by low field 2D NMR relaxometry V. Tudisca at.al. Journal of Archaeological Science, 2011
6. Nuclear magnetic resonance spectroscopic and isotopic analysis of carbonized residues from subarctic canadian prehistoric pottery. B. L. Sherriff, M. A. Tisdale, B. G. Sayer, H. P. Schwarcz and M. Knyf. Archaeometry 37, 1 1995.
7. Natural science methods in field archaeology, with the case study of Crimea T. N. Smekalova, E. B. Yatsishina, A. S. Garipov, A. E. Pasumanskii, R. S. Ketsko, A. V. Chudin, Crystallography Reports, Volume 61, Issue 4, 1 July 2016, DOI 10.1134/S1063774516030251

A ^{1}H-NMR-based Metabonomic Study of the Nephroprotective Role of Taurine against Gentamycin Poisoning in Rats

Jean-Marie Colet, David Barbarino, Marilyn Duquesne

Faculty of Medicine & Pharmacy, University of Mons, 7000 Mons, Belgium
E-mail: jean-marie.colet@umons.ac.be
http://www.umons.ac.be

Introduction

Taurine is a sulfur amino acid derivative found mainly in the diet but also synthesized by the body. It plays several important roles within the body, including nephroprotection especially in the proximal tubules in the nephrons.

Gentamicin extracted from the bacterium *Micromonospora purpurea* is an antibiotic of the aminoglycoside family. The use of gentamicin is limited due to cochleo-vestibular and renal toxicities reported in animal models but also in patients. It is mainly used in the hospital by parenteral administration to fight severe infections.

Metabonomics is part of the omics approaches. It enables an accurate and detailed description of the metabolite composition of cells, tissues and cellular liquids. It allows the detection of metabolic disturbances due to any adverse effect on the organism from the environment, stress, pathologies, nutrition, toxicity and pharmacology. Approximately 2,500 endogenous metabolites are present in the human body. They are organic molecules of low molecular weight (<1000 kDa) derived from the endogenous metabolism. Abnormal fluctuations in any of those metabolites can be simultaneously assessed thanks to the use of proton NMR (^{1}H-NMR) spectroscopy. Due to the large number pf observation and variables involved in such metabonomic analysis, the spectral data are next binned and integrated in order to retrieve numerical values for each resonance arising from the detected metabolites. Those numerical values are then analyzed by using multivariate statistical analysis tools such as Principal Component Analysis (PCA) which give a simplified representation of the dataset.

Objective of the study

The aim of the present work was to demonstrate the protective role of taurine against the renal damages induced by the exposure of rats to gentamycin. To do so, the renal function of rats exposed to gentamicin with or without concurrent exposure to taurine was assessed by a metabonomic analysis of urine samples, histology, and clinical chemistry.

Experimental protocol

The study was carried out on 14 male Wistar-Han rats weighing 200 g (Janvier, France) randomly distributed in 3 groups:

- Group 1: 5 rats treated with gentamycin + taurine
- Group 2: 5 rats treated with gentamycin alone
- Group 3: 4 control rats

The animals received food and water ad libitum. Depending on the group, gentamycin (100 mg/kg) and/or taurine (750 mg/kg) were injected subcutaneously once daily for 7 consecutive days. When needed, rats were moved to metabolism cages placed on refrigerated racks for urine collection. Urines were centrifuged, added with phosphate buffer in D_2O for further ^{1}H-NMR analysis (using a 500,16 MHz Bruker Avance spectrometer with a 5 mm DUX 3H-1H probe). Blood samples were taken from the caudal vein for further dry clinical chemistry analysis (parameters: total proteins, albumin, urea nitrogen, uric acid and creatinine). Finally, kidneys were removed for histological exams.

Figure 1. Metabolism cage for urine collection

Results

Clinical Chemistry and Histology

Significant increases in the urine and/or plasma levels of creatinine and BUN were noticed in rats exposed to gentamycin alone as compared to control group. The concurrent exposure of gentamycin and taurine significantly reduced those effects on creatinine and BUN. From an histological point of view, early onset of necrosis as well as the presence of several elements (cytoplasmic vacuoles, necrotic bodies, infiltrates, ...) were seen in rats treated with gentamicin alone. Rats treated with gentamicin + taurine showed less severe lesions (Fig. 2).

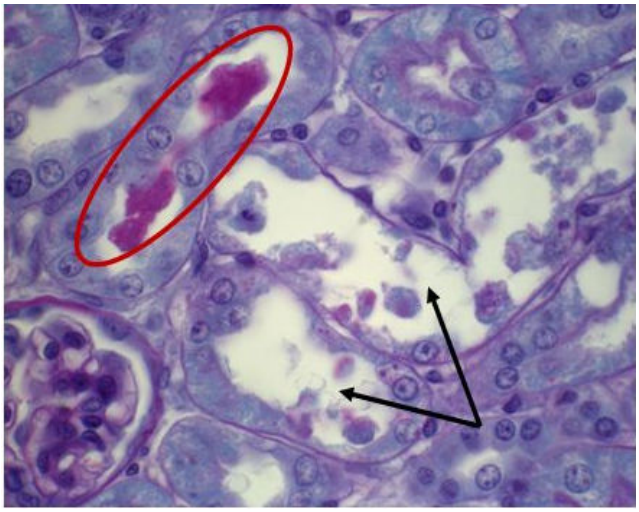

Figure 2. Histological exam of a kidney section from a rat exposed to gentamycin alone

As for the metabonomic evaluation, the time evolution of the urine composition as measured by ^{1}H-NMR is displayed on the PCA (scores plot, Fig. 3). The discriminating metabolites are shown on the corresponding loadings plot (Fig. 4). Variations in Krebs cycle intermediates and some markers of proximal tubule reabsorption / secretion (i.e., hippurate) were observed in rats exposed to gentamycin alone, as compared to controls and rats co-exposed to taurine.

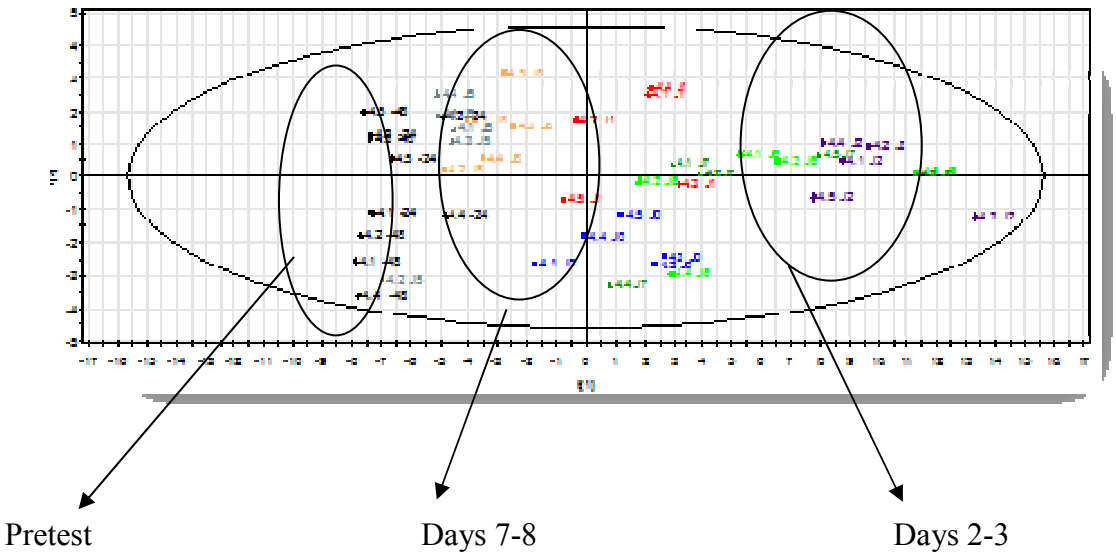

Figure 3. Scores plot showing changes in urine composition over time in rats co-exposed to gentamycin and taurine

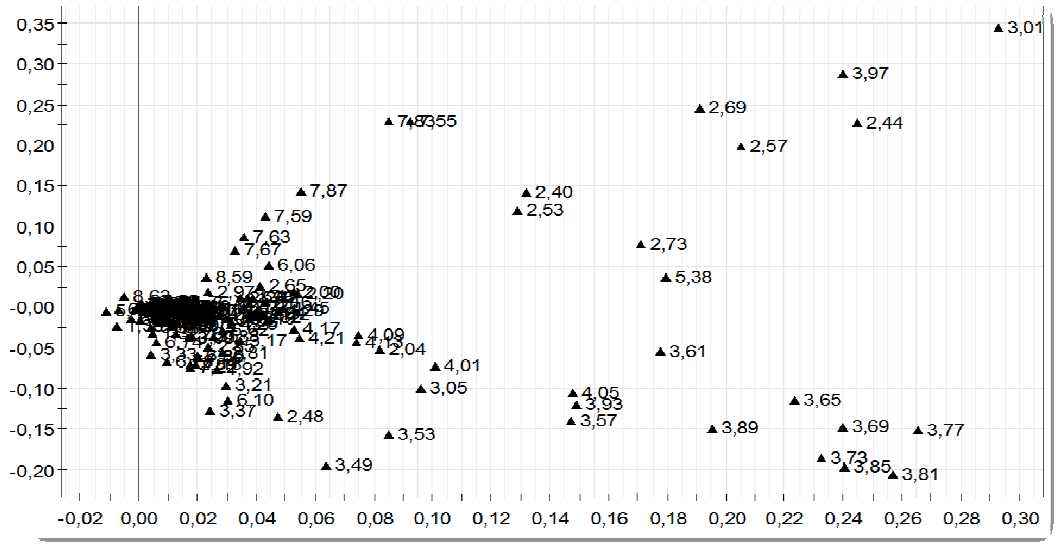

Figure 4. Corresponding loadings plots displaying the major discriminating metabolites

Discussion/Conclusion

All these results confirm the nephroprotective role of taurine against the nephrotoxicity of gentamicin. Given alone, this antibiotic caused renal tissue necrosis in rats. This toxic effect was supported by some alterations in urine biomarkers as well as clinical chemistry parameters of tubular damages. It was confirmed by histopathology. Co-exposure to taurine was able to preserved, at least partially, the renal tissue of rats thanks to its role as an antioxidant, thus fighting against the oxidative stress caused by gentamicin, as well as by to its role as a cell membrane stabilizer.

Acknowledgements

The laboratory of General, Organic, and biomedical chemistry at UMONS, headed by Prof. Sophie Laurent, is acknowledged for NMR support.

Paramagnetic terpyridine complexes of *d*-metals by methods of the magnetic resonance spectroscopy

Gleb L. Denisov[1,2], *Alexander A. Pavlov*[2], *Valentin V. Novikov*[2]

[1]*Higher Chemical College of the Russian Academy of Sciences*
[2]*Nesmeyanov Institute of Organoelement Compounds of Russian Academy of Sciences*
E-mail: denisov0gleb@gmail.com

Molecular devices, such as spin switches and molecule magnets, attract the attention of scientists as potential storage devices due to its bistability effect. One of the most promising compounds in this field is the *d*-metals complexes [1].

Within this work, a number of cobalt(II), iron(II) and nickel(II) complexes based on terpyridine (terpy) ligands were selected (Fig. 1) The Fe^{2+} complexes are diamagnetic, so the signals assignment of ^{1}H and ^{13}C spectra was a trivial task. The obtained data were used as a diamagnetic contribution in the study of others paramagnetic complexes.

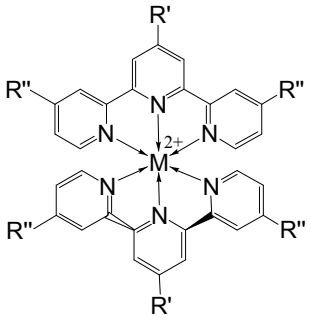

Figure 1. The structure of the complexes,
M^{2+} = Fe^{2+}, Ni^{2+}, Co^{2+};
R' = H, ^{t}Bu, py;
R'' = H, ^{t}Bu.

For the NMR signals assignment of the paramagnetic Co^{2+} and Ni^{2+} complexes the quantum-chemical calculations were carried out in the ORCA [2] software using the density functional theory (DFT) in the B3LYP basis using def2-TZVP basis sets, taking into account the solvent effect (COSMO).

NMR shift of paramagnetic compounds consists of two part: the diamagnetic and the paramagnetic shifts [3]. The latter includes the contact shift (CS) and the pseudocontact shift (PCS):

$$\delta_{exp} = \delta_{dia} + \delta_{para} = \delta_{dia} + \delta_{cs} + \delta_{pcs}$$

The values of the CS for Ni^{2+} ans Co^{2+} compounds were obtained from the calculated spin density at the ^{1}H and ^{13}C nuclei using ORCA. The PCS were calculated from the optimized structure obtained from a single crystal by the X-ray diffraction method. The combined values of CS, PCS, and the diamagnetic component of the chemical shift at ^{1}H and ^{13}C nuclei showed good convergence with the experimental data (Fig. 2).

It should be noted that the value of CS is dominant for Ni^{2+} complexes, whereas for Co^{2+} complexes there is an important contribution of PCS in addition to CS, which makes it possible to more accurately characterize the geometry of the complex in solution by NMR spectroscopy.

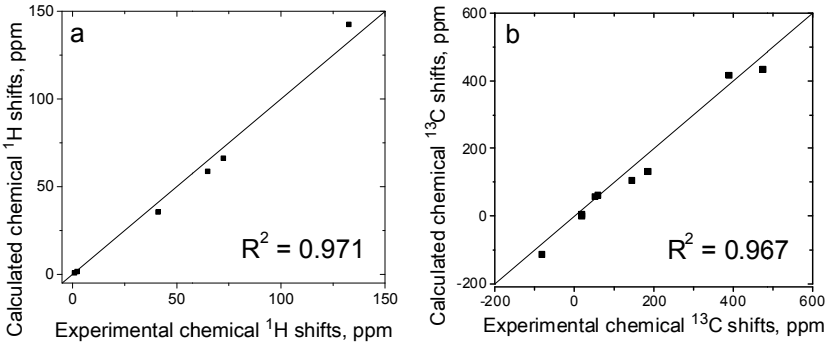

Figure 2. The convergence of the experimental and calculated chemical shifts in the spectra ^{1}H and ^{13}C of the Ni (^{t}Bu-terpy)$_2$ complex

The paramagnetic Co^{2+} compounds can be in two spin states: the low spin (LS) and the high spin (HS) states, which differs in the arrangement of electrons on the *d*-orbitals for the d^7 electronic configuration (Fig. 3) [4].

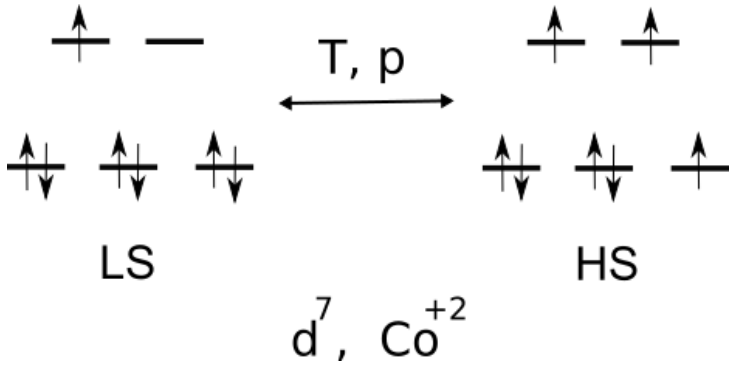

Figure 3. The low spin and high spin states crossover for Co^{+2} d^7 configuration

In this work were used the Evans method [5] and paramagnetic NMR shifts analysis to determine the spin state in a number of Co^{2+} complexes.

References

1. V.V. Novikov, A.A. Pavlov, Y.V. Nelyubina , M.-E. Boulon, O.A. Varzatskii, Y.Z Voloshin, R.E.P. Winpenny - J. Am. Chem. Soc., 137, pp. 9792–9795 (2015)
2. F. Neese - *WIREs Comput Mol Sci* - V. 2, 1, pp 73–78 (2012)
3. I. Bertini, C. Luchinat, G. Parigi - Solution NMR of paramagnetic molecules (2001)
4. H. Goodwin, *Top. Curr. Chem*. - V. 234, pp. 23-47 (2004)
5. D. F. J. Evans - *J. Chem. Soc.* - 36 (1959)

^{1}H NMR relaxation in emimAc-glycerol mixture

A. V. Ievlev

St. Petersburg State University 198504, St. Petersburg, Petergof, Ulyanovskaya str., 1.
E-mail: a.ievlev@spbu.com

Introduction

Imidazolium-based ionic liquids are today one of the most actively studied liquid systems due to broad prospectives of their possible applications. The main purpose of this paper was to find out how the presence of glycerol affects the spin-lattice relaxation of the ionic liquid. Relaxation in pure, without glycerol, 3-methyl-1-ethylimidazolium acetate has been described in detail earlier [1].

Experimental conditions

The spin-lattice relaxation times were measured by a standard inversion-recovery pulse sequence in the temperature range from 302 to 354 K. The ^{1}H NMR frequency was 400 MHz. The processing of the spectral data was carried out in a package of MestReNova v. 11.0.2, and relaxation curves were carried out in a package QtiPlot.

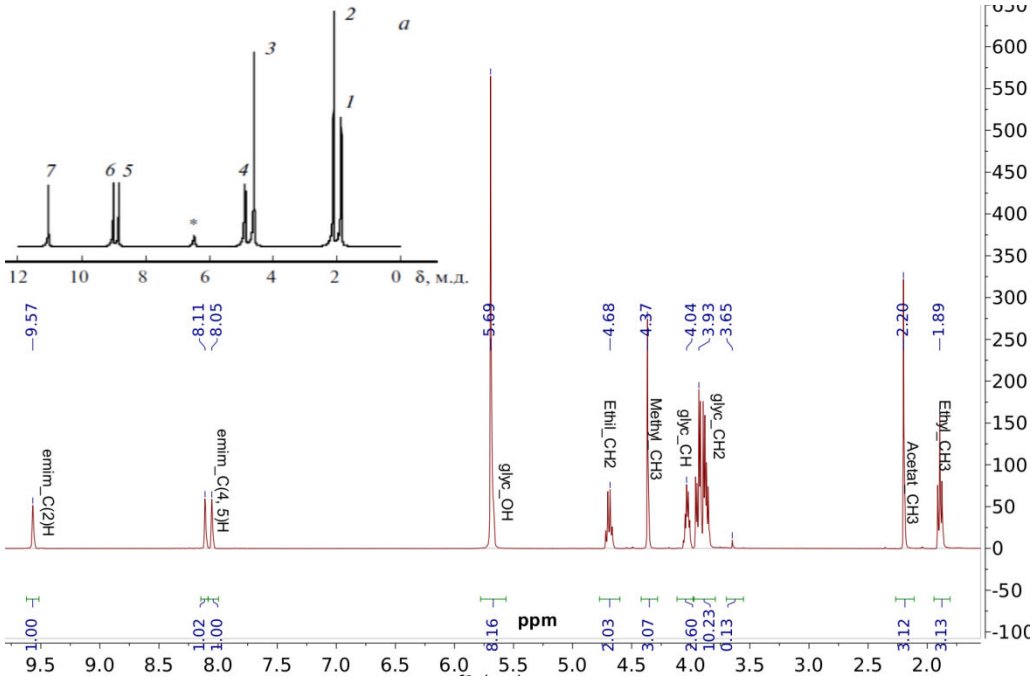

Figure 1. ^{1}H NMR spectra of mixture emimAc and glycerol at temperature 354 K (400 MHz) and pure emimAc on fig. 1a

Figure 1 shows the proton spectrum of the mixture studied. There are clearly visible additional lines corresponding to glycerol. Details of the spin-lattice relaxation behavior in the system and a comparison with the pure emimAc curves will be demonstrated during the report.

Acknowlegments

The part of studies was carried out at the Research Park of Saint Petersburg State University: Centre for Magnetic Resonance. This work was supported by grant RFBR № 17-03-00057. Special thanks are due to Matveev V.V. for his help in analyzing the data obtained.

References

1. В. В. Матвеев и др. Изв. РАН. Серия химическая, 2013, No 9, стр. 1985-1990.

Solid-State NMR Study of Surfactant Mesophases at Solid Interfaces

Boris B. Kharkov[1], *Sergei V. Dvinskikh*[2]

[1]*New York University, New York, United States*
[2]*Royal Institute of Technology, Stockholm, Sweden*
E-mail: sergeid@kth.se

Hybrid organic-inorganic nanostructured composites are now integrated in the field of nanoscience and nanotechnology [1]. Mesogenic organic molecules embedded in solid inorganic framework at nano-scale can form highly dynamic phases with aggregate structures different from those in the bulk. Recent studies of hybrid composites obtained by template synthesis [2] and by intercalation process [3] have shown that rotational, conformational, and translational mobility of organic component is much higher than previously anticipated.

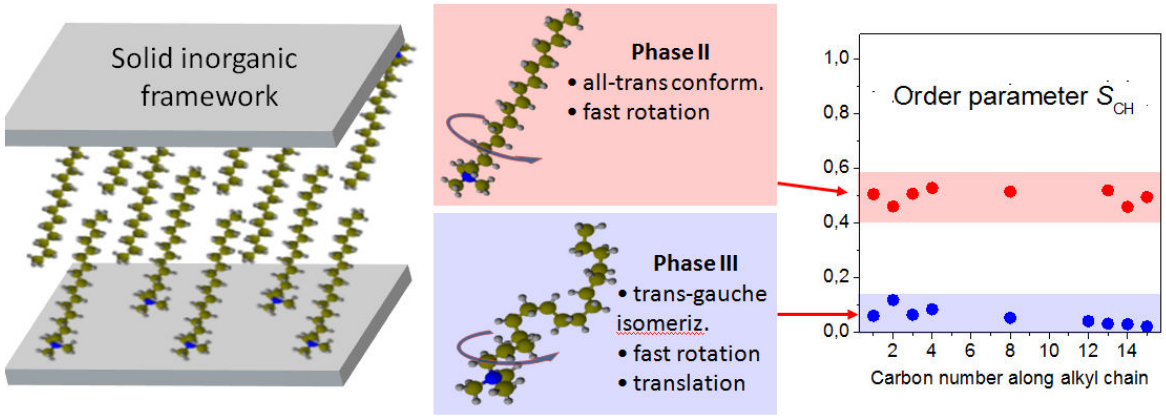

Figure 1. Dynamics models of mesogenic surfactant double-layer. The transition to phase III is associated with chain melting and the onset of translational dynamics and results in an liquid-crystalline state of the organic component

In this presentation, solid-state NMR dipolar spectroscopy techniques will be described. Spin dipolar couplings have well-defined orientational and distance dependence that makes them convenient and informative probes of dynamic processes and structural properties at molecular and atomic levels. A brief theoretical account of anisotropic spin interactions and their partial averaging by molecular dynamics in mesophases will be followed by the description of solid-state NMR experimental techniques for liquid crystals, with emphasis on two-dimensional heteronuclear dipolar NMR spectroscopy. Recent NMR studies of nanostructured LC materials will be presented. Dynamics of surfactant molecules adsorbed at solid surfaces, confined in ordered mesopores, intercalated into inorganic layered structures and aggregated in concentrated aqueous solution are compared. Solid state NMR spectroscopic data are used to quantitatively characterize the surfactant conformational dynamics and to build physical models of nano-confined molecules.

References

1. C. Sanchez, K. J. Shea, and S. Kitagawa. - *Chem. Soc. Rev.* **40**, 471 (2011).
2. (a) B. B. Kharkov and S. V. Dvinskikh. - *J. Phys. Chem. C* **117**, 24511 (2013). (b) B. B. Kharkov and S. V. Dvinskikh. - *Phys. Chem. Chem. Phys.* **15**, 18620 (2013).
3. B. B. Kharkov, R. W. Corkery, and S. V. Dvinskikh. - *Langmuir* **30**, 7859 (2014).

An estimate of the ratio of magnetic resonance frequencies of atoms Cesium-133 and water protons in the range 10 – 25 mT

Denis D. Kosenkov, Yu. I. Neronov, N. N. Seregin, A. E. Shilov, V. Y. Shifrin

Mendeleyev Institute for Metrology, St. Petersburg, Moskovsky pr. 19, Russia
E-mail: wdenkosw@gmail.com; yineronov@mail.ru

Introduction

The measuring range 8.5 - 25 mT is practically important for ensuring the unity of measurements of magnetic induction based on State primary standard for the units of magnetic induction GET12-2011 [1]. Now, there is no direct transfer of the value of T from the standard of magnetic fields of low fields to the medium and strong magnetic fields region (0.01-2 T). The experimental studies presented in this paper are the first step in matching the conversion constants for nuclear magnetic resonance sensors of strong fields with the quantum atomic-resonance (AMR) constants of helium-cesium magnetometers, which use in the low-field region.

As shown by the research of AMR sensors with cesium-133 vapor as an actuating medium with direct optical pumping in fields higher than 0.5 mT, the structures of atomic sublevels completely separated into components are detected. Moreover, the dependence of the AMR frequency on the optical pumping light intensity is reduced to an insignificant level.

At the same time, the use of cesium-133 provides an advantage over the known AMR magnetometers based on other actuating medium in terms of reducing the random component of measurement uncertainty, when a multiple reduction in the volume of the working substance is required (up to 30 or more times).

The advantages of using Cs^{133} in fields with induction up to 25 mT compared to other alkali metals with an equal working volume of sensitive elements (sphere Ø 10 mm) are: the largest amplitude of the AMR signal while working in laboratory conditions (temperature 25 ± 10 ^{0}C) and optimal for the construction of the electronic part of the equipment AMR frequency range (up to 100 MHz).

Hardware description

The required magnetic field in the experiments was provided by: four sectional gauge of magnetic induction; the highly stable direct current power supply system (range 0.05 - 2.0 A); a set of current measuring instruments based on the precision multimeter Agilent 3458A; a measure of electrical resistance with a nominal value of 1 ohm; a system for correcting the uniformity of the magnetic field; compensation unit of the alternating field induced noise.

The main element of the used equipment was a cesium-133 vapor-based magnetometer, which consists of the following four main devices: a cesium measuring transducer; the atomic magnetic resonance signal generation unit; a synthesizer-controller of magnetic resonance frequency and a personal computer with specialized software.

The main difference between this magnetometer and conventional quantum cesium magnetometers of the geomagnetic range (20-100) μT is its purpose for measuring substantially larger magnetic fields (up to 25 mT). A feature of the change in the conditions and parameters of the AMR signal in comparison with traditional analogs in the compared regions and ranges of measurements are the differences in the shape and amplitude of the magnetic resonance line when operating in "weak" and "medium" magnetic fields.

If the unified signal structure is used in "weak" fields, then in the range of "medium" fields, the working one is one of the extreme AMR lines separated with the smaller intensity, compared to the conditions of "weak" fields.

The change in the shape and amplitude of the resonance line, as well as the reduction of the working space with a homogeneous magnetic field, required to maintain the optimum

width of the magnetic resonance line, using up to 30 times the smaller size of the cesium magnetic-sensitive element (sphere diameter 10 mm) than conventional magnetometers (20-40 mm) operating in a homogeneous magnetic field of the Earth.

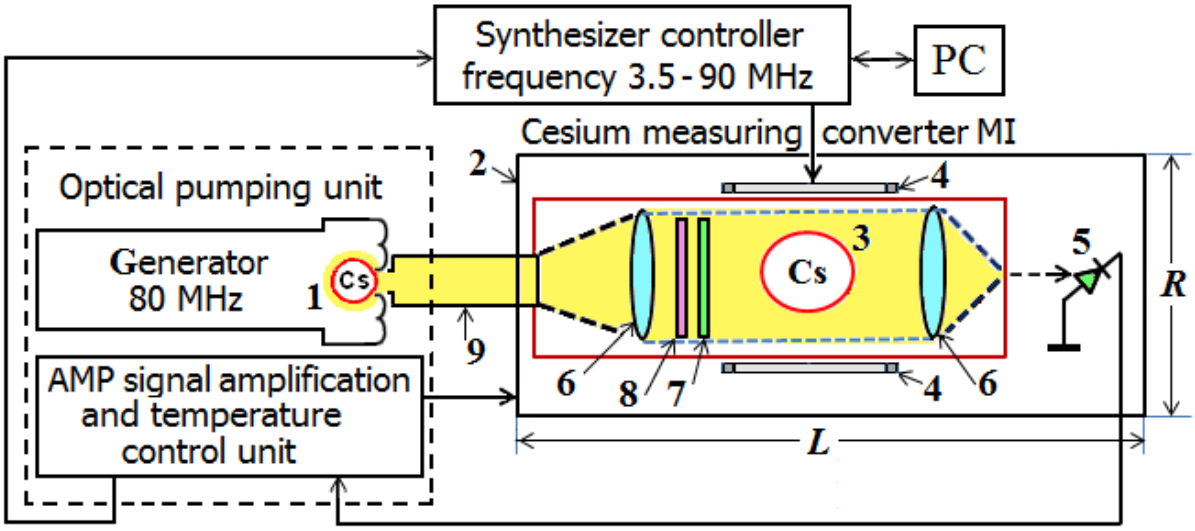

Figure 1. Structural diagram of the magnetometer based on Cesium-133 vapor: 1 - spectral Cs lamp; 2 - thermostat; 3 - Cs absorption chamber (12 mm); 4 - field radio coil; 5 - photodiode; 6 - lenses; 7 - interference filter; 8 - circular polaroid; 9 - optical fiber; R = 38 mm; L = 100 mm

At the same time, the signal-to-noise ratio decreases and, accordingly, the uncertainty of type A measurements increases (the random component of the measurement error). To minimize the uncertainty of AMR frequency measurements, the magnetometer and quantum comparator design provides synchronous detection and integration of the AMP signal implemented by software. As a result, the intensity of the ESR signal was large enough and sufficient to register the resonant frequency with an error at the level of units of the sixth sign.

Radio-electronic modules, which are similar to those previously described [2], were assembled to register signals from water protons. We used a method for determining the frequency of NMR signals using software, compiled on the basis of equations describing the Re and Im NMR signal form [2,3]. The magnetic field was calculated using the relation:

$$\nu(H_2O) = \gamma_p[1 - \sigma(H_2O) - \kappa(H_2O)/6]\times\mathbf{B}_\perp, \quad (1)$$

where γ_p is the gyromagnetic ratio of the proton. Screening of the proton in water $\sigma(H_2O$ and the bulk susceptibility of water $\kappa(H_2O)$ depend on the temperature of the sample. Data on the temperature dependence of these quantities are presented in [4].

Experimental data and discussion

The magnitude of the used magnetic system field depends not only on the current, but also on the temperature, which affects the geometric dimensions. Due to the heating of the winding, the temperature in the center of the magnetic system (signal recording area) varied from 41 to 30 ^{o}C with a current change from 1.6 to 0.55 A. The registration of cesium signals and water proton signals was performed by sequentially placing one of the two primary transducers in the center of the magnetic system after stabilizing the temperature regime.

The Cesium-133 spectrum consists of a group of signals, which frequencies depend on the orientation of the circular polarization vector and the direction vector of the magnetic field. To change the mutual orientation of these vectors, a current direction switch was used. The table shows the frequencies of the maximum intense signal, which was the extreme high

frequency (at -I) and extreme low frequency (at +I) from the AMR signal group. The dependence of the gyromagnetic ratio for Cs^{133} on the field value (Table 1) was estimated from the ratio:

$$\gamma(Cs^*) = [\nu(Cs, -)/(B_{\perp},-) + \nu(Cs,+)/(B_{\perp},+)]/2 \quad (2)$$

It is known that $\gamma(Cs^*)$ has a complex dependence on the field, which is still difficult to calculate theoretically. In this connection, the presented data can serve as a basis for the search for more accurate results.

Table 1. Collation of resonance frequencies of Cesium-133 and water protons

B/mT, range	Current I, A	Sign current	$\nu(Cs^*)$/Hz	$\nu_p(H_2O)$/Hz	B/mT	$\gamma(Cs^*)$,MHz/T
25.0	1.604 903	−I +I	93 686 897 81 961 525	1 064 707.31 1 064 712.01	25.006 958 25.007 069	3511.9837
22.5	1.444 423	−I +I	83 731 697 74 240 127	958 255.20 958 258.91	22.506 699 22.506 786	3509.4337
20.0	1.283 320	−I +I	73 087 890 66 396 837	851 527.28 851 530.84	19.999 963 20.000 046	3507.1731
17.5	1.123 400	−I +I	64 231 570 58 501 647	745 368.22 745 476.50	17.506 587 17.509 130	3505.1013
15.0	0.962 370	−I +I	54 657 033 50 445 263	638 645.89 638 645.91	14.999 981 14.999 982	3503.3549
12.5	0.801 870	−I +I	45 236 193 42 312 393	532 202.42 532 205.74	12.499 926 12.500 004	3501.9599
10.0	0.641 490	−I +I	35 943 076 34 072 445	425 767.54 425 772.30	10.000 073 10.000 184	3500.7312

From the data of the table, it follows that the functional dependence for γ (Cs) is well described by a quadratic dependence on the magnitude of the magnetic field:

$$\gamma(Cs) = 3498.57(+/- 0.02)[MHz/T] + 21438.7[MHz/T^3]\times(B[T])^2 \quad (3)$$

The dependence (3) obtained by us on average differs from the data presented in the table by $\Delta\{\gamma(Cs, \text{experiment})/\gamma(Cs, \text{calculation})\} = 6 \times 10^{-6}$.

References

1. V.Y. Shifrin, V.N. Khorev, V.N. Kalabin, S.L. Voronov, A.E. Shilov; «State primary standard for the units of magnetic induction, magnetic flux, magnetic moment, and magnetic induction gradient», Measurement Techniques, **55**, 739-744 (2012).
2. Yu. Neronov, N.N. Seregin; «The development of an NMR spectrometer for the precision determination of the ratio of the resonance frequencies of nuclei», Measurement Techniques**, 53**, N 8, 926-935 (2010).
3. Yu. I. Neronov and N. N. Seregin; «Precision determination of the difference in shielding by protons in water and hydrogen and an estimate of the absolute shielding by protons in water», Metrologia **51**, 54-60 (2014).
4. Yu. I. Neronov; «Determination of the temperature dependence of the shielding protons of water and a method for estimating the temperature of living tissues»; Izmeritel'naya Tekhnika, No. 1, pp. 67–71, (2017).

The "Hollow Core" Structure of Copolymeric Dendrimers

D. A. Markelov,[1] A. A. Polotsky[2], T. M. Birshtein[2,1]

[1]St. Petersburg State University, 7/9 Universitetskaya nab., St. Petersburg, 199034 Russia.
[2]Institute of Macromolecular Compounds, Russian Academy of Sciences,
Bolshoi Prospect 31, V.O., St. Petersburg 199004, Russia
E-mail: markeloved@gmail.com

Results

Copolymer dendrimers with attached terminal linear fragments that differ from inner segments in physical or chemical properties are considered by using the Scheutjens−Fleer self-consistent field approach. We find that the incompatibility between the terminal and the inner segments is the main factor favoring formation of a "hollow" interior in the dendrimer [1]. It is shown that the solvent quality with respect to terminal groups plays an important additional role.

Influence of structural parameters of the dendrimer, such as the terminal segment length, lend, and the generation, G, is also studied. We show that increasing terminal segment length enhances the segregation effect at the onset of the conformational rearrangement. At the same time, the size of the hollow in the dendrimer does not change with variation in lend. On the other hand, if the number of generations G increases, both the extent of the segregation effect, corresponding to the conformational change, and the hollow size grows.

Our results allow us to explain molecular dynamics simulation results [2] and experimental data [3, 4] for G=4 generation carbosilane dendrimer with terminal mesogenic groups in dilute chloroform solution. In this copolymer dendrimer the "hollow" interior is formed with decreasing temperature which corresponds to increasing segregation effect.

Acknowledgements

This work was supported by Russian Foundation for Basic Research (Grants 17-03-01115-a and 14-03-00926-a).

References

1. D.A. Markelov, A.A. Polotsky, T.M. Birshtein, Formation of a "Hollow" Interior in the Fourth-Generation Dendrimer with Attached Oligonneric Terminal Segments, J. Phys. Chem. B. 118 (2014) 14961–14971. doi:10.1021/jp509151w.
2. D.A. Markelov, M.A. Mazo, N.K. Balabaev, Y.Y. Gotlib, Temperature dependence of the structure of a carbosilane dendrimer with terminal cyanobiphenyl groups: Molecular-dynamics simulation, Polym. Sci. Ser. A. 55 (2013) 53–60. doi:10.1134/S0965545X13010045.
3. D.A. Markelov, V. V. Matveev, P. Ingman, M.N. Nikolaeva, E. Lähderanta, V.A. Shevelev, N.I. Boiko, NMR studies of carbosilane dendrimer with terminal mesogenic groups, J. Phys. Chem. B. 114 (2010) 4159–4165. doi:10.1021/jp909658v.
4. D.A. Markelov, V. V Matveev, P. Ingman, M.N. Nikolaeva, A. V Penkova, E. Lahderanta, N.I. Boiko, V.I. Chizhik, Unexpected Temperature Behavior of Polyethylene Glycol Spacers in Copolymer Dendrimers in Chloroform, Sci. Rep. 6 (2016) 24270. doi:10.1038/srep24270.

Spin dynamics studied by solid-state nuclear magnetic resonance and electron paramagnetic resonance in 29Si:B crystals

Oksana V. Koplak[1,2], *Eduard A. Shteynman*[3], *Alexey. N. Tereschenko*[3], *Roman B. Morgunov*[1,2]

[1]*Institute of Problems of Chemical Physics, RAS, Chernogolovka, 142432 Russia*
[2]*Taras Shevchenko National University of Kyiv, Kyiv, 01601 Ukraine*
[3]*Institute of Solid State Physics, RAS, Chernogolovka, 142432 Russia*
E-mail: o.koplak@gmail.com

Introduction

Interest in investigation magnetic resonance in silicon crystals enriched with magnetic isotope has been revived in recent years in connection with the fact that the nuclear spins in silicon have abnormally long spin relaxation times [1]. Nuclear magnetic resonance (NMR) and electron paramagnetic resonance (EPR), as well as their combinations, have opened a simple way for processing of quantum information and initialization of the quantum spin system (its conversion to the initial state). Silicon spintronics and the related quantum computing activated the studying the spin-dependent phenomena in silicon.

Magnetic (mass-independent) isotope effect in silicon crystals

Silicon has three stable isotopes 28Si, 29Si and 30Si. Just one of them, 29Si, is magnetic (nuclear spin 1/2, nuclear magnetic moment 0.555). In [2] magnetic (mass-independent) isotope effect (MIE) on silicon oxidization was observed. MIE is a dependence of the reaction rates on the nuclear spin and nuclear magnetic moment of reactants. In order to analyze chemical and silicon isotope composition the secondary ion mass spectrometry (SIMS technique) was applied. Silicon oxidation by oxygen depends on the magnetic field and exhibits isotope effect: silicon atoms 29Si with magnetic nuclei are oxidized up to two times faster in comparison with 28Si and 30Si atoms with nonmagnetic nuclei [2]. The MIE effect verifies that the oxidation is a spin selective reaction controlled by radical pairs (electron spins of Si and O atoms). The dominating oxidizing species are oxygen molecules in triplet spin state, which generate triplet radical pairs. This fact indicates that the silicon oxidation is a spin selective radical (or ion–radical) process. The rate of this reaction is comparable with that of triplet–singlet spin conversion in the radical pair [Si O2Si], containing paramagnetic centers. Broadening of the 28Si, 29Si isotope distribution in the subsurface layers of Si:B single crystals under plastic deformation has been observed near the surface in [3]. The 28Si, 29Si profiles broaden with increasing dislocation density (Fig. 1).

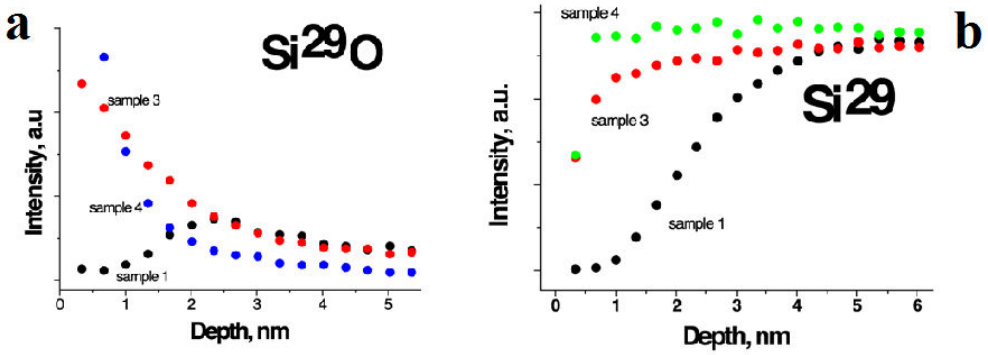

Figure 1. Dependences of secondary ion current of ^{29}Si and $^{29}Si^{16}O$ complexes on ionic etching depth in the reference samples (3 and 4) and deformed sample 1 $Fz^{29}Si$

Accompanying changes in the $^{29}Si^{16}O$ profile caused by plastic deformation have been found. The shift of the $^{29}Si^{16}O$ profile to the crystal bulk correlates well with the $^{29}Si+$ isotope redistribution. The uphill diffusion or dislocation movement are possible driving factors of Si and SiO redistribution, whereas selectivity of the isotopes in oxidation reaction is provided by singlet–triplet transitions in Si··O short living pairs.

Electron paramagnetic resonance of oxygen defects in ^{29}Si

Dipole–dipole nuclear interaction and electron– nuclear interaction controlled by spins of paramagnetic defects are the main driving channels of quantum computing in silicon media. Quantum devices based on 29Si:B crystals is more complicate due to high electron spin of the holes S= 3/2, high values of nuclear spins of the stable boron isotopes 10B and 11B (I(10B)=3 and I(11B) =3/2), and the contribution of spin–orbital interaction to the splitting of the spin sublevels of "light" and "heavy" holes. We have studied light doped (2 1014 cm-3 boron concentration) 29Si crystals. Furthermore, we have introduced 1015 cm3 paramagnetic deformation defects that stimulated electron–nuclear relaxation and contributed to nuclear spin relaxation kinetics. The ESR spectra of these defects are anisotropic and have a significant line-width (up to 1 kOe) (Fig. 2). The nonuniform broadening of the ESR lines is caused by the variation of the internal magnetic field in correlated defect clusters [4].

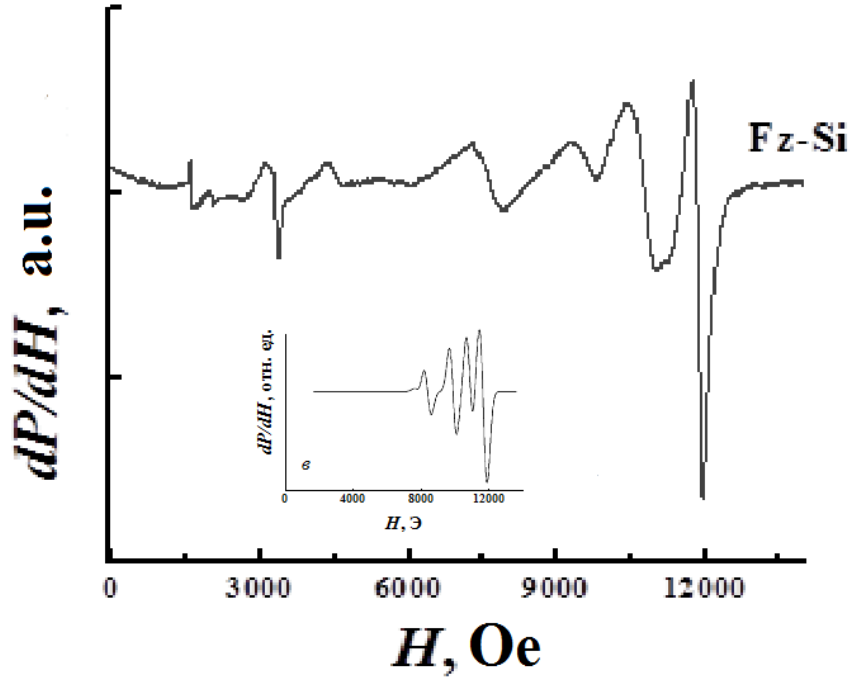

Figure 2. ESR spectra in the deformed sample Fz^{29}Si enriched with ^{29}Si up to 99 % and numerical simulation of the ESR spectrum of deformation defects in the deformed sample

The defects observed in the deformed crystal ESR have deformation origin. The defects are three dimensional, or placed in the surface layers, but not in the crystal bulk, because their ESR spectrum is anisotropic; the pronounced anisotropy is evidence of the fact that the defects are in those positions of the crystal lattice, whose symmetry is lowered by plastic deformation and dislocations; the width of the ESR lines of the defects under investigation attains 1 kOe, which considerably exceeds the estimates within the framework of usually considered broadening mechanisms related to hyperfine interaction (to 0.1 kOe); the most probable mechanism of line broadening in our experiments is inhomogeneity of the effective field in spin correlated clusters; The best fitting of the spectrum (Figure 2, insert) was implemented for the following parameters of the spin Hamiltonian: the electron spin

S = 1, the components of the g - tensor are gxx = 0.61, gyy = 0.78, and gzz = 0.75, the splitting parameters in the crystal field are D = 2000 Oe, and E = 1000 Oe, and the nucleus spin is I = 1/2. This makes it possible to assume that we observe the ESR of anisotropic exchange coupled clusters of triplet oxygen with the spin S = 1 embedded in the surface lattice under high temperature plastic deformation. The photoluminescence spectra of the deformed crystal 29Si:B has been demonstrated "standard" set of lines D1, D2, and D4 of the dislocation luminescence. The high dislocation density in the crystal results in luminescence line broadening, especially, in the long wavelength region of the spectrum [5].

NMR Spectra of isotope enriched crystals

The main contribution to the NMR spectrum width of 29Si causes a nuclear dipole interaction between the neighboring nuclear spins of 29Si–29Si. We established that the position of the NMR signal peak and the distance Hpp between peaks depend on the crystallographic orientation of the sample with respect to the magnetic field H (Fig. 3a). The narrowest resonance lines (700 Hz) were observed in the field orientation parallel to [100], the widest lines (1980 Hz), is in the field orientation along [110]. The strongest line splitting (1300 Hz) was observed in the field directed along [111].

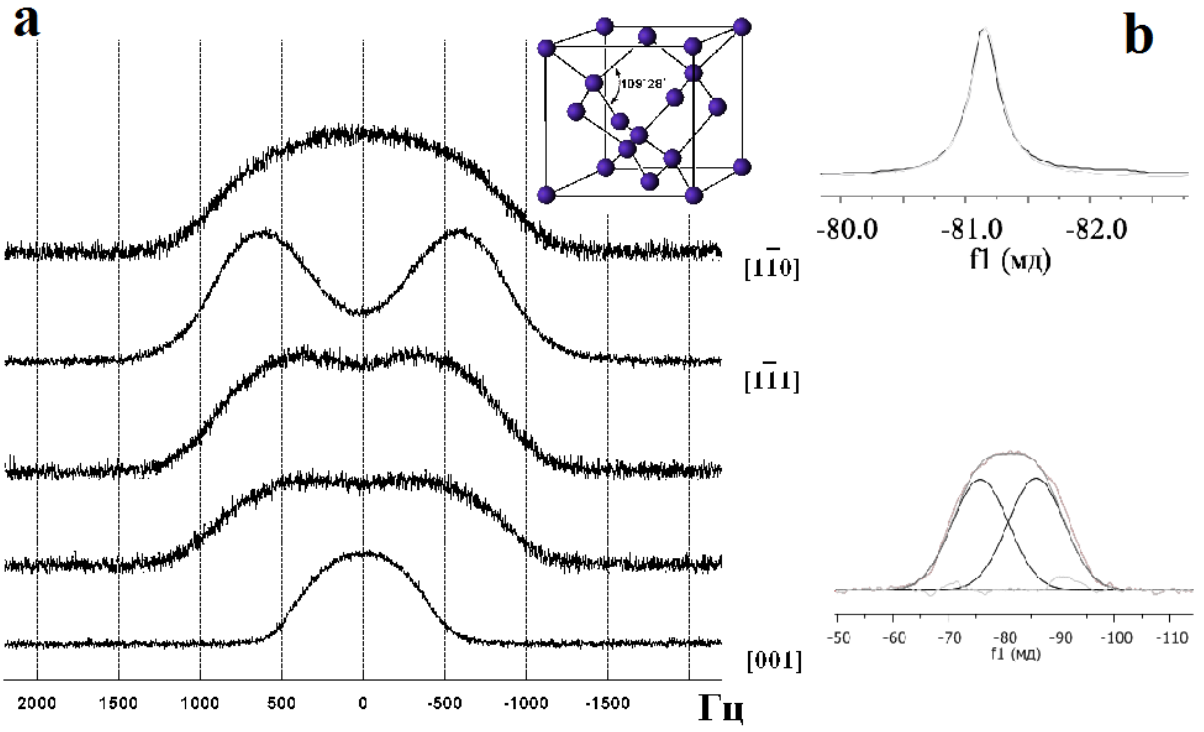

Figure 3. NMR spectra: a)in the deformed sample Fz^{29}Si at different orientations of the magnetic field of the spectrometer with respect to crystallographic directions ; b) silicon crystals with a concentration of ^{29}Si 4,5% (a) and 99 % enriched ^{29}Si:B crystals

A pair of lines at –88.8 ppm and –78.4 ± 0.1 ppm corresponds to the Pake doublet of the fourfold-coordinated ^{29}Si atoms. The NMR line width of ^{29}Si in silicon depends on the percentage fraction of the magnetic ^{29}Si. For example, the NMR line width for silicon crystals with a concentration of magnetic nuclei ^{29}Si from 5 to 100% increases from ~100 to 2000 (Fig. 3b). The NMR line width $\Delta\nu_{dd}$ caused by the dipole– dipole interaction of nuclei can be estimated from the formula $\Delta\nu_{dd} = 30/T_2$, where $\Delta\nu_{dd} \sim 1000$ Hz and $T_2 \sim 300$ s is the nuclear spin–spin relaxation time. The average distance between ^{29}Si nuclei can be estimated from the formula $a \approx (8f/d^3)^{-1/3} = 3.35$ nm, where eight is the number of atoms in the diamond crystal structure cell, $d = 0.543$ nm is the silicon lattice constant, and $f = 99\%$ is the fraction of the

magnetic nuclei ^{29}Si of the total number of all nuclei. However, the Poisson distribution used above for estimating electron pairs shows that the nuclei pairs are also meet with the probability of 37% in neighboring crystal lattice sites. Hence, for such random formations, the dipole– dipole interaction is very intense [5,6].

In plastically deformed isotopically enriched crystals ^{29}Si (99%), paramagnetic defects of a new type with anisotropic ESR spectra and a significant line width (up to 1 kOe) were found. The effective g- factors of the ESR spectrum lines testify that deformation defects have the electron spin S = 1 being impurity exchange coupled clusters. ESR spectra and the photo luminescence are related to the involvement of the same groups of paramagnetic centers in formation of the spectra; the presence of these centers depends on the deformation of crystals. The NMR line width is determined by the electron– nuclear and nuclear dipole–dipole interactions.

Acknowledgements

This work is supported by the RFBR (grant 16-02-00420 A).

References

1. M. Veldhorst, C. H. Yang, J. C. C. Hwang, W. Huang, J. P. Dehollain, J. T. Muhonen, S. Simmons, K. M. Itoh, A. Morello, and A. S. Dzurak – Nature., **526**, 410-414 (2015).
2. Koplak O., Morgunov R., Buchachenko A - *Chemical Physics Letters.,* 560. 29-31 (2013).
3. O.V. Koplak, R.B. Morgunov - *Chemical Physics Letters.*, 643, 39–42 (2016).
4. O. V. Koplak, A. I. Dmitriev, S. G. Vasil'ev, E. A. Shteinman, R. B. Morgunov - *Journal of Experimental and Theoretical Physics. 118, 621–629* (2014).
5. O. V. Koplak, A. I. Dmitriev, S. G. Vasiliev, E. A. Shteinmann, S. I. Alekseev, R. B. Morgunov *// Semiconductors., 48, 989–995* (2014).
6. R. B. Morgunov, O. V. Koplak - *Silicon., 8, 331–336* (2016).

NMR study of water dynamics in copper-exchanged mordenites

Ekaterina Krylova[1], *Lyudmila Surova*[1], *Dmitrii Bogdanov*[1], *Yurii Zukov*[1], *Marina Shelyapina*[1], *Alexei Privalov*[2], *Vitalii Petranovskii*[3]

[1] *Saint-Petersburg State University*
[2] *Technical University of Darmstadt, Darmstadt, Germany*
[3] *CNyN, National Autonomous University of Mexico, Ensenada, Mexico*

Copper-exchange zeolites are highly promising materials for heterogeneous catalysis, especially for reduction of NO*x* (de-NO*x* catalysts) [1, 2]. According to numerous researches their catalytic properties are governed by both the valence state of copper ions, their location and coordination in the zeolite lattice and copper content as well [3, 4]. Water molecules, which easily enter inside zeolite channels, is another crucial factor that influences zeolite properties. Moreover, it is well known that water is a promoter of many physical and chemical processes proceeding in porous materials. From this perspective, the study of water dynamics is zeolites are highly required.

Being sensitive to the rate of molecular displacements over submicrometric distances during observation times of hundred microseconds till seconds, the nuclear magnetic resonance (NMR) diffusometry has proved itself to be a powerful tool for studying translational dynamics of guest molecules in porous materials including zeolites [5].

In this contribution, we report on the results of the ^{1}H NMR study of the dynamics of water molecules in a series of copper-exchange mordenites.

The samples CuNaMorM*X* (where *X* = 1, 2, 3 and 6 is the number of ion-exchange procedures) were synthetized from Na-mordenites (NaMor) supplied by Zeolist Int. (product CBV10A) with Si/Al atomic ratio equal to 6.5. The ion-exchange procedure was done by using the microwave assisted method. For more details see Ref. [6]. To increase the copper content, the exchange procedure was repeated several times up to six copper-exchange procedures. The copper exchange level for the studied samples is 58, 75, 89 and 127 % for *X* = 1, 2, 3 and 6, respectively.

The X-ray diffraction confirms that after the ion-exchange procedures the samples keep the mordenite crystalline structure. According to the scanning electronic microscopy for all the samples the size of crystallites is about 100 nm.

To determine the water content and activation energy of water desorption, thermal analysis (TGA) was carried out using a Netzsch STA 449 F1 Jupiter coupled with a quadrupole mass spectrometer QMS 403 Aëolos. Analysis of the samples was done in the temperature range 40-700°C at the heating rate of 2, 10 and 20°C/min in argon stream at the rate of 50 ml/min.

The proton diffusion measurements were performed using NMR in a static field gradient (SFG NMR) applying the stimulated echo pulse sequence. This method allows us to measure diffusion coefficients in systems with short spin-spin relaxation times values, which are typical for solids.

The NMR experiment was carried out using relaxometer at 91 MHz in a static field gradient of 134.1 ± 0.3 T/m within the temperature range from 300 K to 380 K. Waiting time between the pulse series was more than proton spin-lattice relaxation time in 10 times. The temperature of the samples was controlled with the accuracy of 1 K.

It has been found that at room temperature in the parent NaMor sample the water diffusion coefficient is close to the value in the bulk water: $D^{300K} = 5.2 \times 10^{-10}$ m^2/s. However, a partial substitution Cu^{2+} for Na^+ slow it down to 1.2×10^{-10} m^2/s that does not change noticeably with following increasing of the copper content. The activation energy of water

diffusion is 0.25 ± 0.01 eV for Na^+ mordenite and slightly increases with copper loading up to 0.32 ± 0.01 eV.

The both diffusivity and activation energy values obtained for the NaMor zeolite are in fair agreement with results reported in Ref. [7, 8] for Na-BEA and NaX zeolites and can be attributed to the intracrystalline diffusivity, as for zeolites in the Na^+-form, the heat of water adsorption and, correspondingly, the activation energy of long-range diffusion, is about of 60 kJ/mol [8]. This value notably exceeds the activation energies obtained from NMR experiment. Such a deviation points out that the water molecules remain in the matrix of the host materials, namely in the main channel of the mordenite matrix. The size of the main channel is about 6.5 × 7.0 Å, and if in NaMor the Na^+ cations are mainly placed in the small channels, the Cu^{2+} cations are in the main channel and are surrounded by water molecules, $[Cu(H_2O)_n]^{2+}$ complexes. However, they do not impede the translational motion of water molecules.

Acknowledgements

The XRD, SEM and TGA studies were done at the Research Park of Saint Petersburg State University: Centre for X-ray Diffraction Studies, Centre for Innovative Technologies of Composite Nanomaterials, Thermogravimetric and Calorimetric Research Centre. The diffusion measurements were carried out in TU Darmstadt with support of the G-RISC (E. Krylova and L. Surova).

References

1. D. Berthomieu, G. Delahay // Catal. Rev. Sci. Eng., 48, 269–313 (2006)
2. Chen Y. // Prog. Chem., 26, 248–258 (2014)
3. P. Vanelderen et al. // Coord. Chem., 257, 483–494 (2013)
4. S. Grundner et al. // Nat. Commun., 6, 7546 (2015)
5. S. Beckert et. al. // J. Phys. Chem. C, 117, 24866–24872 (2013)
6. Y.M. Zhukov, et al. // Microp. Mesopor. Mat., 224, 415–419 (2016)
7. H. Pfeifer // NMR Basic Princ. Prog., 7, 53-153 (1972
8. J. Kärger, P. Volkmer // J. Chem. Soc. Faraday Trans. I, 76, 597-615 (1980)

Investigation of α–casein translational mobility by NMR methods

Daria L. Melnikova[1], Irina V. Nesmelova[2,3], Vladimir D. Skirda[1]

[1]Department of Physics, Kazan Federal University, Kazan 420011, Russia
[2]Department of Physics and Optical Sciences, and [3]Center for Biomedical Engineering and Science, University of North Carolina, Charlotte, NC 28223, USA
E-mail: melndaria@gmail.com

Introduction

In the last decade it became known, that proteins have functional activity not only in globular condition, but in partly or whole disordered form [1]. Globular structure in common is inherent for proteins with a strictly defined function – for enzymes. Much higher lability is needed for the proteins, which could interact with a greater amount of partners, hence, macromolecules of such proteins in native condition is partly or whole unstructured. The intrinsically disordered proteins functional role could be bound to the need of molecular plasticity for more effective identification by the partner-molecules [2-4].

The degree of compactness of the polypeptide chain depends on the amino acid residue composition of a given protein and on environmental conditions, including the concentration of the protein itself and/or the crowders. Hence, there is a great interest to understand how the intrinsically disordered proteins (IDPs) behave in the wide range of concentrations, from dilute to highly concentrated solutions. In particular, understanding the translational diffusion of IDPs, which is the major mode of macromolecular transport in biological or chemical systems (e.g., the self-diffusion, hereafter denoted simply as diffusion), becomes important. Although translational diffusion of proteins has received considerable theoretical and experimental scrutiny, much of that attention has been directed towards the description of globular proteins. The translational diffusion of intrinsically disordered proteins (IDPs), however, is much less studied [5-10].

The purpose of current work was to study structural and dynamical features of translational mobility of the intrinsically disordered protein α – casein in water solutions in a wide range of concentrations by NMR with pulsed field gradient (PFG).

Results

All NMR measurements were performed at 298 K on a 400 MHz Bruker Avance – III TM spectrometer equipped with gradient system that allowed a maximum gradient, g, of 28 T/m (e.g., 2800 G/cm). Self-diffusion coefficients (hereinafter referred to simply as diffusion coefficients) were measured using the stimulated-echo pulse sequence (PGSTE) [11]. Samples were prepared by dissolving the lyophilized powder of α–casein in D_2O in order to minimize the signal from water protons in NMR spectra.

A typical form of diffusion attenuation of spin echo amplitude, for example of 7% α–casein solution, is shown in the figure 1. This form clearly indicates the presence of two components with different diffusion coefficients, obviously related to molecules of water (region A) and the protein (region B). It demonstrates the opportunity to define diffusion coefficients both for solvent and the protein. The section of diffusion attenuation related to the protein, as it is clear from figure 1, could not be described only by one exponential decay. As it is known in such cases, the value of average diffusion coefficient could be applied to characterise the protein molecules. It could be defined from the slope of the tangent (solid line) to the initial section of the protein diffusion attenuation (region B).

Fourier transformed ^{1}H NMR spectra of the protein solution showed well-separated signals from residual water (region 5 ppm) and protein molecules (from 0.16 to 3.61 ppm),

permitting the selective registration of protein diffusion coefficient. In further, relying on the spectral resolved registration, we obtained diffusion attenuation only for the protein molecules

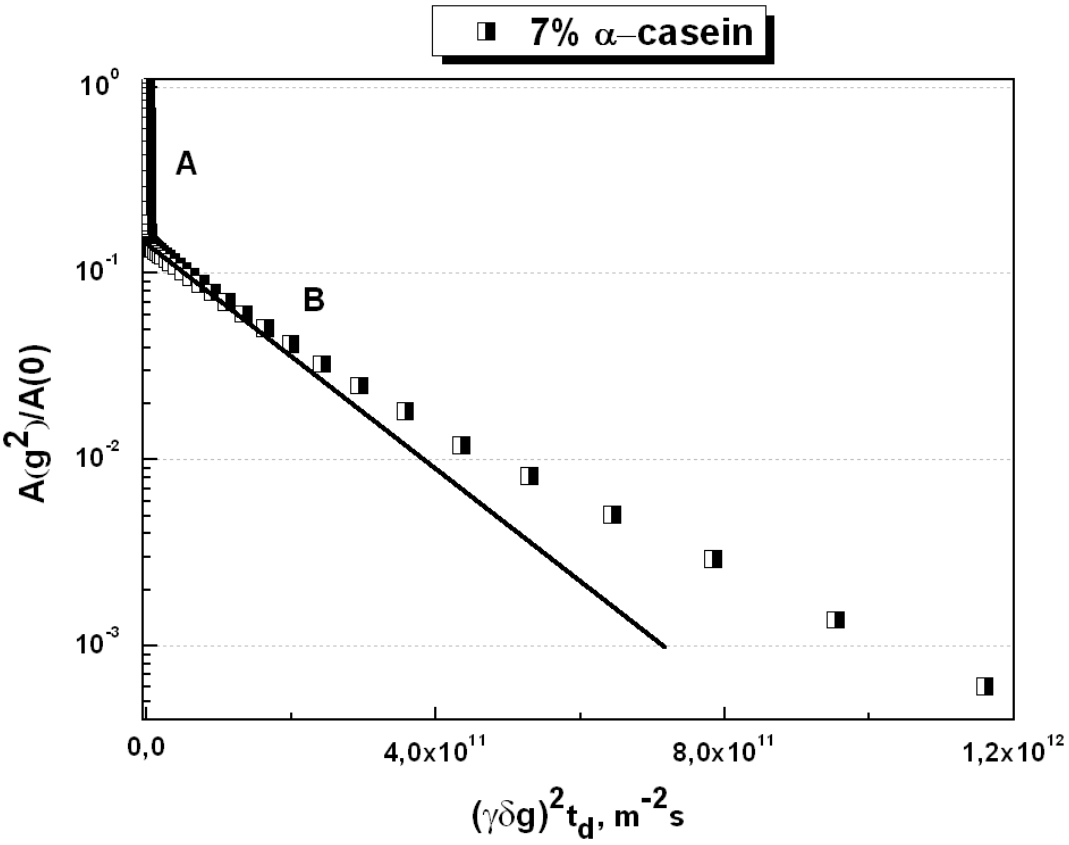

Figure 1. Diffusion attenuation of spin-echo signal for 7% α–casein solution in D_2O. It shows diffusion attenuations related to molecules of water (region A) and the protein (region B) in this protein solution. All measurements were done at 298 K

As a result of a detailed study of the translational diffusion of an intrinsically disordered alpha-casein protein, we found several interesting features. We have found that in the concentrated solutions the translational mobility of alpha-casein molecules is characterized by a wide range of self-diffusion coefficients. In this study, we observe that α–casein reversibly self-associates in concentration-dependent manner to form labile, three-dimensional, gel-like structures. Thus, the choice of α–casein also allowed us to access the effect of self-association on the concentration dependence of the diffusion coefficient of a disordered protein.

Acknowledgements

This work was supported by the Faculty Research Grant from the University of North Carolina to I.V.N. NMR measurement were carried out on the equipment of the Federal Centre of Shared Facilities at Kazan Federal University.

References

1. V. N. Uversky, J. R. Gillspie, A. L. Fink. Why are “natively unfolded” proteins unstructured under physiologic conditions? – Proteins. 41, 415–427 (2000).
2. A. K. Dunker, D. J. Lawson. Intrinsically disordered protein. – J. Mol. Graphics and Modelling. 19, 26–59 (2001).

3. V. N. Uversky. A protein-chameleon: conformational plasticity of alpha-synuclein, a disordered protein involved in neurodegenerative disorders. – J. Biomol. Struct. Dyn. 21, 211—234 (2003).
4. C. J. Oldfield, Y. Chemg, M. S. Cortese, C. J. Brown, V. N. Uverskiy, A. K. Dunker. Comparing and combining of mostly disordered proteins. – Biochemistry. 44, 1989–2000 (2005).
5. H. M. Berman, J. Westbrook, Z. Feng, G. Gilliland, T. N. Bhat, H. Weissig, I. N. Shindyalov, P. E. Bourne. The Protein Data Bank. – Nucleic Acids Res. 28 (1), 235-242 (2000).
6. H. J. Dyson, P. E. Wright. Intrinsically Unstructured Proteins and Their Functions. – Nat. Rev. Mol. Cell Biol., 6 (3), 197-208 (2005).
7. J. Habchi, P. Tompa, S. Longhi, V. N. Uversky. Introducing Protein Intrinsic Disorder. – Chem. Rev., 114 (13), 6561-88 (2014).
8. A. H. Mao, S. L. Crick, A. Vitalis, C. L. Chicoine, R. V. Pappu. Net Charge Per Residue Modulates Conformational Ensembles of Intrinsically Disordered Proteins. – Proc. Natl. Acad. Sci. USA, 107 (18), 8183-8 (2010).
9. V. N. Uversky. Unusual Biophysics of Intrinsically Disordered Proteins. – Biochim. Biophys. Acta, 1834 (5), 932-51 (2013).
10. Y. Wang, L. A. Benton, V. Singh; G. J Pielak. Disordered Protein Diffusion under Crowded Conditions. – J. Phys. Chem. Lett., 3 (18), 2703-2706 (2012).
11. J. E. Tanner. Use of Stimulated Echo in NMR-Diffusion Studies. – J. Chem. Phys., 52 (5), 2523-2537 (1970).

Reconstruction of particle size-distribution from conjunction of NMR and DLS diffusion data

Sevastyan O. Rabdano[1], Ivan S. Podkorytov[1], Nikolai R. Skrynnikov[1,2]

[1]Laboratory of Biomolecular NMR, SPbSU, 199034, 7/9 Universitetskaya nab., St. Petersburg
[2]Department of Chemistry, Purdue University, 47907, 560, Oval Drive,
West Lafayette IN, USA
E-mail: sevastyan@rabdano.ru
http://bio-nmr.spbu.ru

The aqueous systems with polydispersity are challenging to tackle by experimental methods. The methods like dynamic light scattering (DLS) or small angle X-ray scattering can provide some information on the morphology of aggregates. However this techniques fail when particle sizes are distributed broadly. Scattering methods have biased weighting of large particles in comparison to small ones [1, 2]. The NMR diffusometry on the other hand can deal only with relatively small particles posing auspicious magnetic relaxation characteristics. Fortunately NMR could characterize large protein systems when certain amino acid residues located at flexible tails are dynamic enough to produce sharp spectral peaks [3]. The present study deals with aggregate particles (AP) of RRM2 domain of TDP-43 protein that are formed upon treatment of protein sample by hydrogen peroxide. Upon H_2O_2 treatment RRM2 forms intermolecular disulfide bonds leading to unfolding and consecutive cross-linking of monomeric units to multimers.

The NMR signal is proportional to the molecular weight M_w of molecule, while intensity of scattered light is proportional to M_w^2. Thus measured diffusion coefficients of APs have different values because of different weighting of size distribution. Here we report the method of reconstruction of particle size-distribution from two measured diffusion coefficients. The apparent diffusion coefficients of RRM2 aggregates were measured by pulsed field gradient NMR and DLS. The distribution functions were guessed and then their parameters were fitted to experimental diffusion coefficients taking into account M_w and M_w^2 weighting for NMR and DLS respectively.

The parameters of distribution functions for studied system cannot be obtained individually by either of methods, but their combination was fruitful. Proposed approach could likely be used for determination of particle size-distribution of important biological aggregates such as amyloid fibrils, polydisperse polymer systems or any other ensemble of soluble particles with size heterogeneity on a nanometer scale.

References

1. Pecora R. Dynamic Light Scattering Measurement of Nanometer Particles in Liquids // J. Nanoparticle Res. 2000. Vol. 2, № 2. P. 123–131.
2. Shibayama M., Karino T., Okabe S. Distribution analyses of multi-modal dynamic light scattering data // Polymer. 2006. Vol. 47, № 18. P. 6446–6456.
3. Christodoulou J. et al. Heteronuclear NMR investigations of dynamic regions of intact Escherichia coli ribosomes // Proc. Natl. Acad. Sci. 2004. Vol. 101, № 30. P. 10949–10954.

Analysis of NMR spectra of alizarin and alizarin red S

Vladislav Salikov, Andrei V. Komolkin

Faculty of Physics, Saint-Petersburg University
E-mail: vladislav.salikov@inboxl.ru

Introduction

Oxidative stress is phenomenon that entity is damaging living cells as a result of oxidation. This process has a certainly impact on every biological objects. For this reason an investigation of compounds for antioxidative properties is important for practical issue. Anthraquinone may have an antioxidative activity [1]. Two of them are alizarin [2, 3] and alizarin red S [2] (Figure 1). The purpose of this work is analysis of NMR spectra of pure solutions of these two compounds.

Methods and materials

Alizarin is practically indissoluble in water including deuterated water. DMSO-d6 (with 99.8% deuterium) was used as solvent for both compounds. Alizarin was dissolved in solvent at concentration of 35.4 mg/832.6 mg of DMSO-d6 and alizarin red S was dissolved at concentration of 36.8 mg/896.4 mg of solvent. The solutions were prepared and researched at 25 °C. Experimental data was obtained with Bruker 500 MHz Avance III spectrometer at "Research Park" of SPbU. Spectrometer operates at 500.03 MHz for ^{1}H nuclei and 125.74 MHz for ^{13}C nuclei.

As a result of the experiments, the following spectra of each substances were obtained:

1. ^{1}H; pulse sequence: zg30;
2. ^{13}C NOE coupling with hydrogen; pulse sequence: zggd30;
3. ^{13}C NOE decoupling with hydrogen; pulse sequence: zgpg30;
4. ^{1}H and ^{13}C 2D HSQC; pulse sequence: hsqcetgpsi2.

The proton spectrum provides us information about the chemical shifts of hydrogen atoms and indirect spin-spin interactions. Thus, it is possible to determine the chemical environment of atoms, using implicit evidences, which helps to assign the lines.

The carbon spectra can establish the chemical shifts of all carbons, as well as determine the carbon atoms bonded to hydrogens. Doublets with splitting of 150-180 Hz are caused by the interactions with the bonded hydrogen atom. There is possibility of splitting each line of doublet into another doublet due to weaker interactions with hydrogen atoms linked with two or more chemical bonds. The use of nuclear Overhauser effect (NOE) leads to doubling the intensity of spectral lines of the carbons linked to hydrogens with respect to the intensity of the lines of the carbons which do not link to protons.

The 2D HSQC (Heteronuclear Single-Quantum Correlation) NMR spectrum on ^{1}H and ^{13}C atoms allows us to determine the chemical shifts of carbon atoms and bonded to them hydrogen atoms.

NMR spectra were processed using the ACD\lab v.12.01 package. The assignment of experimental lines to atoms of compound was performed with ACD/labs ChemSketch, ACD/labs NMR Predictor, Magic Plot, author's program in an environment Matlab R2015b[4].

Discussion and results

The first substance is alizarin (Figure 1). The 2D spectrum showed the resonances of 7 cross peaks of ^{1}H - ^{13}C (except solvent). These peaks are joined in two groups: with weak (w) and strong (s) intensity 119 ppm (C), 6.78 ppm (H), s; 123.03 ppm (C), 8.36 ppm (H), w;

123.07 ppm (C), 7.97 ppm (H), s; 125.35 ppm (C), 8.37 ppm (H), s; 125.39 ppm (C), 7.96 ppm (H), w; 128.09 ppm (C), 8.36 ppm (H), s; 127.61 ppm (C), 7.86 ppm (H), s.

The ^{1}H NMR spectrum exhibited the resonances of the aromatic protons (d. 6.785, H-9, J 8.9 Hz; dd. 7.875, H-8; J 8.9, 2.7 Hz; m. 7.972, H-2, H-3; m. 8.365, H-1, H-4) and hydroxyl proton (s. 8.368, H-15). Here "s" denotes singlet, "d." denotes doublet, "dd." denotes doublet of doublets, "m." denotes multiplet.

The ^{13}C NMR spectrum with coupling showed the resonance of carbons (dd. 119.12, C-9, J_H 160.5 Hz, J_{H2} 3.2 Hz; s. 119.49; dd. 123.09, J_H 167.4 Hz, J_{H2} 5.8 Hz; dd. 125.43, C-1, C-2, J_H 169.7 Hz, J_{H2} 4.9 Hz; dd. 127.68, C-8, J_H 160.3 Hz, J_{H2} 6.3 Hz; dd. 128.24, C-4, J_H 160.6 Hz, J_{H2} 6.0 Hz; s. 142.8; s.147.61; s. 156.5; s. 171; s. 172.12).

The second substance is alizarin red S (Figure 1). The 2D spectrum showed the resonances of 7 cross peaks of ^{1}H - ^{13}C (except solvent). These peaks are 127 ppm (C), 8.17 ppm (H), s; 127 ppm (C), 7.9 ppm (H), w; 134.5 ppm (C), 7.89 ppm (H), s; 134.5 ppm (C),8.92 ppm (H), w; 135.5 ppm (C), 7.92 ppm (H), s; 135.5 ppm (C), 8.15 ppm (H), w; 118.7 ppm (C), 7.87 ppm (H), s.

The ^{1}H NMR spectrum revealed the resonances of the protons (m. 8.2, H-1, H-4; m. 7.914, H-2, H-3, H-8) and hydroxyl protons (s. 11.451, H-16; s. 12.624, H-15).

The ^{13}C NMR spectrum with coupling exhibited the resonance of carbons (s. 116.68; d. 118.78, C-8, J_H 167.5 Hz; s. 123.37; dd. 127.06, C-1/C-4, J_H 166.5 Hz, J_{H2} 8.1 Hz; dd. 127.29, C-2/C-3, J_H 163.9 Hz, J_{H2} 7.5 Hz; s. 133.4; s. 133.96; m. 134.71, C-1/C-4, J_H 163.9 Hz, J_{H2} 7.0 Hz, J_{H3} 8.4 Hz; s. 135.44; dd. 135.65, C-2/C-3, J_H 163.94 Hz, J_{H2} 7.55 Hz; s. 149.15; s. 152.04; s. 180.89; s. 188.74).

All data are represented in *Table 1*.

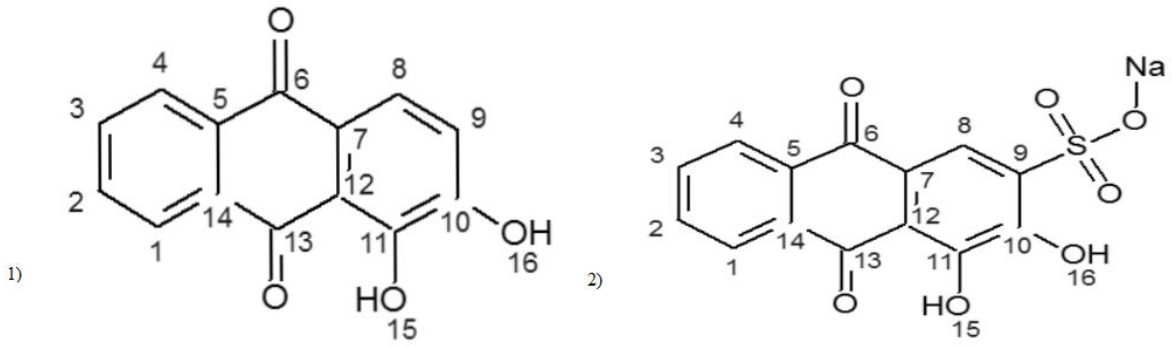

Figure 1. Structure of molecules: 1) alizarin, 2) alizarin red S

Table 1. ^{1}H-, ^{13}C- NMR, spectral data of alizarin and alizarin red S

No. C/H	Alizarin		No. C/H	Alizarin		No. C/H	Alizarin red S*		No. C/H	Alizarin red S*	
	δH	δC		δH	δC		δH	δC		δH	δC
1	8.379	125.43	8	7.873	127.68	1,4	8.21	134.71	8	7.89	118.78
2	7.958	125.43	9	6.785	119.12	2,3	7.92	135.65	9	-	-
3	7.976	123.09	-/16	8.368	-	2,3	7.9	127.29	-/16	11.451	-
4	8.361	128.24	-/15	**	-	1,4	8.17	127.06	-/15	12.624	-

*Assign was performed without calculation in author's program. Assign is based on article [5] and 2D spectrum.

**There is no line in the spectrum.

Conclusion

Proton and ^{13}C NMR spectra of alizarin and alizarin red S were obtained and lines were assigned.

These data will be used in the investigation of interaction of these two substances with peptide.

Acknowledgements

Experiments were performed at Center for Magnetic Resonance of St. Petersburg State University.

References

1. Lishuang Lv, Huadong Chen4, Chi-Tang Ho ,Shengmin Sanga Chemical components of the roots of Noni (Morinda citrifolia) and their cytotoxic effects //Fitoterapia 82 (2011) 704–708
2. S. Jeremic, N. Filipovic, A. Peulic, Z. Markovic. Thermodynamical aspect of radical scavenging activity of alizarin and alizarin red S. Theoretical comparative study// Computational and Theoretical Chemistry, 2014, v. 1047, p. 15–21.
3. G Zengin, NS Degirmenci, L Alpsoy, A Aktumsek Evaluation of antioxidant, enzymeinhibition, and cytotoxic activity of three anthraquinones (alizarin,purpurin, and quinizarin) // (2016) Vol. 35(5) 544–553
4. Саликов, В. А. Комолкин, А. В. Программа расчета спектров ЯМР изотропных жидкостей // Материалы конференции: тез. конф, 12 «Spinus» - Санкт-Петербургский гос. университет. 209-211.
5. Yuk Ping Chin, Siti Farhana Abdul Raof, Subathra Sinniah, Vannajan Sanghiran Lee, Sharifah Mohamad, Ninie Suhana Abdul Manan Inclusion complex of Alizarin Red S with b-cyclodextrin: Synthesis, spectral, electrochemical and computational studies //Journal of Molecular Structure 1083 (2015) 236–244

The sensitivity of local dynamics and its manifestation in NMR to excluded volume in dendrimers

Oleg V. Shavykin, Anatolii A. Darinskii[1,2], Igor M. Neelov[1,2], Frans A. M. Leermakers[3]

[1]St. Petersburg National Research University of Information Technologies, Mechanics and Optics (ITMO University)
[2]Institute of Macromolecular Compound of Russian Academy of Sciences
[3]Laboratory of Physical Chemistry and Colloid Science, Wageningen University, Dreijenplein 6, 6307 HB Wageningen, The Netherlands
E-mail: kupala-89@mail.ru

Introduction

Dendrimers are regular hierarchically branched polymers. Orientational mobility in dendrimers could be described by the second order orientational autocorrelation function (ACF):

$$P_2(t) = \frac{3}{2}\langle\frac{\big(r(0)r(t)\big)^2}{|r(0)|^2|r(t)|^2}\rangle - \frac{1}{2},$$

where $r(t)$ – for an internuclear vector in time t. Using this ACF we can find the spin–lattice relaxation rate T_{1H} for case ^{1}H:

$$\frac{1}{T_{1H}}(\omega_H) = A_0(H)[J(\omega_H) + 4J(2\omega_H)],$$

where ω_H – is the angular frequency, $A_0(H)$ – is a constant, which is insensitive to temperature or frequency, $J(\omega)$ – spectral density:

$$J(\omega) = 2\int_0^\infty P_2(t)\cos(\omega t)\,dt$$

Theory of NMR relaxation for flexibly dendrimers was developed in [1] using Gaussian model of dendrimer. This model does not consider effect of excluded volume interactions (phantom model) and position of maximum not depend on radial position of segment in dendrimer. For phantom model (q=0) position of maximum of $[1/T_{1H}(\omega_H)]$ for different shells are the same. But experimental data for different dendrimers demonstrate differences between local orientational mobility of inner and termial segments [2, 3].

Introduction of semiflexibility in Gaussian model [1] means introduction of correlation q between orientation of segments in different shells of dendrimers. Parameter q equal to average cosine between neighboring segments. Introduction of semiflexibility in Gaussian model leads to dependency of position maximum on radial position of segments in dendrimer.

Orientational dynamics of bonds

The effect of excluded volume (EV) interactions on the manifestation of the local dynamics in the spin–lattice NMR relaxation in dendrimers has been studied by using Brownian dynamics simulations. We have shown here the occurrence of shift of maxima of $[1/T_{1H}(\omega_H)]$ dependence due to introduction of angle potential in model of dendrimer with excluded volume interaction, if correlation parameter q is the same.

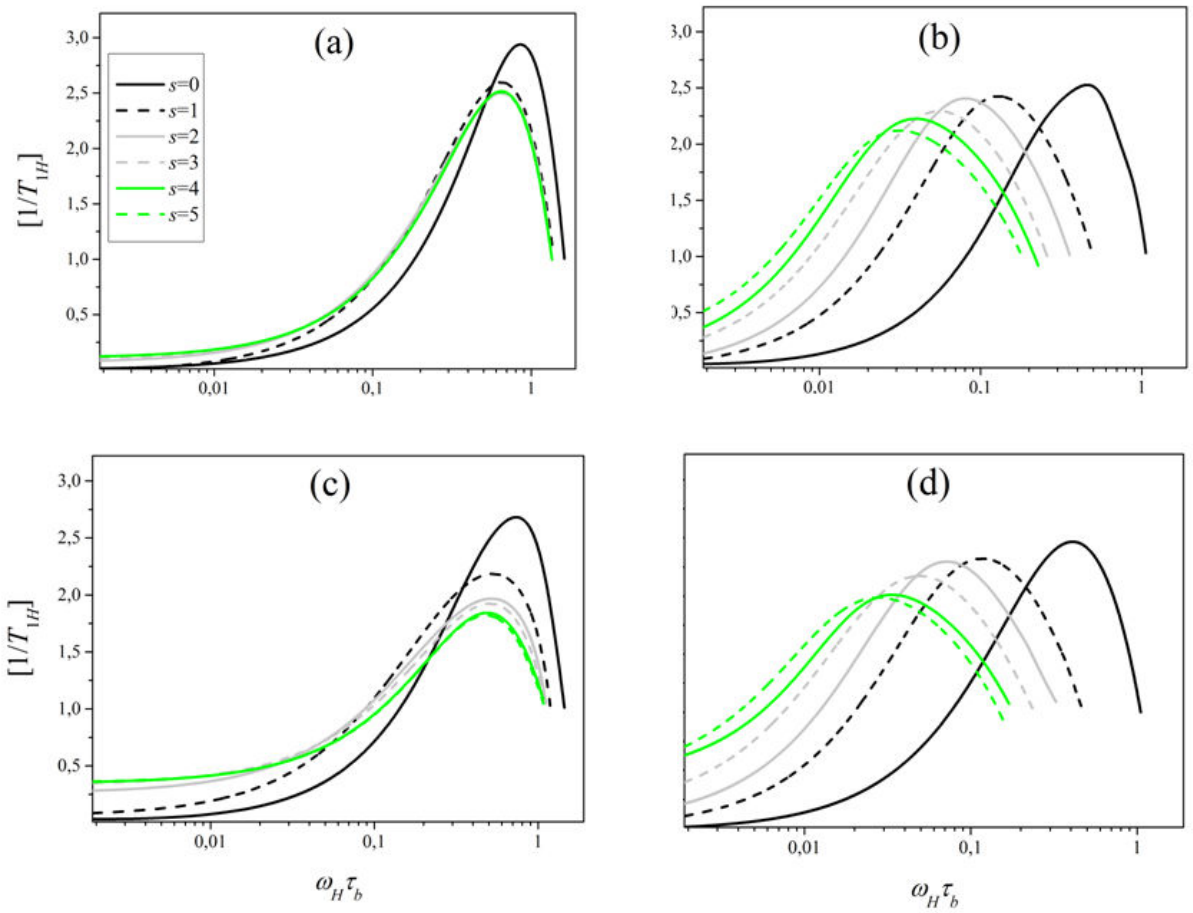

Figure 1. Frequency dependence of $[1/T_{1H}(\omega_H)]_s$ for bonds belonging to different subshells for the flexible (a), semiflexible (b) Ph and flexible (c), semiflexible (d) EV models [4, 5]

Manifestation of the orientational dynamics of segments in NMR relaxation

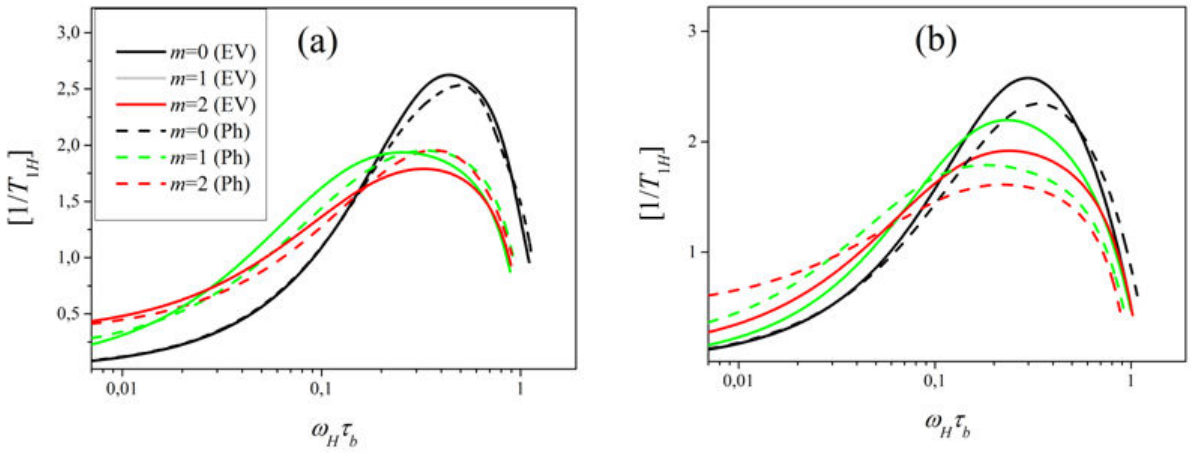

Figure 2. Frequency dependence of $[1/T_{1H}(\omega_H)]_m$ for segments belonging to different subgeneration for the symmetrical (a), asymmetrical (b) Ph and EV models [5]

We also have shown that the main effect of EV interactions consist in much stronger contribution of dendrimer rotation as whole to the dynamics of dendrimer segments in comparison with phantom models. After the exclusion of this contribution the manifestation of internal dynamics in spin–lattice NMR relaxation become practically insensitive to EV

interactions (see, fig. 2 (a)). In paper [6] it was shown, that low asymmetry of branching of dendrimer not influences the structural properties of dendrimers. We also have shown, that asymmetrical dendrimers demonstrates the same behavior in local dynamics, but the more the number of segments in dendrimer the stronger contribution of dendrimer rotation as a whole (see, fig. 2 (b)).

Acknowledgements

This work was partly supported by grant 074-U01 of Government of RF and RFBR grants 16-03-00775. Computing resources on supercomputers "Lomonosov" were provided by supercomputer center of Moscow State University [7].

References

1. D. A. Markelov, M. Dolgushev, Y. Y. Gotlib and A. Blumen. NMR relaxation of the orientation of single segments in semiflexible dendrimers // J. Chem. Phys., 2014, 140, 244904.
2. I.M.Neelov, D.A.Markelov, S.G.Falkovich, M.Yu.Ilyash, B.M.Okrugin, A.A.Darinskii Mathematical simulation of lysine dendrimers: temperature dependences // Polymer Science, Series C. 2013. V. 55. N 1. P. 154–161
3. D.A Markelov, S.G.Falkovich, I.M.Neelov, M.Yu. Ilyash, V.V.Matveev, E.Lahderanta, P.Ingman, A.A.Darinskii Molecular dynamics simulation of spin-lattice NMR relaxation in poly-L-lysine dendrimers. Manifestation of the semiflexibility effect // Physical Chemistry and Chemical Physics. 2015. V. 17. P. 3214–3226
4. O.V.Shavykin, I.M. Neelov, Anatolii A. Darinskii. Is the manifestation of the local dynamics in the spin–lattice NMR relaxation in dendrimers sensitive to excluded volume interactions? // Phys. Chem. Chem. Phys., 2016,18, 24307-24317.
5. O.V.Shavykin, E.V.Popova, A.A.Darinskii, I.M.Neelov, F.A.M.Leermakers Computer simulation of local mobility in dendrimers with asymmetric branching by brownian dynamics method. *Scientific and Technical Journal of Information Technologies, Mechanics and Optics*, 2016, vol. 16, no. 5, pp. 893–902
6. I.V.Mikhailov, A.A. Darinskii. Does symmetry of branching affect the properties of dendrimers? *Polymer Science. Series A*, 2014, vol. 56, no. 4, pp. 534–544.
7. V. Sadovnichy, A. Tikhonravov, V. Voevodin, V. Opanasenko Contemporary High Performance Computing: From Petascale toward Exascale, Boca Raton, 2013.

NMR study of photoisomerization of AzoTAB and CTAB when interacting with cardiomyocytes

Nataliia S. Shubina, Ekaterina S. Babicheva, Alexander M. Perepukhov, Alexander V. Maximychev, Sheyda R. Frolova, Konstantin I. Agladze

Moscow Institute of Physics and Technology (State University)

Introduction

E-isomers AzoTAB and CTAB (Fig. 1) may interact with the lipid bilayer, which can be used for the treatment of arrhythmia [1]. CTAB and AzoTAB have the ability to modulate voltage-gated ion channels of cardiomyocytes [2, 3].

Isomerization AzoTAB and CTAB are achieved through UV irradiation (365nm). Photoregulation is resulted by a double bond photoisomerization azobenzene and stilbene fragments, respectively (Fig. 1). In this paper, interaction AzoTAB and CTAB with neonatal rat cardiomyocytes was studied using high-resolution NMR spectroscopy.

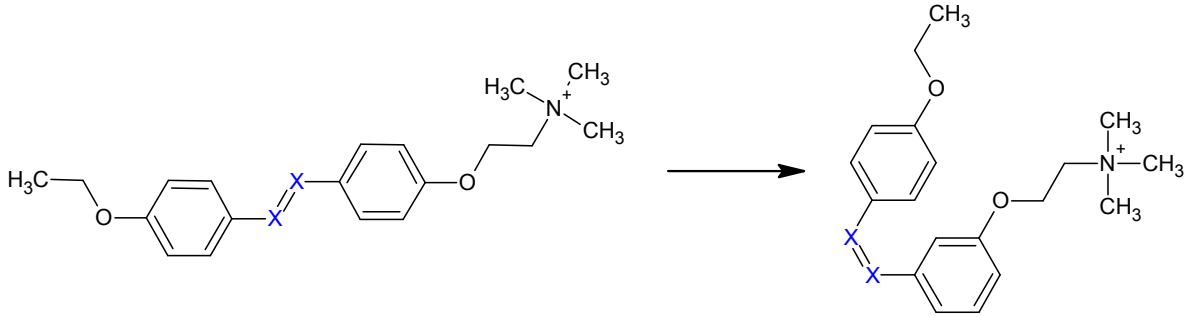

Figure 1. The photochemical isomerization of AzoTAB (X = N) and CTAB (X = C)

Results and discussion

It is found that the photoisomerization of AzoTAB is reversible ($K=3\times10^{-5}$ c^{-1}) and CTAB is irreversible. Bounded molecular mobility causes to a broadening of the signals in ^{1}H-NMR spectra and indicates on the interaction of *(E)*-AzoTAB with the cell membrane of cardiomyocyte.

UV *(E)-(Z)* isomerization causes a disturbance of the interaction between molecules AzoTAB and cell membrane that is observed as a significant narrowing of the signals in the spectrum of the mixture AzoTAB with a cell membrane. Analysis of ^{1}H-NMR spectra of AzoTAB and CTAB shows that the properties of CTAB differ from the properties of AzoTAB. Thus, E- CTAB interacts with the cell membrane, a broadening of the peaks. Unlike AzoTAB, after UV irradiation this binding is not lost, the Z-CTAB signals are significantly broadened.

Thus, high-resolution NMR spectroscopy show that AzoTAB and CTAB interacts with the cell membrane, the results correspond to the results obtained in experiments with a lipid bilayer. In addition, when Z-CTAB are added to cells insertion also takes place.This fact indicates that the ability of CTAB and AzoTAB modulating voltage-gated ion channels of cardiomyocytes is not associated with the formation of covalent bonds on irradiation.

References

1. Abbas A. Cardioprotective effect of resveratrol analogue isorhapontigenin versus omega-3 fatty acids in isoproterenol-induced myocardial infarction in rats // *J Physiol Biochem* 2016. V. 72(3)

2. Magome N., Kanaporis G., Moisan N., Tanaka K., Agladze K. Photo-controlofexcitation waves in cardiomyocyte tissue culture // *Tissue Eng Part* A. 2011. V. 17 I. p. 21–22.
3. Sheyda R. Frolova1, Olga Gaiko1, Valeriya A. Tsvelaya1, Oleg Y. Pimenov, Konstantin I. Agladze Photocontrol of Voltage-Gated Ion Channel Activity by Azobenzene Trimethylammonium Bromide in Neonatal Rat Cardiomyocytes // *PLoS One*. 2016 V. 11(3)

NMR analysis of calixarenes-sulfonic acids

N. A. Slesarenko[1], *A. V. Chernyak*[1,2]

[1]*Institute of Problems of Chemical Physics, Russian Academy of Sciences, Chernogolovka*
[2]*Science Center in Chernogolovka, Russian Academy of Sciences, Chernogolovka*
E-mail: wownik007@mail.ru

Due to their conformational flexibility, calixarenes have the ability to capture and retain various molecules and ions, forming the so-called guest-host structure.

Another promising but little studied feature of the calixarene structure is the formation of layered structures by them, which are stabilized as a result of the formation of strong intermolecular hydrogen bonds. In recent years have begun to show interest to water soluble sulfo calixarenes as potential solid electrolytes. High proton conductivity is associated with the formation of a layered structure. The layers contain water molecules bound to sulfo groups by means of hydrogen bonds.

The aim of this work was to establish the features of the structural and dynamic changes caused by the change in the number of water molecules included in the calixarene-sulphonic acid structure.

The high-resolution ^{1}H NMR spectra in D_2O have been obtained. It confirms the purity and corresponds to the spectra of the individual calixarenes.

^{13}C NMR spectra of high resolution in D_2O also confirm the structure of the samples under study. The $-CH_2$ group signal locates in the region of 30 ppm. It indicates that all compounds have a cone conformation.

The number of water molecules per molecule of calixarene from the 1H magic angle spinning spectrum for tetra calixarene at a relative humidity of 10% by the intensity of the number of signals has been determined. It amounted to about 12-13 water molecules. It was found that the SO_3H signal and water shifted to strong fields with increasing cycle. It indicates the weakening of hydrogen bonds of calixarenes with a large number of cycles. Analysis of the NMR spectra showed a marked rearrangement of the structure upon transition to calixarenes at 32% relative humidity.

When comparing the spectra of ^{13}C tetrasulfo calixarene at different humidities, it was found that the carbon signals of the $-CH_2$ group and the aromatic carbon atom bound to it are most sensitive to the change in the number of water molecules in the structure.

The self-diffusion coefficients on 1H nuclei were measured by the PFG NMR method. The nonexponential nature of diffusion decay indicates the presence of water molecules with different mobilities. A decrease in the coefficients of self-diffusion of mobile protons as the size of the calixarene molecule cycle is increased was found.

NMR study of $LiBH_4$ and solid solutions $LiBH_4$-LiI

Alexey V. Soloninin[1], Alexander V. Skripov[1], Line H. Rude[2], Torben R. Jensen[2], Yaroslav Filinchuk[3]

[1]Institute of Metal Physics, Ural Division of the Russian Academy of Sciences, S. Kovalevskoi 18, Ekaterinburg 620990, Russia
[2]Center for Materials Crystallography, Interdisciplinary Nanoscience Center (iNANO), and Department of Chemistry, Aarhus University, Langelandsgade 140, DK-8000 Aarhus C, Denmark
[3]Institute of Condensed Matter and Nanosciences, Universite catholique de Louvain, Place L. Pasteur 1, B-1348 Louvain-la-Neuve, Belgium
E-mail: alex.soloninin@imp.uran.ru

Introduction

Lithium borohydride, $LiBH_4$, containing 18.4 mass percent of hydrogen is considered as one of the most promising materials for hydrogen storage. $LiBH_4$ has an orthorhombic structure at low temperatures (LT) and undergoes a first-order phase transition to a hexagonal structure at $T_0 \approx 381$ K. This transition is accompanied by the 3 orders of magnitude increase in the electrical conductivity, so that the high-temperature (HT) phase of $LiBH_4$ can be considered as a superionic conductor. The HT phase of $LiBH_4$ can be stabilized down to low temperatures by a partial halide ion substitution of $[BH_4]^-$ anions. Such a substitution results in the formation of $Li(BH_4)_{1-y}I_y$ solid solutions with the hexagonal structure. Using the stabilizing effect of I^- substitution, it is possible to obtain compounds with rather high Li ion mobility at room temperature. The aim of the present work is to investigate the reorientational motion of BH_4 groups and Li diffusion in LT and HT phases of lithium borohydride and in $LiBH_4$–LiI solid solutions with 2:1, 1:1, and 1:2 molar ratios using ^1H, ^{11}B, and ^7Li NMR measurements.

Experimental results

The temperature dependences of the proton spin-lattice relaxation rates R_1 measured at three resonance frequencies for the low-temperature phase of $LiBH_4$ are shown in Figure 1.

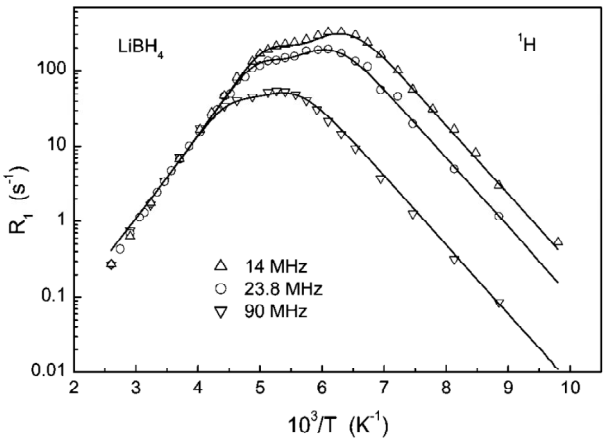

Figure 1. The proton spin-lattice relaxation rates measured at 14, 23.8 and 90 MHz as functions of the inverse temperature for the orthorhombic phase of $LiBH_4$. The solid curves show the simultaneous fits based on the two-peak model

The general features of the observed behavior of R_1 are typical of the relaxation mechanism due to nuclear dipole-dipole interaction modulated by thermally activated atomic motion. For this mechanism, the R_1 maximum is expected to occur at the temperature, at

which the atomic jump rate τ^{-1} becomes nearly equal to the resonance frequency ω. The data presented in Figure 1 exhibit the inflection point near 180 K; this suggests that the observed temperature dependence of R_1 can be described as a superposition of two peaks with different slopes. Our interpretation of the R_1 data for the low-temperature phase of $LiBH_4$ is based on assumption that each BH_4 tetrahedron participates in two types of rotational motion (most probably, two-fold and three-fold jump rotations) having different rates[1]. We have denoted the two types of motion assuming that $i = 1$ corresponds to the faster motion (i.e., the one giving rise to the R_1 peak at lower T). The results of the simultaneous fit based on the standard model with two types of motion are shown by solid curves in Figure 1. The values of the amplitude parameters resulting from the fits are $\Delta M_{HB1} = 8.2\times10^9$ s^{-2}, $\Delta M_{HH1} = 9.6\times10^9$ s^{-2}, $\Delta M_{HB2} = 4.0\times10^9$ s^{-2}, and $\Delta M_{HH2} = 4.6\times10^9$ s^{-2}, and the corresponding motional parameters are $\tau_{01} = (1.9\pm0.1)\times10^{-14}$ s, $E_{a1} = 0.182\pm0.003$ eV, $\tau_{02} = (3.1\pm0.2)\times10^{-15}$ s, and $E_{a2} = 0.251\pm0.004$ eV.

The transition from the low-temperature orthorhombic phase to the high-temperature hexagonal phase leads to a sharp increase in ^{1}H, ^{7}Li and ^{11}B relaxation rates[2]. The temperature dependences of the spin-lattice relaxation rates R_1^H, R_1^{Li}, and R_1^B measured at different resonance frequencies for the HT phase of $LiBH_4$ are shown in Figure 2. As can be seen from Figure 2, all the spin-lattice relaxation data for different nuclei (^{1}H, ^{7}Li and ^{11}B) and at different resonance frequencies are satisfactorily described in terms of a single thermally-activated process of Li diffusion with $\tau_0 = 1.1\times10^{-15}$ s and $E_a = 0.56$ eV.

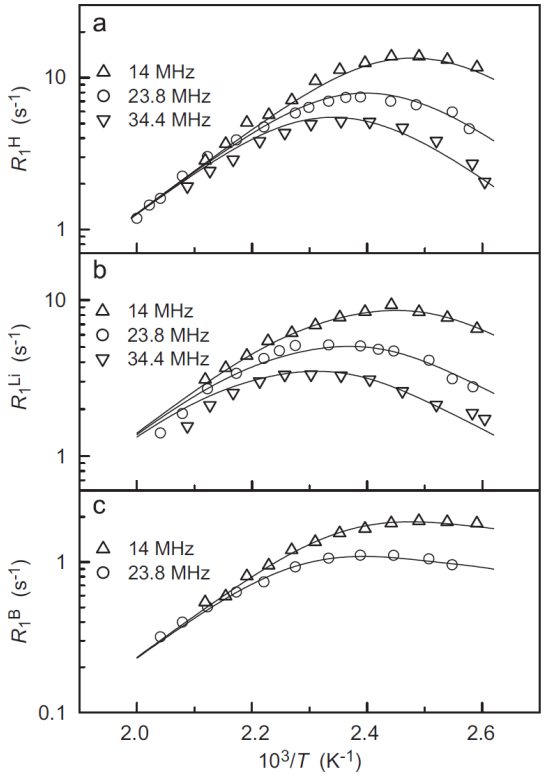

Figure 2. The ^{1}H, ^{7}Li and ^{11}B spin-lattice relaxation rates as functions of the inverse temperature for the high-temperature phase of $LiBH_4$. The solid curves show the simultaneous Bloembergen – Purcell – Pound fits to the data with the fixed parameters of Li motion: (a) the ^{1}H relaxation data; (b) the ^{7}Li relaxation data; (c) the ^{11}B relaxation data

To study the reorientational motion of the BH_4 groups and the translational diffusion of Li^+ ions in $LiBH_4$–LiI solid solutions with 2:1, 1:1, and 1:2 molar ratios, we have measured the ^{1}H, ^{11}B, and ^{7}Li NMR spectra and spin-lattice relaxation rates in these compounds over

the temperature range of 18 – 520 K. For all the studied $LiBH_4$-LiI solid solutions, the measured temperature dependences of the proton spin-lattice relaxation rate R_1^H exhibit two peaks. As an example of the data, Figure 3 shows the behavior of the proton spin-lattice relaxation rates measured at three resonance frequencies for the 2:1 sample.

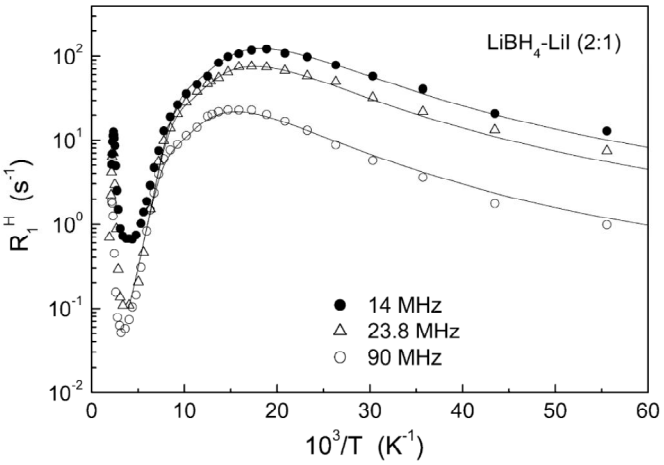

Figure 3. Proton spin-lattice relaxation rates measured at 14, 23.8 and 90 MHz for $LiBH_4$-LiI (2:1) as functions of the inverse temperature. The solid lines show the simultaneous fits of the model with a two-peak distribution of the activation energies to the data in the range of the low-temperature $R_1^H(T)$ peak

The analysis of the measured ^1H, ^{11}B, and ^7Li spin-lattice relaxation rates for hexagonal $LiBH_4$–LiI solid solutions with 2:1, 1:1, and 1:2 molar ratios has revealed the parameters of BH_4 reorientations and Li diffusion in these compounds. The low-temperature rates of BH_4 reorientations increase with increasing iodine content. Our results are consistent with a coexistence of at least two types of reorientational processes with different characteristic rates, and each of these processes can be described by a certain distribution of the activation energies[3]. For the faster reorientational process, the average activation energies derived from our data are 53 ± 4 meV, 39 ± 4 meV, and 33 ± 4 meV for the samples with 2:1, 1:1, and 1:2 molar ratios, respectively. For the slower process, the corresponding average activation energies are 104 ± 7 meV (2:1), 57 ± 8 meV (1:1), and 49 ± 7 meV (1:2). Above 350 K, BH_4 reorientations in $LiBH_4$–LiI solid solutions become too fast to be probed by NMR, and the measured spin-lattice relaxation rates in this range are governed by the translational diffusion of Li ions. For the studied $LiBH_4$–LiI samples with 2:1, 1:1, and 1:2 molar ratios, the Li jump rates are found to decrease with increasing iodine content. The activation energies for Li diffusion derived from our data are 0.63 eV, 0.65 eV, and 0.68 eV for the samples with 2:1, 1:1, and 1:2 molar ratios, respectively.

Acknowledgements

This work is supported by the Russian Federal Agency of Scientific Organizations under Program "Spin" No. 01201463330 and the Russian Foundation for Basic Research under Grant No. 15-03-01114.

References

1. A. V. Skripov, A. V. Soloninin, Y. Filinchuk, D. Chernyshov. – *J. Phys. Chem. C,* **112**, 18701-18705 (2008).
2. A. V. Soloninin, A. V. Skripov, A. L. Buzlukov, A. P. Stepanov. – *J. Solid State Chem.*, **182**, 2357-2361 (2009).
3. A. V. Skripov, A. V. Soloninin, L. H. Rude, T. R. Jensen, Y. Filinchuk. – *J. Phys. Chem. C,* **116**, 26177-26184 (2012).

Poster Session

Using MRI to visualize blood derivatives

V. Y. Adelson[1], V. V. Frolov[1], V. M. Cheremisin[2]

[1]Saint-Petersburg State University, Faculty of Physics
198504, St. Petersburg, Peterhof, st. Ulyanovskaya, 1
[2]Saint-Peterburg State University, Faculty of Medicine
199034, St. Petersburg, V.O. 21-line, 8a
E-mail: adelson_v@outlook.com

When interpreting MRI data in case of posttraumatic hemorrhage, it is important to know about the development of posttraumatic hematoma and to visualize it using MR tomograms in various regimes. SWI (Susceptibility Weighted Imagining) allows you to visualize traces of tiny hemorrhages after a long time, depositions of the brain and also to contrast venous blood decently [1, 2].

An experiment has been conducted on a high-field tomograph Siemens Magnetom Avanto (magnetic field strength is 1.5 T). The subject of the study was human blood with an addition of a 0.9% NaCl solution. The change in the visualization of blood in time was of particular interest. Impulse sequences of the spin echo and SWI sequence have been used (Fig. 1, 2). The measurements have been being carried out for 14 days. Sequence parameters in the experimental part were chosen according to the most informative contrast (short TE and TR for T1-weighted images and long ones for T2-weighted images). Table 1 shows the distribution of signal intensity for ampoule's height of one of the samples during measurements using different sequences.

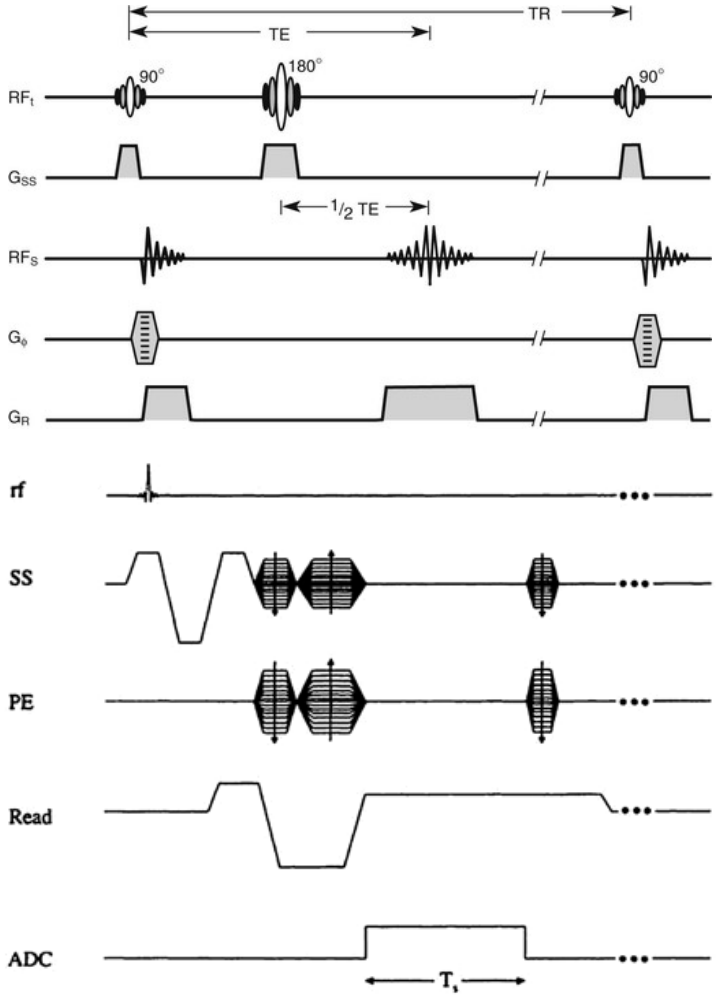

Figure 1. Spin-echo impulse sequence diagram

Figure 2. Gradient echo impulse sequence diagram for obtaining perceptually-weighted images

Table 1. Distribution of signal intensity

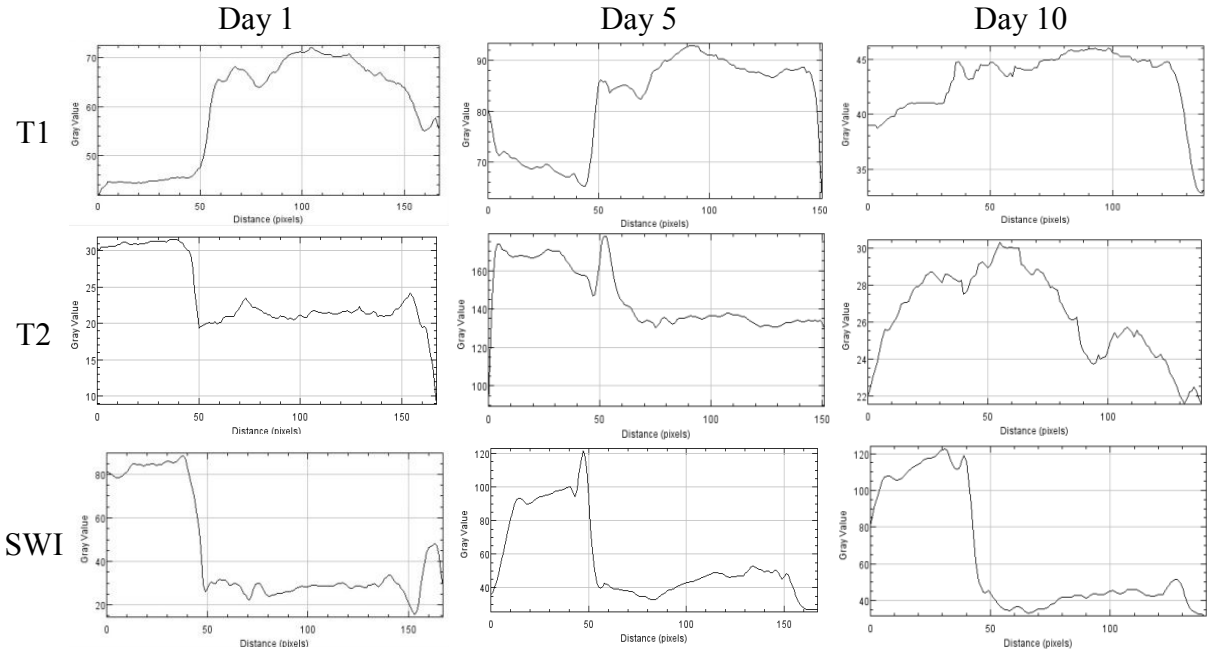

References

1. Haacke EM., Xu Y., Cheng YN., JR Reichenbach. Susceptibility weighted imaging (SWI) // Magnetic Resonance in Medicine, Vol.52(3), 2004. – P. 612 - 618.
2. Haacke EM., Xu Y., Cheng YN., JR Reichenbach Susceptibility-Weighted Imaging: Technical Aspects and Clinical Applications Part1 and Part 2// Physics Review, AJNR Am J Neuroradiol 30:19 –30, Jan 2009

Terbium(III) tetraphenylporphyrinate as potential single molecular magnet

D. Yu. Aleshin, A. A. Pavlov, S. V. Dudkin

[1]*Higher Chemical College of the Russian Academy of Science*
[2]*A. N. Nesmeyanov Insitute of Organoelement Compounds. 119991, Moscow, Vavilova st., 28*
E-mail: dima.aleshin26@gmail.com

Introduction

The porphyrins and metalloporphyrins are versatile functional dyes with a wide range of applications. At last decade the lanthanide mono- and bis-porphyrinates have been investigated as a single-molecular magnets [1, 2]. However, until recently, lanthanide mono-porphyrinates have been less investigated in contrast with their sandwiches analogues.

The presence of a paramagnetic ion in the complex leads to a large shift and broadening of its signals in the NMR spectra due to their interaction with unpaired electrons. This interaction is consists of two parts: diamagnetic and paramagnetic [3], the latter including a contact shift(CS) and a pseudocontact shift(PCS) contributions:

$$\delta_{obs} = \delta_{dia} + \delta_{CS} + \delta_{PCS} \quad (1)$$

(δ_{obs} - observed chemical shift, ppm; δ_{dia} - diamagnetic contribution; δ_{cs} - contact shift(2) that arises from spin polarization conveyed through molecular orbitals and becomes negligible at a distance of 5-6 covalent bonds; δ_{pcs} - pseudocontact shift (3) that arises from dipolar coupling between magnetic moments of a nucleus and of an unpaired electron and has a $1/r^3$ dependence on the distance to the paramagnetic species).

1) Contact shift.

$$\delta_{cs} = \frac{A2\pi}{h}\frac{g_e\mu_b S(S+1)}{3\gamma kT}. \quad (2)$$

2) Pseudocontact shift.

$$\delta_{iso}^{pc} = \frac{1}{12\pi r^3}\left(\Delta\chi_{ax}(3cos^2\theta - 1) + \frac{3}{2}\Delta\chi_{rh}sin^2(\theta)\,cos(2\varphi)\right) \quad (3)$$

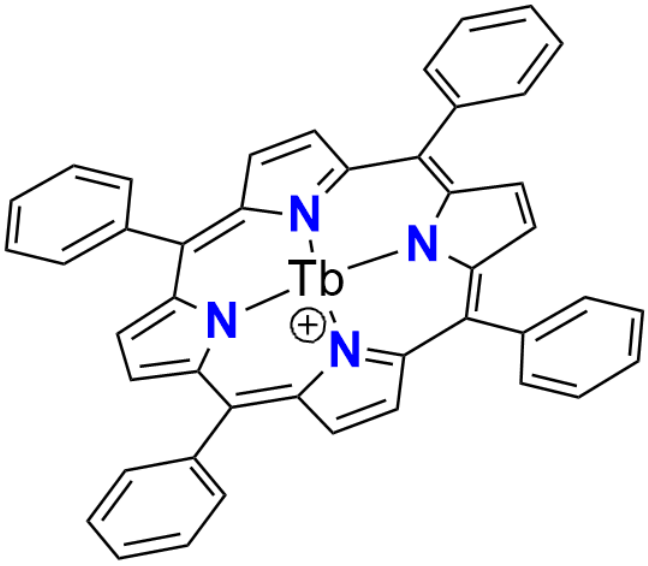

Figure 1. Structure of the studied complex

Results and discussion

The terbium(III) mono-porphyrinate have been obtained with moderate yield via refluxing of a metal-free *meso*-tetraphenylporphyrin with a terbium(III) acetylacetonate in boiling 1,2,4-trichlorobenzene [4].

For cations of lanthanide and actinides, the contact contribution can be neglected, since 4f, the level containing unpaired electrons is screened by 5s and 5p levels and as a result, practically does not interact with ligands [3]. The values of pseudocontact shifts depend on the polar coordinates of the nucleus in the magnetic susceptibility tensor frame r and θ and on the anisotropy of this tensor $\Delta\chi$. Formula (3) in the case of axial symmetry takes the form (4).

$$\delta_{iso}^{pc} = \frac{1}{12\pi r^3}(\Delta\chi_{ax}(3cos^2\theta - 1) \quad (4)$$

We can choose a value $\Delta\chi_{ax}$, providing the best convergence between experiment and calculations. The calculated values of chemical shifts for the analyzed nuclei are determined by the formula (3). The use of the described approach showed good convergence of the experimental and calculated data, as demonstrated in Fig. 2. At $\Delta\chi_{ax} = 5.85 * 10^{-31} m^{-3}$, the standard deviation is 0.9931.

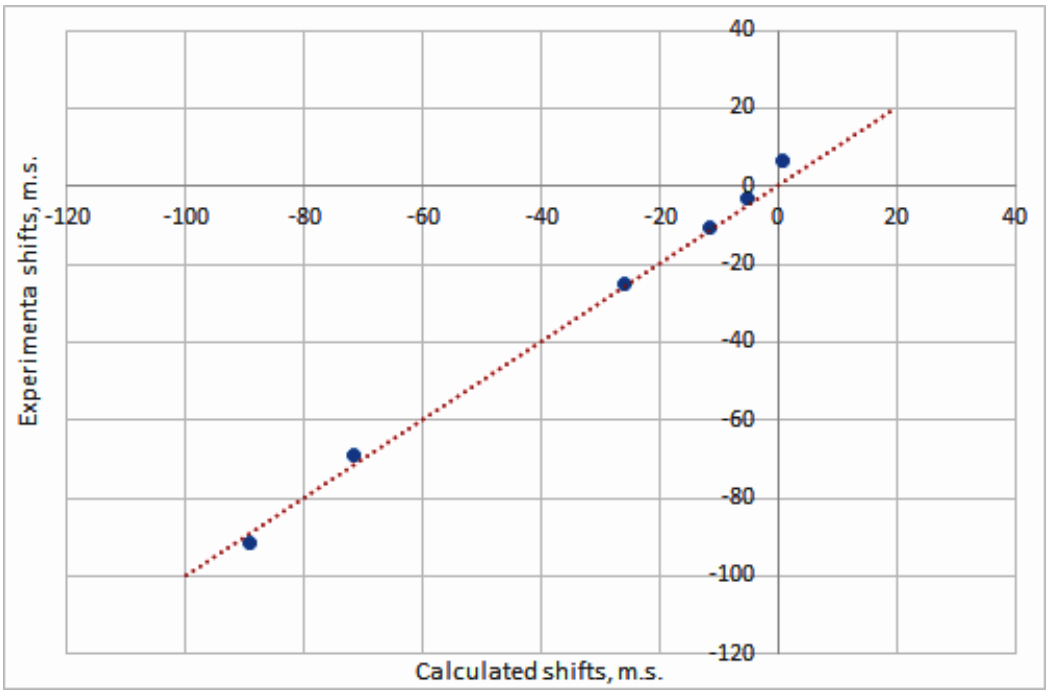

Figure 2. Experimental and calculated paramagnetic shifts in the ^1H spectra of the complex

Acknowledgements

The financial support from the Russian Science Foundation (project 14-13-00724) and the Russian Foundation for Basic Research (grants 16-03-00368) are gratefully acknowledged.

References

1. Wang H, Wang B. W., Bian Y., Gao S, Jiang J.–*Coord. Chem. Rev.,*306, 195–216 (2016).
2. Sunri Lee S., Ogawa T. – *Chem. Lett.,* 46, 10-18 (2017).
3. Bertini I., Luchinat C., Parigi G, Ravera E. NMR of paramagnetic molecules applications metallobiomolecules and models, Elsevier B.V., Amsterdam, 2017.
4. Wong C.P.– *Inorg.Synth.,*22**,** 156-162 (1983).

NMR self-diffusion study of amino acid ionic liquids based on 1-methyl-3-octylimidazolium in water

Yu. S. Chernyshev, A. S. Koneva, E. A. Safonova

St. Petersburg State University, Russia, 199034, St. Petersburg, Universitetskaya nab., 7/9.
E-mail: a.koneva@spbu.ru

Amino acid ionic liquids (AAILs) are a novel class of chiral ionic liquids, which properties expand significantly the field of their application in various technologies. AAILs are considered as the chemicals with higher biodegradability, lower toxicity and can be utilized as a reaction medium in gas separation or heterogeneous catalysis or as a selector in the chiral liquid extraction etc. [1-4]. The thermophysical properties of AAILs are strongly depend on both the side-chain structure of the amino acid anion and the alkyl chain length of imidazolium cation. In the present work, the molecular transport properties of long-chain AAIL (1-methyl-3-octylimidazolium) with two amino acid anions (L-Leucine and L-Valine) in aqueous (D_2O) solutions were investigated by means of the self-diffusion coefficients at the temperature range 273-343 K for the IL's concentrations below and above its critical micelle concentration (cmc). The CMC values for both AAILs in water are assumed to be close to the CMC value for the aqueous solution of 1-methyl-3-octylimidazolium glutamate [C_8mim][Glu] [4], i.e. CMC ~ 0.2 mol/L.

^{1}H NMR diffusion experiments were performed at the Centre for Magnetic Resonance, St. Petersburg State University on the 500 MHz Bruker Avance III spectrometer equipped with GREAT 1/60A gradients and 5 mm MIC DIFF/30 probe with ^{1}H insert. The self-diffusion coefficients were measured by pulse gradient stimulated echo (PGSTE) NMR for cation, anion and water spectral components.

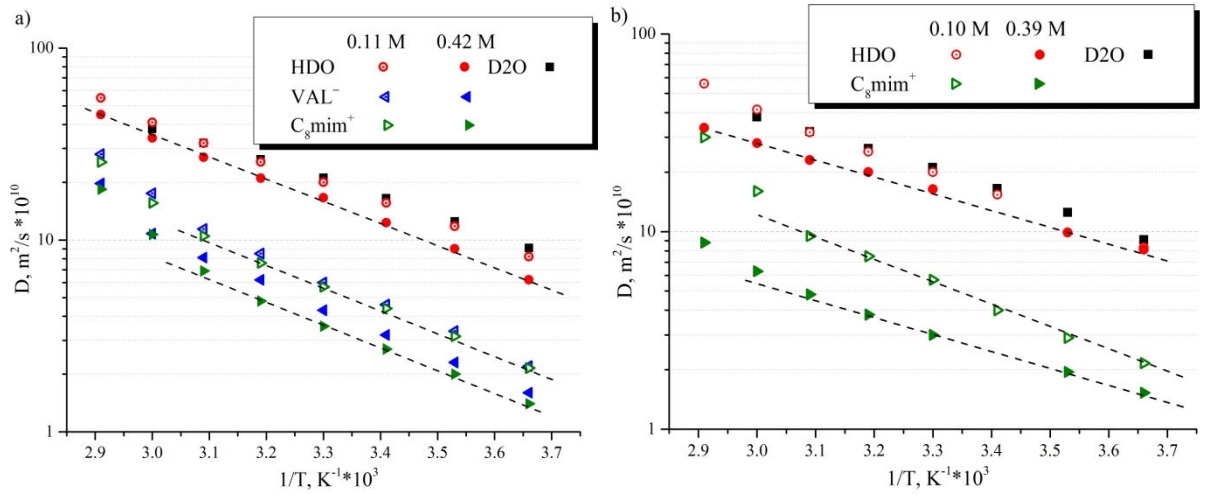

Figure 1. Temperature dependencies of the measured self-diffusion coefficients in aqueous solution of [C_8mim][Val](a) or [C_8mim][Leu] (b) of heavy water (circles), anion (left triangle), cation [C_8mim]$^+$ (right triangle) or free heavy water (squares). Open symbols are for the AAIL concentrations 0.11 mol/L (a), 0.10 mol/L (b), full symbols are for 0.42 mol/L (a) or 0.39 mol/L (b) of AAILs

As following from the data (Figures 1), the temperature dependences in the range of 273 ÷ 323 K have Arrhenius character. The activation energy of translational movement E_a in the range 0.05 ÷ 0.4 mol/L for [C_8mim][Val] retains its value both for the solvent (D_2O), and for anion and cation, that is typical for the structure of the free water ($E_a \simeq 19$ kJmol^{-1}). However for [C_8mim][Leu] the value of $E_a \simeq 19$ kJmol^{-1} is retained only for the small AAIL's concentrations (namely, at 0.05 ÷ 0.1 mol/L of AAIL, i.e. below the cmc). For the

concentration of AAIL 0.39 mol/L (Figure 1b), some decrease in the value of $E_a \simeq 14$ kJmol^{-1} is observed. This may indicate a violation of the structure of the solvent. In the range 323 ÷ 343 K, a deviation from linearity occurs for all the D(1/T)-dependences for anions and cations, what associated with the destruction of the aggregate structure.

Acknowledgements

This work is supported by the grant RFBR 16-03-00723a.

References

1. F.Tang, Q.Zhang, D.Ren, Z.Nie, Q.Liu. S.Yao. Functional amino acid liquids as solvent and selector in chiral extraction. J. Chromatography A, **1217 (28)**, 4669-4674, (2010).
2. K.Fukumoto, M.Yoshizawo, H.Ohno. Room temperature ionic liquid from 20 natural amino acids. J.Am. Chem. Soc., **127 (8)**, 2398-2399 (2005).
3. R. Gardes, R.Ge, P.Goodrich, C.Hardacre, A.Hussein, D.Roonley. Thermophysical properties of amino acid-based ionic liquids. J.Chem. Eng. Data, **55 (4)**, 1505-1515 (2009).
4. E.Alopina, E.Safonova, I.Pukinsky, N.Smirnova. Liquid- liquid equilibria in aqueous mixtures of alkilmrthylimidazolium glutamate with potassium carbonate and some physicochemical properties of aqueous [$C_n$mim][Glu](n=4,6,8) solutions. J.Chem.Eng.Data, **61 (6)**, 2013–2019 (2016).

^{1}H-NMR based metabonomics as a potential tool to assess cardiotoxicity in drug development

Matthieu Dallons, Manuel Podrecca, Jean-Marie Colet

Department of Human Biology and Toxicology, Faculty of Medicine & Pharmarcy, University of Mons, Belgium
E-mail: matthieu.DALLONS@umons.ac.be
http://www.umons.ac.be

Introduction

Currently, the main cause of drug post-approval withdrawal from the market is cardiovascular toxicity. Indeed, safety cardiovascular issues account for 45% of the total post-approval withdrawal, compared to 32% for hepatic issues [1]. The severity and the high incidence of cardiovascular toxicity in the late-stage of clinical drug development can lead to several consequences: restrictions of medical use, special pre- and/or post-approval monitoring and drug withdrawal. However, cardiovascular toxicity accounts only for 9% of drug attrition during phase I of clinical development [2]. The data suggest that there is a need to develop more predictive methods to assess cardiotoxicity in preclinical studies and in early stages of clinical trials to avoid the progression of drug candidates with a high risk for the cardiovascular system. Therefore, a ^{1}H-NMR based metabonomics was used to reassess the cardiotoxicity of 2 nonsteroidal anti-inflammatory drugs (NSAIDs), Diclofenac and Rofecoxib, recently incriminated with an increased incidence of heart infarct [3, 4].

Methods

Two molecules were selected for our investigations : Diclofenac and Rofecoxib. The SHR and DAHL/SS rat strains were used as a hypertension model in view to potentiate the NSAIDs cardiotoxicity. One study was performed for the Diclofenac in SHR rats. For the Rofecoxib, one study in SHR rats and one study in DAHL/SS rats were carried out. The rats were exposed *per os* daily to the molecules during a 28 days treatment and were randomly divided into 3 groups: a control group, a low dose group and a high dose group. Urine and blood samples were collected at different times during the treatment. The rats were euthanazed at different times of the studies for cardiac histological investigations. For each study, a metabonomics analysis was carried out on the urine samples, using a 500,16 MHz Bruker Avance spectrometer with a 5 mm DUX 3H-1H probe. A multivariate data analysis was performed to highlight discriminant metabolites concentration changes. The data obtained were compared to data from histological and *serum* conventional protein biomarkers measurement.

Results and conclusions

Myocardial histological analysis did not show any difference between the exposed and control rats. Moreover, no significant change was found in the measurement of 3 conventional protein biomarkers (cardiac troponin I (cTnI), cardiac myosin light chain-1 (CMLC-1) and myoglobin). The metabonomics study identified metabolic changes in the rats exposed to the high dose of Diclonefac and Rofecoxib. These changes allowed us to highlight several biochimical pathways alterations, which could be linked to early myocardial necrosis events: Krebs cycle alteration, acidosis with creatinine synthesis increase, oxidative stress, osmotic stress, choline and purines metabolism disturbance and adaptative protection mechanisms such as cellular osmolytes concentration adaptation and glutathione synsthesis.

Acknowledgements

This work was funded by the Walloon Region (Belgium) in the context of the First Spin-off project "Optimized Preclinical Toxicological Assessment".

We sincerely thank the department of General, Organic and Biomedical Chemistry (Faculty of Medicine & Pharmacy, University of Mons) for the technical support related to the 1H-MRN spectrometry.

We are grateful to the department of Histology (Faculty of Medicine & Pharmacy, University of Mons) for the assistance provided in our histological investigations.

References

1. Ferri N, Siegl P, Corsini A, et al. Drug attrition during pre-clinical and clinical development: understanding and managing drug-induced cardiotoxicity. Pharmacology & Therapeutics. 2013 Jun; 138(3):470–84.
2. Sibille M, Deigat N, Janin A, et al. Adverse events in phase-I studies: a report in 1015 healthy volunteers. Eur J Clin Pharmacol. 1998 Mar; 54(1):13–20.
3. Bhosale U, Quraishi N, Yegnanarayan R, et al. A cohort study to evaluate cardiovascular risk of selective and nonselective cyclooxygenase inhibitors (COX-Is) in arthritic patients attending orthopedic department of a tertiary care hospital. Nigerian Medical Journal. 2014; 55(5):417.
4. Harirforoosh S, Asghar W, Jamali F. Adverse effects of nonsteroidal antiinflammatory drugs: an update of gastrointestinal, cardiovascular and renal complications. Journal of Pharmacy & Pharmaceutical Sciences. 2014; 16(5):821–47.

Relative influence of LF and microwave resonance in quantum magnetometers system with laser pumping of alkali atoms

Sergey V. Ermak, Eduard A. Sagitov, Vladimir V. Semenov

Dept. of Quantum electronics, Peter the Great St. Petersburg Polytechnic University, Saint Petersburg, 195251, Russia
E-mail: e-sagitov@mail.ru

Introduction

In paper of authors [1] results of researches of long term stability of the measured frequency of two quantum magnetometers with laser pumping of vapors ^{87}Rb in function of averaging time and correlation coefficient of the detected signals were provided. One of the magnetometers was based on a LF spin generator principle, while the second one was built as passive microwave spectrometer with a resonance frequency lock loop. By this device the effect of relative compensation of different light shift components of resonance frequency of magnetometers [2] was researched, however at the same time the inevitable relative influence of LF and microwave channels connected to effect of coherence circulation between hyperfine structure states of alkali atoms wasn't considered [3, 4].

Theory of "dressed" atom in quantum magnetometers system

To a certain extent this lack is removed by the represented work in which frequency shifts in the LF and microwave channels of a magnetometers tandem connected to simultaneous force on alkali metal atoms of resonant radio fields are analyzed. Physical nature of such frequency shifts is associated with coherence circulation between magnetic sublevels of an alkali atom "dressed" by spin oscillator LF field. Absolute value of this shift strongly depends on magnetic-dipole transition number and reaches its maximum at 0-0 microwave transition, which is commonly used in atomic frequency standards.

In accordance with quantum theory of the "dressed" atom, simultaneous action of the LF and microwave fields on alkali atoms yields in multiphoton absorption and reemission of LF field quants, and probing microwave field absorption. [5] The spectrum of microwave transitions between the sublevels of the hyperfine structure takes the form of the central group of satellite lines. As an example, arrows on fig.1 show the possible microwave transitions between the hyperfine structure sublevels of alkali "dressed" atom with a nuclear spin of 3/2 for the center line.

For example, in accordance with Figure 1 at 0-0 resonance frequency transitions, indicated in Table 1 are induced simultaneously. In the second column of the table probabilities of the corresponding transitions are indicated.

Table 1. Microwave transitions probabilities, $F=1, m_F \leftrightarrow F=2, m_F$

$F = 1, m_F \leftrightarrow F = 2, m_F$ transitions	**Probability of transition**
$F = 1, m_F = -1 \leftrightarrow F = 2, m_F = 1$	$\frac{3}{64}\left[J_0\left(\frac{\omega_1}{\omega}\right) - J_0\left(3\frac{\omega_1}{\omega}\right)\right]^2$
$F = 1, m_F = 0 \leftrightarrow F = 2, m_F = 0$	$\frac{1}{64}\left[J_0\left(\frac{\omega_1}{\omega}\right) + 3J_0\left(3\frac{\omega_1}{\omega}\right)\right]^2$
$F = 1, m_F = 1 \leftrightarrow F = 2, m_F = -1$	$\frac{3}{64}\left[J_0\left(\frac{\omega_1}{\omega}\right) - J_0\left(3\frac{\omega_1}{\omega}\right)\right]^2$

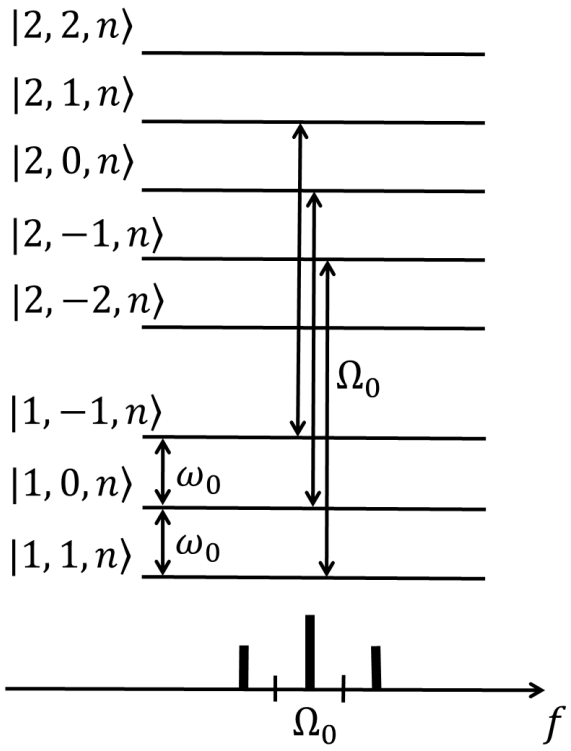

Figure 1. The spectrum of microwave transitions "dressed" alkali atom with a nuclear spin equals 3/2

Experiment

Experiments were provided in the conditions of optical pumping of laser source which is set up on LF D_2 - line component of transition of $S_{1/2}$-$P_{3/2}$ from hyperfine structure level with $F_g = 2$ where the most polarization of alkali atoms is reached. Tuning of the laser on a high-frequency component from HFS level with $F_g = 1$ of main state doesn't give positive result because of feedback omission owing to the low concentration of atoms on considered level. Other situation takes place in case laser pumping of D_1 - line of a head doublet. In this case, as shows elementary calculation of diagonal elements difference of density matrix, it is possible to receive higher level of atoms polarization both on a microwave transition, and in structure of magnetic levels with $F_g = 2$ and $F_g = 1$. In the experiment with laser pumping of D_1 - line the tandem of magnetometers worked both at LF components of electrodipole transition of this line (transitions of $F_g = 2 \leftrightarrow F_e = 1$ and $F_g = 2 \leftrightarrow F_e = 2$) and at a short wave component of $F_g = 1 \leftrightarrow F_e = 2$, though with considerably smaller signal-to-noise ratio. The last fact has a basic role in a choice optimal pumping mode which would allow to realize the minimum level of a flicker noise of Allan deviation in function of averaging time [6]. Equality of intensity of the detected signals in a microwave and LF channels of a magnetometers tandem is satisfied to such conditions as both of these channels have equivalent value. The relative influence of a microwave and LF signals shown as in dynamics of their intensity and spectrum changing. As an example in fig. 2 the experimental recordings of the self-generating magnetometer signal and a microwave absorption spectrum of Rb^{87} atoms are provided when scanning frequency field of microwave diapason.

Relative influence of LF and the microwave channels in magnetometers tandem was checked during the experiment in two modes: a) measurements of a frequency shift of the spin generator $\delta\nu_{SG}$ at the fixed detuning of microwave frequency $\delta\nu_{UHF}$; b) measurements of a frequency shift of the microwave resonance $\Delta\nu_{UHF}$ at the fixed detuning of the spin generator frequency $\Delta\nu_{SG}$ due to change of phase shift in feedback circuit.

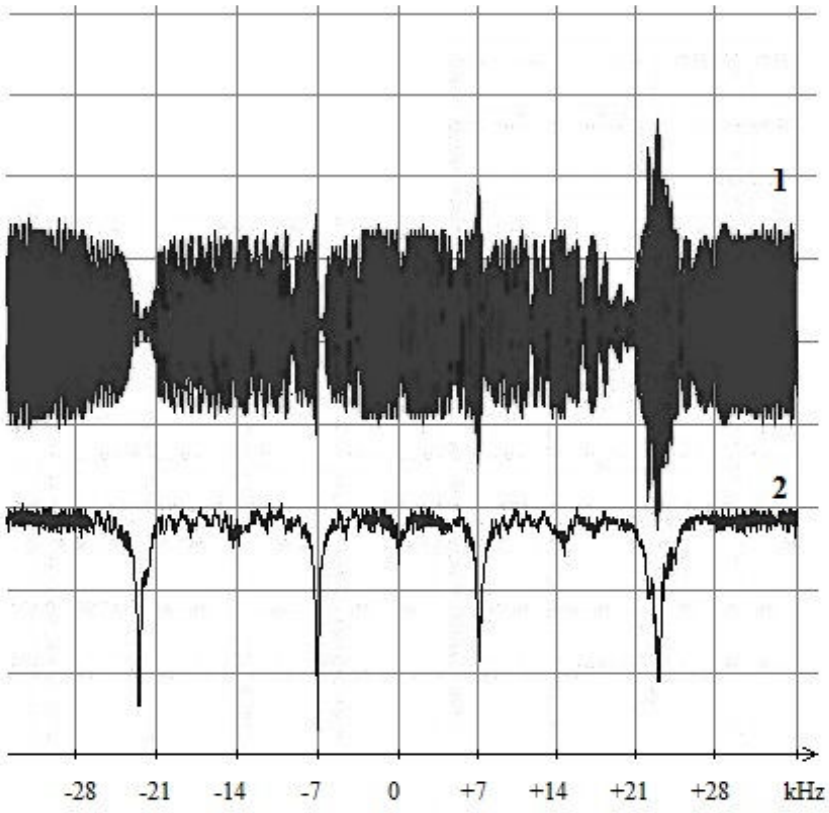

Figure 2. Recordings of the self-generating magnetometer signal and a microwave absorption spectrum of optical-oriented Rb^{87} atoms: 1 – signal of self-generating magnetometer, 2 – absorption signal of RF resonance in case of scanning frequency field of microwave diapason

The experiment showed a radical difference of interaction of LF and microwave channels tandem of magnetometers while they are working in modes "a" and "b": so for example, when the same artificial deviations $\delta\nu_{UHF}$ and $\Delta\nu_{SG}$ in magnetic field of 0.01 Oe $\delta\nu_{SG}$ respect to $\Delta\nu_{UHF}$ was the order of magnitude of 10^2.

References

1. Baranov A. A., Ermak S. V., Sagitov E. A., Smolin R. V. and Semenov V. V. – JEPT, 121(3), 393-403 (2015).
2. Happer W. - Review of Modern Phys., 44(2), 170-249 (1972).
3. Mathur B. S., Tang H., Happer W. - Phys. Rev., 171(1), 11-19, (1968).
4. Kornienko L. S., Mayorshin V. V., Kotkin L. A. and Umarkhodgaev R. M. - Optics and Spectroscopy, 53(6), 370–372 (1982).
5. Haroche S. - Ann. De Phys.6, 4-5, 189-387 (1971).
6. Riehle F. – "Frequency Standards: Basics and Applications" (Wiley-VCH), 2004.

Study of oil model sample's by NMR

Dmitry Ivanov

Faculty of Physics, Kazan Federal University
E-mail: f.ma.dima@mail.ru

Introduction

In nowadays the production of high-viscosity oil is becoming an increasingly urgent issue, as the stocks of light oil are rapidly depleting. Qualitative and effective work with such systems in the field of solving fundamental and applied problems directly depends on a deep and comprehensive analysis of various properties, in particular the influence of the component composition on the characteristics of oil [1, 2].

In our opinion, an essential impulse of development in this area could be obtained in the case of the implementation of model series of oil samples with a prescribed and, consequently, controlled composition. Such an approach on the one hand will make it possible to establish the influence of the component composition of oil on the magnetic resonance characteristics of oil. On the other hand, it is the first step towards constructing a unique correlation between the rheological properties of oil and the characteristics of nuclear magnetic resonance (NMR).

Discussion of results

As we said earlier, the existing approach to constructing correlation dependencies between the dynamic viscosity η and the relaxation characteristics for oil is highly controversial. Therefore, in order to unambiguously interpretation the influence of some component (in our case of resin) on the characteristics studied, was studied a model oil-resin sample.

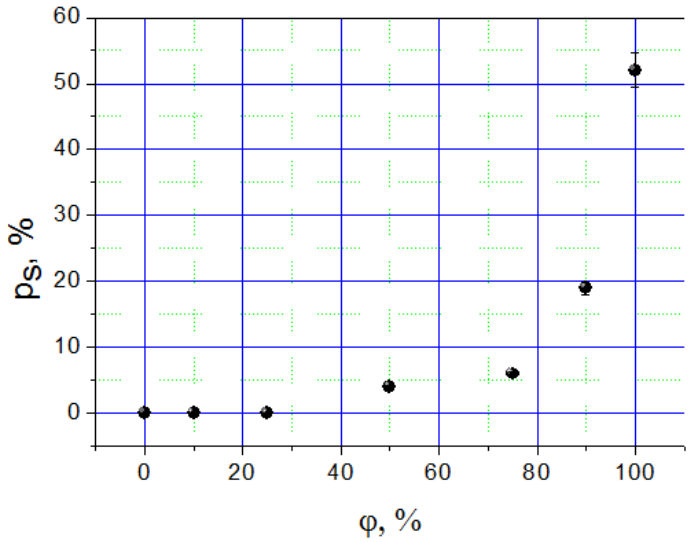

Figure 1. The fraction of solid component in the model system "oil + paraffin + resin" obtained using the method of Solid-Echo: 0% - corresponds to oil with 7% paraffin, 100% - pure resin

The realization of the idea of model samples makes it possible to reveal the influence of the resin not only on the average spin-spin relaxation rate, but also on the fraction of the solid-state component p_s (Fig. 1). It is seen that p_s, depending on the resin content, as well as the average spin-spin relaxation rate does not grow linearly. In fact, the solid component in

the test mixture appears with a resin content of more than 25%. This effect can be explained by dissolving the resin in oil at low concentrations in the system and forming solid formations above this concentration.

Conclusion

It is shown that viscosity correlates with contents solid-state components in backs – a spin relaxation which depends on the content of resin in this system not linearly.

We show exist what the basic possibility and prospects exist of use of model samples for studying of in-fluence of component structure on relaxation characteristics and dynamic viscosity of samples of high-viscosity oil.

References

1. Klaus H. Altgelt Composition and Analysis of Heavy Petroleum Fractions, 1993 by CRC Press, 512 Pages
2. Influence viscosity oils of texturizing ingredients N. Abbakumova, L. Petrova, T. Foss, G. Romanov, A. Elpidinsky Oil and gas technology 2011. *№ 1 (72)*. Pages 3-6.

Investigation of mobility of ionic liquid molecules $[C_8mim^+][Cl^-]$ in water solution by computer simulation and NMR-experiment

Aleksey A. Kazarinov, Andrei V. Komolkin

Faculty of Physics, Saint-Petersburg University, Russia
E-mail: aleksey.kaz@mail.ru

Introduction

Ionic liquids, which actually are salts with low melting temperatures (lower than 100 degrees Celsius), are interesting as the new substance class, which is not completely researched. One of their properties is formation of aggregates in aqueous solution, when the concentration of ionic liquids exceeds critical micelle concentration (CMC) [1].

A researched system is a solution 1-octyl-3-methyl-imidazolium chloride $[C_8mim^+][Cl^-]$ in water. At the present work used two ways of investigation of self-aggregation process in the system: computer simulation and NMR-experiment. From both ways can be calculated basic characteristics of system: diffusion, conformations and other. These parameters could be compared with each other, what would provide of results to research.

Computer simulation

This type of investigation is a continuation of previous work [2]. In the system included 256 molecules of imidazolium, 15872 molecules of water. That configuration corresponds to solution, exceeded the critical micelle concentration 4 times at the temperature 298K. Measurements of main parameters in the system have been doing during 10 ns. A snapshot of the system is presented in Figure 1. Different colors show various aggregates in the solution. There are 13 ones. Average size of the aggregates is approximately 14 molecules.

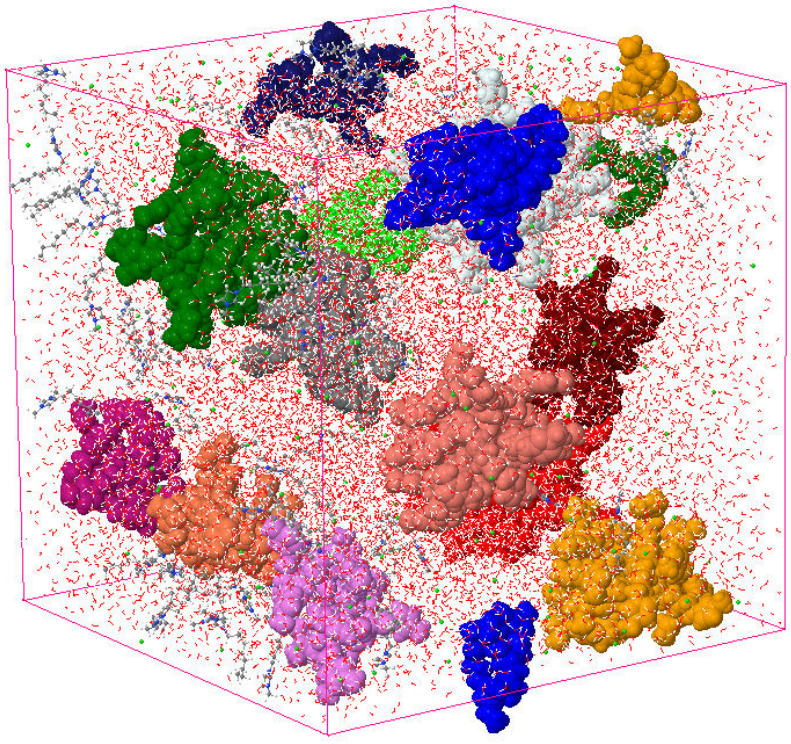

Figure 1. Example of investigated system

A program, created in [2], provides to display numbers of molecules in aggregates. By these numbers, may be calculated as diffusion of molecules in micelles so diffusion of free-floating monomers in water. Also specified numbers of molecules are used for calculation of conformations.

NMR-experiment

Seeking parameters are coefficients of self-diffusion for different types of molecules.

Used Diffusion-Ordered NMR Spectroscopy seeks to separate the NMR signals of different species according to their diffusion coefficient. By NMR spectra it is possible to calculate conformations of molecules in the system. Researched systems corresponds to 0.5 CMC (0.1 mol/l), 2 and 4 CMC.

Acknowledgements

The experiment was performed by equipment of Magnetic resonance resource centre in "Research park of SPbSU".

References

1. Мицеллообразование // Химическая энциклопедия. Т. 2. — М.: Большая Российская энциклопедия, 1992. С. 95–96.
2. Kazarinov A. Research of the Structure of Micelles in Ionic Liquid Aqua Solution / A. A. Kazarinov, A. V. Komolkin // Conference Abstracts, International Student Conference "Science and Progress" St. Petersburg, 2016. P. 247.

Development of software for routine analysis of 3-dimensional arrays of experimental data

M. A. Khasanov, A. V. Ievlev, A. V. Chudin

Department of nuclear physical research methods, Faculty of Physics, Saint Petersburg State University
E-mail: makhas18@gmail.com

Introduction

Data visualization is an integral part of any activity related to the processing and presentation of data. It is a process of data transformation, providing the most convenient and effective form for a person. Data visualization is widely used in various fields: journalism, economics, education, statistics, science, etc.

In this paper, the data taken with a magnetometer, which measured the magnitude of the magnetic field in a certain area, are presented in the form of a table. The table shows the profile, picket, fixation time, value (Fig. 1) and field variation (Fig. 2). It is necessary for each profile and picket value to correlate its field value and thus obtain a three-dimensional array of data. On the basis of this array, it is possible to construct magnetic field maps, from which a lot of useful information can be obtained during further analysis.

Данные измерения магнитометра ПКМ
Файл: C:\data\2016.03.21.Koporie\2103ar.txt

Дата: 22.03.16
Участок: 0

Поле	Время	Профиль	Пикет
051431.590	11:48:22.7	000000	000099
051446.664	11:48:23.7	000000	000100
051451.465	11:48:24.6	000000	000101
051514.734	11:48:25.5	000000	000102
051602.977	11:48:26.2	000000	000103
051675.617	11:48:26.7	000000	000104
051759.938	11:48:27.2	000000	000105
051828.156	11:48:27.6	000000	000106
051860.254	11:48:28.1	000000	000107
051918.914	11:48:28.6	000000	000108
051951.617	11:48:29.1	000000	000109
051975.980	11:48:29.6	000000	000110
051999.672	11:48:30.1	000000	000111
052020.480	11:48:30.6	000000	000112
052034.820	11:48:31.1	000000	000113
052039.680	11:48:31.6	000000	000114
052041.500	11:48:32.1	000000	000115
052039.965	11:48:32.6	000000	000116
052043.004	11:48:33.1	000000	000117
052041.789	11:48:33.5	000000	000118
052044.586	11:48:34.0	000000	000119
052034.965	11:48:34.5	000000	000120
052062.359	11:48:35.0	000000	000121
052081.480	11:48:35.5	000000	000122
052090.969	11:48:36.0	000000	000123
052090.730	11:48:36.5	000000	000124
052085.621	11:48:36.9	000000	000125
052076.910	11:48:37.4	000000	000126
052075.691	11:48:37.9	000000	000127
052091.477	11:48:38.4	000000	000128
052099.414	11:48:39.0	000000	000129
052104.074	11:48:39.6	000000	000130

Figure 1. The level of the magnetic field, depending on the coordinates

Данные измерения магнитометра ММПГ-1 (МИНИМАГ)
Файл: C:\data\2016.03.21.Koporie\2103vr.txt

Дата: 22.03.16
Участок: 0
Автоматический режим, цикл - 15 сек.

Поле1	Д	Время
52169.21	1	11:32:15
52169.41	0	11:32:30
52169.37	0	11:32:45
52169.52	0	11:33:00
52169.54	0	11:33:15
52169.32	1	11:33:30
52169.15	0	11:33:45
52169.28	0	11:34:00
52168.99	1	11:34:15
52168.82	1	11:34:30
52168.73	1	11:34:45
52168.75	1	11:35:00
52168.53	0	11:35:15
52168.20	0	11:35:30
52168.08	0	11:35:45
52167.53	1	11:36:00
52167.38	1	11:36:15
52166.96	0	11:36:30
52166.95	1	11:36:45
52167.20	0	11:37:00
52167.33	1	11:37:15
52167.60	1	11:37:30
52167.48	1	11:37:45
52167.46	1	11:38:00
52167.44	0	11:38:15
52167.38	0	11:38:30
52167.27	1	11:38:45
52166.80	0	11:39:00
52166.67	0	11:39:15
52166.69	1	11:39:30
52166.64	1	11:39:45

Figure 2. Time variation of the magnetic field

In this work it was necessary to analyze the possibility of visualizing data in packages such as LabView, Matlab, Mathcad and compare them with others.

Results

At this stage, the program was written in the Mathcad package (Fig. 3) and Matlab (Fig. 4). The main part of the program is occupied by a node that converts data from a magnetometer into a pseudo-three-dimensional array, which is then displayed as a three-dimensional graph. After that, the researcher can work with the visualized data, highlighting

patterns characteristic of this or that magnetic anomaly. The main advantage of this project is the ability to collect and visualize data from any magnetometers.

M := READPRN("C:\Users\Admin\Desktop\12\2709ICV.dat")

M0 := $M^{\langle 0 \rangle}$ M4 := $M^{\langle 4 \rangle}$ cols(M) = 5 rows(M) = 946

k := j ← 0; while $M0_j < 1$: j ← j + 1; j

$m := \frac{rows(M)}{k}$

m = 21.022

round(m) = 21

k = 45

$L :=$ for l ∈ 0.. round(m) − 1; for i ∈ 0.. k − 1: $L_{i,l} \leftarrow M4_s$; s ← s + 1; return L

limit := 0

Figure 3. The code of the program in Mathcad

```
function search
clear
clc
tic
A = dlmread('2709ICV.dat');
B1 = A(:,1);
k = max(find(B1==0));
disp(k);
m = length(B1)/k;
disp(round(m));
B5=A(:,5);
s=1;
for l=1:round(m)
    for j=1:k
        L(j,l)=B5(s);
        s=s+1;
    end
end
disp(L);
H=L;
assignin('base', 'H_base', H);
disp(H);
y=0:1:k-1;
x=0:1:round(m)-1;
[X,Y]=meshgrid(x,y);
surf(X,Y,H);
toc
```

Figure 4. The code of the program in Matlab

The results of the program are shown in the following figures:

	0	1	2	3	4
0	860	825	$1.125 \cdot 10^3$	972	921
1	860	$-7.917 \cdot 10^3$	$1.018 \cdot 10^3$	997	834
2	864	$1.126 \cdot 10^3$	$1.021 \cdot 10^3$	$1.134 \cdot 10^3$	863
3	864	$1.191 \cdot 10^3$	$1.004 \cdot 10^3$	980	839
4	848	$1.058 \cdot 10^3$	976	899	822
5	885	$1.122 \cdot 10^3$	$1.04 \cdot 10^3$	$1.097 \cdot 10^3$	857
6	835	$1.09 \cdot 10^3$	975	982	792
7	836	$1.118 \cdot 10^3$	$1.189 \cdot 10^3$	$1.062 \cdot 10^3$	882
8	852	$1.077 \cdot 10^3$	992	917	902
9	837	$1.116 \cdot 10^3$	991	$1.15 \cdot 10^3$	913
10	832	$1.049 \cdot 10^3$	984	889	875
11	790	$1.133 \cdot 10^3$	986	$1.14 \cdot 10^3$	893
12	844	$1.075 \cdot 10^3$	969	916	843
13	876	$1.076 \cdot 10^3$	987	912	809
14	860	$1.11 \cdot 10^3$	$1.011 \cdot 10^3$	$1.005 \cdot 10^3$	877
15	836	$1.121 \cdot 10^3$	964	887	...

Figure 5. Pseudo-3D array in Mathcad

	1	2	3	4	5
1	860	825	1125	972	921
2	860	-7917	1018	997	834
3	864	1126	1021	1134	863
4	864	1191	1004	980	839
5	848	1058	976	899	822
6	885	1122	1040	1097	857
7	835	1090	975	982	792
8	836	1118	1189	1062	882
9	852	1077	992	917	902
10	837	1116	991	1150	913
11	832	1049	984	889	875
12	790	1133	986	1140	893
13	844	1075	969	916	843
14	876	1076	987	912	809
15	860	1110	1011	1005	877
16	836	1121	964	887	859

Figure 6. Pseudo-3D array in Matlab

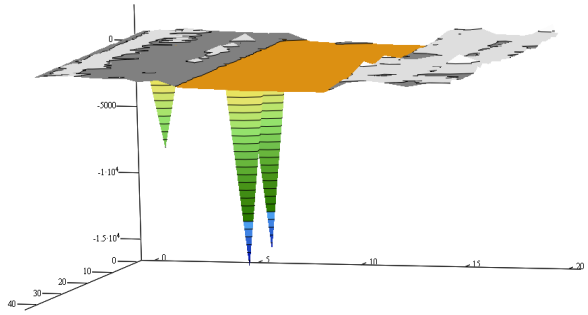

Figure 7. Visualization of data in Mathcad

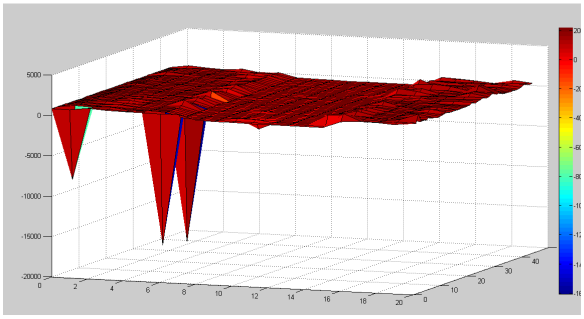

Figure 8. Visualization of data in Matlab

References

1. Fedosov V.P., Nesterenko A.K. Digital signal processing in LabView / ed. V.P. Fedosov. - Moscow: DMK Press, 2007. - 472 p.
2. Matlab Primer, https://www.mathworks.com/help/pdf_doc/matlab/getstart.pdf

Paramagnetic intermediates in reactions of carbon dioxide electrocatalytic reduction

Kirill V. Kholin[1], Pavel A. Abramov[2], Maxim N. Sokolov[2], Marsil K. Kadirov[1]

[1]A.E. Arbuzov Institute of Organic and Physical Chemistry, Kazan Scientific Center, Russian Academy of Sciences, Arbuzov str. 8, Kazan, 420088, Russian Federation
[2]Nikolaev Institute of Inorganic Chemistry Siberian Branch of Russian Academy of Sciences, Acad. Lavrentiev Ave. 3, Novosibirsk, 630090, Russian Federation
E-mail: kholin06@mail.ru

Introduction

In Nature, the carbon cycle has the ability to recycle some 203 gigatons (Gt) of carbon dioxide each year. Anthropogenic ("man - made") CO_2 (about 7 Gt per year) represents approximately 3.4% of the total CO_2 converted in the natural cycle. As a result, CO_2 becomes accumulated in the atmosphere. Hence, it is vital that strategies are developed to limit CO_2 accumulation in the atmosphere.

Many ideas have involved trapping the "greenhouse gas" and converting it into fuels and organic materials, using either light or electrical energy [1]. The idea of synthesizing valuable organics from CO_2, however, is not new. Some of the earliest reports of CO_2 reduction date back to the late 1800s, when formic acid was first synthesized from aqueous bicarbonate [2].

The negative electron affinity of CO_2 in the gas phase translates in solution into a one-electron transfer that converts linear CO_2 into bent $CO_2^{-\bullet}$ both hindered by unfavorable thermodynamics $E°(CO_2/CO_2^{-\bullet}) = -2.14$ V (versus SCE) and very slow self-exchange rates. The two-electron (hydride) transfer into $HCOO^-$ ($E° = -0.55$ V versus SCE) or the stabilization of $CO_2^{-\bullet}$ into bound intermediates appear to be more favorable pathways to initiate the reduction of CO_2 toward CH_3OH and CH_4. Mononuclear tricarbonyl Re (I) complexes attract attention as catalysts for the reduction of CO_2, including due to its ability to absorb light. The catalytically-active reduced form of such complexes is paramagnetic "18 + δ" electron complexes [3].

A combination of electrochemical methods and ESR creates new opportunities for deeper studies of heterogeneous electron transfer and subsequent chemical reactions. The concept of a coaxial cavity [4] was used to create a three electrode electrochemical-ESR (El-ESR) cell with a large surface comprised of a helical working electrode for the purpose of increasing sensitivity and ensuring the accuracy of the electrochemical experiments due to the relatively small voltage drop between the working and reference electrodes. Placing the cell in the cavity and recording the ESR spectrum or measuring its intensity simultaneously with electrochemical characterization has led to interesting results.

Results and discussion

We studied redox processes of a firstly synthesized complex [(Aryl-BIAN)Re(I)$(CO)_3$Br] (fig. 1a). Cyclic voltammetry curves curried out during the complex reduction in DMF are shown in fig. 1b. A first cycle is marked by a black curve (without peak 1) and a second cycle (with peak 1) is marked by a red curve. It can be seen that only cathode peak 2 is observed for the first cycle (black curve) and peak 1 is not observed. However, during reoxidation, a peak opposite to the cathode peak 1 appears. Peak 2 corresponds to the original complex [(Aryl-BIAN)Re$(CO)_3$Br]^0 reduction to [(Aryl-BIAN)Re$(CO)_3$Br]$^{1-}$. Peak 1 corresponds to a fact that particle is reduced earlier than a complex [(Aryl-BIAN)Re$(CO)_3$Br]^0 Moreover, the fact shows that this particle is formed from a reduced form [(Aryl-BIAN)Re$(CO)_3$Br]$^{1-}$. It can also be seen, the cathodic peaks of the [(Aryl-BIAN)Re(I)$(CO)_3$Br] complex reduction (peaks 2,4,5) are decreased at a second cycle, which

is due to a near-electrode layer depletion by this complexes. The peaks corresponding to a second unknown particle reduction (peaks 1,3) are increased, on the contrary. The near-electrode layer is enriched by this particles.

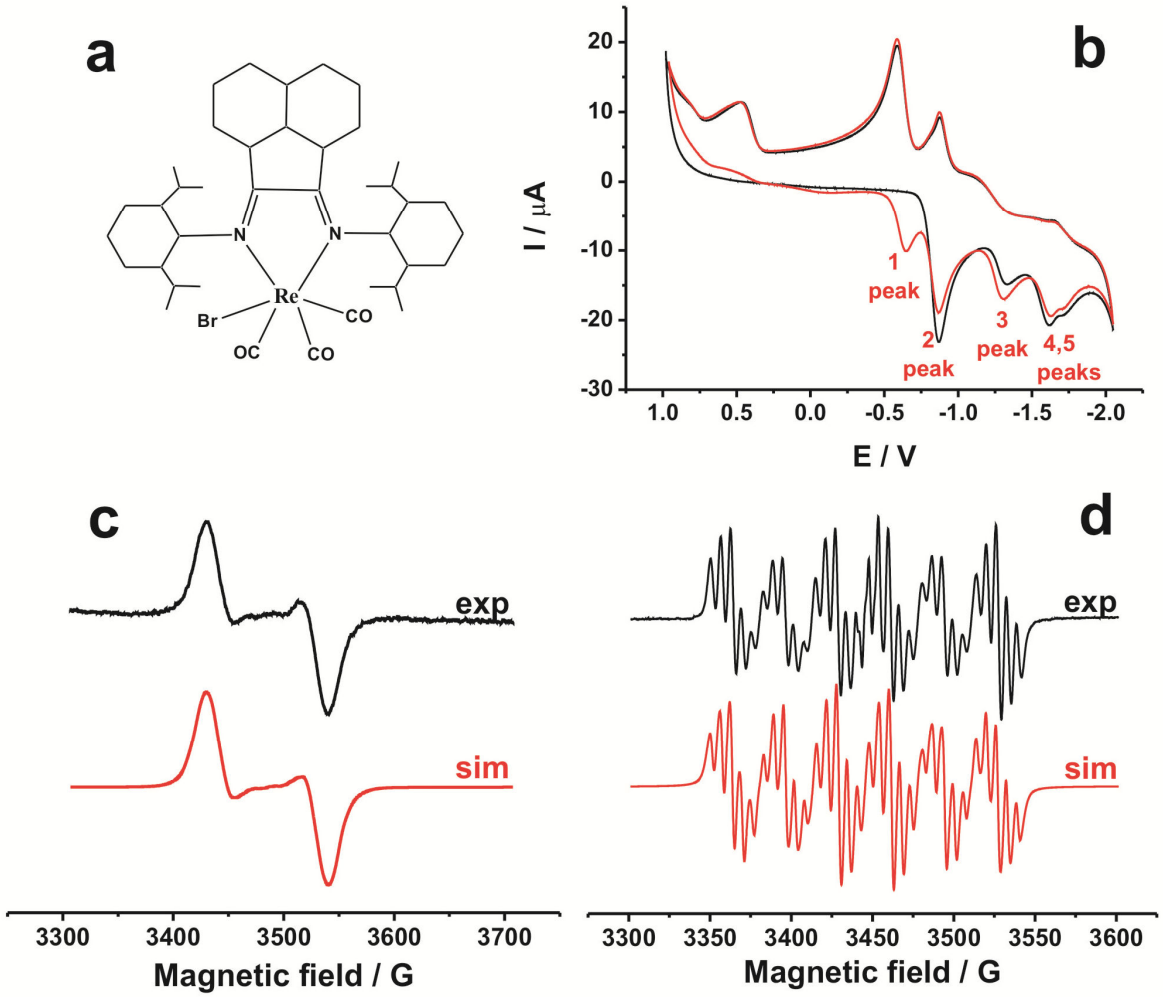

Figure 1.a) Structural formula of a [(Aryl-BIAN)Re(I)(CO)$_3$Br] complex
*b) The CV curves of the complex in DMF (n = 5 * 10^{-3} M) at a first cycle (black curve) and at a second cycle (red curve)*
c) The EPR spectrum obtained in DMF during a complex reduction in an electrochemical-ESR cell at a potential -0.8 V and its simulation
d) The EPR spectrum obtained in DMF during a complex reduction in an electrochemical-ESR cell at a potential -1.7 V and its simulation

An ESR signal (Fig. 1) starts to increase if we study the same complex solution in the electrolysis-ESR cell at -0.8 V. The observed EPR spectrum corresponds to a reduced form [(Aryl-BIAN)Re(CO)$_3$Br]$^{1-}$ and it was simulated. The simulation was done with following magnetic resonance parameters: g = 2.005, a_{Re} = 19 G; 2: a_N = 9.5 G. The spectrum is sextet of quintets with relatively large line width. Sextet is formed due to a splitting on Re nucleus with a nuclear spin 5/2 (two isotopes ^{185}Re and ^{187}Re), and quintet is split on two nitrogen nuclei of ligand (Aryl-BIAN). The g-factor is close to a value of free electrons .This fact indicates an existence of ligand-centered electron transfer - [(Aryl-BIAN)$^{\cdot-}$Re(I)(CO)$_3$Br]$^{1-}$. It is known from the literature [5,6], this type complexes can "throw out" halogen after reduction, and dimerization Re-Re can occur after that. Moreover, intramolecular electron

transfer from a ligand to a metal center takes place in these processes, and complexes [(α-diimine)Re(0)$(CO)_3$] are formed. The EPR spectra of dimers are not detected in the X-band due to a paramagnetic Re(0)centers exchange interaction presence.

The EPR spectrum (fig. 1c) disappears at a potential of peak 4. If the ligand-centered electron transfer occurs again a diamagnetic complex $[(\text{Aryl-BIAN})^{2-}\text{Re(I)}(CO)_3\text{Br}]^{2-}$ is formed, and if the metal-centered electron transfer occurs an extremely unstable form $[(\text{bian})^{\cdot-}\text{Re(0)}(CO)_3\text{Br}]^{2-}$ is formed.

But another EPR spectrum appears at a potential of peak 3. The spectrum and its simulation are shown in fig. 1d. The EPR spectrum represents sextet of quintets too, but it is resolved much better due to much narrower lines. The simulation was done with following magnetic resonance parameters: g = 2.006, a_{187Re} = 32.6 G; a_{185Re} = 31.0 G; 2: a_N = 6.2 G. This spectrum indicates to a Re(I) complex with "ligand paramagnetic center", but an increased HFS constant on Re nucleus and a decreased line width indicate to bromide ion absence in a complex axial position [7].

Thus, existence of a paramagnetic intermediate with a coordinatively unsaturated metal center which was detected during electrochemical reduction of the complex allows us to expect a manifestation of catalytic properties of a complex [(Aryl-BIAN)Re(I)$(CO)_3$Br] in a carbon dioxide reduction processes.

Acknowledgements

The reported study was funded by RFBR according to the research project No. 16-33-00536 мол_а.

References

1. Aresta, Michele, and Angela Dibenedetto. "Carbon dioxide fixation into organic compounds." Carbon Dioxide Recovery and Utilization. Springer Netherlands, 2003. 211-260.
2. Royer, E. "Reduction of carbonic acid into formic acid." CR Acad Sci 70 (1870): 731-735.
3. Klein, Axel, Conny Vogler, and Wolfgang Kaim. "The δ in 18+ δ electron complexes: importance of the metal/ligand interface for the substitutional reactivity of "Re (0)" complexes (α-diimine-) ReI (CO) 3 (X)." Organometallics 15.1 (1996): 236-244.
4. Allendoerfer, R. D., G. A. Martinchek, and Stanley Bruckenstein. "Simultaneous electrochemical-electron spin resonance measurements with a coaxial microwave cavity." Analytical Chemistry 47.6 (1975): 890-894.
5. Machan, Charles W., et al. "Developing a mechanistic understanding of molecular electrocatalysts for CO2 reduction using infrared spectroelectrochemistry." Organometallics 33.18 (2014): 4550-4559.
6. Benson, Eric E., and Clifford P. Kubiak. "Structural investigations into the deactivation pathway of the CO_2 reduction electrocatalyst Re (bpy)(CO) 3 Cl." Chemical Communications 48.59 (2012): 7374-7376.
7. Shakeri, Jamaladin, et al. "Photoreduction of CO_2 to CO by a mononuclear Re (i) complex and DFT evaluation of the photocatalytic mechanism." RSC Advances 5.51 (2015): 41125-41134.

Peculiarities of creatine concentration in semioval centers white matter and medial cortex in patients with dementia: MRS study

Y. G. Khomenko, G. V. Kataeva, A. A. Bogdan, E. M. Chernysheva, D. S. Susin, E. A. Gromova

N. P. Bechtereva Institute of the Human Brain RAS, St.Petersburg
E-mail: julkhom@rambler.ru

Introduction

Magnetic resonance spectroscopy (MRS) allows to receive data on various metabolites concentration in brain tissue in vivo, that is of great interest for the study of pathogenesis of neurodegenerative diseases and clinical practice. The multivoxel MRS is of particular interest because it allows to evaluate metabolite concentrations in white and gray matter in different brain regions simultaneously.

In neurological pathology, in particular, in neurodegenerative diseases, the ratio of N-acethylaspartate (NAA) to creatine (Cr) is commonly used, as NAA is usually considered to be the neuronal integrity marker [1]. Since estimation of the absolute concentrations of metabolites with in vivo MRS is complicated, the internal reference is required, and the most common is Cr concentration. As the Cr concentration is traditionally considered to be quite stable, usually it does not evaluated in the medical examinations.

At the same time, Cr concentration differs in white and gray matter. Widerman et al. (2001) reported that Cr concentration in parietal gray matter was 113% of the concentration in the white matter [2], they also reported about the regional variations in metabolite concentrations. Wang&Li (1998) showed that the levels of NAA, creatine and phosphocreatine (Cr), and choline-containing compounds (Cho) in gray matter were significantly higher than in white matter. The averaged NAA, Cr, and Cho concentrations in gray matter were 11.0, 9.7, and 1.9 mM/liter, respectively, in comparison with 7.5, 5.2, and 1.6 mM/liter in white matter [3]. Hetherington et al. (1994) estimated that in healthy subjects Cr content was significantly lower in white matter than gray ($p<0.01$), with a white/gray content ratio of 0.8, in agreement with biopsy [4].

The aim of our research was to evaluate the Cr ratio in white and gray matter in supraventricular brain regions in patients with dementia and mild cognitive impairment.

Methods

Group consisted of 26 patients with different types of dementia (age 69,6±7,7), and 27 patients with mild cognitive impairment (MCI) (64,1±10,1) and 2 control groups (age-matched and young control group) were examined.

All patients underwent the standard neurological examination. Evaluation of the cognitive impairment severity was performed using the following scales: a mini-mental State Examination (MMSE), a maximum score of 30 points; The Montreal Cognitive Status Assessment Scale (MoCog), the frontal assessment battery (FAB) with a maximum score of 18 points; clock drawing test (CDT) with a maximum score of 10 points, and the “5 words memory test“ to assess short-term memory. The choice of short screening scales was due to the possibility of their use in a neurologist daily practice.

Multivoxel H-MRS in supraventricular region was performed on Achieva 3T scanner, Philips (2D PRESS, TE/TR=144/1500 ms). Anatomical localization of voxels is presented on Figure 1. The area of MRS study - 8*9 voxels (10*10*15 mm), whole volume 80*90*15 mm was divided into 9 regions of interest (ROI): 6 in white matter (WM) of semioval centers (3 ROIs: anterior, medium and posterior for each hemisphere) and 3 ROIs in gray matter (GM)

of medial cortex. NAA/Cr, NAA/Cho, Cho/Cr ratios (NAA – N-acethyl aspartate, Cr – creatine, Cho – choline) were analyzed separately for each ROI.

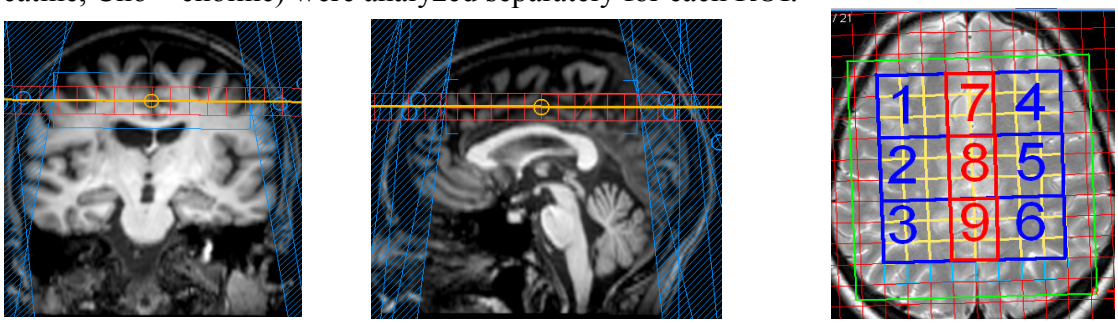

a *b*

Figure 1. (a) — MRS anatomical localization in the supraventricular region; (b) — localization of regions of interest in white (1-3 and 4-6) and gray matter (7-9)

Results

NAA/Cr, Cho/Cr and NAA/Cho ratios were significantly lower in dementia group compared to both MCI and controls ($p<0,01$). These findings are in accordance with our previous studies [6]. However, we did not find differences between different dementia types (possibly because of the too small size of some groups).

The ratio of Cr in WM to Cr in GM were significantly higher ($p<0.01$) in the dementia group (possibly due to the cortex atrophy) (Fig.2).

Area	Control	Dementia	p
Cr-1/Cr-7	89±8%	109±20%	0.0001
Cr-2/Cr-8	92±10%	105±14%	<0.01
Cr-3/Cr-9	101±12%	112±10%	<0.01
Cr-4/Cr-7	86±6%	107±18%	0.0001
Cr-5/Cr-8	88±5%	96±11%	<0.01
Cr-6/Cr-9	93±10%	98±11%	-

Figure 2. Ratios of Cr content in white matter to the corresponding areas of medial cortex. Numbers of areas given in accordance with ROIs in Fig. 1

The interrelations of Cr-WM/Cr-GM ratios with cognitive tests scores were also revealed. As shown in Table 2, Cr-WM/Cr-GM ratios correlated negatively with tests scores reflected better functional state of brain tissue.

Thus, it was found that the content of Cr in the white matter with respect to their content in the adjacent regions of gray matter (medial cortex) differs significantly in dementia and mild cognitive impairment: in dementia the relative Cr concentration in white matter increase with respect to the gray, probably due to a significant decrease in the concentrations of Cr in the gray matter or due to the cortex atrophy. The ratio of Cr in the white matter to Cr in the medial cortex increases with dementia and negatively correlated with the cognitive tests scores.

It is known that normal concentration of Cr is higher in gray matter than in white, and the Cr content slowly increasing with age. Despite this, it is believed that the Cr concentration remains sufficiently stable to use it as an internal referent.

Table 2. Correlations of metabolite ratios with cognitive tests scores

Area*	Cognitive tests									
	MMSE		MoCog		FAB		CDT		«5 words» memory test	
	r	p	r	p	r	p	r	p	r	p
Cr 1/7	-	-	-	-	-	-	-0,48	0,0008	-	-
Cr 2/8	-0,43	0,0031	-0,47	0,0010	-	-	-0,44	0,0026	-	-
Cr 3/9	-0,61	0,0000	-0,61	0,0000	-0,44	0,0054	-0,57	0,0001	-0,47	0,0021
Cr 4/7	-	-	-0,42	0,0040	-0,41	0,0068	-0,55	0,0001	-	-
Cr 5/8	-0,41	0,0059	-0,45	0,0021	-0,56	0,0001	-0,50	0,0005	-0,42	0,0046
Cr 6/9	-	-	-0,44	0,0029	-0,49	0,0012	-	-	-0,40	0,0071

** Numbers of areas given in accordance with ROIs in Fig.1.*

Nevertheless, the revealed dependencies can evidence that significant alterations of Cr concentration in the brain tissue of patients with dementia exist. Notably, changes of ratio of Cr concentration in white and gray matter were revealed, that brings into a question its use as an internal reference for the evaluation of other metabolites concentrations (NAA, Cho and others) in this category of patients. For example, in case of simultaneous decrease of NAA and Cr concentrations the implementation of commonly used NAA/Cr ratio for the neuronal integrity evaluation will mask NAA decrease. Thus, the diagnostic significance of NAA/Cr ratio for the evaluation of neuronal integrity in such cases will have quite limited diagnostic value.

The obtained results show that for the correct interpretation of MRS data both for the clinical and scientific purposes it is necessary to evaluate not only traditional metabolites ratios, but also creatine concentration, ratios of metabolite concentrations in white and gray matter and the cortex atrophy level. Follow-up study is needed to clarify the diagnostic significance of changes of Cr concentration ratio in white and gray matter in neurodegenerative diseases.

References

1. Barker P.B., Bizzi A., De Stefano N., Gullapalli R.P., Lin D. M. Clinical MR Spectroscopy: Techniques and Applications. Cambridge University Press, 2009.
2. Widerman, D., Schuff, N., Matson, G.B., Soher, B.J., Du, A.T., Maudsley, A.A., Weiner, M.W., Short echo time multislice proton magnetic resonance spectroscopic imaging in human brain: metabolite distributions and reliability. Magn. Reson. Imaging. 19 (8), 10873–11080 (2001)
3. Wang Y., Li S.J. Differentiation of metabolic concentrations between gray matter and white matter of human brain by in vivo 1H magnetic resonance spectroscopy. Magn Reson Med. 39(1):28-33 (1998)
4. Mason G.F., Pan J.W., Ponder S.L., Twieg D.B., Pohost G.M., Hetherington H.P. Detection of brain glutamate and glutamine in spectroscopic images at 4.1 T. Magn Reson Med 32(1): 142–145 (1994)
5. Khomenko Y.G., Bogdan A.A., Kataeva G.V., Chernysheva E.M., Multivoxel magnetic resonance spectroscopy in the examination of patients with cognitive disorders (in Russian). Bulletin of St. Petersburg University. Series 4. Physics. Chemistry. T. 3. No. 1. P. 82-89 (2016)

Using MRI method for studies of forced diffusion in pore medium

P. P. Kobchikova, M. M. Doroginitsky

Institute of Physics, Kazan (Volga region) Federal University, Russia
E-mail: pollymoon@ya.ru
http://kpfu.ru/physics/struktura/kafedry/kafedra-fiziki-molekulyarnyh-sistem

Introduction

To study translational molecular dynamics, the nuclear magnetic resonance (NMR) method is used, based on measuring the diffusion attenuation of the spin echo [1]. The time range of the study is limited to the interval: from 10^{-3} to 1 s due to nuclear magnetic relaxation of the NMR signal. Through the use of NMR method with impulse gradient magnetic field [2] the phenomenon of faster self-diffusion of a fluid under partial saturation of pore medium was discovered [3] compared to self-diffusion of a free fluid under the same thermodynamic conditions. The authors proposed the name "forced" diffusion for this phenomenon.

In the present work, we investigated the possibility of using the MRI method to extend the time range of the investigation of diffusion transport of matter in pore medium with the aim to study the phenomenon of forced diffusion.

Object and method

As a porous medium, dolomite core samples were extracted from the Universitetskaya-1 well. The core samples have a cylindrical shape with a diameter of 10 cm, (Fig. 1.A). The samples were pre-dried at 50 ° C for several days. The residual water saturation was monitored by means of an NMR tomograph (Fig. 1.B). Measurement of the distribution of fluid in the process of saturation was carried out on a specialized magnetic-resonance tomograph «MR Scanex» (RTI, Moscow). The magnetic system of the device is a closed cycle cryosystem that ensures 1,5 T induction magnetic field in the work zone with a 20 cm gap. To obtain the image, we used the standard spin echo sequence [3]. The relative fluid saturation was determined from the optical density of the image.

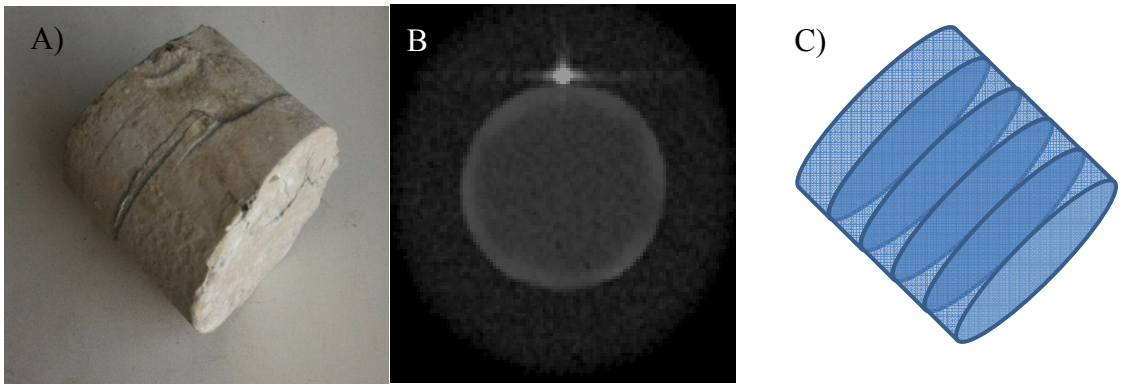

Figure 1. A) Sample of dolomite; B) Monitoring of the saturation of a sample; C) Transversal tomograms

To saturate the sample it was immersed entirely in a container filled with water. Sample saturation was carried out continuously throughout the entire experiment, with the exception for when it was removed from the container for measurements and isolated from the air with a polymer film. Thus, a condition was ensured for maintaining a constant fluid saturation on the sample surface. Five transverse NMR tomograms of the saturable sample

were obtained (Fig. 1.B-C) for 7 time points in the range from 5 to 320 minutes. The obtained images of the fluid distribution in the process of saturation were stored in the graphic format Dicom. In order to process fluid distribution tomograms "Inobitech DICOM viewer 1.8.6" software was used that allowed us to obtain optical density of the picture along the selected straight line. To take into account the heterogeneity and anisotropy of the sample, the radial saturation profiles of fluid were averaged over 8 directions (Fig. 2.A) and 3 sections (Fig. 2.B). When calculating the relative fluid content, the mean optical noise density was determined and taken into account (Fig. 2.C). As the porous medium was saturated with fluid, the optical density of the tomograms increased. (Fig. 2.D). According to the digitized data, the radial distribution density of the fluid was calculated in the MathCad program software as a function of the saturation period.

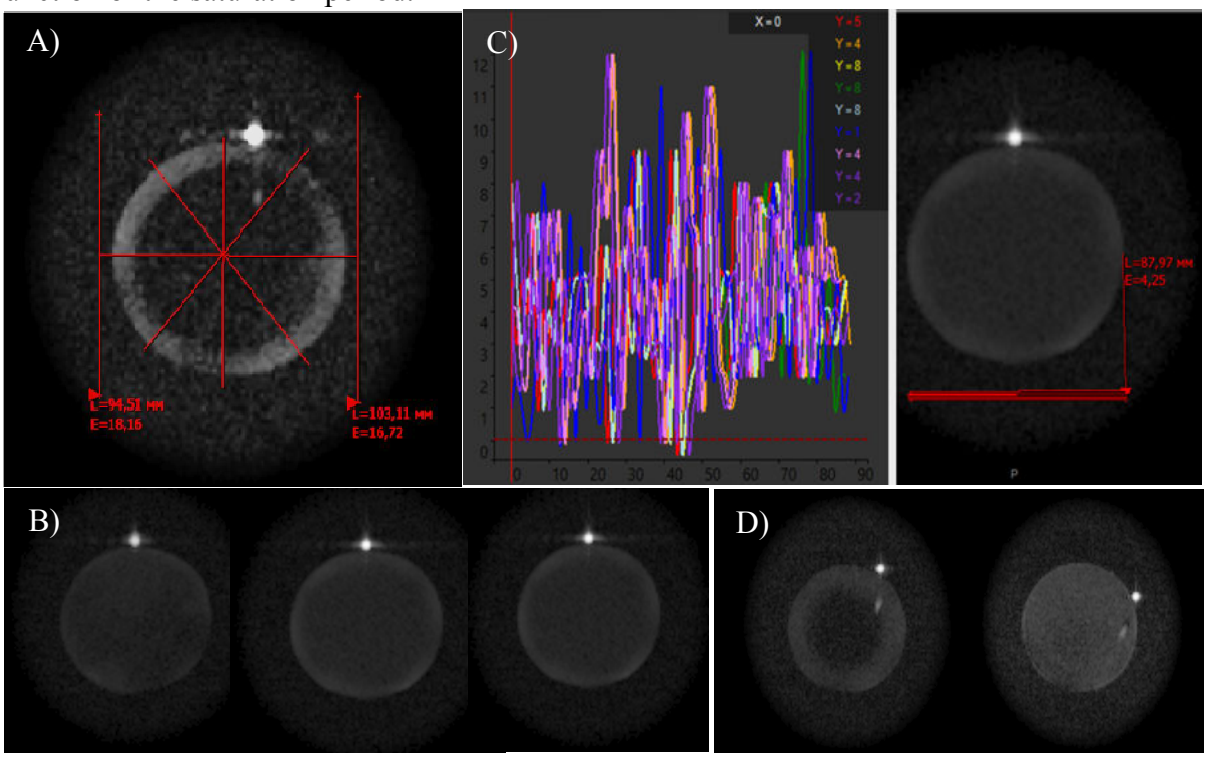

Figure 2. A) An average radial profile of an optical density B) Three tomograms for the same time of saturation C) Determination of noise level D) Comparison of tomograms for two times of saturation: 5 min and 80 min

Results

The MRI method makes it possible to significantly supplement the time range for investigating the diffusion transport of matter to the time range for studying diffusion by traditional NMR methods. The method of the analysis of an optical density of MRT used in this work allows investigating diffusion processes in large-size objects.

The main experimental result of this work is the radial distribution profiles of the fluid $w(r,t)$ obtained by the MRI method during the saturation process in the interval from 5 to 320 min (Fig. 3.A).

For diffusion processes of saturation of a pore medium were considered next models: model of Fick's diffusion and model of the "forced" diffusion. Comparison of the experimental data with Fick's model of diffusion shows the overestimated self-diffusion coefficient. The model of the forced diffusion gives more precise consent with experimental data.

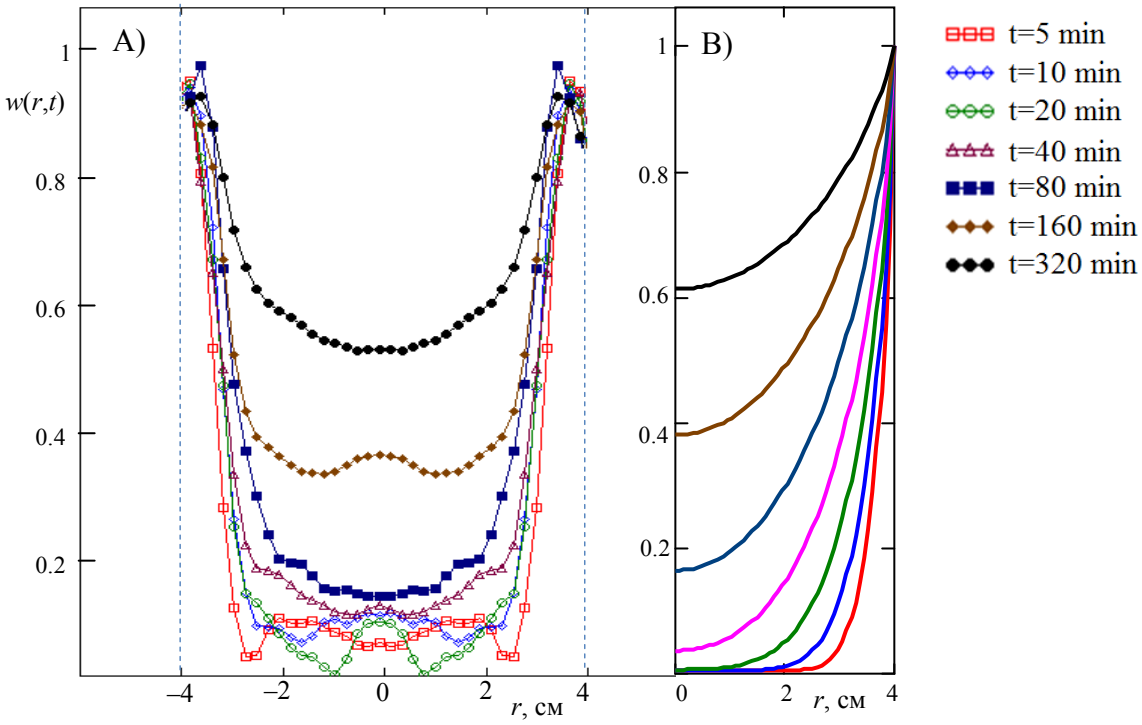

Figure 3. A) Radial profiles of distribution of a fluid in a saturation history for various times of saturation B) Calculations for the equation of "the porous medium"

Discussion

To interpret the obtained data, the equation of "porous medium" was used [4], recorded for the fluid concentration-controlled diffusion coefficient: $D(w)=D_f-(D_f-D_s)w$.

$$\frac{\partial}{\partial t}D(w)=\Delta D^2(w),$$

where D_w – is self-diffusion coefficient of fluid in free volume, and D_f – is coefficient of forced self-diffusion of the substance in a dispersed state. Comparison of calculations with experimental results shows (Fig 3.B), that the coefficient of forced self-diffusion of water in the pore medium of dolomite is $D_f \approx 2{,}5\cdot10^{-8}$ m^2/s, which is an order of magnitude greater than the self-diffusion coefficient of water under the same thermodynamic conditions $D_s \approx 2{,}5\cdot10^{-9}$ m^2/s. At the same time D_f on 3 decimal orders less than the coefficient of self-diffusion of water vapor $D_v \approx 2\cdot10^{-5}$ м^2/с. The question of the dispersed fluid phase in remains is open.

Acknowledgements

We express gratitude to Fattakhov A. V. (Institute of geology and oil and gas technologies of K(P)FU and Melnikova D. L. (Institute of physics of KFU) for the help in carrying out the experiments.

References

1. E.I. Hahn. Spin-echoes – *Phys. Rev.*, v.80, n.4, 580-594 (1950)
2. E.O. Stejskal, J.E. Tanner. Spin diffusion measurements: spin echoes in the presence of a time-dependent field gradient – *J. Chem. Phys.*, v.42, n.1, 288-292 (1965)
3. R.R. Ernst, G. Bodenhausen and A. Wokaun. Principles of Nuclear Magnetic Resonance in One and Two Dimensions – "Clarendon Press" Oxford (1987)
4. N.M. Ivanova. Exact Solutions of Diffusion-Convection Equations – *Dynamics of PDE*, v.5, n.2.139-171 (2008)

Water diffusion in "water-in-decane" microemulsions stabilized with the mixture of nonionic surfactants Span 80 and Tween 80

A. S. Koneva, E. A. Safonova

St. Petersburg State University, Russia, 199034, St. Petersburg, Universitetskaya nab., 7/9.
E-mail: a.koneva@spbu.ru

Introduction

Microemulsions are transparent, thermodynamically stable isotropic liquid mixtures of oil, water and surfactant. There are many applications of microemulsions e.g. in oil recovery, drug delivery, cleaning processes, chemical synthesis etc. There is a growing interest in the usage of water-in-diesel microemulsions and emulsions as alternative fuels [1]. For the application, a study on the microstructure of "water-in-hydrocarbon" microemulsions is of high importance.

Previously, we have investigated the self-diffusion of the surfactant molecules in "water-in-decane" microemulsions stabilized with the mixture of nonionic surfactants Span 80 (sorbitane monooleate) and Tween 80 (polyoxyethylene sorbitan monooleate). It was shown that the bimodal distributions of the diffusion coefficients (D) are specified for the system [2]. The data on D were obtained by the different methods, PGSTE NMR and dynamic light scattering (DLS). The slower diffusion mode (D_{agg} values) was related to the diffusion of the mixed microemulsion droplets with the hydrodynamic radii Rh ~ 10–20 nm. The second diffusion mode (D_m values) was corresponded to the diffusion of micelles with Rh ~ 1–2 nm. These smaller aggregates contain probably Span 80. In the present work, the water diffusion in the same microemulsion system is considered.

Water diffusion

The microemulsions with 0, 4, 6, 8, 10, 13 wt.% (weight percent) of water content at the constant weight ratio of n-decane and both surfactants 65 : 35 (wt.%/wt.%) were studied. Based on the water signals the self-diffusion coefficients of hydroxyl protons in the microemulsions were determined. The self-diffusion coefficients were measured by pulse gradient stimulated echo (PGSTE) NMR. ^{1}H NMR diffusion experiments were performed on the 500 MHz Bruker Avance III spectrometer equipped with GREAT 1/60A gradients and 5 mm MIC DIFF/30 probe with ^{1}H insert. The self-diffusion coefficient D is directly related to the decaying intensities of NMR signal according to the following equation:

$$I/I_0 = e^{-D\gamma^2 G^2 \delta^2 \left(\Delta - \delta/3\right)},$$

where I and I_0 are the intensities of the NMR signal in presence and absence of the field gradient pulses, respectively, G is the gradient strength, Δ is the diffusion time, δ is the gradient pulse length, γ is the gyromagnetic ratio. The values δ = 1 ms and Δ = 50 ms were used. For the microemulsion with 8 wt.% of water the self-diffusion coefficients of water molecules were additionally measured at the diffusion time Δ in the range of 7.5 – 200 ms. The decaying intensities of the water signal were single exponential, in contrast to the bimodal distributions observed for the surfactant molecules [2].

The self-diffusion of water molecules (D_w) was faster than the diffusion of the microemulsion droplets (D_{agg}). The values of the difference ΔD between D_w and D_{agg} in dependence on the water concentrations are presented in Figure 1 at several temperatures. As one can see, the ΔD values at some fixed water content increase with the temperature. At the same temperature from the range of 298 – 313 K, the ΔD values decrease with the increase in

water content. Only at 318 K the maximum of ΔD is observed for the mixture with 8 wt.% of water. These results demonstrate that not all water molecules diffuse as a part of the microemulsion droplets.

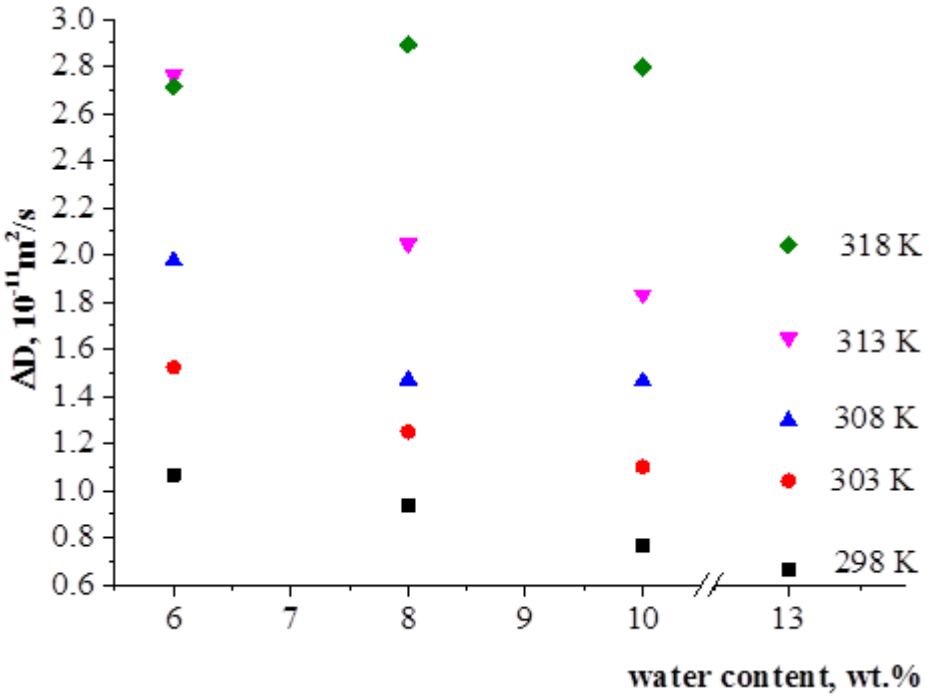

Figure 1. Differences in the self-diffusion coefficients of water molecules and of microemulsion droplets (ΔD) versus the water content at different temperatures

The obtained dependences of D_w versus the diffusion time Δ show that the D_w values increase slightly with the Δ increase. Thus, there are no restrictions (such as boundaries of the microemulsion droplets) for the water diffusion. Otherwise, D_w values would decrease with the Δ increase. Obviously, the aggregates could easy exchange of the water molecules. According to the preliminary data of molecular dynamic (MD) simulation for the mixed reverse micelles of Span 80 + Tween 80 the water molecules are able to leave a microemulsion droplet (Figure 2).

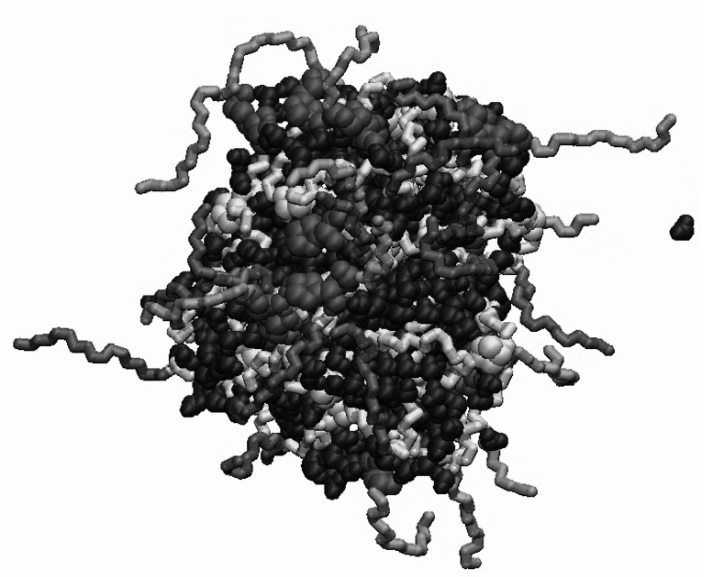

Figure 2. The snapshot from MD simulation of the mixed reverse micelles of Span 80 and Tween 80 when the water molecule leaves the aggregate

The main contribution to the water diffusion gives the molecules associated with the microemulsion droplets. Additionally, there are the water molecules as a part of small Span 80 micelles (i.e. aggregates with faster diffusion) [2]. For a better understanding of the water states in the reverse micellar system, the microemulsions were investigated also by means of Fourier transform infrared (FT-IR) spectroscopy. The preliminary MD data for the small micelles demonstrate that all water molecules are bonded with the hydrophilic groups of the surfactants and that there is no water pool inside the micelles.

Using the data on D_{agg} and on D_m for the small aggregates, the fractions of water molecules in each state (p, q, p+q=1) were calculated with the following equation:

$$D^{w}_{\exp} = pD_{agg} + qD_{m},$$

where $D^{w}_{\exp}$ is the observed diffusion coefficient of water molecules.

The calculations showed that the water fraction in the small Span 80 micelles decrease with water concentration, but a number of water molecules associated with the micelles remains the same. The water fraction as well as a number of water molecules in the microemulsion droplets increase with the water content. The obtained results are correlated with the data on Rh of the microemulsion droplets increasing with the water content, and with the data on Rh of small Span 80 micelles demonstrating no size change [2]. It can be assumed that in case of the maximum of water solubilization, a number of the water molecules bounded with the micelles is constant and thereby the size of aggregates does not change.

Acknowledgements

For the useful discussion of NMR data authors thank Dr. Yu. S. Chernyshev (Faculty of Physics, St. Petersburg State University).

For MD simulation authors thank I. V. Kopanichuk, E. A. Vedenchuk, and Dr. A. A. Vanin (Institute of Chemistry, St.Petersburg State University).

The NMR studies were performed at the Center for Magnetic Resonance, St. Petersburg State University.

The FT-IR studies were performed at the Centre for Optical and Laser Materials Research, St. Petersburg State University.

This work is supported by the Russian Science Foundation (grant 16-13-10042).

References

1. Neuma de Castro Dantas , T.; da Silva, A. C.; Neto, A. A. D. New microemulsion systems using diesel and vegetable oils. *Fuel***, 80 (1)**, 75-81 (2001)
2. Koneva, A. S., Safonova, E. A., Kondrakhina, P. S., Vovk, M. A., Lezov, A. A., Chernyshev, Y. S., & Smirnova, N. A. Effect of Water Content on Structural and Phase Behavior of Water-in-Oil (n-Decane) Microemulsion System Stabilized by Mixed Nonionic Surfactants SPAN80/TWEEN80. *Colloids and Surfaces A: Physicochemical and Engineering Aspects*. **518,** 273–282 (2017)

Investigation of quasi-periodic regimes of spin-wave self-generation in nonlinear active ring oscillator

A. V. Koryukin, V. M. Kislitsyn, A. A. Tolubaeva, A. V. Kondrashov, A. V. Drozdovskii, A. B. Ustinov

Saint Petersburg State Electrotechnical University "LETI"
197022, Saint-Petersburg, 5 Professor Popov st.
E-mail: parnaz@mail.ru

Introduction

In recent years an increased interest to study the self-generation of microwave (MW) dynamic chaos [1-3]. It is due to possible application of dynamic chaos to construct a new generation of communications and radar systems. The advantages of such systems are large noise immunity and good security during information transmission. The purpose of this work is investigation of new regimes of quasi-periodic oscillations of the spin-wave oscillator.

Experimental prototype

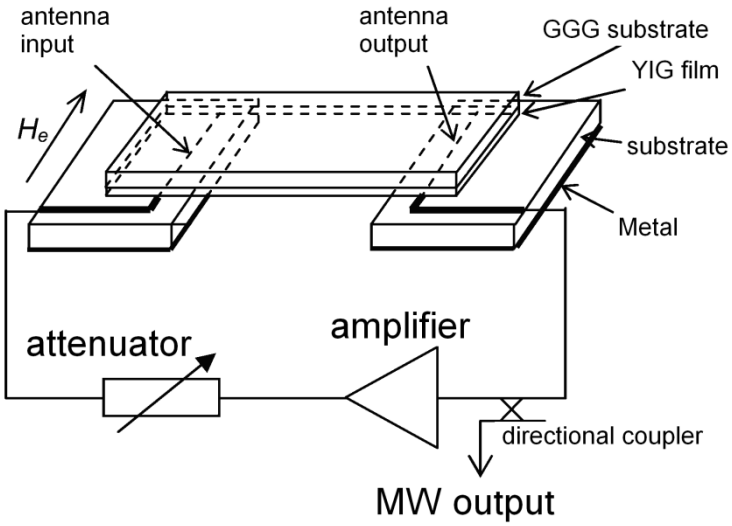

Figure 1. Block-diagram of the experimental prototype of the spin-wave oscillator

Experimental prototype of the oscillator has a ring circuitry consisting of an original spin-wave delay line, a microwave amplifier, a variable attenuator, and a directional coupler to lead the signal out from the ring. The attenuator is used to control the total gain of the ring, allowed to increase the power of the circulating waves. The delay line was made with the yttrium iron garnet film having a thickness of 13.6 μm. The growth of the power of spin waves led to the development of nonlinear processes in the film. The delay line is a nonlinear element that determines the the nonlinear properties of the generated waves. Spin waves excited and received by microstrip antennas having a width of 50 μm. The distance between the antennas was 4.9 mm. The film was magnetized tangentially so as to provide the self-generation of surface spin waves.

Results and discussion

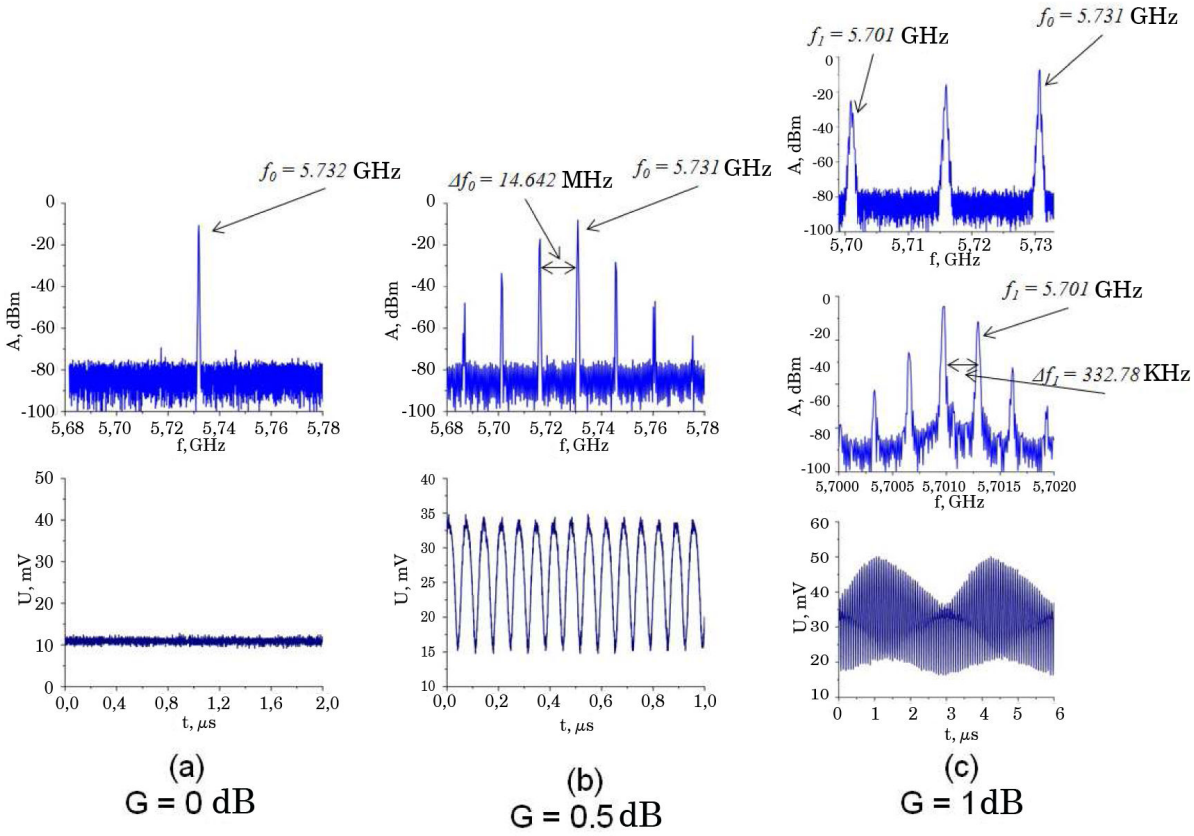

Figure 2. Regimes of generation: (a) – monochromatic, (b) – periodic, (c) – quasiperiodic

Methods of the research consisted of systematic increase in the ring gain G above a self-generation threshold, and to observe waveforms and spectra of the microwave signal in different regimes of generation. At the self-generation threshold, for which the value of G was taken to be zero, we obtained a generation of monochromatic signal at a frequency of 5.732 GHz. By increasing the G increased the power of the microwave signal which circulated in the ring. This led to the increase of the modulation instability which was the reason of amplitude modulation of the signal which was registered by oscilloscope. In the frequency domain the spectrum had additional harmonics with detuning Δf_0. When G was 0.5 dB the amplitude modulation had evolved into a periodic sequence of dark solitons. For this regime Δf_0 = 14.642 MHz. When G was 1 dB each additional harmonic decayed and in the spectrum appeared new harmonic with incommensurate frequency Δf_1 = 332.78 kHz. In the time domain we observed the amplitude modulation of solitons.

It is known, that the oscillations become chaotic after the second bifurcation. However, further with an increase of G after the third bifurcation there was a new quasi-periodic regime instead of a chaotic regime. In this regime the secondary harmonics decayed again and there was a new incommensurate frequency Δf_2 = 1.814 MHz. Reaching the G = 2 dB the oscillations became stochastic. The waveform became complex and non-periodic and the spectrum had a form of a set of broadened harmonics with noise pedestal.

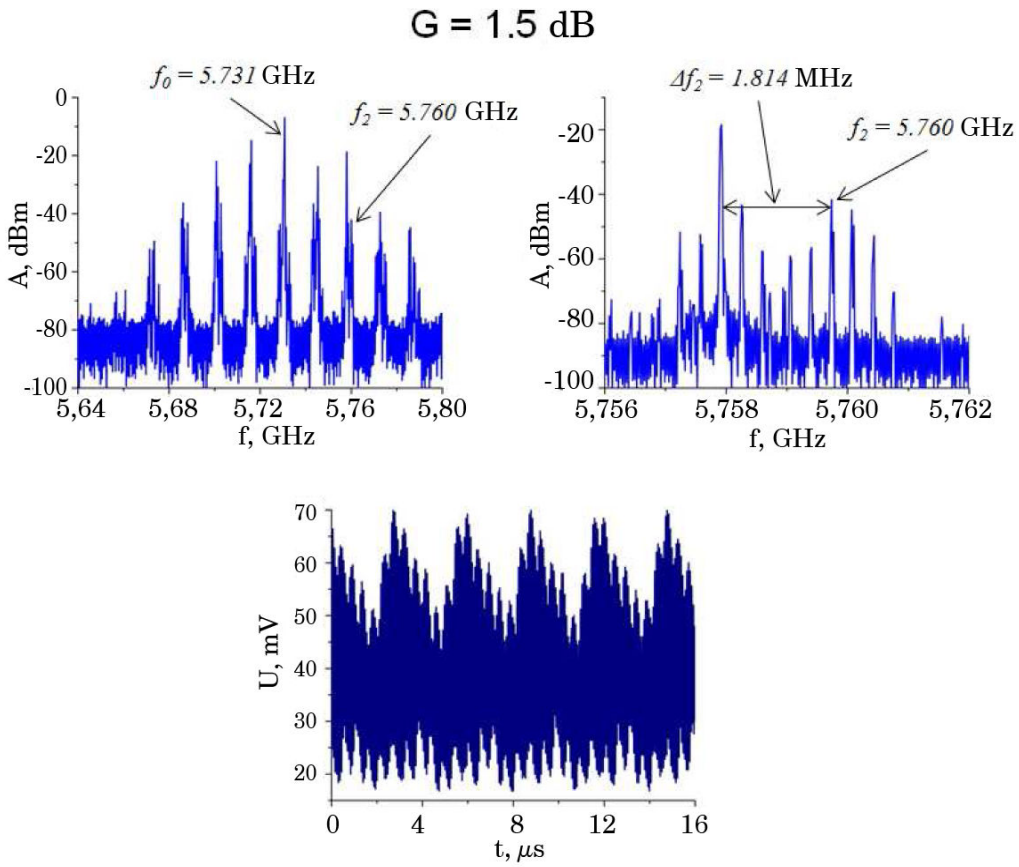

Figure 3. Quasi-periodic regime with 3 incommensurate frequencies

Phase portraits of the observed waveforms were constructed on the basis of the measured self-generation regimes. The phase portraits allowed to determine the system state. As a result the following phase portraits were obtained: for soliton regime - a limit cycle; for quasi-periodic regime with two incommensurable frequencies - two-dimensional torus; for quasi-periodic regime with three incommensurable frequencies we obtained, for the first time, a three-dimensional torus. Phase portrait was a strange attractor for the chaotic oscillation regime. The analysis of phase portraits was carried out with a Grassberger-Procaccia method. As a result, the value of fractal dimensions of attractors identified for various generation regimes.

Thus, we obtained and studied, for the first time, a self-generation regime for which there was a three-dimensional torus in the phase space.

References

1. Dmitriev A. S., Panas A. I. Dynamic Chaos: New data carriers for communication systems (in Russian). - FIZMATLIT 2002.
2. Kuznetsov S. P. Dynamic chaos (in Russian). - FIZMATLIT 2006.
3. Grishin S. V., Grishin V. S., Romanenko D.V., Sharaevsky Y.P. // Technical Physics Letters. 2014. T. 40. N. 19. P. 51-59.

The residual magnetic field measurement in compact shielding construction

Nikita K. Kulachenkov[1], Aleksandra S. Bublikova[2], Georgii S. Chashkin[2], Sergey V. Ermak[2], Vladimir V. Semenov[2]

[1]State Research Center of the Russian Federation Concern CSRI Elektropribor, JSC, St. Petersburg, Russia
[2]Peter the Great Saint-Petersburg Polytechnic University, St. Petersburg, Russia
E-mail: Nik.k2710@gmail.com

The necessary element of compact atomic devices (e.g. atomic clock, nuclear magnetic resonance gyroscope) is existed multilayer magnetic shields. The residual magnetic field significantly influence on a sensitivity (parameters) of such devices [1-2]. In this regard, the components measurement of the residual magnetic field in compact shielding construction and definition of static and dynamic shielding factors are essential problems.

In this paper the absorption signal processing in optical oriented pumping alkali metal atoms is considered. The simplified experimental scheme is shown on fig. 1.

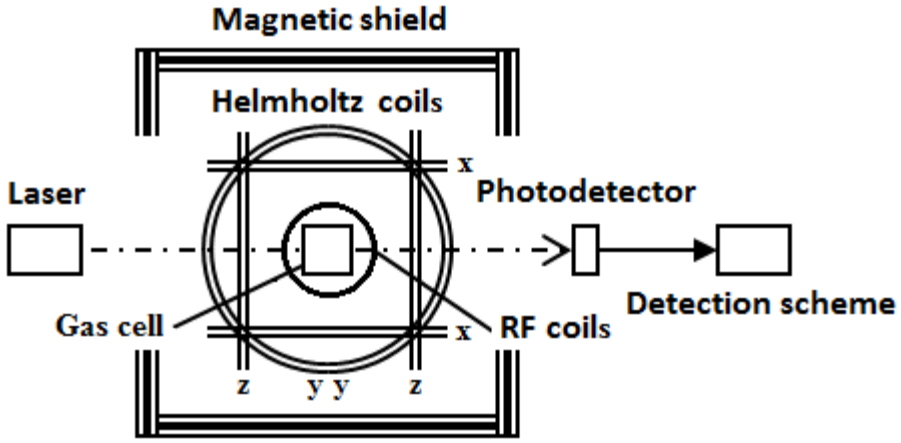

Figure 1. Experimental scheme

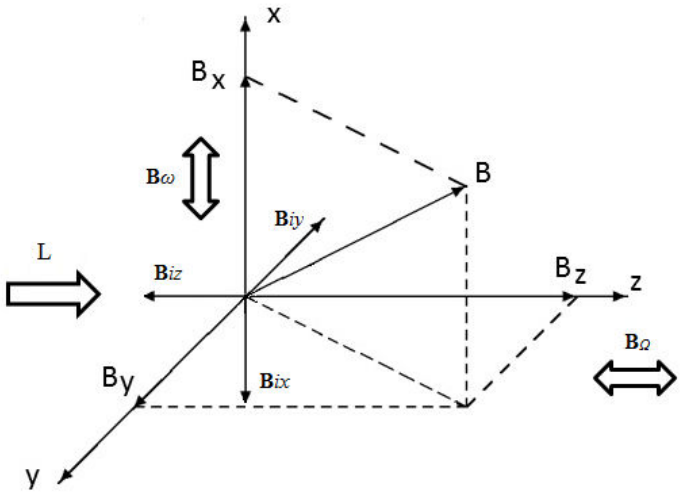

Figure 2. Experimental scheme

The applied vector fields is shown on fig. 2, where **B** is the measuring magnetic field, **L** is the pumping light, $\mathbf{B}_{\Omega}$ is modulation magnetic field, $\mathbf{B}\omega$ is the resonance radio frequency field, **B***iz*, **B***ix*, **B***iy* are the Helmholtz magnetic system components.

The gas cell with alkali metal atoms in the center of three pairs Helmholtz coils system. The residual magnetic field of the shielding system is compensated in three orthogonal **x**, **y**, **z** directions.

The inversion of the current direction has provided in Z - coils oriented along optical axis provides the measurement of the residual magnetic field Z-component by using radio-optical resonance frequency signal. The transverse components of the residual magnetic field were compensated by using Hanle (effect) resonance signal. Zero signal of Hanle resonance is corresponded to the moment of the transverse components compensation [3]. The adjustment parameters of X and Y Helmholtz coils were provided information about the residual magnetic field inside shielding construction using radio-optical resonance frequency signal.

The shielding construction is consider in this paper includes several nested magnetic shields constructed of high-permeability material with 30 mm length and 30 mm middle diameter. The static shielding factor as a ratio of the field applied to the outside of a shielded volume to the field measured inside not exceeds 10^3 in **x**, **y**, **z** directions. The linewidth of the radio optical resonance was defined as 1 kHz with the signal to noise ratio of 10^3 in one Hz bandwidth. The 5 mm spherical gas cell with cesium was used.

The theoretical calculation of the static shielding factor is defined of more than 10^5. The significant difference of values is explained by the functional holes using for the optical trace (in accordance with fig. 1 the laser and photodetector are placed outside shielding construction) and the electrical connections.

The preliminary experimental estimation of dynamic shielding factor was shown. Noted parameter is significantly bigger than static shielding factor for the case of an external alternating low frequency magnetic field (part of Hz). The investigation of the external magnetic field slow variations influence as an important for shielding construction well be continued.

References

1. Y.-Y Jau, A.B.Post, N.N.Kuzma, A.M.Braun, M.V.Romalis W.Happer – *Phys. Rev. Letters*, 11, 110801-1 – 110801-4 (2004).
2. B.C.Grover, E.Kanegsberg, J.G.Mark and R.L.Meyer. – *U.S. Patent №4157495* (1979).
3. C.Cohen-Tannoudji, J.Dupon-Roc, S.Haroche, F.Laloe. – *Rev.Phys. Appl*, 1, 102-108 (1970).

NMR study of transformer oil

Olga E. Kurakina[1], Vladimir K. Kozlov[1], Alexander N. Turanov[1,2], Ruslan A. Giniatullin[3]

[1]Kazan State University of Power and Engineering, Kazan, Russia
[2]Zavoisky Physical-Technical Institute, Kazan, Russia
[3]Kazan National Research Technological University, Kazan, Russia
E-mail: random_jj@mail.ru

Introduction

The condition of transformer oil is one of main factors of stable operation of power oil-filled electrical equipment. An oil composition change occurs as a result of adverse factors influence during exploitation, this leads to a degradation of insulating properties of oil and, consequently, to transformer breakdown. Periodic monitoring of insulating oil composition helps to avoid such problems.

Research

Samples of GK grade oil fresh, used in real power transformer, as well as samples of same grade oil, aged in model conditions were studied by ^{1}H, ^{13}C, ^{17}O NMR spectroscopy (Bruker Avance 400 MHz) and ^{1}H NMR relaxation (Carr-Purcell-Meiboom-Gill and solid-state echo pulse sequences, 19 MHz) techniques.

It was found that percentage of aromatic molecular groups increases at aging of transformer oil (^{1}H, ^{13}C NMR spectroscopy). This can occur both as a result of exchange processes with insulating materials, and as a result of chemical processes of aromatization. Over time aromatic compounds, reaching some concentration, self-organized into columnar supramolecular structures. Such structures grow, condense and precipitate subsequently (^{1}H NMR relaxation).

In addition, it has been shown that ^{1}H NMR spectroscopy makes it possible to determine the water content of oil with high accuracy. This result has practical importance, since to date there is no simple and accurate method for measuring a small amount of water, about 10 g per 1 ton of oil. The techniques used in power grid companies, both in Russia and abroad, have serious shortcomings.

The process of sediment formation in transformer oils

The generally recognized mechanism of sediment formation during the aging of transformer oils is the formation of peroxides, oxides, products of deep oxidation (confirmed by ^{17}O NMR spectroscopy), and the formation of solid particles, which subsequently precipitate.

New mechanism of aging (aromatization) and sedimentation in petroleum transformer oils was discovered and proved on the basis of the results obtained. Analysis of Raman scattering and IR spectra of same samples, as well as the precipitates taken from them, confirms the occurrence of such processes in studied oils.

Conclusion

The obtained results confirmed high potential of NMR spectroscopy for monitoring the degradation processes during the of transformer oil exploitation. It has been described a new mechanism of sedimentation in oils.

References

1. A.C.M. Wilson. Insulating liquids: their uses, manufacture and properties. – London, New York: Peter Peregrinus LTD, 221 p. 1980.
2. R.A. Lipshtein, M.I. Shakhnovich. Transformer Oil. – Israel Program for Scientific Translations, 257 p., 1970.
3. V. Kozlov, A. Turanov. – IEEE Transactions on Dielectrics and Electrical Insulation, 19, 1485-1497 (2012).

The correlation of structure peculiarity with transport properties of mixed-matrix PVA membranes

Anna I. Kuzminova, Anastasia V. Penkova, Maria E. Dmitrenko

St. Petersburg State University, St. Petersburg, 199034 Russia
E-mail: ai.kuzminova@mail.ru

Introduction

Nowadays, the essential improvement of the transport properties of polymer membranes can be achieved by the modification of the polymer matrix by inorganic filler that yields in developing the mixed – matrix membranes (MMMs). The introduction of inorganic filler in the polymer matrix of the membrane allows getting tailoring properties. Hybrid or mixed matrix membranes prepared by dispersing of inorganic filler in a polymeric matrix offer the possibility to overcome the trade-off between the permeability and selectivity of the polymeric membranes. MMMs combine the simplicity of processing polymer membranes with the superior transport properties of inorganic particles. Among the inorganic particles fullerene takes and important place as this nanoparticle saves its unique π-electron structure inside of the polymer matrix.

This work focuses on preparation and characterization of mixed-matrix membranes based on polyvinyl alcohol modified by a water soluble fullerene derivative (fullerenol). The most important investigation of fillers inclusion in polymers is analysis of membranes by spectroscopic methods. Among these methods, nuclear magnetic resonance (NMR) is the best tool for the investigation of polymer nanocomposite materials. NMR allowed to study the interaction between fullerenol and polymer matrix and to confirm the complex structure of MMMs in the present work. The additional characterizations of the polymer samples were done by microscopy methods (SEM, AFM). Transport properties of the membranes were studied during the separation of organic-water mixture. The correlation of structure peculiarity with transport properties of developed mixed matrix membranes was studied. It was shown that the transport characteristics of mixed-matrix membranes were essentially changed as compared to membranes based on parent polymers due to the change of structure and morphology of the polymer membranes.

Acknowledgements

This work was supported by Fellowship of President of Russian Federation СП-1153.2015.1 (Penkova A.V.) and the support of Région Lorraine and CNRS. The experimental work was facilitated by equipment from Resource Centers: Research Centre for Nanotechnology, Research Centre for X-ray Diffraction, Research Centre for Physical Methods Surface Investigation, Thermal Analysis and Calorimetry, Chemical Analysis and Materials Research Centre and GEOMODEL at St. Petersburg State University.

Methodology of intravital labeling of human mesenchymal stromal cells with superparamagnetic iron oxide nanoparticles

K. A. Levchuk[1,2], A. N. Shumeev[2], T. L. Zolina[2], A. V. Kotova[2], L. V. Aleksandrova[2], B. V. Bagaeva[2], A. A. Aizenstadt[1,2], I. E. Kotkas[1], I. I. Maslennikova[1], N. I. Enukashvili[1,3]

Scientific adviser: Senior researcher, Ph. D. Enukashvili N. I.[1]
[1]North-West I.I. Mechnikov State Medical University, St. Petersburg.
[2]Pokrovsky Bank of Stem Cells, St. Petersburg.
[3]Institute of Cytology RAS, St. Petersburg.

Introduction

Nowadays accurate and complex treatment of a variety of diseases with different genesis is available due to application of cell technologies. Though, intravital method of cell labeling for biomedical cell products (BMCP) kinetics examining is still to investigate. Kinetics of medicine for BMCP is a tracking of cell migration and adhesion within organism. Fluorescent labeling of cells is impossible for visualization in organism. Radioactive labeling of cells is harmful for patient and affects the physiology of transplanted cells. MRI is considered to be a perspective method of transplantat visualization. Use of MRI demands the development of intravital cell labeling with contrast agents. Reporter particles should be uptaken by cells, persist within them without changing of biological properties, be visualized by MRI and safe for transplanted cells and recipient organism. Superparamagnetic nanoparticles of ferrum oxide Fe_3O_4 (magnetite) are considered as an appropriate material.

Aim

Set conditions and realize *in vitro* labeling of cell cultures by superparamagnetic iron oxide (SPIO) nanoparticles of Fe_3O_4 (magnetite), verify viability and characterize immunophenotype of cells with inclusion of magnetite.

Materials and methods

Primary cultures of multipotent mesenchymal stromal cells (MMSC) were obtained from human vein of umbilical cord (UC) and human adipose tissue (AT). Each sample had an informed donor agreement. UC and AT MMSC were incubated in cultural medium contained different concentrations of magnetite nanoparticles (5-20 nm) (Powder nanotechnology, Russia). After 24 hours an uptake of particles was estimated due to light microscopy. Immunophenotype of cells with nanoparticles was evaluated by flow cytometry and compared with control cultures of MMSC.

Results

After 24 hours of incubation with SPIO magnetite nanoparticles cell cultures of MMSC maintained viability (95%) as control ones and contained magnetite particles. We found the optimal concentration for good uptake to be of 200 ng/ml. Also, effective labeling needs SPIO nanoparticles to be sonified with 37 kHz ultrasound. Surface markers of cells maintained MMSC immunophenotype as control cultures without uptake.

Conclusion

Obtained data demonstrates a retention of viability and immunophenotype of MMSC for chosen labeling parameters. Subsequently, we are planning to select the conditions for visualization of particles by MRI *in vivo* and *in vitro*. Furthermore, we are going to elucidate stem properties of labeled cells due to functional tests, verify an uptake of particles and optimize the recognition of cells with particles by means of flow cytometry (direct and lateral scattering).

Modern tractography methods: an overview

Nadezhda V. Luzhetckaia, Svetlana V. Ievleva

St. Petersburg State University, 1, Ulyanovskaya str., St. Petersburg, 198504, Russian Federation
E-mail: jennet24@mail.ru

Introduction

Tractography is a technique which is used mostly in neuroscience in order to visualize nerve fiber passes (or tracts) in a human brain. The approach is based on a combination of magnetic resonance imaging techniques, anisotropic diffusion properties of fibrous tissues and special data processing methods. Tractography techniques have been developing for over two decades and have become some of the most promising approaches in biological and medical imaging.

DTI

The base of tractography is diffusion-tensor imaging (DTI or DT-MRI). The technique is quite similar to diffusion-weighted imaging (well-known to every MRI specialist) in a way of data collecting and underlying physical principles, but the number of directions of diffusion gradients applications is higher and equal to that which is optimal to calculate a characteristic of the diffusion anisotropy - the diffusion tensor. Since the work of *Peter J. Basser et.al.* [1], DTI with a simple reconstruction based on diffusion ellipsoids has been the main technique for fiber reconstructions, but it was shown that this type of visualization gives wrong results in areas with fiber crossing, kissing, and so on (see for example, [2]). Therefore, a need for better approaches arose.

HARDI/Q-ball imaging

One of the ways to resolve intravoxel fiber crossing is using high angular resolution diffusion imaging techniques (HARDI). The disadvantage of this method is a requirement of a model of the underlying diffusion process. Fortunately, a new approach, Q-ball imaging, was proposed. It is an implementation of the HARDI approach which uses a spherical tomographic inversion called Funk Random Transform. This technique can resolve complex intravoxel structures and does not require special knowledge about the diffusion process [3].

Conclusion

As one can see, tractography is a quite complex technique which includes usage of MRI pulse sequences, mathematical and statistical methods of data processing and deep understanding of underlying principles for making right conclusions about real tissue structure. It has its own pitfalls and difficulties, but solving them can promise us better understanding of biological processes in a human brain.

References

1. *Peter J. Basser, James Mattiello, Denis LeBihan* MR Diffusion Tensor Spectroscopy and Imaging // Biophysical Journal 66:259-267 (1994).
2. *Derek K. Jones, Thomas R. Knöschec, Robert Turnerc* White matter integrity, fiber count, and other fallacies: The do's and don'ts of diffusion MRI // NeuroImage 73:239–254 (2013).
3. *David S. Tuch* Q-Ball Imaging // Magnetic Resonance in Medicine 52:1358–1372 (2004)

Application of two-frequency NQR and DFT method for assignment of ^{14}N NQR spectra

Sultonazar Mamadazizov[1], Marina G. Shelyapina[2], Anna Neniukhina[1], Galina S. Kupriyanova[1]

[1]Institute of physics and mathematics, Immanuel K ant Baltic Federal University,
[2]Department of Nuclear-Physics Research Methods, Saint Petersburg State University
Kaliningrad, 236016, Russia
E-mail: sultonazar.mamadazizov@mail.ru

Introduction

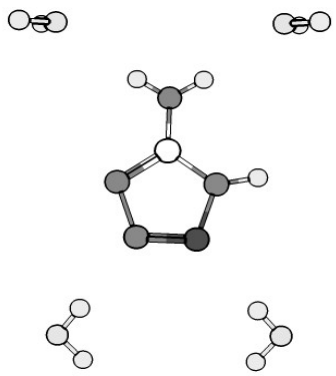

Figure 1. Molecule of 5 aminotetrazole monohydrate

Nuclear Quadrupole Resonance (NQR) is an effective technique for investigation of solid samples. NQR frequency depends on interaction of electric field gradient with nuclei quadrupole moment. Number of NQR transitions is determined by nuclei`s spin. Each nonequivalent nitrogen has three NQR frequencies ω_+, ω_- and ω_0, because of spin I=1. Thus, ^{14}N NQR spectra of 5 aminotetrazole monohydrate (ATZH) consist of fifteen lines. Determination of related transitions and assignment of triplets to corresponding nuclei in a molecule is a difficult task. For this purpose, two-frequency NQR is usually used. It is a reliable technique for determination of related transitions in complex structures. Also quantum mechanical calculations of ^{14}N NQR spectra of molecule are needed to finalize assignment. Accuracy of calculations depends on structural parameters such as bond lengths and angles od molecule. In our work result of theoretical calculations compared to experimental NQR spectra of 5-aminotetrzole monohydrate. It is shown that in combination these techniques could make easier identification and assignment of unknown NQR lines. Also, the assignment based on quantum chemical calculation is more reliable, especially in the cases when the fractional coordinates are known. Even in difficult cases, such as tetrazoles, where 4 or 5 nitrogen have a close NQR frequency it is possible to make correct assignment.

Two-frequency NQR

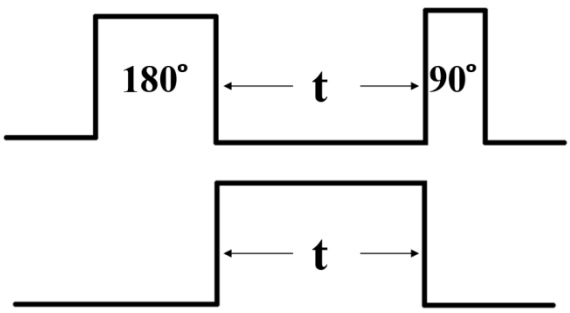

Figure 2. Scheme of spin echo NQR pulse sequence with saturation on second channel

In our work, we investigated nuclei with spin I=1. Single nonequivalent nuclei in this case has three NQR lines ν_+, ν_- and ν_0. After NQR lines had been detected, it is time to identify pairs ν_+ and ν_- of nonequivalent nuclei. One of the most fastest methods is two-

frequency NQR. In this case saturation of one of the lines, for example, ν_+ influence on free induction decay of observed frequency ν_- [1]. To determine related lines spin echo NQR pulse sequence with saturation of transition ν_- was used (Fig. 2). Fourier transform of ATZH spin echo signal of single frequency 3.615 MHz experiment is shown in the fig. 3. Saturation pulse with frequency 2.804 MHz applied on second channel destroys the detected echo signal. Corresponding ν_0 is determined from condition

$$\nu_0 = \nu_+ - \nu_-$$

Determined related transitions are given in the table 1.

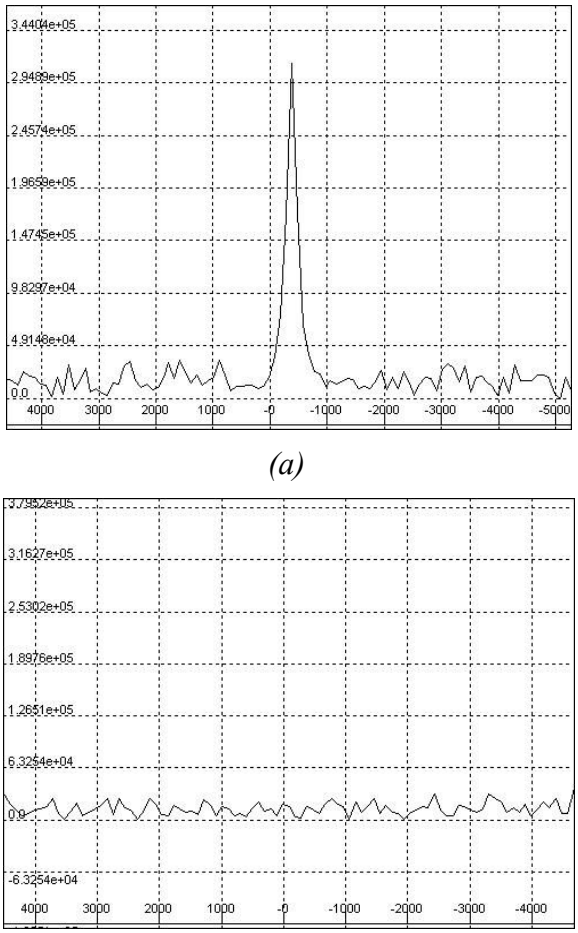

(a)

(b)

Figure 3. Fourier transform of ATZH spin echo signals detected at room temperature on frequency ν_+ = 3.615MHz. (a) One-frequency NQR echo signal; (b) sequence with saturation pulse on ν_- = 2.803 MHz (pulse length t = 3.5 ms)

DFT calculation of ^{14}N NQR spectra of ATZH

Assignment of identified triplets were based on calculated ^{14}N NQR spectra by DFT method. All calculations were performed by the GAUSSIAN09 package [2]. Fractional coordinates for ATZH are given in literature [3]. B3LYP/6-311++G(3df,3pd) is the most suitable basis set for the task. In this case, additional polarization d and p orbitals were added to provide flexibility to hydrogen molecular orbitals. Thus, bonded atoms asymmetric electronic cloud distribution is described more precisely. In case of ATZH water molecules hydrogens and bridge proton in N(1)-H(1)···N(4) has a direct influence on ^{14}N NQR.

Theoretical ^{14}N NQR spectra are given in table 1. Calculated and experimental data are in a perfect agreement. Particularly, average percentage deviation of ν_+(c) lines from

$\nu_+(e)$ is less than 8% and for ν_- lines it is about 5%. Correlation analysis also proves high accuracy of calculated ^{14}N NQR spectra for ATZH (Fig. 4). Determination coefficient for experimental and theoretical NQR lines is about 98%.

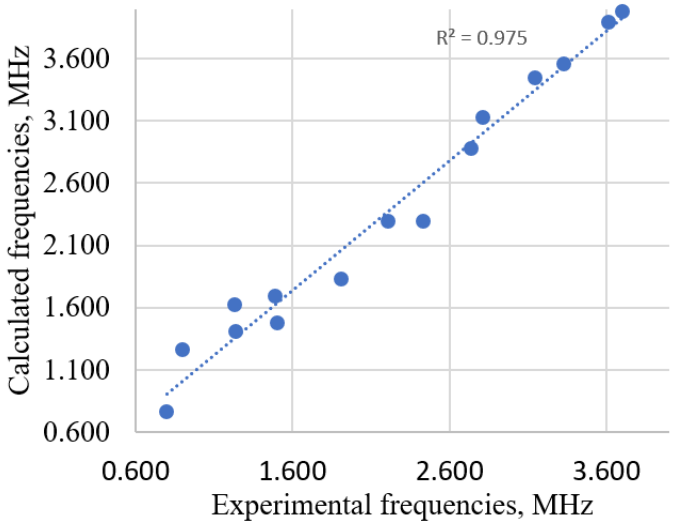

Figure 4. Correlation analysis of calculated frequencies

Table 1. Calculated and experimental ^{14}N NQR spectra of ATZH

N(i)	$\nu_+(c)$, MHz	$\nu_+(e)$, MHz	$\nu_-(c)$, MHz	$\nu_-(e)$, MHz	$\nu_0(c)$, MHz	$\nu_0(e)$, MHz
1	2.881	2.740	1.475	1.500	1.405	1.240
2	3.982	3.700	2.293	2.210	1.688	1.490
3	3.892	3.615	3.132	2.815	0.760	0.800
4	3.451	3.143	1.827	1.910	1.624	1.233
5	3.559	3.331	2.295	2.430	1.264	0.901

Conclusion

Related NQR frequencies of five nonequivalent nitrogen in ATZH were determined. ^{14}N NQR spectra of 5 aminotetrazole monohydrate were calculated with correlation coefficient of 98%. New assignment based on experimental and theoretical data was proposed.

References

1. J Supercond Nov Magn (2011) 24: 653–658
2. Gaussian 09, Revision A.02, M. J. Frisch, G. W. Trucks, H. B. Schlegel…2009
3. Journal of Molecular Structure, 83 (1982) 35-55

Accounting for the effects of conformational structure of the spin labels on the parameters of the EPR spectra by DFT method

Alina Mamatova[1], *Liudmila Savostina*[1,2]

[1]*Institute of physics, Kazan Federal University, Kazan, Russia*
[2]*Zavoisky Physical-Technical Institute, Kazan, Russia*
E-mail: mamatovaalinka@mail.ru

Introduction

Correct interpretation of the EPR signal from free radicals are known as spin labels is necessary and useful information for EPR experiment. Spin labels EPR spectra give characteristic, in turn dependent on the molecular mobility and the physicochemical properties of the environment. However, some spin labels with different conformations can be reflected in the EPR spectra and this fact must be considered for explanation of the EPR data.

The influence of conformational changes in the molecules on their physico-chemical properties is one of the most pressing problems in organic chemistry (the influence of the conformation of the molecule to its reactivity), biology (the dependence of the biological activity of substances on the conformation), and physics (influence of the conformation of the spin labels on the parameters of the spectra of electron paramagnetic resonance (EPR), such as the g-factor and the hyperfine interaction constant (HFC)). Different conformations are characteristic of molecules containing rings: a five-, six-, seven-membered ring, etc. The objects of our research are spin labels. They are derivatives of nitroxyl radicals containing a six-membered heterocyclic ring: 2,2,6,6-tetramethyl -piperidine-1-oxyl - TEMPO, 4-oxo-2,2,6,6- tetramethyl -piperidine-1 -oxyl -TEMPOL, 4-hydroxy -2,2,6,6-tetramethyl -piperidine-1-oxy -TEMPONE. These six-membered stable nitroxyl radicals are widely used in the method of spin labels.

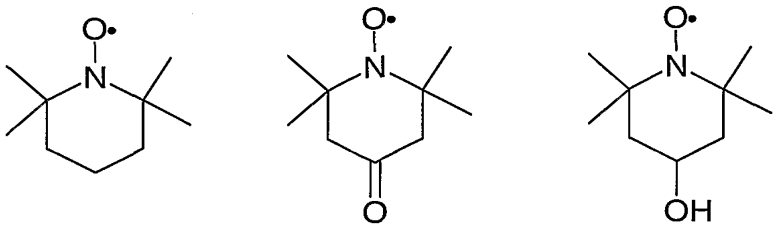

TEMPO TEMPONE TEMPOL

All of six-membered cyclic molecules characterized three different conformations: "chair", "bath", "twist". From stereochemistry the most stable conformation is "chair" and the less stable conformation is the "bath."

Method and results

The stable conformation (chair, twist) of nitroxyl radicals were obtained by the method of density functional theory (DFT). The calculations were performed with full geometry optimization using the BP86, B3LYP, BHandHLYP functionals [1] and several basis sets SVP, TZVP, EPRII, EPRIII [2] in ORCA software package [3]. Calculations of the EPR parameters - g-factor and the constant of hyperfine interaction (HFC) were carried.

For calculations of the EPR spectra parameters (constant HFC and g-factor), we used the following procedure: for each of the conformation of the radical molecule selected geometry with the most stable (lowest) energy and use it as the starting geometry for the calculation in the same functional but with the use of special bases developed for calculations

of the EPR spectrum parameters, EPRII and EPRIII. At the same time, we carried out a full optimization of the geometry of the molecule.

Calculations for each of the conformation of the radical molecules by use three functionals were carried out. The results are shown in Table 1.

Table 1

		TEMPONE		**TEMPO**		**TEMPOL**	
BP86		***TWIST***	***CHAIR***	***TWIST***	***CHAIR***	***TWIST***	***CHAIR***
HFC (MHz)	EPRII	16.21	29.07	16.51	28.76	16.36	28.48
	EPRIII	18.05	29.24	18.39	28.91	18.25	28.67
g-factor	EPRII	2.0056	2.0058	2.0055	2.0058	2.0056	2.0058
	EPRIII	2.0057	2.0059	2.0057	2.0059	2.0057	2.0059
B3LYP		***TWIST***	***TWIST***	***CHAIR***	***CHAIR***	***TWIST***	***CHAIR***
HFC (MHz)	EPRII	26.31	36.87	26.76	36.04	36.40	36.40
	EPRIII	27.42	29.23	27.57	35.29	35.82	35.82
g-factor	EPRII	2.0059	2.0061	2.0058	2.0059	2.0061	2.0061
	EPRIII	2.0060	2.0059	2.0060	2.0061	2.0063	2.0063
BHandHLYP		***TWIST***	***TWIST***	***CHAIR***	***CHAIR***	***TWIST***	***CHAIR***
HFC (MHz)	EPRII	38.27	**45.13**	39.03	**45.45**	45.12	**45.12**
	EPRIII	38.44	44.49	39.20	44.82	44.48	44.48
g-factor	EPRII	2.0061	2.0064	2.0061	2.0063	2.0064	2.0064
	EPRIII	2.0063	2.0065	2.0062	2.0064	2.0065	2.0065
Experiment [4]		**TEMPONE**		**TEMPO**		**TEMPOL**	
HFC (MHz)		49.44		45.66		48.32	
g-factor		2.0068		2.0070		2.0078	

Since experimental data obtained at room temperature, it can be assumed that the environment can be investigated in equilibrium multiple conformations. Our calculations have shown that on the potential energy surface of nitroxyl radicals is possible to locate only two of the three possible conformations: "chair" and "twist". The energetically stable conformation is a "chair".

However, the other conformation "twist" is not be totally excluded for studying. The energy barrier between the possible conformations were obtained. Calculations have shown that the activation barrier for transition nitroxyl radical one conformation into another conformation is of the order of 2.18 kcal/mol for TEMPO radical and in the reverse path (from the "chair «conformation in» twist conformation) the activation barrier of the same molecule is 1.89 kcal/mol. Such an order of magnitude of the activation barrier suggests that at room temperature overcoming the activation barrier of this is possible due to thermal motion (Brownian motion). Based on these data, we can assume that at room temperature there is a mixture of conformers.

The final value hyperfine coupling constants for a mixture of several conformations can be calculated by the formula [5]:

$$A_F = \sum_i A_{F,i} n_i / N$$

where n_i - mole fraction conformation, $N = \sum_j n_j$,

According to the Boltzmann distribution of the statistical population is one configuration $\frac{n_i}{N}$ given its energy ε_i: $\frac{n_i}{N} = \frac{\exp(-\beta\varepsilon_i)}{\sum_j \exp(-\beta\varepsilon_j)}$,

where $\beta = {}^{1}/_{kT}$ (k- Boltzmann constant, T =293,15 K), ε_i- SCF energy i-conformer relative to the lowest energy.

The calculations of the average constant of the hyperfine interaction (HFI) on the nitrogen atom to radicals TEMPO, TEMPONE и TEMPOL are showed in Table 2.

Table 2

TEMPONE					
i	*conformation*	ε_i	n_i/N	A_i	A_s
1	twist		0,474235	38,2	41,88
2	chair	0	0,525765	45,1	
TEMPO					
i	*conformation*	ε_i	n_i/N	A_i	A_s
1	twist		0,003233	39,2	44,71
2	chair	0	0,996767	45,0	
TEMPOL					
i	*conformation*	ε_i	n_i/N	A_i	A_s
1	twist		0,001134	38,7	45,10
2	chair	0	0,998866	45,1	

Conclusions

Our quantum chemical calculations showed that:

1. The energetically stable structure of nitroxyl radicals is the structure of a conformation "chair".
2. The calculated value of the g-factor for the conformation of the "chair" (for all investigated derivatives of nitroxyl radicals) is closest to the experimental data.
3. The most optimal combination of the functional / the basis for quantum chemical calculations of nitroxyl radicals of six-membered (using the ORCA software package) are:
   - BP86 / TZVP to find electronic and spatial structure of the molecule;
   - BHandHLYP/EPRII to calculate the parameters of EPR spectra. The calculated values of the isotropic hyperfine coupling constants and the g-factor of the molecules are as closest to the experimental data.

References

1. Becke, A. D. A new mixing of Hartree–Fock and local density-functional theories /A. D. Becke // The Journal of Chemical Physics, 1993. – Vol. 98. – P. 1372-1377.
2. Barone, V. Recent Advances in Density Functional Methods, Part I, ed. D. P. Chong // World Scientific Publ. Co., Singapore. - 1995.
3. Neese F. The ORCA program system. // WIREs Comput. Mol. Sci, 2012. – Vol. 2. – P. 73-78.
4. M. Kumara Dhas," Electron spin resonance spectroscopy studies on reduction process of nitroxyl radicals used in molecular Imaging," European Journal of Biophysics, 2014. - Vol. 2, No. 1. - P. 1-6.
5. Malcek M., Calculation of hyperfine coupling constant of the TMPD molecule // Acta Chimica Slovaca, 2012. - Vol.5, №1. - P.100-108.

Principles of image fusion of CT and MRI using external labels

Veronika V. Mamontova, Anna V. Lebedeva, Andrei V. Komolkin

Saint Petersburg State University, 7/9 Universitetskaya emb., St. Petersburg, 199034, Russia
E-mail: st048848@student.spbu.ru

Introduction

At the present time tomography is frequently used for patient health research. This technique allows one to identify pathologies without direct intervention to the body. In this work two tomographic methods are used: magnetic resonance imaging (MRI) and computed tomography (CT). MR distinguishes soft tissues, such as muscle and fat ones, while the X-ray used in CT clearly distinguishes bone tissues [1].

Therefore, it is useful to fuse the images obtained by these methods.

The main idea of this work is to employ the special labels attached to the patient's body as the reference for image fusion.

Choice of the label substance

The problem was to find substances, which are contrast in both computed tomography and magnetic resonance imaging, or two substances to make labels which consist of X-ray contrast shell filled with MRI-contrast liquid (combined label). Solutions of Copper sulfate and Urografin 76% (Sodium amidotrizoate), Iodine (5% alcohol solution), Bar-VIPS (Barium sulphate) were chosen for the experiment. Further studies were carried out using magnetic resonance imager TOSHIBA MRT200PP2 and CT scanner TOSHIBA Aquilion. There were applied T1-weighted, T2-weighted, and T1 with suppression of the signal of water (FLAIR) methods in the MRI experiment.

The table shows density of the most suitable substances. The first three could be used as contrast agents for both CT and MRI, while the remaining ones as part of combined labels.

Table. The list of the most suitable substances and their density (in units of Hounsfield scale for CT, in relative units for MRI)

Substance	CT	MRI		
		T1	T2	FLAIR
Urografin 76% (25% vol/vol aqua solution)	2300	3100	5700	2900
Urografin 76% (13% vol/vol aqua solution)	1200	2700	7400	2800
I_2 (5% alcohol solution)	1700	2200	4800	3600
Bar-VIPS ($BaSO_4$)	14000	-	-	-
$CuSO_4$ (0.45 g/l aqua solution)	0	7000	8200	8400
$CuSO_4$ (0.75 g/l aqua solution)	0	5800	5600	5600

Principle of image fusion

It is supposed to combine tomograms by dividing the field of research into tetrahedra, the vertices of which are in the centres of spherical labels. This method is called triangulation.

Let us consider the fusion of 2 slices (fig.1). To align them, it is needed to perform rotation transformations, scaling, and reflection of images, due to the fact that image resolution (pixel size) and slice thickness in CT and MRI examinations are different as well as an image of MRI could be turned in the laboratory reference frame, hence two slices may be not parallel to each other. Position of voxel in the reference frame is carried out by reading the tags that determine the orientation of the patient from a DICOM file.

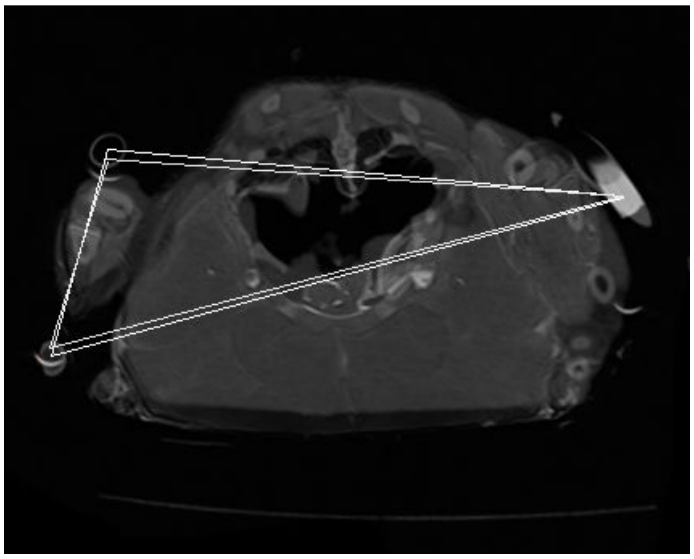

Figure 1. The triangulation principle

Program for data visualization

Processing of a series of planar images (MRI or CT results) was carried out in Python version 3, using "pydicom" package [2]. The data of each slice in the series are converted to image in PNG format. The color of each pixel depends on the density of body tissue.

3D reconstruction is written in C++ without the use of additional packages.

There are many different methods of 3D reconstruction. This work used the most common Voxel-based volume model. The voxel contains a color value (density). The coordinates of each voxel are calculated from its relative location.

Building 3D model involves combining the sequence of images (fig. 2). Distance between the images is determined by the orientation of each image in space, as well as its spatial coordinates and thickness of each layer.

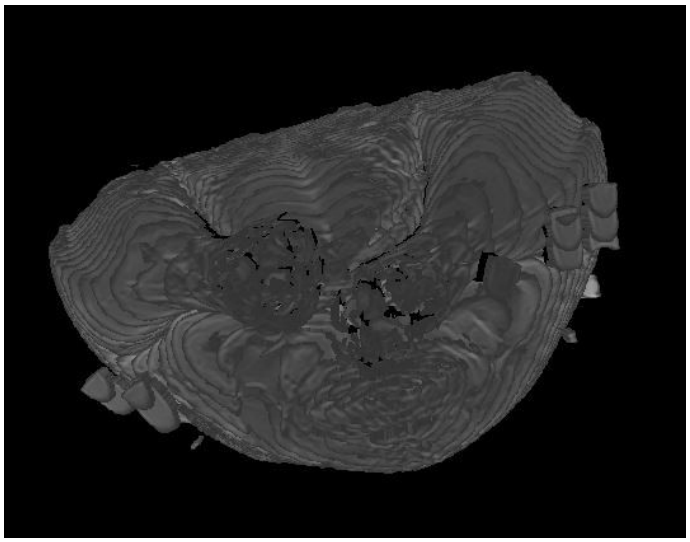

Figure 2. Building 3D model of chicken with external labels

Showing voxels on the screen is produced using OpenGL and OpenGL Shading Language.

Using CUDA in the future will optimize the program performance.

As a result, the graphical user interface was developed. At this stage it involves drawing arrays on the screen and the ability to work with three-dimensional object (building grid, navigate, zoom). It contains the classic menu toolbar.

The workspace is divided into several parts: a preview window and a window view 3D-image (or 2D).

Additional functionality such as simultaneous display of CT and MRI and their combination in 3D format can be added as the project progresses.

Acknowledgements

Authors would like to express gratitude to the University Clinic of St. Petersburg State University ("SPMC" of the Ministry of Health of Russia) providing us with the opportunity to conduct studies using CT scanner and magnetic resonance imager.

References

1. The radiology information resource for patients [Electronic resource] – Access mode: https://www.radiologyinfo.org/ (23.03.2017)
2. Pydicom User Guide [Electronic resource]. — Access mode: http://pydicom.readthedocs.io/en/latest/pydicom_user_guide.html (06.01.2017)

Molecular Dynamics Simulation of Lysine Dendrimer of 5th Generation and Oppositely Charged Semax Peptide

Igor Neelov[1,2], *Elena Popova*[2,3]

[1]*Institute of Macromolecular Compounds, Bolshoy prospect 31, St. Petersburg, Russia*
[2]*ITMO University, Kronverksky prospect 49, St. Petersburg, Russia*
[3]*Institute of Hygiene, Occupational Pathology & Human Ecology, Kuzmolovo, Russia*
E-mail: i.neelov@mail.ru

Introduction

Starting from 80th years of the last century, when the first dendrimers were synthesized [1], interest to them grows every year and a great number of papers on dendrimer synthesis behaviour and applications were published. Dendrimers are the macromolecules with regular star-like ("star-burst") branched structure, spherical shape, constant size and a constant number of terminal groups under normal conditions. It makes possible the creation of well-characterized complexes of dendrimers with other compounds.

It is shown in [2] that in some cases dendrimer complexes with some drugs are hundred and thousand times more effective than drugs without dendrimers at the same concentration. Dendrimers improve the solubility of drugs in water, increase the time of their circulation, and could be used for targeted delivery of drugs to specific tissues, improve the transfection and crossing different biological barriers. Dendrimers also protect drugs from degradation and from contact with healthy cells during delivery process.

Therapeutic Semax peptide (Met-Glu-His-Phe-Pro-Gly-Pro) was selected as a model peptide in our study because it belongs to a class of regulatory peptides and has an antioxidant, antihypoxic and neuroprotective properrties. Semax peptide is used for acute ischemic stroke prevention, for traumatic brain injury treatment, for recovery of patients after a stroke, in the case of optic nerve disease and glaucoma optic neuropathy.

The goal of this paper is to study the interaction between lysine dendrimer and therapeutic Semax peptides using molecular dynamics method to determine whether the dendrimer could form a complex with peptide molecules and thus could be used for delivery of these peptides into cells.

Model and Calculation Method

Modeling was performed using the molecular dynamics method for systems consisting of one lysine dendrimer of fifth generation with positively charged $NH3^+$ end groups, 8 or 24 Semax peptides (with charge -1 each), water molecules and chlorine counterions in a cubic cell with periodic boundary conditions. The initial conformations for peptides with internal rotation angles in main chain equal (–135º, 135º, 180º) was prepared using Avogadro chemical editor. The structures were optimized in vacuum using molecular mechanics of AMBER force field. Further energy minimizations and simulations were performed using the GROMACS 4.5.6 software package and AMBER_99SB-ildn force fields. The potential energy of this force field consists of valence bonds and angles deformation energy, internal rotation angles, van der Waals and electrostatic interactions. The procedure of molecular dynamics simulation used for lysine dendrimers and polyelectolytes has been described earlier in [3-7]. In all calculations the normal conditions (temperature 300 K, pressure 1 atm) were used.

Results and Discussion

Modeling of Equilibrium Process Establishment

The time dependence of gyration radius R_g at the beginning of calculation describes the process of equilibrium establishment during complex formation. From Fig. 1 it can be seen that dendrimer complex with 8 peptides forms within 20 ns. In case of system 24 peptides, complex forms for the first time nearly within 30 ns (see local peak of R_g on curves 2 of Fig.1). Some peptide molecules in second complex were detached (we checked it using snapshots; not shown) from dendrimer and finally it takes almost 1.5 to get stable comlex in the system. After that the complex sizes R_g fluctuate slightly, but their average values practically do not change with time. Therefore, we can assume that the systems are in equilibrium state.

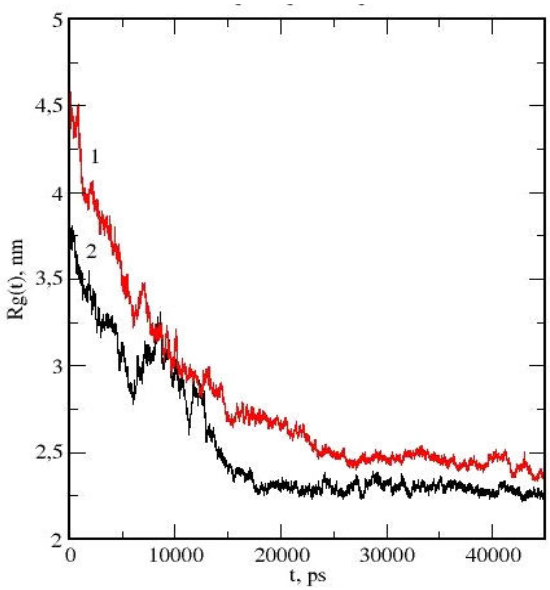

Figure 1. Time dependence of gyration radius. For systems consting of dendrimer G5 and: 8 Semax peptides (1); G5 and 24 Semax peptides (2)

Modeling of the equilibrium state

In equilibrium state the size R_g of the complex G5 with 24 Semax peptides is larger than the size of G5 with 8Semax which is greater then size of dendrimer G5 without perptides (see Table 1). It is quite natural, since it correlates with increase of the molecular weight of the complexes in comparison with the molecular weight of the dendrimer itself. The shape of both complexes can be characterized by their tensor of inertia main component (R_g^{11}, R_g^{22}, R_g^{33}), that are in Tab. 1 and in the simplest case, anisotropy by ratio R_g^{33} / R_g^{11} . The values of this anisotropy for our systems are presented in Tab. 1 and only slightly fluctuate with change of size of the complex

*Table 1. The eigenvalues R_g^{11}, R_g^{22}, R_g^{33} of inertia tensor, gyration radius **R_g** , anisotropy of shape R_g^{33}/R_g^{11} and diffusion coefficients D of G5 and two peptide complexes*

System	R_g^{11} (nm)	R_g^{22} (nm)	R_g^{33} (nm)	R_g (nm)	R_g^{33}/R_g^{11}	$D \times 10^5$ (sm^2/s)
Dendrimer (*G5*)	1.30	1.49	1.61	1.81	1.24	-
G5 & 8 Semax	1.32	1.65	1.75	1.88	1.35	0.12
G5 & 24 Semax	1.736	1.89	2.11	2.50	1.21	0.10

Information about the internal structure of the equilibrium complex could be obtained using radial density distribution of different groups of atoms relatively center of inertia of

system. Figure 2 demonstrates that dendrimer (curve 1) is located in the centre of the complexes while peptides (curve 2) are mainly on surface of both complexes with 8 and 24 peptides and do not penetrate in the center of complex. But it is necessary to mention that at intermediate distances from center of complexes the dedrimer and peptides densities overlap.

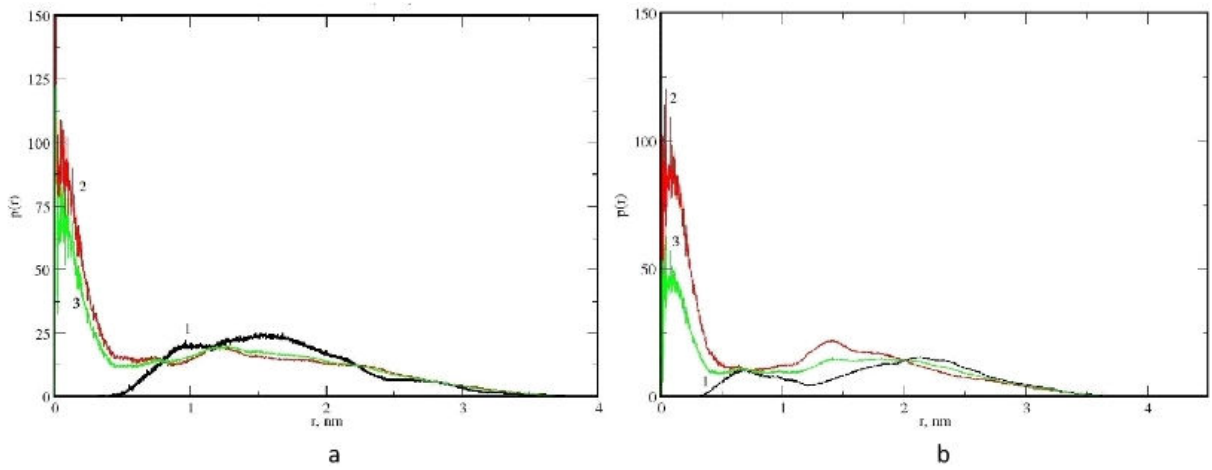

Figure 2. Radial distribution p(r) curves: dendrimer G5 and 8 Semax (a), dendrimer G5 and 24 Semax (b). Distribution curves: peptide atoms (1); dendrimer atoms (2); all atoms of complex (3)

Thus MD simulation shows that dendrimer-peptides complex formation is possible and occurs rather quickly (in 20-40 ns) for both systems. The equilibrium size (radius of gyration) and the anisotropy of both complexes are rather close to each other. The radial distribution function of atom number in all complexes shows that dendrimer is mainly inside the complex, while the peptides are mainly on its surface.

Acknowledgements

This work was partly supported by grant 074-U01 of Government of RF and RFBR grants 16-03-00775. Computing resources on supercomputers "Lomonosov" were provided by supercomputer center of Moscow State University [8].

References

1. E. Buhleier, W. Wehner, F. Vögtle. - *Synthesis*, **9,** 155–158 (1978).
2. E. Abbasi, S.F. Aval, A. Akbarzadeh, M. Milani, et. al. - *Nanoscale Res Lett,* **9**, 247 (2014).
3. I.M. Neelov, D.A. Markelov, S.G. Falkovich, M.Y. Ilyash, B.M. Okrugin, A.A. Darinskii - *Polymer Science*, **55**, 154-161 (2013).
4. S. Falkovich, D. Markelov, I. Neelov, A. Darinskii -. *Journal of Chemical Physics*, **139**, 064903 (2013).
5. I. Neelov, S. Falkovich, D. Markelov, E. Paci, A. Darinskii, H. Tenhu Dendrimers in Biomedical Applications, RSC Publ., London, 2013
6. I.M. Neelov, A. Janaszewska, B. Klajnert, M. Bryszewska, N. Makova, D. Hicks, N. Pearson, G.P. Vlasov, M.Y. Ilyash, D.S. Vasilev, N.L. Dubrovskaya, et al. - *Current Medical Chemistry*, **20**, 134–143 (2013)
7. D.A. Markelov, S.G. Falkovich, I.M. Neelov, M.Y. Ilyash, V.V. Matveev, E. Lahderanta, P. Ingman, A.A. Darinskii - *Physical Chemistry and Chemical Physics*, **17**, 3214-3226 (2015)
8. V. Sadovnichy, A. Tikhonravov, V. Voevodin, V. Opanasenko Contemporary High Performance Computing: From Petascale toward Exascale, Boca Raton,. 2013

Studies of spin-lattice relaxation in liquid Ga-In eutectic alloy embedded into opal

D. Yu. Nefedov[1], A. V. Uskov[1], E. V. Charnaya[1], J. Haase[2], D. Michel[2], Yu. A. Kumzerov[3]

[1]*St. Petersburg State University, St. Petersburg, 198504 Russia*
[2]*Faculty of Physics and Geosciences, Leipzig University, 04103 Germany*
[3]*A.F. Ioffe Physico-Technical Institute RAS, St. Petersburg 194021, Russia*
E-mail: iverson89@yandex.ru

Introduction

Investigations of properties of liquids under nanoconfinement are of great interest. Especially phase transitions in such systems attract the increasing attention of investigators. The aim of the present work consists in studies of melted Ga-In eutectic alloy embedded into an opal matrix. Crystallization of the eutectic alloy occurs gradually. Within the temperature range of crystallization different interesting effects are observed. In particular, in the temperature range 180 to 169 K two components of the NMR line appear. It is known that in some liquids, like water, there are phase transitions between different structural phases [1]. Tien et al [2] reported NMR measurements carried out for supercooling Ga in an opal-confined environment. The appearance of two distinct peaks was interpreted in terms of the possible existence of two different liquid forms of Ga at the temperature range between 260 and 220 K. In [3] the existence of a transition from a high-density to a low-density liquid Ga in the supercooled regime was predicted using molecular dynamics simulation.

Sample and experiment

Sample is a nanocomposite consisted of the Ga-In alloy (Ga – 94 at.%, In – 6 at.%) embedded into pores of artificial opal with the size of silica spheres about 260 nm. Pore sizes of opal were less than theoretical for the octahedral and tetrahedral pores due to deformation of silica spheres during opal preparation. Spin-lattice relaxation time and line shape measurements were carried out for ^{71}Ga isotope at magnetic field of 11.7 T using Bruker Avance 500 NMR pulse spectrometer.

Results

At room temperature the NMR signal of ^{71}Ga is a narrow single line. By cooling within the temperature range between 180 to 169 K two components of the NMR line appear. During cooling the low-frequency component disappears, and high-frequency component gets more intensive. One can say that intensity from the low frequency component is pumped to the high frequency component. From appearance of two components in the NMR signal we suggested that structural changes were observed before total freezing in liquid alloy. Peaks have rather different Knight shifts to allow us to fit the NMR line by two Lorentz functions (Fig.1).

Also, the similar deconvolution of the NMR line into two Lorentz functions was carried out for each time point in inversion-recovery experiments for different temperatures in the temperature range of coexistence of two components to calculate the relaxation times for the components. It was found that components had different spin-lattice relaxation times (Fig.2).

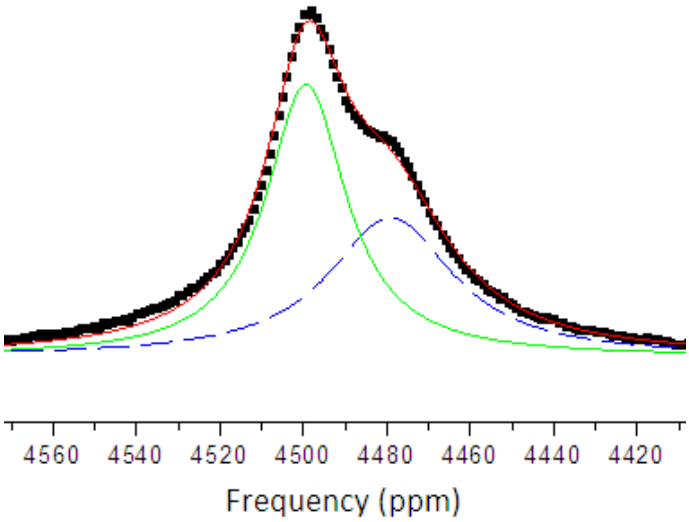

Figure 1. NMR line of ^{71}Ga at 173K. Black squares – experimental data, solid red line – fitting curve of total line, solid green line – fitting curve of high frequency peak, dashed blue line – fitting curve of low frequency peak

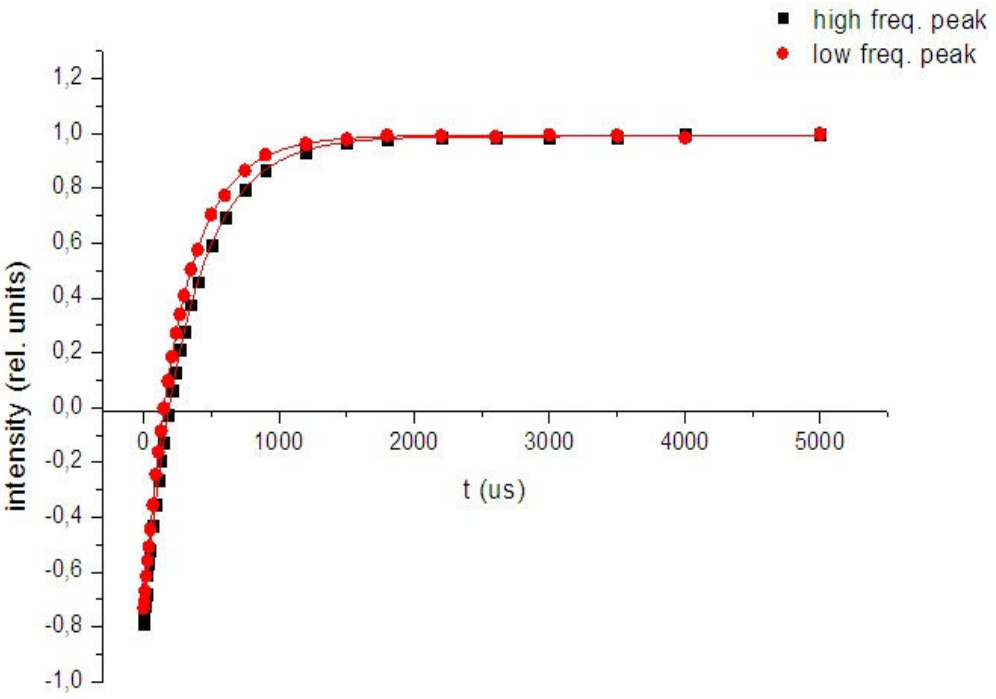

Figure 2. Spin-lattice relaxation curve of high and low frequency components of ^{71}Ga at 173K

Correlation time of atomic motion and quadruple constant were found by fitting the magnetisation recovery with the expression

$$\frac{M(t)}{M_0} = 1 - b\left[\frac{4}{5}\exp\left(-\frac{C\tau_c t}{1+4\omega_0^2\tau_c^2}\right) + \frac{1}{5}\exp\left(-\frac{C\tau_c t}{1+\omega_0^2\tau_c^2}\right)\right]\exp\left(-\frac{t}{T_{1m}}\right), \qquad (1)$$

where M_0 is equilibrium magnetisation, b accounts for nonideal inversion of magnetisation, C is constant of quadruple interaction, ω_0 is Larmor frequency, τ_c is correlation time of atomic motion, T_{1m} is time of longitudinal relaxation due to magnetic interaction.

The obtained temperature dependences of the product of the correlation time and quadruple constant for both components are shown in Fig. 3.

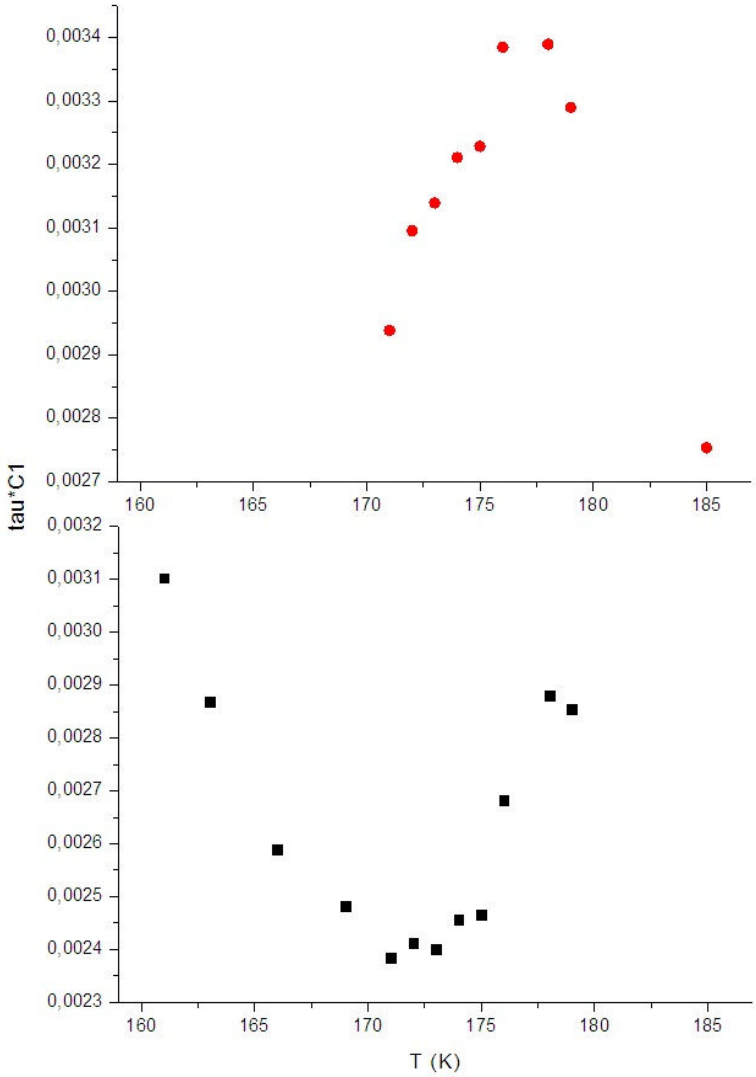

Figure 3. Temperature dependence of $\tau_c C$. Black squares – high frequency component, red circles – low frequency component

In addition to the NMR-line behavior of Ga in the Ga-In alloy within opal at the temperature range between 180 to 169 K, different spin-lattice relaxation times for two components evidence the coexistence of two different phases of liquid alloy. This effect corresponds to the supposition about structural transformations. Further investigations of structural changes in the liquid Ga-In alloy with current composition and with other compositions in porous matrices with different size of pores are of great interest.

References

1. P. H. Poole, F. Sciortino, and H. E. Stanley, Nature London **360**, 324 1992.
2. C. Tien, E. V. Charnaya, W. Wang, Y. A. Kumzerov, and D. Michel, Phys. Rev. B **74**, 024116 2006.
3. D. A. C. Jara, M. F. Michelon, A. Antonelli, and M. de Koning, J. Chem. Phys., **130**, 221101 (2009).

Adsorption of n-hexane on silicalite-1 studied by NMR

Tatiana V. Nikiforova, Andrey V. Savinkov, Bulat I. Gizatullin

Institute of Physics, Kazan Federal University, Kazan, Russia
E-mail: 44tanuxa44@mail.ru

Introduction

Detailed study of the dynamics of adsorbed hydrocarbon molecules in the zeolitic pores is subject of particular interests of scientists, because the molecular motion of the adsorbed hydrocarbon may have a close relation to the process of hydrocarbon separation [1] and to the shape selective behavior exhibited by zeolite [2]. Therefore, many experimental and theoretical works have been done to clarify the dynamic behavior of adsorbed hydrocarbons in the porous media of the MFI-type zeolites and silicalites. However, some aspects of hydrocarbon's adsorption in silicalite-1 are unclear until the present time.

The crystal structure of silicalite-1 is the aluminum-free analogue of MFI zeolite. The silicalite-1 contains two channel systems. The first type of channel is straight and has dimensions of 5.3 Å by 5.6 Å, while the second channel system follows a zig-zag path and has pores with dimensions of 5.1 Å by 5.5 Å. Porous media of zeolite and silicalite samples also includes the inter-crystallite pores with wide distributed dimensions of ~1 – 100 μm.

Two-dimensional nuclear magnetic resonance (2D NMR) is one of powerful methods to study of dynamic and exchange processes in porous media, such as mass transfer though space via molecular transport or magnetization transfer though cross-relaxation and spin-diffusion. In this report, we represent results of intensive study by 2D ^{1}H NMR of *n*-hexane adsorption kinetics in silicalite-1 sample, molecular mobility and dynamical NMR-characteristics of *n*-hexane in silicalite-1 channels at different stages of the *n*-hexane adsorption.

Experimental and Results

The measurements were performed with a 20 MHz NMR Xromatech Proton-20M relaxometer at low magnetic field. Powder of silicalite-1 was annealed at $T \sim 250\ ^0$C and pumped during 1 hour. Then the silicalite-1 sample was exposed on *n*-hexane atmosphere during different time periods; every time a content of *n*-hexane was controlled by weighting the sample and 2D ^{1}H NMR measurements were performed. The *n*-hexane content was increased from 0% (wt.) and saturated on the 14.6% (wt.). The experiment was performed at room temperature.

Two-dimensional NMR relaxation measurements provide a correlation between the initial (encoding) and final (detection) parts of the NMR experiment. The encoding sequence may involve longitudinal T_1 or transverse T_2 decay whereas decoding period may involve the transverse T_2 decay providing the T_1-T_2 and T_2-T_2 correlations in the sample. Obtained 2D NMR data are processed by the two-dimensional inverse Laplace transform [3,4] resulting T_1-T_2 and T_2-T_2 2D NMR correlation maps. The resulting T_2-T_2 correlation maps are interpreted in terms of diagonal peaks that represent the molecular population from sites in which the properties remain unchanged and off-diagonal peaks that indicate the molecular exchange [5, 6]. In this report we focused on investigation of the dynamical relaxation characteristics of adsorbed *n*-hexane in silicalite-1 by 2D NMR T_1-T_2 pulse sequence and on molecular mobility of *n*-hexane molecules inside the silicalite-1 channels studied by means of 2D NMR T_2-T_2 pulse sequence.

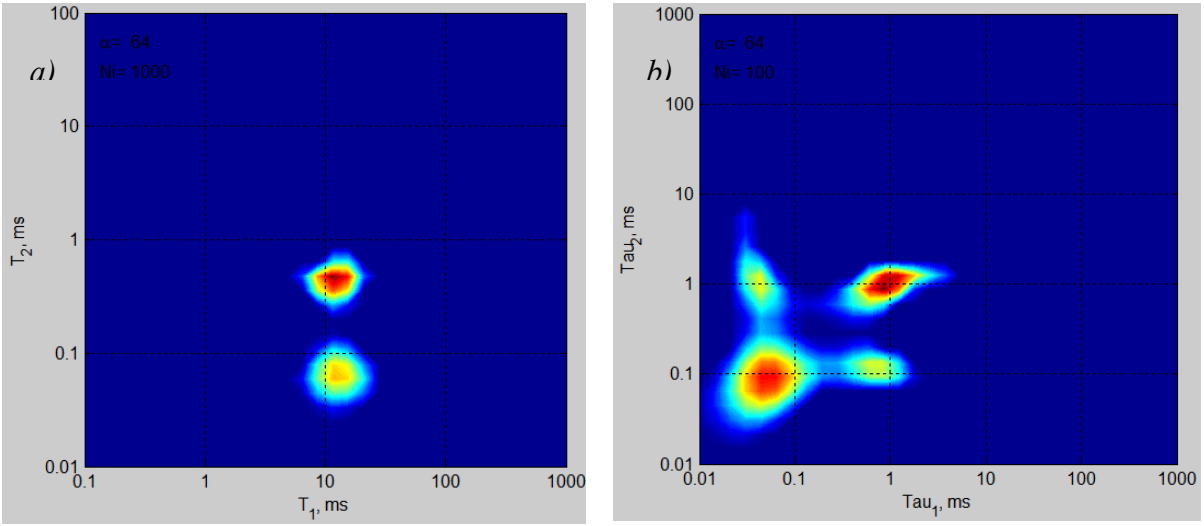

Figure 1. a) The T_1-T_2 and b) T_2-T_2 correlation map obtained for the silicalite-1 sample with maximum of n-hexane content of 14.6% (wt.). The T_2-T_2 2D NMR experiment was performed at t_{mix} = 0.45 ms

The T_1-T_2 2D NMR data unambiguously identify *n*-hexane in two different environments within the silicalite-1. These two NMR phases of *n*-hexane are characterized by two different T_2 relaxation times, but they have the same T_1 (Fig.1a) in the whole concentration range. Increasing of *n*-hexane content gives rise to decreasing of T_2 for slow relaxing phase and part of this phase in ^{1}H NMR signal is increasing. The T_2-T_2 measurements performed in the silicalite-1 sample at the same *n*-hexane contents revealed the exchange processes between these two NMR phases, which are evidenced in appearance of the off-diagonal peaks on the T_2-T_2 correlation map (Fig.1b). The exchange processes are probably related to molecular mobility of n-hexane between the channel systems and mesopores (defects) in the silicalite-1 structure. This is suggested by very short exchange time of $t_{ex} = 1 \pm 0.3$ ms obtained in the fully saturated sample.

Acknowledgements

This work is supported by the Russian Foundation for Basic Research (Project No. 16-32-00169 mol_a).

References

1. R. Krishna, B. Smit, T.J.H. Vlugt. – *J. Phys. Chem. A,* 102, 7727 (1998).
2. N.Y. Chen, W.W. Kaeding, J. Dwyer. – *J. Am. Chem. Soc.*, 101, 6783 (1979).
3. J.-H. Lee, Ch. Labadie, Ch.S. Springer, Jr., and G.S. Harbison. – *J. Am. Chem Soc.*, 115, 7761-7764 (1993).
4. J. Cox, P.J. McDonald and B.A. Gardiner. – *Holzfoschung*, 64, 259-266 (2010).
5. K. E. Washburn, P. T. Callaghan. – *Phys. Rev. Lett.*, 97, 175502 (2006).
6. L. Monteilhet, J.-P. Korb, J. Mitchell, and P. J. McDonald. – *Phys. Rev. E*, 74, 051404 (2006).

Aggregation stages of CTAB molecules in aqueous solutions

Irek R. Nizameev[1], Vyacheslav A. Semenov[2], Alexey I. Litvinov[1], Lucia Ya. Zakharova[1], Marsil K. Kadirov[1]

[1]A.E. Arbuzov Institute of Organic and Physical Chemistry, Kazan Scientific Center, Russian Academy of Sciences, 8, Akad. Arbuzov str., Kazan 420088, Russia.
[2]Kazan National Research Technological University, K. Marx str., Kazan 420015, Russia
E-mail: irek.rash@gmail.com

One of the most simple and advanced strategy for metal clusters obtaining at the moment is the using template constructed by surfactant aggregates [1-3]. In order to minimize aggregation of metallic particles various stabilizers are applied. In case of chemical deposition of metal clusters amphiphilic compounds are often used as stabilizers. Therefore, purpose of this work is to investigate the aggregation of surfactants at the glass surface. The work is additionally stimulated by our recent investigations of amphiphilic solutions by ESR-spectroscopy [4]. They evidenced some pre-micellar changes in the correlation times of a spin probe, TEMPO. These results are in agreement with ref.[5] revealing pre-micellar association in SDS solutions.

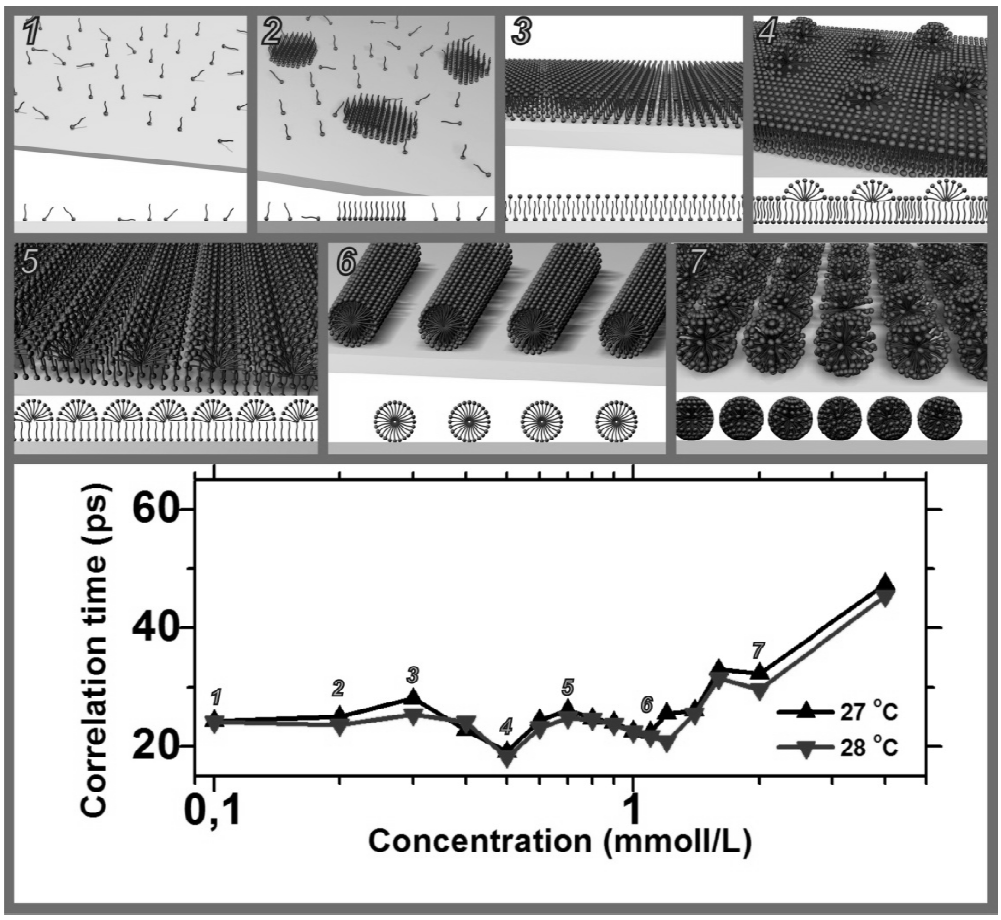

Figure 1. Simplified representation of the adsorbed structures for low and intermediate concentrations of CTAB in water solutions at the glass/solution interface with the increase of surfactant concentration: 1 – sparse monomers of surfactant at the surface of glass; 2 – the formation of hemimicells; 3 – bilayer film of adsorbed surfactant; 4 – hemispherical surface micelles at surfactant monolayer film; 5 – hemicylindrical surface micelles on the surfactant layer; 6 – cylindrical and 7 - spherical admicelles

Electron spin resonance (ESR) is widely used in research of both homogeneous and microheterogeneous systems. Surfactant molecules usually do not have paramagnetic properties and as a result do not give rise to ESR spectrum. In order to investigate their aggregation behavior with ESR method spin probes were added into the solution. Among the stable nitroxyl radicals, TEMPO (2,2,6,6-tetramethyl-1-piperidinyloxy) is a most widely used spin probe[6-7].

The object of our investigation is cetyltrimethylammonium bromide (CTAB) because it has very interesting properties (such as temperature-dependent morphology) that were discovered in our previous work [8].

TEMPO was used as spin probe. Although some limitations of the use of TEMPO occur due to its partition between two phases in micellar systems, we used it, since many classical surfactants were explored by the spine probe technique with TEMPO [7].

In the dependence of correlation time τ_c *vs.* the CTAB concentration three discontinuities were revealed within 0.2-0.5, 0.5-1.02 and 1.02-1.1 mM narrow concentration ranges, which are assumed to be connected with the formation of bilayer and hemispherical, hemicylindrical, cylindrical and spherical admicelles (Fig. 1). These images of some of them at the surface of the glass have been independently obtained by AFM.

To visualize the micellar surface aggregates atomic force microscopy (AFM) technique was used. CTAB molecules morphology was investigated at the glass/solution interface.

We carried out careful investigation of the CTAB solution focusing on the premicellar range and taking into account data on CTAB adsorption on the glass surface that can markedly contribute to the experimental results (Fig. 2).

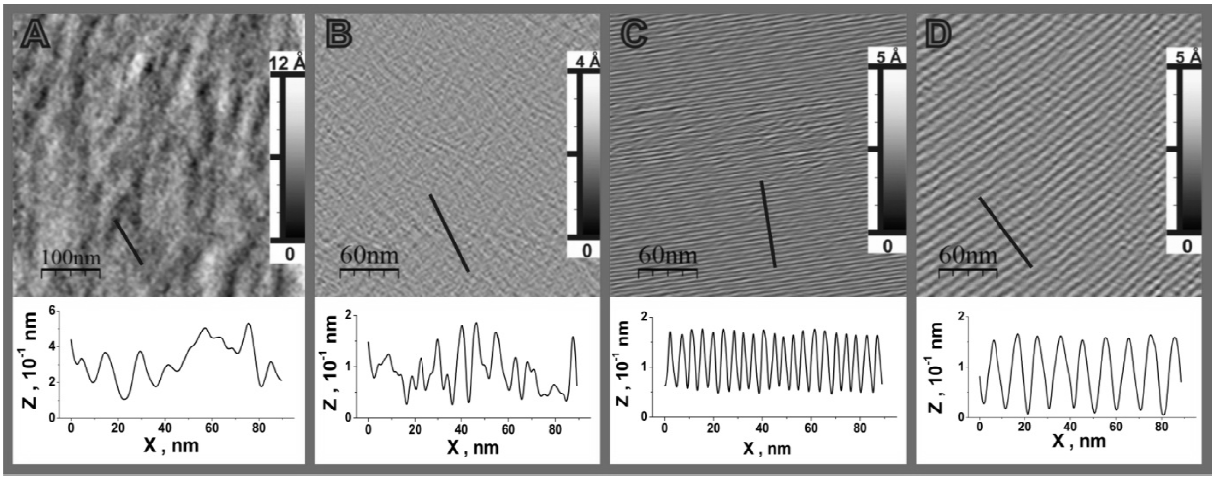

Figure 2. AFM images of glass substrate (A) and adsorbed structures (B - D) for different concentrations of CTAB solutions in water (B - 0.35 mM, C - 0.80 mM, D - 1.02 mM) and corresponding histogram plots of the surface height at the glass/solution interface at 27 °C

Conclusions

Saw shaped discontinuities at ESR spin probe correlation times plot were explained by AFM method and attributed to surfactant aggregate formation on the inner surface of ESR glass tube. These aggregates were imaged by AFM on the surface of the same glass plate and were shown to be shaped as film, hemicylinders, admicellar cylinders, with transitions between them with the increase of surfactant concentrations.

Acknowledgements

The reported study was funded by RFBR according to the research project No. 16-33-00145 мол_а.

References

1. O.P. Yadav, A. Palmqvist, N. Cruise, K. Holmberg. – *Colloids Surf., A,* **221**, 131–134 (2003).
2. E.M. Gaigneaux, M. Devillers, D.E.De. Vos *et al.* – *Stud. Surf. Sci. Catal.,* **162**, 561–567 (2006).
3. S. Zhang, Y. Zhao. – *ACS Nano,***5**, 2637–2646 (2011).
4. A.I. Litvinov, F.G. Valeeva, L.Y. Zakharova, S.E. Solovieva, I.S. Antipin, M.K. Kadirov. – *Russian Chemical Bulletin,* **62**, 1350-1353 (2013).
5. S. Vijayan, C. Ramachandran, D.R. Woods. – *The Canadian Journal of Chemical Engineering,* **58**, 485-496 (1980).
6. D. Kivelson. – *J. Chem. Phys.,* **33**, 1094 (1960).
7. A.M. Wasserman. – *Russ. Chem. Rev.,* **63**, 373-382 (1994).
8. M.K. Kadirov, I.R. Nizameev, L.Y. Zakharova. – *J. Chem. Phys.,* **116**, 11326-11335 (2012).

70-kDa heat shock protein (Hsp70) detection using magnetic nanoparticles-based biosensor

Marina Parr[1], Roman Illarionov[2], Yaroslav Marchenko[3], Grigorii Timin[4], Lyudmila Yakovleva[3], Boris Nikolaev[3] and Maxim Shevtsov[4,5]

[1]Peter the Great St.Petersburg Polytechnic University, Saint-Petersburg, Russia
[2]Faculty of Chemical and Biotechnology, Saint-Petersburg State Institute of Technology (Technical University), Saint-Petersburg, Russia
[3]Research Institute of Highly Pure Biopreparations, Saint-Petersburg, Russia
[4]Institute of Cytology of the Russian Academy of Sciences (RAS), Saint-Petersburg, Russia
[5]Klinikum rechts der Isar, Technical University of Munich, Munich, Germany
E-mail: mar.ark.parr@gmail.com

Introduction

Molecular chaperone Hsp70 is involved in the folding and stabilization of numerous proteins, including many that contribute to the development of cancer. Hsp70 can be exposed on the cell surface or/and released into the circulation. Quantitative studies for detection of the Hsp70 demonstrated the association of the protein levels with various chronic diseases and cancers thus indicating the role of Hsp70 as a plausible biomarker in clinical trials [1-5]. In the current study analysis of the blood plasma levels of Hsp70 for the assessment of the brain tumor progression in the orthotopic glioblastoma model in rats was performed. Additionally the correlation analysis of the glioma progression and Hsp70 plasma levels was conducted. For the detection of chaperone highly sensitive method of magnetic switching assay based on magnetic nanoparticles and NMR-relaxometry was applied [6].

Materials and Methods

Dextran coated superparamagnetic iron oxide nanoparticles (SPIONs) were conjugated with anti-Hsp70 monoclonal antibodies. Detailed protocols for magnetic conjugates synthesis can be found in [7]. In the current study monoclonal antibodies cmHsp70.1 targeted to TKD-fragment of Hsp70 [8], and antibodies 2E4 and 3B5 targeted to C-terminus and N-terminus domain of Hsp70 respectively [9] were used.

Intracranial model of the C6 glioma in Wistar rats was employed in this study [7]. The stage of glioma progression (i.e. tumor volume) was evaluated by scoring visible manifestations of the disease (exhaustion, loss of locomotor activity, lethargy, porphyrin secretion from eyes and nose, movement uncoordination, difficulty in breathing) and magnetic resonance imaging (MRI). Four groups of animals (5 animals in each group) were used: non-injected healthy rats (control I), sham-operated rats (control II) (15 days following operation), early stage of glioma growth (10 days following C6 cells injection), later stage of glioma progression (21 days following tumor implantation). Blood plasma was obtained by collecting peripheral blood from tail vein and centrifuged at 1500*g* for 15 minutes. For performing NMR-relaxometry measurements 0.125 ml of collected blood plasma, 0.125 ml of distilled water and 0.250 ml of SPION-Abs suspension with [Fe] = 0,04 mM were mixed in Eppendorf and co-incubated for 1 hour at room temperature. Following co-incubation with magnetic conjugates the NMR-relaxometry studies were performed for detection of Hsp70 concentration in plasma.

Results and Discussion

Relaxometry studies clearly demonstrated that T2-relaxation time was higher in blood plasma samples obtained from glioma-bearing animal in comparison to the samples from control animals ($P<0.001$) (Figure 1). The observed change in T2-relaxation was not related to the type of the antibodies applied (i.e., 2E4, 3B5 and cmHsp70.1).

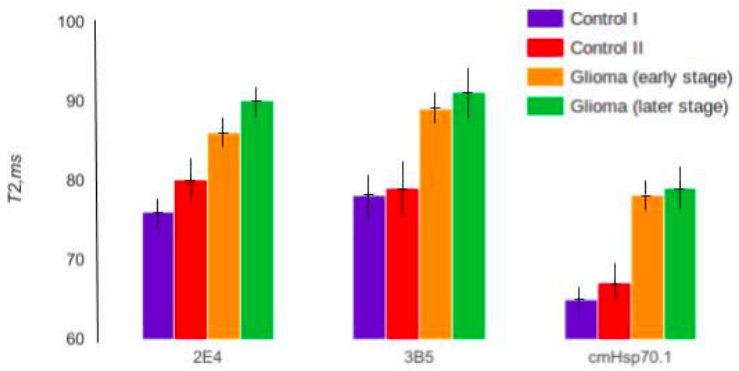

Figure 1. T2-relaxation times (ms) for the detection of the Hsp70 using 2E4, 3B5 and cmHsp70.1 magnetic conjugates in control and tumor-bearing animals. Data are presented as M±SD

The relative increment in T2-relaxation times growth for blood plasma from rats with early stage of glioma progression as compared to the control group (control I) constituted 13%, 14% and 20%, respectively for 2E4, 3B5, and cmHsp70.1 magnetic conjugates. Increase of T2-relaxation time for samples from glioma-bearing rats is explained by the increase of the Hsp70 concentration in plasma. Intriguingly, the sham-operation also resulted in the elevation of Hsp70 in plasma due to the inflammation in the zone of operation though the protein levels were significantly lower as compared to the glioma-bearing animals ($P<0.001$).

Assessment of the tumor volume in animals using high-field (11T) MR scanner (Bruker, Germany) revealed that medium tumor volume in the early stage progression animals corresponded to 32±7 mm^3 while at later stage it increased up to 71±8 mm^3 (Figure 2). Subsequent analysis of the correlation of the tumor volume with Hsp70 levels in plasma demonstrated a positive correlation. Thus Hsp70 plasma concentration in animals with early stage of glioma progression constituted 34±7 pg/ml. Significant increase of the tumor volume in the later stage of tumor progression resulted in further elevation of Hsp70 concentration up to 91±5 pg/ml ($P<0.001$).

In conclusion, the developed magnetic conjugates for detection of Hsp70 using NMR-relaxometry studies demonstrated high sensitivity in the protein concentration assessment. Increase of the Hsp70 levels in plasma of the glioma-bearing animals evidences the possible application of the protein as a biomarker for detection of the glioblastoma progression.

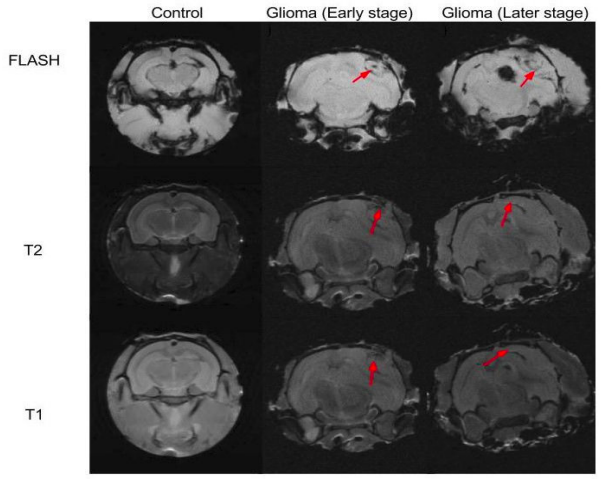

Figure 2. MR images of C6 glioma in the animals at early (middle column) and late (right column) stages of tumor progression. Sham-operated animals (left column) were used as control. The images were obtained at RARE-T1, TurboRARE-T2 and FLASH regimens

Acknowledgements

This work is supported by the Russian Foundation for Basic Research 15-08-08148A. Authors would like to thank Olga Genbach and Prof. Dr. Oleg Galibin for help in experiments with animals and Center for Magnetic Resonance of Saint-Petersburg State University Research Park for MRI (especially Prof. Dr. Peter M. Tolstoy and Anton Mazur).

References

1. B. Dybdahl, S. Slordahl, A. Waage, P. Kierulf, T. Espevik, A. Sundan. Myocardial ischemia and the inflammatory response: release of heat shock protein 70 after myocardial infarction. – *Heart,* 91, 299-304 (2005) .
2. X. Zhang, Z. Xu, L. Zhou, Y. Chen, M. He, L. Cheng, F. B. Hu, R. M. Tanguay, T. Wu. Plasma levels of Hsp70 and anti-Hsp70 antibody predict risk of acute coronary syndrome. – *Cell Stress Chaperones,* 15, 675-686 (2010).
3. M. T. Ganter, L. B. Ware, M. Howard, J. Roux, B. Gartland, M. A. Matthay, M. Fleshner, J. F. Pittet. Extracellular heat shock protein 72 is a marker of the stress protein response in acute lung injury. – *Amer. J. Physiol. Lung Cell. Mol. Physiol.,* 291, 354-361 (2006).
4. R. Njemini, M. Lambert, C. Demanet, R. Kooijman, T. Mets Basal and infection-induced levels of heat shock proteins in human aging. – *Biogerontology*, 8, 353-364 (2007).
5. M.Gehrmann, H.M. Specht, C. Bayer, M. Brandstetter, B. Chizzali, M. Duma, S. Breuninger, K. Hube, S. Lehnerer, V. van Phi, E. Sage, T.E. Schmid, M. Sedelmayr, D. Schilling, W. Sievert, S. Stangl and G. Multhoff. Hsp70 - a biomarker for tumor detection and monitoring of outcome of radiation therapy in patients with squamous cell carcinoma of the head and neck. – *Radiation Oncology,* 9:131, (2014).
6. M. Parr, R. Illarionov, Y. Marchenko, L. Yakovleva, B. Nikolaev, A. Ischenko and M. Shevtsov. Switching assay as a novel approach for specific antigen-antibody interaction analysis using magnetic nanoparticles. – *Journal of Physics: Conference Series*, 741(1) (2016).
7. M. Shevtsov, L. Yakovleva, B. Nikolaev, Y. Marchenko, A. Dobrodumov, K. Onokhin, Y. Onokhina, S. Selkov, A. Mikhrina, I. Guzhova, M. Martynova, O. Bystrova, A. Ischenko and B. Margulis. Tumor targeting using magnetic nanoparticle Hsp70 conjugate in a model of C6 glioma. – *Neuro Oncol.*, 16(1), 38–49 (2014).
8. S. Stangl, M. Gehrmann, J. Riegger, K. Kuhs, I. Riederer, W. Sievert, K. Hube, R. Mocikat, R. Dressel, E. Kremmer, A.G. Pockley, L. Friedrich, L. Vigh, A. Skerra, G. Multhoff. Targeting membrane heat-shock protein 70 (Hsp70) on tumors by cmHsp70.1 antibody. – *Proc.Natl.Acad.Sci.USA,* 108(2), 733-8 (2011).
9. Russian Federation patent № 2 381 271 C1

Experimental investigation of ^{87}Rb-absorption cells with two anti-relaxation components (coating + buffer gas) for stability improvement of atomic clock

Evgeny N. Pestov[1], Alla N. Besedina[2] and Vladimir V. Semenov[3]

[1]The Federal State Scientific /Prod. Enterprise "Geologorazvedka", Saint-Petersburg, Russia
[2]Joint- Stock Company "Russian Institute of Radio Navigation and Time"("RIRT"), Saint-Petersburg, 192012, Russia
[3]Dept. of Quantum electronics, Peter the Great St. Petersburg Polytechnic University, Saint-Petersburg, 195251, Russia
E-mail: infra-balt@peterlink.ru

Introduction

The creation of a quantum small-size frequency discriminator at the ^{87}Rb-absorption cell with a mixture of buffer gases for the on-board atomic clock of GPS, Galileo and GLONASS systems with relative instability $\sigma_y(\tau) \leq 1 \cdot 10^{-13} \cdot \tau^{-1/2}$ per day is a problem [1].

One of the problems is connected with updating of the electronic systems of the standard, another one – with the creation of ^{87}Rb-absorption cells with high physical and operational characteristics. To achieve a high medium-term stability of the frequency over a time interval of ~ 10^4 s, it is necessary, first of all, to increase the quality factor Q of the quantum discriminator and to provide a temperature frequency coefficient (TFC) at the level of ~ $1 \cdot 10^{-13}$.

The perspective for solving these issues is the use of ^{87}Rb-cells with anti-relaxation wall (ARW) coating [2,3], which have an undoubted advantage in realization a small width of 0-0 resonance and a larger value of Q as compared with ^{87}Rb-cells, that use known mixture of buffer gases, for example, ^{40}Ar + ^{20}Ne; ^{40}Ar + N_2; etc.

The application of ^{87}Rb-cells with ARW coating in quantum frequency standards was constrained by the opinion that the coating characteristics were not sufficiently stable in time. However, the results of [4] can change this situation. Thus, Russian researchers made a significant contribution to the study of the physical properties of ARW coatings and the development of a new technology to stabilize the ARW coating in time (Aleksandrov E.B., Balabas M.V.) [5,6].

To increase the medium- time stability of the atomic clocks over a time interval of $10^4 \div 10^5$ s, the authors of this paper propose to use of a new type ^{87}Rb-cells with two anti-relaxation components: ARW coating + buffer gas with low pressure [7,8].

In this paper we present the following

1. Comparative research of the longitudinal and transverse relaxation times (τ_1 and τ_2) of ^{87}Rb atoms was studied as a function of the temperature t° and light intensity $I(D_1)$ under lamp pumping for ^{87}Rb- cells of two types: 1) with ARW coating; 2) with ARW coating + buffer gas, ^{40}Ar (p = 4 Torr).

2. The shift in the frequency $\delta\nu_{0\text{-}0}(t^0)$ of the hyperfine reference transition ($\nu_{0\text{-}0}$ = 6.834 GHz) was studied as a function of the temperature, $\nu_{0\text{-}0}(t^0)$, of ^{87}Rb-cells of small dimensions (ARW coating + buffer gas, ^{40}Ar). As a result, a nonlinear dependence with steep-inflection (extremum) was obtained for cylindrical cells (Ø 19x19 mm) in the vicinity of t* ~ 42°C. In the vicinity of this temperature point t* ~ 42°C, frequency shifts from the spin-exchange processes of various nature are compensated.

The inflection zone in the vicinity of t* (°C) is < 0.5°C, which makes it possible to technically achieve the value TCF ~ $1 \cdot 10^{-13}$ Hz/grad with the modern element base.

3. The quality parameter Q of the ^{87}Rb-cell (ARW coating + ^{40}Ar) discriminator was evaluated under the conditions of operation with laser pumping. A value of Q ~ 100 was achieved, which exceeds the analogous parameter of traditional discriminators using cells with buffer gases by more than 5 times.

4. Analysis of the obtained experimental data shows that under the theoretical study of the results it is necessary to take into account the joint action of the following four relaxation mechanisms of the spin system of ^{87}Rb atoms: spin-wall and spin-exchange relaxation of ^{87}Rb atoms in a ^{40}Ar buffer gas and relaxation from the action of the pump light intensity.

Conclusion

The addition at ^{87}Rb-cell with an ARW coating of a buffer gas (^{40}Ar) with low pressure and negative frequency shift value [$-\delta\nu_{0\text{-}0}$ (t°)] shows the possibility of compensating for the frequency shift $\delta\nu_{0\text{-}0}$ in the vicinity of a certain temperature t*(°C), which is the inflection point of the characteristic $\nu_{0\text{-}0}$ (t°) of the reference 0-0 resonance.

The application of modern electronic systems makes it possible to achieve in the vicinity of the temperature point t* the TFC value at the level of units 10^{-13} Hz/grad, and in combination with laser pumping to obtain the medium-term frequency stability of the quantum discriminator of atomic clocks $\leq 1\cdot10^{-13}$ for an averaging time of 1 day.

References

1. Camparo J.C., Hagerman J.O. and McClelland T.A. "Long-Term Behavior of Rubidium Clocks in Space" – IEEE, 2(12), 501-508 (2012).
2. Pellaton M., Affolderbach C., Mileti G., et al. "Wall-coated cells for Rb atomic clocks" – Proc. Joint Conf. of the IFCS-EFTF, Gottenberg, Sweden, 87-90 (2012).
3. Pestov E.N., Azarov V.P. and Besedina A.N. "Creation of ^{87}Rb-absorption cells with anti-relaxation wall coating for highly stable atomic clocks" – Proc. IAA RAS., St.-Petersburg, Russia, № 27, 507-511 (2013).
4. Gusman J.S., Wojciechowski A. et. al. "Nonlinear magneto-optical rotation and Zeeman and Hyperfine relaxation of potassium atoms in a paraffin-coated cell" – Phys. Rev. A, 74, 053415 (2006).
5. Alexandrov E.B., Balabas M.V., Budker D., et al. "Light-induced desorption of alkali-metal atoms from paraffin coating" – Phys. Rev. A, 66(4), 1-12 (2002).
6. Balabas M.V., Karaulanov T., Ledbetter M.P., et al. "Polarized alkali vapor with minute-long transverse spin-relaxation time" – Phys. Rev. Lett., 105(8), R 070801 (2010).
7. Knappe S. and Robinson H.G. "Double-resonance lineshapes in a cell with wall coating and buffer gas" – New Journal of Physics, 12(6), 065021 (2010).
8. Pestov E.N., Pestov D.E. and Azarov V.P. "Rubidium absorption cell"– Patent Russia, № 151192 (2014).

Imaging of phosphorus-containing materials by double magnetic resonance

S. A. Shubin, V. V. Frolov, K. V. Tyutyukin

St. Petersburg State University, 1, Ulyanovskaya str.,
St. Petersburg, 198504, Russian Federation
E-mail: shubinsa1@gmail.com

Introduction

Current trends in MRI methodology go beyond the classical experiment of mapping the ^{1}H nuclei distribution in a body. To obtain additional diagnostic information, new techniques have been developed for visualization of various physical parameters, e.g. diffusion coefficients or fluid flows mapping, for MRI of blood vessels.

One of perspective directions of further development of MRI diagnostics is using the nuclei different from ^{1}H. It is due to abundance of such nuclei in molecules participating in important biological processes. Using the information about spatial distribution of these nuclei in a body one can draw conclusions about possible undergoing pathological processes. One of such nuclei is phosphorus-31. The aim of this work is the development the techniques for MRI of ^{31}P-containing compounds in weak static magnetic fields (7 mT) by double magnetic resonance. In this work, trimethyl phosphate, $(CH_3O)_3PO$, was used as model system for studying the performance of the method.

Methods

Let us consider a J-coupled two-spin ^{31}P-^{1}H system. In the described experiment, the two-spin system is initially driven from the equilibrium by a 90^0 excitation pulse on the proton channel, followed by two periods of free evolution separated by a pair of inversion pulses on both channels (Fig. 1). The evolution of the spin state of those ^{31}P nuclei that are coupled to ^{1}H nuclei would differ from evolution of the nuclei that are not J-coupled. The observed signal can be calculated according to the following equation [3]:

$$S(t) = Tr\{(\hat{I}_x(\cos(2\pi J\tau) + 2\hat{I}_y\hat{S}_z \sin(2\pi J\tau)) + \hat{S}_z)(\hat{I}_x + i\hat{I}_y)\}.$$

Since in the experiment only the first term is directly detected, for minimization of the observed signal from the coupled ^{31}P-^{1}H pairs, the following condition must be fulfilled: $2\pi J\tau = \pi$, which leads to $\tau = \frac{1}{2J}$. In this case, one achieves the maximal contrast between different parts of the sample, where coupled and non-coupled subsystems are localized. The echo signal detected by the receiving rf-coil from the J-coupled spins is minimal in this case.

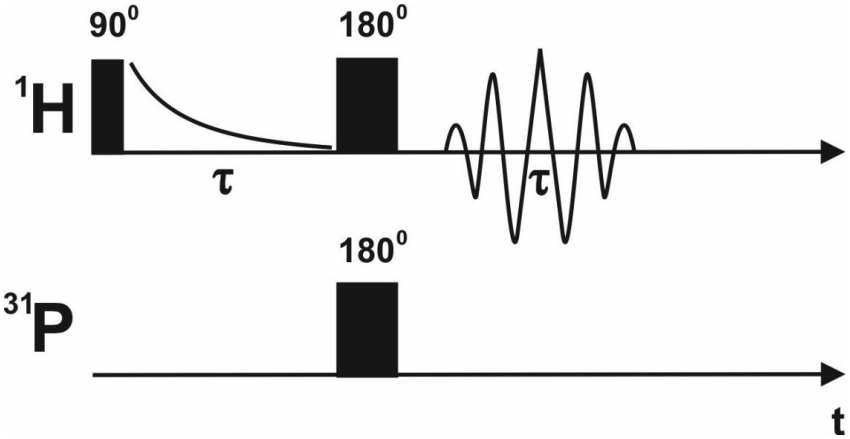

Figure 1. RF pulse sequence applied to the H-P two-spin system

When the 90^0-τ-180^0-τ-echo pulse sequence is executed on the ω_{0H} frequency and the additional 180^0 pulse is applied to phosphorus simultaneously with 180^0 ^{1}H pulse, one can obtain a MR image of ^{1}H not coupled to phosphorus via indirect spin-spin coupling. By subtracting this image from a total proton distribution, we obtain an image of ^{1}H nuclei coupled to ^{31}P. Thus, we map the spatial distribution of components containing phosphorus in the sample.

Taking into account the fact that gyromagnetic ratio of ^{1}H is 2.5 times higher than that for ^{31}P, and, generally, NMR signal intensity is proportional to γ^3, one gains ca. 16-fold in intensity. Accordingly, it is expedient to obtain MR images of ^{1}H spins coupled to ^{31}P nuclei, obtaining the distribution of phosphorus in the sample as the result [2,3].

Summary

In this work, we used dual water-trimethyl phosphate system as a model sample ("phantom"). The sample consisted of a two-sectioned glass cylindrical flask (Fig. 2). In the first section of the flask was water (outer radius), while in the second section we placed trimethyl phosphate (inner radius).

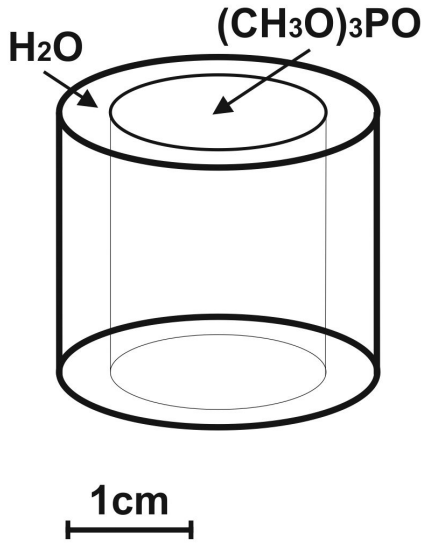

Figure 2. Sample water-trimethyl phosphate

As the result of the described experiment, we have got series of MR images with suppression of signal from ^{31}P-containing component. Fig.3 shows the pairs of pictures that were obtained by varying the impact that refocusing ^{31}P pulse had on the system. The left images in the depicted series were measured when the refocusing pulse was switched off, thus we have obtain the total distribution of protons in the sample. The right images were recorded with phosphorus refocusing pulse switched on. The series demonstrate how the suppression depends on the echo delay parameter τ. It can be seen, that the maximal effect is obtained when τ = 45 ms, which correspond to theoretical value calculated from the ^{31}P-^{1}H J-coupling constant (11 Hz).

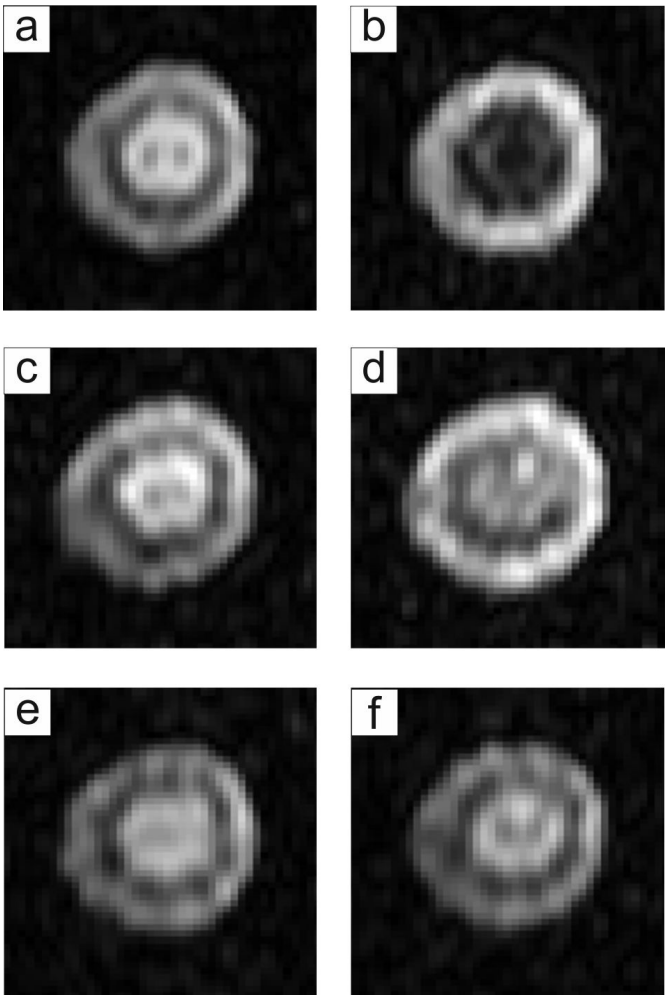

Figure 3. MRI images with phosphorus signal suppression:
a) Rf pulse on ^{31}P channel is off, τ=45 ms b) ^{31}P rf pulse is on, τ =45 ms
c) Rf pulse on ^{31}P channel is off, τ =67.5 ms d) ^{31}P rf pulse is on, τ =67.5 ms
e) Rf pulse on ^{31}P channel is off, τ =90 ms f) ^{31}P rf pulse is on, τ =90 ms

References

1. Laurance D. Hall, Timothy J. Norwood, and Steve C.R. Williams. Coupled-Spin-Filtered Imaging in an Inhomogeneous Magnetic Field. Journal of Magnetic Resonance 79 p.363-368 (1988).
2. A. G. Webb, S.C.R. Williams, and L. D. Hall. Generation of Coupled Spin-Only Images Using Multiple-Echo Acquisition. Journal of Magnetic Resonance 84 p.159-165 (1989).
3. Ernst R. R., Bodenhausen G., Wokaun A., Principles of Nuclear Magnetic Resonance in One and Two Dimensions. Clarendon Press, Oxford 1987. 610 Seiten: 1988.

NMR relaxation and diffusion in aqueous solutions of fullerenols and fullerenes with PVP and dextrine complexes

S. V. Sokratilin[1], *Yu. S. Chernyshev*[1], *V. I. Chizhik*[1], *A. V. Ievlev*[1], *A. A. Szhogina*[2], *M. V. Suyasova*[2], *V. P. Sedov*[2]

[1]*St. Petersburg State University 198504, St. Petersburg, Petergof, str. Ulyanovskaya, 1.*
[2]*NRC "Kurchatov Institute", B.P. Konstantinov St. Petersburg Nuclear Physics Institute, Gatchina, Orlova roscha mcr 1.*
E-mail: Sergey.Sokratilin@gmail.com

Introduction

Currently, there is a wide range of methods for the study of human internal tissues. One of the most promising methods is the magnetic resonance imaging (MRI). To improve the accuracy of diagnostics by MRI so called “contrast agents” are used. Salt-chelates are usually used as a contrast agent, in particular rare-earth metal of the lanthanide group.

Fullerene is a molecular carbon formation in the shape of a truncated icosahedron. Carbon atoms in the fullerene molecules are arranged at the vertices of regular hexagons and pentagons that make up the surface of a sphere or ellipsoid. All atoms are equivalent, as evidenced by the spectrum of ^{13}C, which comprises only one spectral line. Fullerenol is a molecular compound, which is a fullerene, upgraded OH - hydroxyl groups, that provide good solubility [1-4]

Endohedral metallofullerenes (EMF) with greater efficiency also can be used as a contrast agent. As contrast agents, the endohedral metallofullerenes were suggested that was expected to increase the efficiency and sensitivity of the method [5].

In this work we investigate the aqueous solutions of endohedral fullerenols with Fe atoms and fullerenes with PVP (polyvinylpyrrolidone) and dextrine complexes. The investigated solutions were of different fullerene concentrations (10 *mM/l*; 6 *mM/l*; 4 *mM/l*; 2 *mM/l*). This work is a continuation of work on the study of Fe and Gd ions inside fullerenols [6].

The choice of the object studied, namely Fe ions in aqueous solutions of fullerenols, is explained by the relevance of the work [7] to find effective relaxant for MRI.

Results and discussion

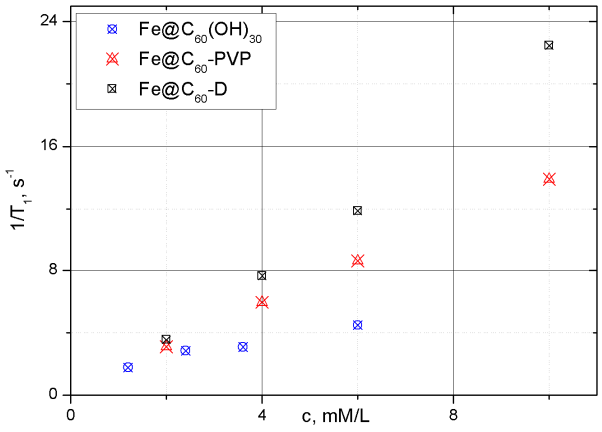

Figure 1. The dependence of the relaxation rates ($1/T_1$) on solution concentration (C mM/ l), 20 MHz

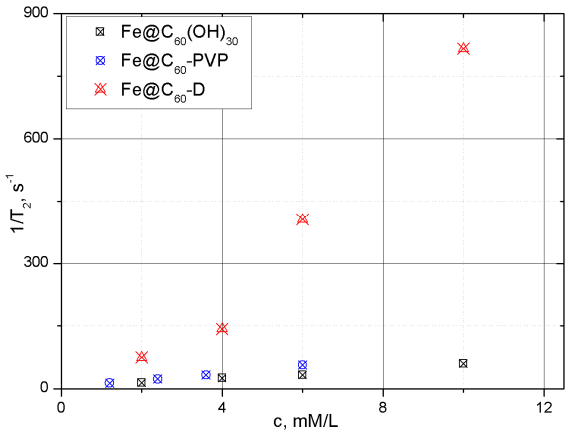

Figure 2. The dependence of the relaxation rates ($1/T_2$) on solution concentration (C mM / l), 20 MHz

We made a series of measurements of relaxation rates for three different sets of samples. The first series of samples contained fullerenols with Fe, the second and third series

contained endohedral metallofullerenes with Fe ions and their complexes with PVP and Dextrine. A series of measurements was carried out on five different spectrometers with different proton resonance frequency of 20 MHz, 90 MHz, 300 MHz, 400 MHz, 500 MHz at the temperature T = 25 ℃.

Temperature dependence at 500 MHz in the temperature range of 295-360˚K were also obtained.

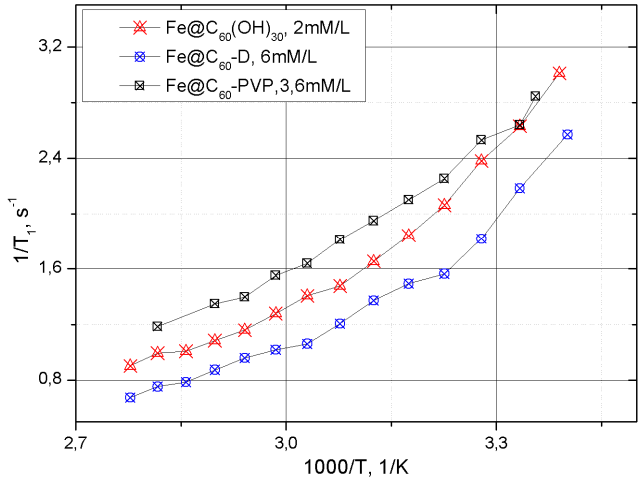

Figure 3. The dependence of the relaxation rate ($1/T_1$) on the temperature (295-360˚K), 500 MHz

The dependence of the diffusion coefficient on solution concentration (C mM/L), 500 MHz were obtained.

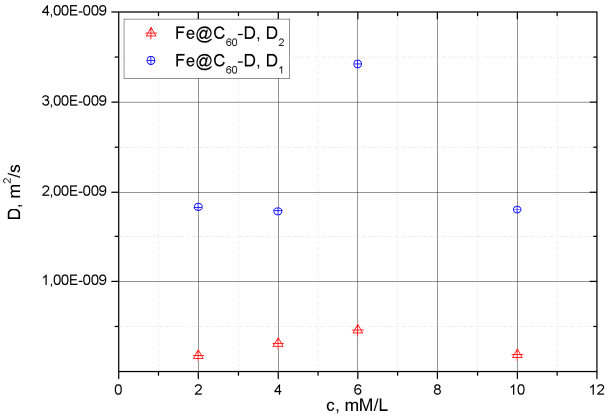

Figure 4. The dependence of the diffusion coefficient on solution concentration (C mmol / l), 500 MHz

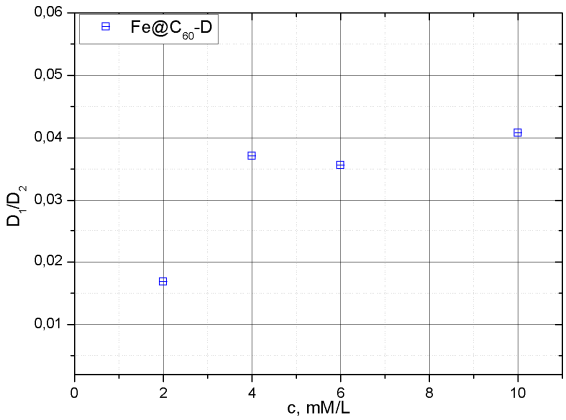

Figure 5. The dependence of the ratio of diffusion coefficient on solution concentration (C mmol / l), 500 MHz

The part of studies was carried out at the Research Park of Saint Petersburg State University: Centre for Magnetic Resonance.

References

1. *Lin A., Fang S., Chou C., Luh T., Ho L.* Local Carboxyfullerene Protects Cortical Infraction in Rat Brain, Neuro Science Research. 2002. V. 43. P. 317-321.
2. *Tabata Y., Ishii T., Aoyama T., Oki R., Hirano Y., Ogawa O., Ikada Y.* Perspectives of Fullerene Nanotechnology. Dordrecht – Boston – London: Kluwer Academ. Publ., 2001.

3. *Nikolaev I. V., Lebedev V.T., Grushko Yu. S., Sedov V. P., Shilin V. A., Török Gy., Melenevskaya E. Yu.* Ordering of Hydroxylated Fullerenes in Aqueous Solution: Fullerenes, Nanotubes and Carbon Nanostructure, V. 20 No. 4-7, P. 345-350, 2012.
4. *Lebedev V.T., Grushko Yu. S., Török Gy.* Structure and self-assembly of fullerene-containing molecular systems, Journal of optoelectronics and advanced materials, V. 15, No. 3-4, P. 193-198, 2013.
5. *Calucci L., Ciofani G., Mattoli V., Mazzolai B., Boni A., Forte C.,* NMR relaxation enhancement of water proton by Gd-doped boron nitride nanotubes, The journal of physical chemistry, 118, 6473-6479, 2014.
6. *S. V. Sokratilin., Yu. S. Chernyshev., V. I. Chazhik, A. V. Ievlev, A. A. Szhogina., M. V. Suyasova., V. P. Sedov., V. T. Lebedev,* Study of the relaxation efficiency of Gd and Fe ions inside fullerenols and they complexes with PVP and Dextrine in aqueous solutions, 13 International Youth School – Conference, Magnetic resonance and its application, p. 232 – 234, 2016.
7. *Ferrucci J. T., Stark D. D.* Iron oxide-enhanced MR imaging of the liver and spleen: review of the first 5 years // Am. J. Roentgenol. — 1990. — V. 155. — P. 943— 950.

NMR magnetometry on the historical and cultural heritage sites

A. A. Stomma[1], K. M. Shataev[1], A. V. Ievlev[2], A. V. Chudin[2]

[1]MBGEA Gymnasium number 2, Tosno
[2]St. Petersburg State University 198504, St. Petersburg, Petergof, str. Ulyanovskaya, 1.
E-mail: Shataevkirill@mail.ru, anton-stomma@mail.ru

Introduction

The method of magnetic reconnaissance is based on measuring the earth's magnetic field with a shallow step and close to the surface of the monument. Local changes in the magnetic field, or "magnetic anomalies", are most often caused by the contrast of the magnetic properties of the objects sought and the environment that surrounds them. For successful application of the method, a sufficient contrast of the magnetic properties is necessary. Figure 1 shows the region of magnetometric survey, and Table 1 shows the geographical coordinates of the site.

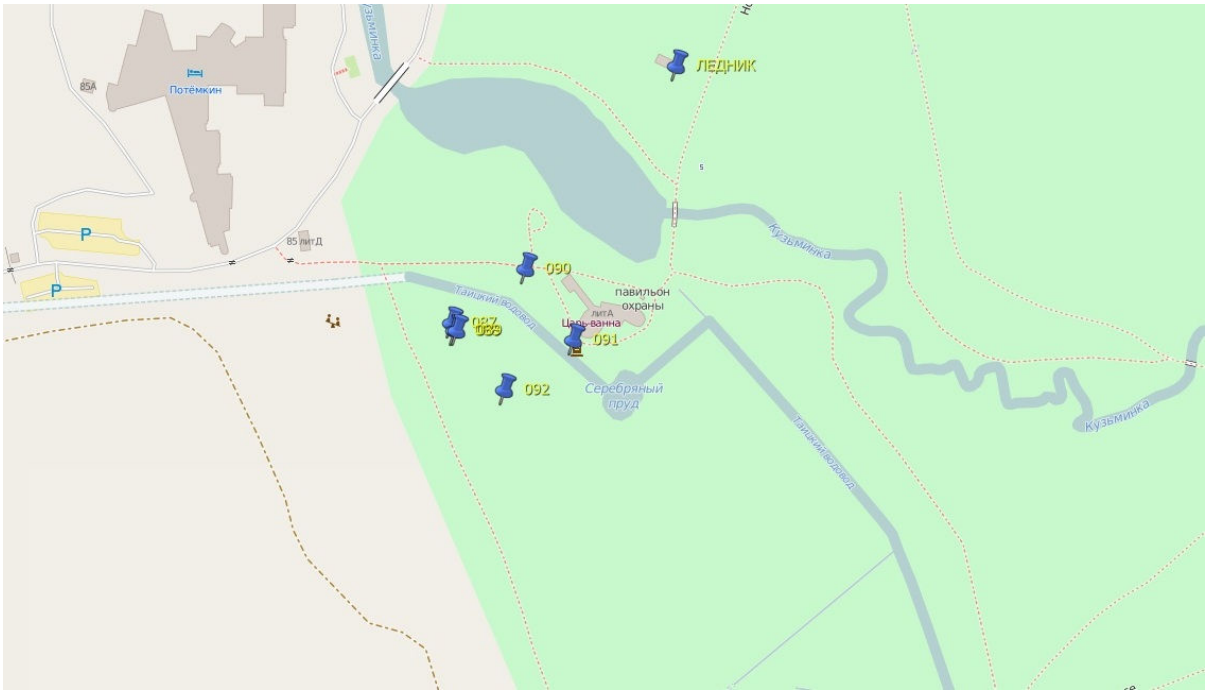

Figure 1. The location of the site of the magnetic survey

Table 1

Latitude	N59°42'31,91"	N59°42'30,71"	N59°42'29,44"	N59°42'30,60"
Longitude	E30°20'37,60"	E30°20'33,57"	E30°20'35,50"	E30°20'39,36"

Results

The second figure shows a 3-D map of the level of the magnetic field in the area of the magnetic survey. As can be seen, the section is crossed by a linear magnetic anomaly, presumably a metal pipe about a meter in diameter. Also in the area of magnetic survey are single high-intensity anomalies, which apparently corresponds to metal debris. Which can be identified as traces of human economic activity.

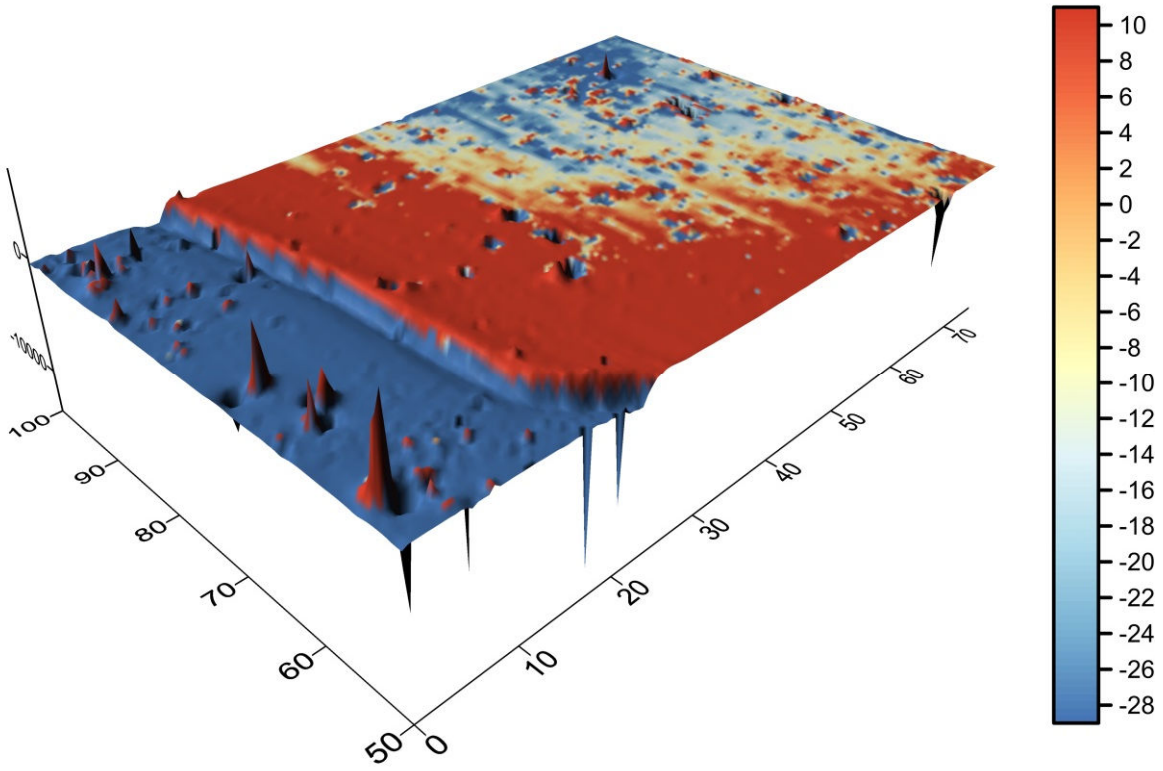

Figure 2. 3D-map of magnetic field

Magnetic detection of SPIONs-labeled mesenchymal stem cells in orthotopic glioblastoma model

Grigorii V. Timin[1,2], Boris P. Nikolaev[3], Vyacheslav A. Ryzhov[4], Yaroslav Yu. Marchenko[3], Ludmila Y. Yakovleva[3] and Maxim A. Shevtsov[1,5]

[1]*Institute of Cytology of the Russian Academy of Sciences, St. Petersburg, Russia*
[2]*Peter the Great St. Petersburg Polytechnic University, Saint-Petersburg, Russia*
[3]*Research Institute of Highly Pure Biopreparations, St. Petersburg, Russia*
[4]*Petersburg Nuclear Physics Institute, NRC Kurchatov Institute, Gatchina, Russia*
[5]*Klinikum rechts der Isar, Technical University of Munich, Munich, Germany*
E-mail: grifonsky@rambler.ru

Background

Mesenchymal stem cells (MSCs) have gained much interest as a source for cell-based therapies. Their potential to regenerate damaged tissue has been attributed to their ability of self-renewal, differentiation into a variety of specialized cell types and migration towards gradients of growth factors secreted by damaged tissue. Furthermore, MSCs have demonstrated preferential incorporation into sites of tumor development, including brain tumors, that allows MSCs to be a promising tool for targeted delivery of anticancer agents. For this clinical application the tracking of systemically administrated MSCs migration and distribution need to be defined. The possibility of efficiently labeling cells with superparamagnetic iron oxide nanoparticles (SPIONs) has stimulated their use to noninvasively track cells by magnetic resonance imaging (MRI) following administration. However, in some cases, concentration of systemically injected SPIONs-labeled MSCs in the organs of interest can be too low to be detected by MRI and requires more sensitive methods. We propose MRI combined with method of longitudinal nonlinear response to a weak ac magnetic field (NLR-M_2) to be a novel suitable approach for tracking magnetically labeled cells *in vivo*.

Methods and materials

SPIONs synthesis

SPIONs were prepared from iron salts solutions by co-precipitation in alkaline media at 80°C. $FeSO_4$ and $FeCl_3$ at Fe^{2+}/Fe^{3+} ratio of 1:2 were dissolved in water with the addition CsCl. Magnetite formation was induced by titration with an NH_4OH solution in an inert gas N_2. Dextran (MW 10 kD, Sigma) was added to the dispersion for colloidal stabilization under ultrasound treatment. The Fe content in the suspension was controlled by UV absorption of thiocyanate-Fe(+3) complex at $\lambda = 480$ nm.

Isolation of MSCs and labeling by SPIONs

MSCs were generated from the bone marrow of adult Wistar rats by flushing the rat femurs with culture medium, placed in culturing conditions and separated from the hematopoietic stem cells due to their plastic adherence. MSCs labeling was achieved by incubation in culture medium containing SPIONs at a final Fe concentration of 150 μg/ml for 12 h.

Modeling of intracranial C6 glioma and MSCs treatment

The C6 rat glioma cell line was obtained from the Russian cell culture collection of the Institute of Cytology (St. Petersburg, Russia). Cells were harvested in log phase of growth and stereotactically infused into the *nucl. caudatus dexter* of anesthetized adult Wistar rats (0.5×10^6 cells). On the 15^{th} day following intracranial implantation of C6 cells, SPIONs-labeled MSCs were intravenously administrated via tail vein (1.5×10^5 cells). Following 24 h

of MSCs administration the MRI was performed with subsequent histological verification of the cells retention in glioma.

Transmission electron microscopy (TEM)

For evaluation of the precise intracellular localization of the nanoparticles, electron microscopy was performed. For TEM following co-incubation with SPIONs for 1 and 24 hours, cells were harvested, fixed, sectioned on a LKB ultratome (Leica Microsystems) and examined with a Zeiss Libra 120 electron microscope (Carl Zeiss Meditec AG, Jena, Germany).

Measurements of nonlinear longitudinal response (NLR-M_2)

The main approach to the investigation of MSCs labeling by SPIONs efficiency and the brain tumor targeting by SPIONs-labeled MSCs efficiency was NLR-M_2, consisting in registration of second harmonic of magnetization (M_2) generated in the material under the action of parallel steady *dc* (H) and weak *ac* ($h \cdot \sin(2\pi ft)$) magnetic field (h = 13.8 Oe, f = 15.7 MHz). Both signal components, $ReM_2(H,T)$ and $ImM_2(H,T)$, were recorded simultaneously as functions of H at various temperatures T. The steady field H was slowly scanned symmetrically relative to the point H = 0 with frequency F_{sc} for control of a field hysteresis in the signal, which appearance due to symmetry properties of M_2 indicates the presence of a spontaneous ferromagnetic moment in a sample (the amplitude of H-scan was 300 Oe with frequency F_{sc} = 8 Hz). The method is very sensitive to an appearance of a ferromagnetic component in magnetization owing to its large nonlinearity in weak magnetic fields [2].

Results

On the second passage in culture bone marrow-derived rat MSCs retain the pattern of uniform fibroblast-like cells (Fig. 1, A). Incubation with SPIONs leads to effective labeling of MSCs that was shown using TEM (Fig. 1, B-C) and NLR-M_2 (Fig. 3, A-B) methods. Transmission electron microscopy revealed that SPIONs were located in the endosomal vesicles and cytoplasm of labeled MSCs. The amount of internalized SPIONs was dependent on the time of co-incubation with cells (Fig. 1, B-C). The absence of field hysteresis on the

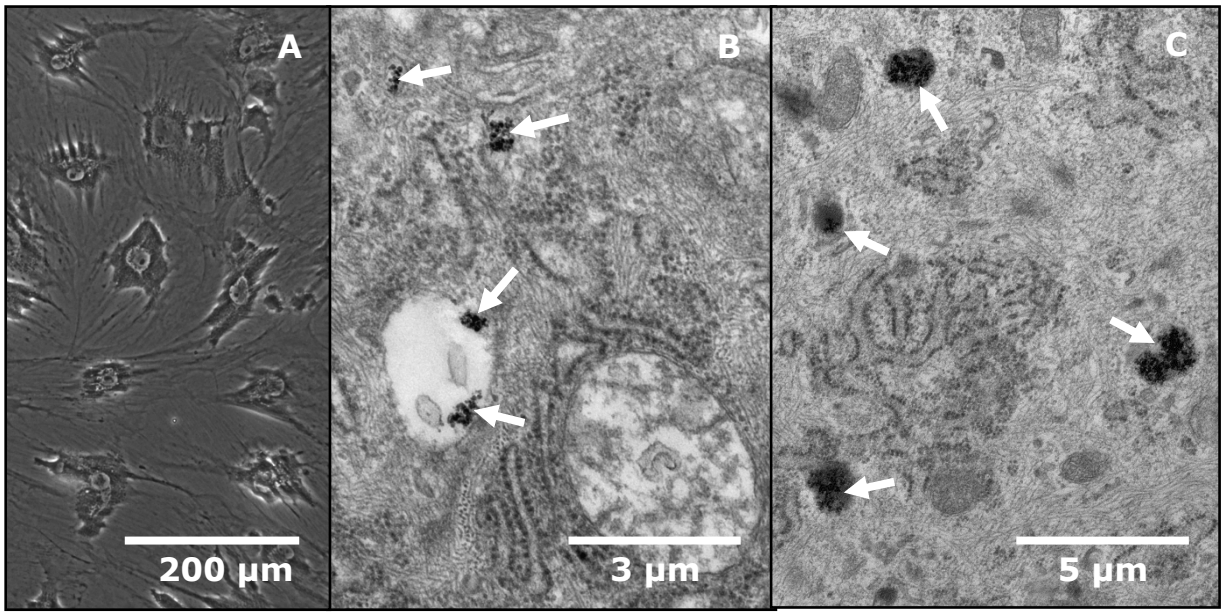

Figure 1. SPIONs-labeled MSCs: 1 hour (B) and 24 hours (A, C) of incubation with SPIONs (A – phase-contrast light microscopy; B, C – transmission electron microscopy, SPIONs clusters in cell cytoplasm and endosomes marked with white arrows)

graphs for $ReM_2(H)$ allows us to consider that SPIONs remain single-domain ferromagnetic nanoparticles in superparamagnetic regime when they are internalized by living cell (Fig. 3). Experimental trial to image MSCs incorporation in brain tumor with the help of MRI yields the homogeneous distribution of contrast agent in tissue (Fig. 2), whereas NLR-M_2 analysis displays the difference in MSCs accumulation between tumor and normal brain tissue (Fig. 3, C-D).

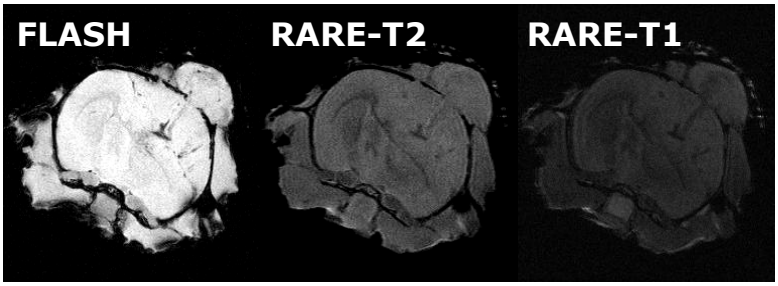

Figure 2. Magnetic resonance images of the glioma-bearing animals following intravenous administration of the SPIONs-labeled MSCs. Images were obtained at RARE-T1, TurboRARE-T2 and FLASH regimens

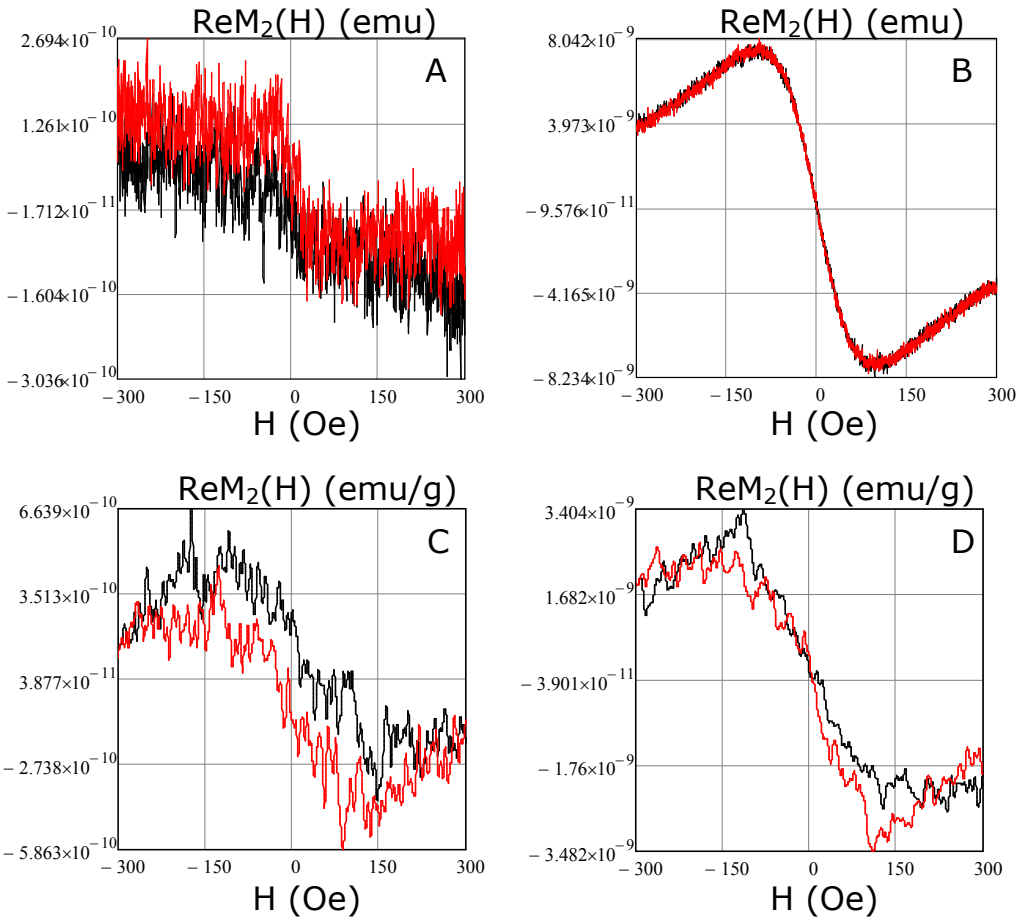

Figure 3. Phase component Re M_2 of second harmonic of magnetization: 1.5×10^5 unlabeled MSCs (A) and 1.5×10^5 SPIONs-labeled MSCs (B); rat brain tissue (C) and glioma (D) 24 hours after injection of 1.5×10^5 SPIONs-labeled MSCs

Conclusions

In the current study we confirmed the migratory capacity of SPOIN-labeled MSCs toward glioma cells following intravenous delivery in the orthotopic C6 glioblastoma model in rodents using highly sensitive method of NLR-M_2 registration. The proposed approach could be applied for the biodistribution analyses of administrated cells in cases of low cells concentration.

Acknowledgements

This work is supported by Russian Science Foundation (14-50-00068) and the Russian Foundation for Basic Research (15-08-08148A). The authors are grateful to Prof. Dr. Peter M. Tolstoy and Anton Mazur from St. Petersburg State University Center for Magneric Resonance for MRI trial, Prof. Marina Martynova and Olga Bystrova from Institute of Cytology (RAS) for the TEM studies.

Low temperature NMR studies of sodium nanoparticles embedded into porous glass and artificial opal

A. V. Uskov[1], D. Yu. Nefedov[1], E. V. Charnaya[1], M. K. Lee[2], L. J. Chang[2], J. Haase[3], D. Michel[3], Yu. A. Kumzerov[4], A. V. Fokin[4], A. S. Bugaev[5]

[1]Physics Department, St. Petersburg State University, St. Petersburg 198504, Russia
[2]Physics Department, National Cheng Kung University, Tainan 70101, Taiwan
[3]Faculty of Physics and Geophysics, Leipzig University, Leipzig D-04103, Germany
[4]A.F. Ioffe Physico-Technical Institute RAS, St. Petersburg 194021, Russia
[5]Moscow Institute of Physics and Technology, Moscow 141700, Russia
E-mail: yskov@yandex.ru

Introduction

NMR is a very powerful method for investigation of nanocomposites on the basis of metals with spin 3/2. It allows investigating both atomic mobility and electronic properties of nanoconfined metals [1, 2]. During the recent time the most of studies were devoted to properties of gallium and its alloys because of existence of two isotopes with different Larmor frequencies and the same spin that seriously simplifies the analysis of quadruple contribution to spin-lattice relaxation. Sodium has only one stable isotope which makes determination of atomic correlation time more complicated. Another disadvantage of sodium is high chemical activity which results in experimental difficulties.

The NMR investigations of bulk sodium were performed in 1965 [3] while the first investigations of nanoconfined sodium were performed recently [4]. It was shown that nanoconfinement impacts on electronic properties, phase transitions and atomic mobility of sodium [5].

Experiment

In order to investigate properties of sodium nanoparticles the liquid sodium was embedded into porous glass with pore size 25 nm and artificial opal matrix. Size of pores was controlled by means of mercury porosimetry for porous glass. Size of globes of artificial opal was determined by means of atomic microscopy. NMR measurements were performed using a Bruker Avance 500 pulse NMR spectrometer. The longitudinal magnetisation recovery curve was measured using the two-pulse sequence consisting of 180^o and 90^o pulses. Measurements were performed in temperature range from 10 K to 290 K.

Results

It was found that T_1 relaxation times are strongly different for different pore sizes at temperature above 200 K. The dependencies of the inverse spin-lattice relaxation time on temperature for different samples are presented in Fig. 1. The obtained results can be explained by influence of atomic mobility on spin-lattice relaxation [2].

The time dependence of longitudinal magnetization after inversion can be written in the following form

$$\frac{M(t)}{M_0} = 1 - b\left[\frac{4}{5}\exp\left(-\frac{C\tau_c t}{1+4\omega_0^2\tau_c^2}\right) + \frac{1}{5}\exp\left(-\frac{C\tau_c t}{1+\omega_0^2\tau_c^2}\right)\right]\exp\left(-\frac{t}{T_{1m}}\right), \quad (1)$$

where M_0 is the equilibrium magnetization, b accounts for nonideal inversion of magnetization, C is the constant of quadruple interaction, ω_0 is the Larmor frequency, τ_c is the correlation time of atomic motion, T_{1m} is time of longitudinal relaxation due to magnetic interaction which is inversely proportional to temperature.

The value of T_{1m} is almost not affected by nanoconfinement, thus at low temperature range the spin-lattice relaxation times are equal for all the samples. At higher temperatures spin-lattice relaxation is mainly governed by atomic mobility. It can be seen from Fig. 1 that the smaller particle size is at the lower temperature the atomic mobility appears.

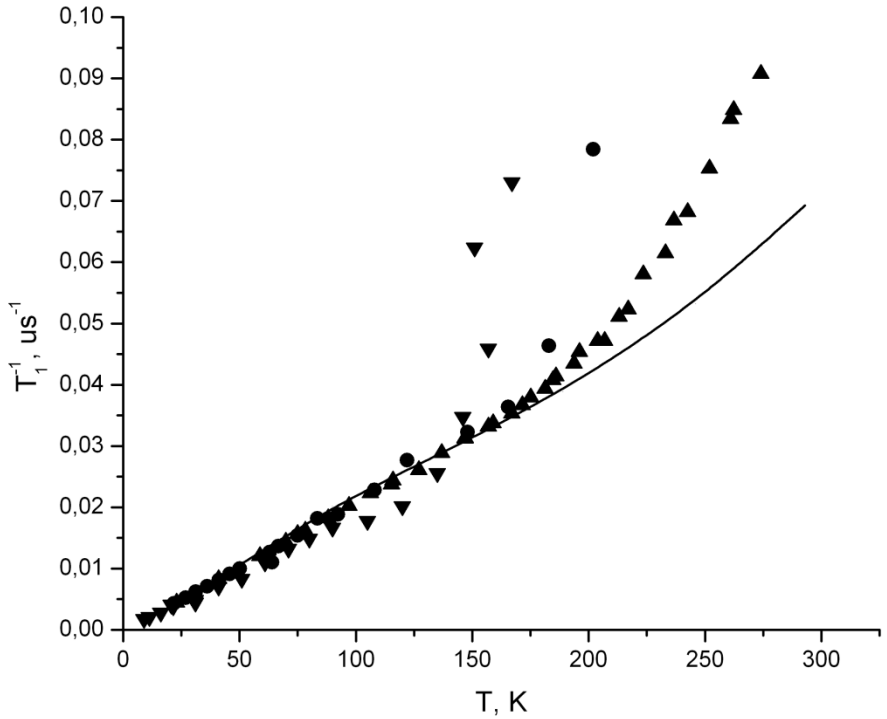

Figure 1. Dependence T_1^{-1} on temperature. Bulk sodium is marked by solid line, up-apex triangles correspond to porous glass 25 nm, down-apex triangles correspond to porous glass 3.5 nm, circles correspond to artificial opal

The dependence of the observed line width on temperature is presented in Fig. 2. It should be mentioned that both lines for sodium in porous glass 25 nm and artificial opal become broad at temperatures below 200 K what can be explained by slowdown of atomic mobility [6]. It should be mentioned that the changes of spin-lattice relaxation time due to atomic mobility are appearing at the same temperature range.

The dependence of the Knight shift on temperature is shown in the insert in Fig. 2. Unlike sodium nanoparticles embedded into porous glass 3.5 nm, the Knight shifts for bulk sodium, sodium particles embedded into artificial opal and porous glass 25 nm increase with increasing temperature.

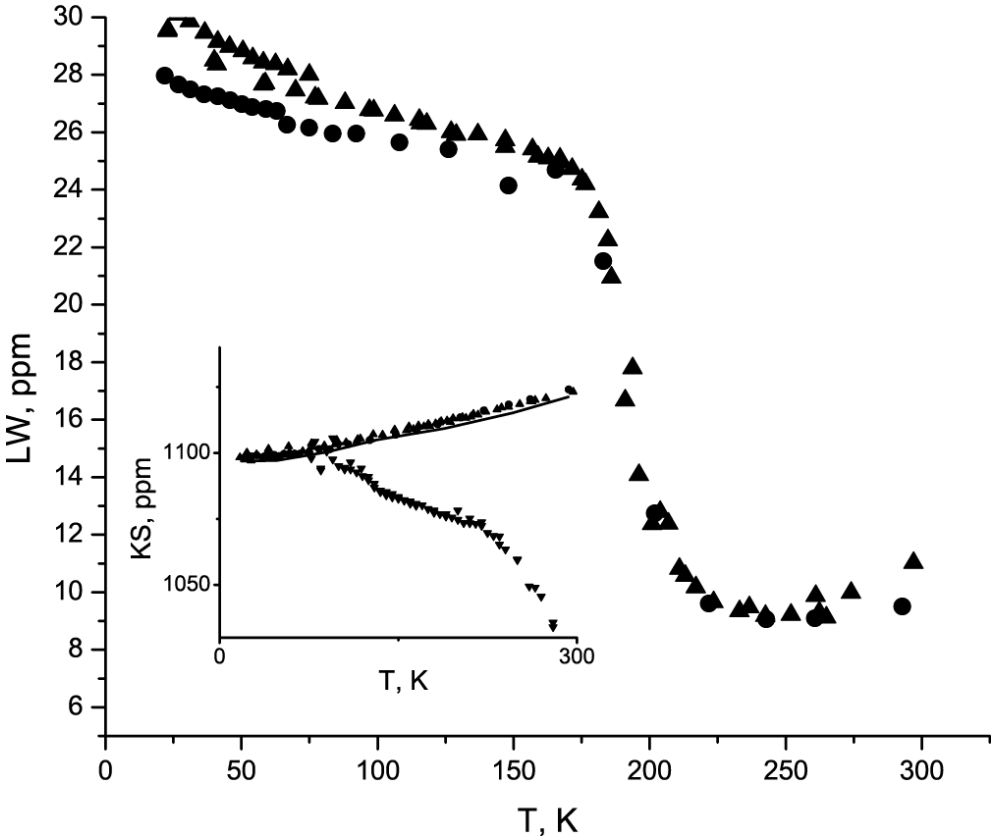

Figure 2. Dependence of line width on temperature. The dependence of Knight shift on temperature is shown in the insert

References

1. E. V. Charnaya, C. Tien, M. K. Lee and Y. A. Kumzerov. J Phys Condens Matter 22, 195108 (2010).
2. E. V. Charnaya, C. Tien, M. K. Lee and Y. A. Kumzerov. Physical Review B 75, (2007).
3. M. Watabe, M. Tanaka, H. Endo and B. K. Jones. Philosophical Magazine 12, 347-354 (1965).
4. E. V. Charnaya, M. K. Lee, L. J. Chang, Y. A. Kumzerov, A. V. Fokin, M. I. Samoylovich and A. S. Bugaev. Physics Letters A 379, 705-709 (2015).
5. A. V. Uskov, D. Y. Nefedov, E. V. Charnaya, J. Haase, D. Michel, Y. A. Kumzerov, A. V. Fokin and A. S. Bugaev. Nano Lett 16, 791-794 (2016).
6. J. R. Hendrickson and P. J. Bray. Journal of Magnetic Resonance (1969) 9, 341-357 (1973).

NMR studies of ferroelectric nanocomposites with KDP and DKDP small particles

N. I. Uskova[1], D. V. Kotkin[2], D. Yu. Podorozhkin[1], E. V. Charnaya[1], D. Yu. Nefedov[1], S. V. Baryshnikov[3]

[1]St. Petersburg State University, St. Petersburg, 198504 Russia
[2]Kostroma State University, Kostroma, 156005 Russia
[3]Blagoveschensk State Pedagogical University, Blagoveschensk, 675002 Russia
E-mail: natalyauskova.spbu@gmail.com

Introduction

Recently, much attention is paid to studies of nanocomposites, especially ferroelectric nanocomposites, because they have properties that can be used in a number of applications. In spite of this, there are ferroelectrics in which size effects are poorly understood.

In this work the main attention was focused on influence of the size effect on temperatures of the ferroelectric phase transitions in potassium dihydrogen phosphate (KDP) and deuterated potassium dihydrogen phosphate (DKDP) and on the phosphorus chemical shift tensor which directly relates to the sample structure. The studies were carried out by nuclear magnetic resonance (NMR), which is sensitive to local structure.

Samples and experiment

The samples under study were KDP embedded in porous glass (pore size 7-8 nm) and DKDP embedded in artificial opal (globe size 220 nm). The results were compared to the results obtained for crystal powders of KDP [1] and DKDP. The measurements were performed using Bruker NMR pulse spectrometer with broad band probehead using magic angle spin technique in large temperature range from 90 K to room temperature.

Results

The changes of ^{31}P NMR line shape and line position due to ferroelectric phase transition were observed for bulk materials. The values of the chemical shift tensor including isotropic shift, anisotropy and asymmetry factor were calculated on the basis of the obtained results. At the temperature of the ferroelectric phase transition the line shifted to low frequencies. The anisotropy of chemical shift tensor rapidly changed and was growing during the further decrease of temperature. The MAS investigations of ^{31}P NMR line allowed revealing a smooth decrease of isotropic shift during the decrease of temperature for bulk DKDP.

The ferroelectric phase transition in KDP embedded into porous glass and DKDP embedded opal was not observed in our temperature range. This conclusion was made because the line shape specific for paraelectric phase was observed. The comparisons of KDP nanoparticles spectra with bulk KDP spectra and of DKDP nanoparticles MAS-spectra with bulk DKDP MAS-spectra are presented below.

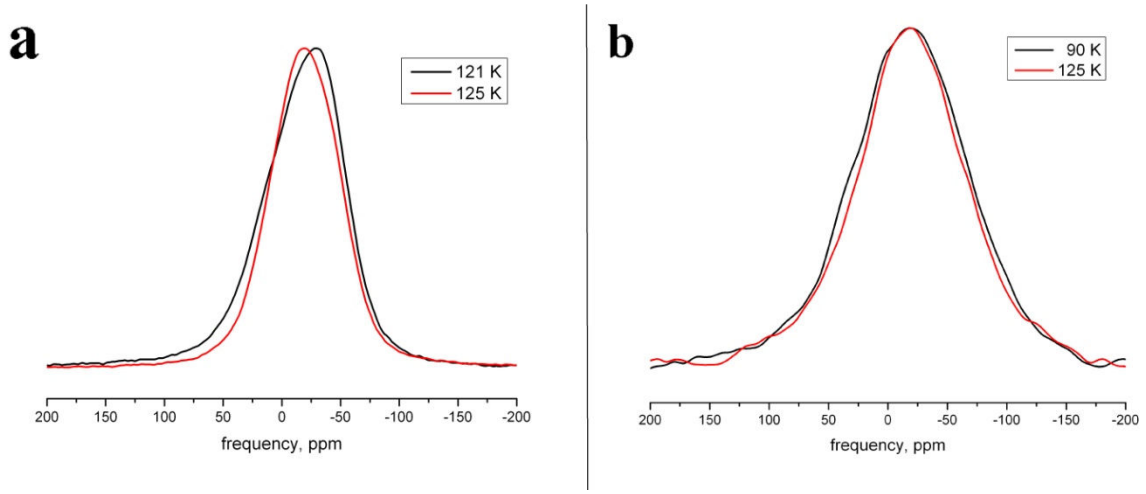

Figure 1. NMR spectra at two different temperatures: a – KDP powder, b – KDP embedded into porous glass with pore size 7-8 nm

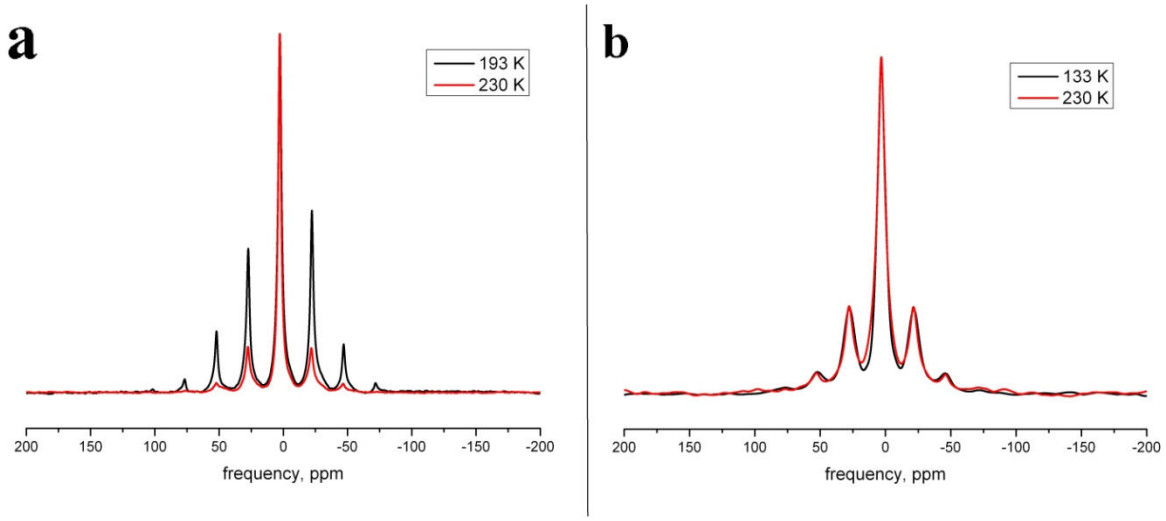

Figure 2. NMR MAS-spectra at two different temperatures: a – DKDP powder, b – DKDP embedded in opal with globe size 220 nm

References

1. N.I. Uskova, D.Y. Podorozhkin, E.V. Charnaya et al. Nuclear magnetic resonance study of potassium dihydrophosphate. – Phys. Solid State 58, 685 (2016).

Resonant properties of microwave spin-wave optoelectronic ring resonator

Vitalii V. Vitko, Andrey A. Nikitin, Alexandr V. Kondrashov, Mikhail I. Martynov and Alexey B. Ustinov

Department of Physical Electronics and Technology, St. Petersburg Electrotechnical University, St. Petersburg, 197376 Russia
E-mail: vitaliy.vitko@gmail.com

Introduction

Modern communication systems have strictest demands for microwave devices with high total bandwidth. Microwave photonics based on combination of electric and photonic circuitries provides practical methods for achievement of subterahertz bandwidth [1, 2]. The use of the photonics and the functional electronics in the same device provides enhancement of functionality and performance characteristics of the device. One of the examples of microwave photonic circuits is closed-loops with delay lines (DLs) which demonstrate wide variety of effects. Closed-loop circuit consisting of series connected active or passive microwave photonic DL and spin-wave DL realize classical configuration of the spin-wave OEO.

Closed-loop circuits with DL operate in two modes due to active or passive regime. The active regime leads to self-oscillations and the circuit operates like an oscillator. Spin-wave optoelectronic oscillators (OEOs) are demonstrative example of the functionality and performance enhancement of such circuit. It combines advantage of low phase noise of OEOs [3] and wide magnetic tuning of spin-wave devices [4, 5]. In the case of passive regime, losses in the DL exceed the amplification that leads to saturation and the circuit operates like a resonator. Closed-loop circuit with passive regime is called an active ring resonator (ARR). The frequency response of the ARR has a comb shape with a pass bands corresponding to the resonant frequencies [6].

The purpose of this work is the experimental investigation of the frequency response of a microwave optoelectronic ring resonator based on cascade connection of the spin-wave and microwave photonic DLs.

Experimental setup

The block diagram of the microwave spin-wave optoelectronic ring resonator experimental prototype is shown in Fig. 1. This resonator is a typical ARR.

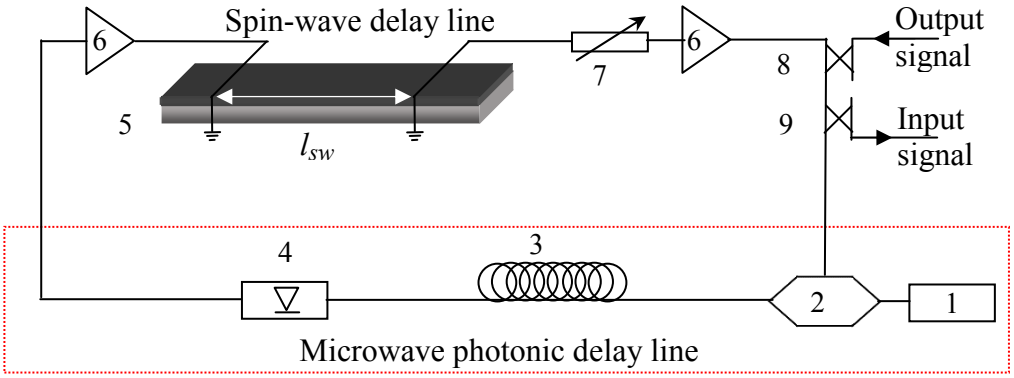

Figure 1. A block diagram of the spin-wave optoelectronic single-loop resonator

The ARR is a closed-loop circuit consisting of microwave photonic and spin-wave DLs. Microwave photonic delay line is formed by a semiconductor laser (1) continuously

emitting at a wavelength of 1.55 μm, the intensity electro-optical modulator (2) of Mach-Zehnder type with a bandwidth of 20 GHz, the single-mode optical fiber (3) with various lengths l_{opt}, and a high-speed photodetector (4) with the bandwidth of 25 GHz. Spin-wave DLs (5) is based on various YIG films with variety of antenna geometries. Two identical microwave amplifiers (6) are used for circuit losses compensation. The amplifiers demonstrate 1 dB suppression at output power of 30 dBm. The gain of each amplifier is 32 dB. These values were almost constant in the nominal frequency range of 4-9 GHz. The ring gain is regulated by a variable attenuator (7). Input and output of a microwave signal is carried out by directional couplers (8) and (9) with a couple coefficient of -10 dB.

The investigated resonator operates as follows. A test microwave signal with frequency $\omega_{mw} = 2\pi f_{mw}$ is supplied through the directional coupler (9) to the microwave photonic DL. It accumulates delay time $\tau_{opt} = l_{opt}\, n / c$, where l_{opt} is a length of optical fiber, the n is its refractive index, c is the speed of light in vacuum. The phase shift of the microwave signal in microwave photonic DL is $\Phi_{opt} = k_{opt}\, l_{opt}$, where k_{opt} is a wave-number of the signal envelope, which is equal to $k_{opt} = \omega_{mw}\, n / c$. After microwave photonic DL the microwave signal is fed in the spin-wave DL accumulating the delay time $\tau_{sw} = l_{sw} / V_g$, where l_{sw} is the propagation path that is equal to the distance between the antennae, V_g is group velocity of the spin wave in YIG film. The phase shift in spin-wave DL is $\Phi_{sw} = k_{sw}\, l_{sw}$, where k_{sw} is wavenumber of spin waves at a frequency f_{mw}. The signal is amplified and supplied to the input of the microwave photonic DL. Thus the loop is closed and the microwave signal starts circulating in the circuit.

The resonance condition in the loop is determined by phase balance $\Phi_{opt} + \Phi_{sw} + \varphi_e = 2\pi m$, where φ_e is phase shift in the electronic interconnections, which is usually small as compared with Φ_{opt} and Φ_{sw}, and m is an integer number. The value of transfer coefficient is defined by values of insertion losses introduced by DLs and a value of amplifier gain coefficient. Damping decrement of the signal in microwave photonic DL is defined by losses in fiber, modulator, and photodetector. Single-mode fiber damping decrement is approximately $\alpha_{opt} = 0.2$ dB/km at 1.55 μm. However, in experiment series the power loss of the microwave signal between electro-optical modulator input and the photodetector output was about -50 dB. This value was almost constant in the frequency range of 4-9 GHz. Contrariwise, the transfer coefficient of the signal in spin-wave DL is defined by the antennae geometry and damping decrement that is $\alpha_{sw} = 2\,\pi\,|g|\,\Delta H / V_g$, where $|g| = 2.8\ 10^{10}\ s^{-1}\cdot T^{-1}$ is gyromagnetic ratio for electron and ΔH is half of ferromagnetic resonance linewidth.

Experimental results

Microwave photonic DL and spin-wave DL with close delay time values $\tau_{opt} \approx \tau_{sw}$ were chosen in order to demonstrate features of frequency response formation in the spin-wave optoelectronic single-loop resonator. The measured frequency response of the resonator in absence of the spin-wave DL for the case of fiber length $l_{opt} = 20$ m is shown in Fig. 2a by curve 1. One can see that the frequency response had a large number of resonant peaks corresponding to the eigen-modes of the closed-loop. Curves 2 and 3 demonstrate frequency responses of DLs with YIG film thickness equal 16.9 μm (curve 2) and 5.4 μm (curve 3). Both these curves were measured in the case of two 50-μm-wide and 2-mm-long microstrip antennae. For all curves the distance between antennae l_{sw} was 3 mm and bias magnetic field was $H_0 = 2090$ Oe.

As shown in the Figs. 2b and 2c the resulting frequency response of the investigated microwave photonic resonator with spin-wave DL contains resonant peaks only within the bandwidth of the spin-wave DL. The free spectra range (FSR) decreases in comparison with curve 1 due to additional delay time τ_{sw} introduced by the spin-wave DL. Decrease of the film thickness provides higher delay time and smaller FSR as it is shown in Figs. 2c. Fig. 3

represents the tuning of the resonant frequencies by variation of the bias magnetic field in the range from 1990 Oe to 2090 Oe. These characteristics were measured for the case of spin-wave DL made of 5.4-μm YIG film with microstrip antennae and microwave photonic delay line with length of 20 m.

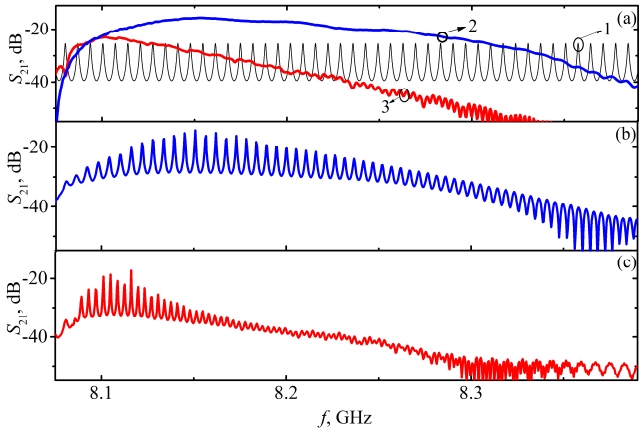

Figure 2. Experimental frequency response characteristics of: ARR based on microwave photonic DL in absence of spin-wave DL and spin-wave DL on YIG film various thicknesses (a); spin-wave optoelectronic ARR with spin-wave DL on YIG film with thickness of 16.9 μm (b), spin-wave DL on YIG film with thickness of 5.4 μm (c)

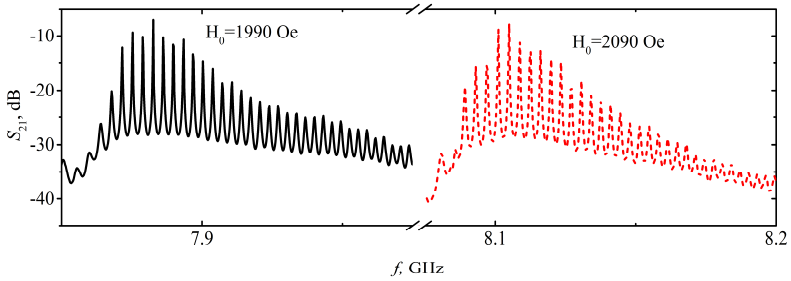

Figure 3. Magnetic tuning of experimental frequency response of the spin-wave optoelectronic ring resonator

In conclusion, the frequency response of microwave spin-wave optoelectronic ring resonator is experimentally investigated. The bandwidth is defined by YIG-film thickness. FSR is defined by delay time in spin-wave and microwave photonic delay lines. Change of bias magnetic field realizes frequency tuning. Performance of described resonator corresponds to tunable comb filter.

Acknowledgements

This work is supported by the Russian Science Foundation (Project 16-12-10440).

References

1. J. Federici, L. Moeller. *Journal of Applied Physics,* 107, No 11, 111101 (2010).
2. D. Marpaung, C. Roeloffzen, R. Heideman, A. Leinse, S. Sales, J. Capmany. – *Laser Photonics Rev.*, 7, 506-538 (2013).
3. Y. Ji, X. S. Yao, L. Maleki. – *Electronics Letters*, 35, No 18, 1554-1555 (1999).
4. V. G. Harris. – *IEEE Transactions on Magnetics,* 48, No 3, 1075-1104 (2012).
5. A. A. Porokhnyuk, A. B. Ustinov, N. G. Kovshikov, B. A. Kalinikos. – *Technical Physics Letters,* 5, No 9, 843-846 (2009).
6. L. F. Stokes, M. Chodorow, H. J. Shaw. – Optics Letters, 7, No 6, 288-290 (1982).

Poems about School

* * *

Чижик-Spinus, где ты был?
– «Я сигнал за хвост ловил!
Сделал я ему “Фурье” –
Закружилось в голове!»

Цели «Spinus»’а просты:
Дать научные мосты!
Пусть у вас здесь будет шанс
Пообщаться «в резонанс»!

В Школе здесь научат всех
Сочетать с наукой смех,
Дискотеки с Э-Пе-эР,
Я-Ка-эР и Я-эМ-эР!

В Школе много новых лиц,
Будем превращать их в птиц:
Вдруг хотя б одной из ста
Дастся «Нобель-высота»!

2010

* * *

Spinus, Spinus, where you were?
Did you dive in the Resonance world?
– “Yes! I dived with my great joy –
Resonance is a pleasant toy!”

“Spinus” school invited you
To look for a knowledge clue.
We will show the signal birth
In the field of our Earth!

If you wish to have success,
At the School achieve progress!
We will teach you all to fly
In the scientific sky!

We desire you to get
Many victories-побед!
It will be a good surprise
If you catch the Nobel prize!

2010

Author Index

Notes

Notes

Notes

Notes

Notes

Magnetic Resonance and its Applications

Abstracts book

Saint Petersburg State University
April 23-29, 2017